Communications Research Centre

HIGH-INTENSITY RAINFALL STATISTICS FOR CANADA

by

B. SEGAL

CRC REPORT NO. 1329-E

Department of Communications
Ministère des Communications

OTTAWA, NOVEMBER 1979

HIGH-INTENSITY RAINFALL STATISTICS FOR CANADA

Examining the tipping-bucket mechanism inside a recording rain gauge. The rain-collecting area is defined by the cylindrical funnel mouth, seen here lying in the foreground. The data analyzed in this report were derived from records taken at locations across Canada with a network of instruments of this type. (Photo courtesy Fisheries and Environment Canada).

COMMUNICATIONS RESEARCH CENTRE

DEPARTMENT OF COMMUNICATIONS

CANADA

HIGH-INTENSITY RAINFALL STATISTICS FOR CANADA

by

B. Segal

(Radio and Radar Research Branch)

CRC REPORT NO. 1329-E

November 1979

OTTAWA

Le présent document est disponible en français,
(Rapport du CRC n° 1329-F)

PREFACE

As the upper limit of the radio spectrum employed in terrestrial and earth-space communications moves ever higher in frequency, the engineer is increasingly confronted by the need to consider climate as an important element in the design of radio systems. As part of its efforts in analyzing and interpreting long-term meteorological observations, the Communications Research Centre has developed an extensive precipitation data base for locations in all parts of the country. A preliminary report presenting the rainfall rate distributions for most of these locations has already been prepared and distributed within the radio engineering community (Segal, 1977). This monograph is an enhanced and expanded version of that earlier document. The analysis employed here includes a number of adjustments and corrections not contained in the earlier work. The graphical presentation has been modified in order to improve the resolution of the high-intensity portion of the distributions.

In addition, an attempt has been made to bring together in this volume a good deal of relevant meteorological information -- much of it coming from sources outside the normal radio-engineering literature. One section, for example, is devoted to a discussion of the influence of land profile on precipitation rates. The topography in parts of this country is sufficiently irregular that corrections either should or must be made when interpolating between stations, or when extending existing knowledge and experience from one site to another. Another topic of relevance to the design of microwave radio systems (but not previously discussed in this context) is that of inadvertent, man-induced modification of the weather through various means. Also included is a critical assessment of some recent experimental observations on rain "cells". This background material should enable the design engineer to assess the validity of many of the assumptions inherent in various models and methods that are used in the prediction of microwave attenuation by hydrometeors. A report presenting the results of detailed numerical calculations of radio wave attenuation for a wide range of transmission parameters will be published in the very near future.

This report has been prepared to serve the needs of the Canadian radio systems designer and of that segment of the scientific community seeking to derive models of atmospheric propagation at microwave frequencies based on available environmental data. It is anticipated that these groups will constitute its major user. However, within other disciplines such as hydrology, agriculture and environmental protection there exist many potential beneficiaries of accurate intense-rainfall statistics. It is hoped that many of these likewise will make use of the results contained here. In this way, it is hoped that this document will prove to be a useful work in its own right as well as serving as a logical companion to the volume specifically devoted to microwave attenuation.

Even within the radio community, much may yet need to be done. Several topics, because they represent relatively novel concepts in systems design, have not been treated with the same depth as other, more prosaic matters. Additional statistics on rainfall variability, for example, could readily be generated for the full complement of stations, if these are required at some future date.

The author would like to express his gratitude to the Radio Relay Committee of the Canadian Radio Technical Planning Board for its continuing interest in these radio climatological studies. The keen interest and concern of Mr. B.S.V. Cudbird from a professional climatologist's vantage point must also be acknowledged. His assistance during the initial stages of this project was most helpful. Thanks are due to Messrs. G. Bristow and B. Yorke of the Atmospheric Environment Service for ensuring the high quality (and quantity) of microfilm records of original precipitation observations. Without question, however, the greatest expression of gratitude must be directed to Mrs. Flora Chyurlia. Her patience and fortitude in tackling what appeared, at times, to be an endless task have made this work possible. Her diligence in so carefully scaling, almost single-handedly, nearly 500 years of Canadian precipitation records, should help to establish this as one of the world's major banks of rainfall data.

B. Segal

Ottawa,
October 1979.

TABLE OF CONTENTS

1. INTRODUCTION

Radio communication has historically enjoyed a position of great importance in Canada; yet few countries in the world face the same diversity in propagation conditions within its borders. This document is concerned entirely with the question of intense rainfall and its potentially detrimental influence on microwave propagation. Figure 1 shows the long-term probability that severe rainfall will produce signal fades of 40 dB or more over a microwave radio link in the Toronto region. Starting at a critical frequency in the vicinity of 8.5 GHz, the attenuation probability increases sharply for the next several GHz. It is not surprising, therefore, that communicators have chosen, wherever possible, to operate in the bands below this frequency. The use of these lower frequencies has been growing rapidly. The rate of growth in licensed assignments in this range has been of the order of 10%–20% per annum over the past decade. The combined pressures of spectral crowding and increased service demands may be expected to produce a marked increase in the use of the frequency spectrum above 10 GHz for both terrestrial and earth-space applications.

In this country, a single long-haul microwave radio relay system may extend more than 4000 kilometres, cover five time zones, and encompass a variety of geographic and climatic regions. Propagation experience gathered in one region of the country may be of little relevance to conditions prevailing thousands or even hundreds of kilometres away. The intent of this report, therefore, is to examine the statistics of rainfall across the entire country in some detail, and in a way that bears upon the design and operation of radio and radar systems.

2. PRECIPITATION DATA BASE

2.1 STATION SELECTION

Along with various other meteorological quantities, rainfall is routinely observed and recorded at a great many stations scattered throughout the country. At some of these, precipitation records have been maintained for many decades – – in some instances, for well over a century. Generally, however, weather stations record only the accumulation of rainfall over a full 24-hour period. Such data are not capable of providing the type of statistics needed to evaluate radio-wave propagation effects. Fortunately, at a smaller number of observation stations, continuously recording rain gauges of the tipping-bucket variety are maintained. These gauges consist of a small, unstably balanced twin-bucket assembly situated immediately beneath the funnel of a much larger rain collector (see frontispiece).

In most of these gauges, the geometry and balance conditions are so arranged that the integrated equivalent of 0.01 inches (0.254 mm) of rain over the collecting surface fills one of the twin buckets sufficiently to cause it to tip away from the neck of the funnel. At this point, the precipitation commences to fill the second bucket, while the first one empties, ready to continue symmetrical operation. At the same time, the tipping of the bucket triggers an electrical impulse which causes the event to be recorded permanently on a paper chart. These tipping-bucket chart recordings offer the best opportunity of utilizing the data contained in the archives of the Canadian Atmospheric Environment Service (AES) to derive precipitation statistics of value to the microwave systems designer.

The AES routinely analyze and maintain summaries of these chart recordings. These summaries consist of the scaled hourly rainfall accumulations as well as the daily 5-min, 10-min, 15-min, etc. maximum rainfall rates. Chen (1976) and Lin (1976a) used published values of the 5 to 180 minute rainfall rates for severe storm events to derive estimates of the five-minute rain rate distributions for several U.S. stations. Lin (1976b) also used the yearly maximum values of 5,10, ... 60 minute rainfall rates to produce distributions for a number of stations where severe rainfall events are infrequent. In the present study, it was decided to use the best available rainfall data base along with sophisticated modelling procedures to provide the Canadian microwave engineer with the radio climatological data required for proper system design.

Since complete, cumulative rainfall rate distributions were desired, it was necessary to analyze the individual rain charts in their entirety, rather than to rely on summaries or brief portions of the rain records. The individual tipping-bucket rain charts were therefore studied for each of the locations shown on the map in Figure 2. The selection of sites was guided by several considerations. Foremost among these was the requirement to cover the entire country as effectively as possible. Without the benefit of hindsight, it was necessary to guess at the probable extent of the various rainfall regimes. Coverage is best in the southern part of the country since (a) this is where most of the early terrestrial microwave system development is likely to take place, (b) most of the available rainfall observation stations are located here, and (c) locations in northern Canada generally exhibit a relatively dry, though otherwise harsh, environment. The St. Lawrence River valley was more heavily sampled because of the immediacy of microwave system implementation along this corridor. Near the east and west coasts, a somewhat higher density of stations was used because it was expected that there would be rapid variation in the character of the rain as a function of distance from the coasts.

Section 4 examines the statistical variation of rainfall rates from year to year, and the length of data sample that is required in order to yield a reliable estimate of the true average distribution. With no prior guideline in this area, it was estimated that 10 years would suffice for most practical applications. For the most part, therefore, 10-year samples of rainfall records were studied for each location. In order to investigate this matter of data convergence, several stations, representing different climatic regions, were analyzed for longer periods of up to 20 years. As this analysis was subsequently to indicate, the estimate of a 10-year data sample was a reasonable presupposition.

At northern sites or at locations where only limited data samples existed, records were studied as available. Table 1 lists all of the locations represented in this investigation, along with the number of years of data for each site. In general, the observation period for each station extended up to (and included) the year 1972, regardless of the actual length of the data sample. Data for 1973 were included for Gagnon, Moosonee, Poste de la Baleine and Stephenville, while the observations for Central Patricia were available for the period 1963 to 1971, only. In all, the 47 stations provided a total of 469 station-years of recorded rainfall data.

2.2 RAIN CHART DIGITIZATION

In operation, each tip of the rain bucket is recorded on a special-purpose pen chart unit. The chart employed for this purpose comprises a strip of paper mounted around the circumference of a cylindrical drum, with the useful area of the chart being a strip approximately 44 mm high by 364 mm long. The drum performs one rotation in the course of a day, thus producing a single strip chart for each 24-hour period(*). The pen is linked to a cam that is controlled by the signal from the tipping bucket. With each tip (i.e., 0.254 mm rain accumulation), the recording pen is stepped vertically about 0.88 mm (either up or down) until the corresponding chart limit is reached. At this point the direction of pen travel is reversed and succeeding impulses are recorded in the opposite direction. The full chart width, from one limit to the other, represents a total of 50 steps, or 12.7 mm rain.

(*) In actual fact, the chart is approximately 380 mm long and allows for up to 25 hours of unattended operation, if necessary.

TABLE 1

List of Tipping-Bucket Rainfall Recording Stations

	LOCATION	LAT deg min	LONG deg min	DATA yrs
1	Calgary, ALTA.	51 06	114 01	10
2	Cambridge Bay, NWT.	69 06	105 07	5
3	Caplan, QUE.	48 06	065 39	9
4	Carmacks, YT.	62 06	136 18	10
5	Central Patricia, ONT.	51 30	090 09	9
6	Churchill, MAN.	58 45	094 04	10
7	Comox, BC.	49 43	124 54	10
8	Dauphin, MAN.	51 06	100 03	10
9	Edmonton, ALTA.	53 34	113 31	10
10	Fredericton, NB.	45 55	066 37	10
11	Gagnon, QUE.	51 57	068 08	9
12	Gander, NFLD.	48 57	054 34	10
13	Geraldton, ONT.	49 41	086 57	10
14	Goose Bay, NFLD.	53 19	060 25	9
15	Halifax, NS.	44 38	063 30	18
16	Hope, BC.	49 23	121 26	10
17	Kentville, NS.	45 04	064 29	10
18	Kingston, ONT.	44 14	076 29	10
19	London, ONT.	43 02	081 09	20
20	Mission, BC.	49 09	122 16	10
21	Montreal, QUE.	45 28	073 45	10
22	Moosonee, ONT.	51 16	080 39	6
23	Normandin, QUE.	48 51	072 32	10
24	North Bay, ONT.	46 22	079 25	10
25	Ottawa, ONT.	45 23	075 43	10
26	Post de la Baleine, QUE.	55 17	077 46	5
27	Prince Albert, SASK.	53 13	105 41	10
28	Prince George, BC.	53 53	122 40	10
29	Quebec, QUE.	46 48	071 23	10
30	Regina, SASK.	50 56	104 40	20
31	Saint John, NB.	45 19	065 53	10
32	St. John's, NFLD.	47 37	052 45	10
33	Sault Ste. Marie, ONT.	46 29	084 30	10
34	Sioux Lookout, ONT.	50 07	091 54	10
35	Stephenville, NFLD.	48 32	058 33	7
36	Summerland, BC.	49 34	119 39	4
37	Summerside, PEI.	46 26	063 50	9
38	Swift Current, SASK.	50 16	107 44	10
39	Sydney, NS.	46 10	060 03	10
40	Toronto, ONT.	43 41	079 38	10
41	Uranium City, SASK.	59 34	108 29	10
42	Val d'Or, QUE.	48 03	077 47	10
43	Vancouver, BC.	49 11	123 10	10
44	Watino, ALTA.	55 43	117 37	9
45	Weyburn, SASK.	49 40	103 51	10
46	Windsor, ONT.	42 16	082 58	10
47	Winnipeg, MAN.	49 54	097 14	10

The small size of the rain charts and of the individual pen steps makes it impractical to undertake any precise scaling of the records without some form of optical magnification. Because of the large number of records involved in this study, the use of microfilm as an intermediate storage medium was the only practical way to proceed. As a result, some 90,000 rain charts were microphotographed onto high-contrast, 16-mm positive film with a 12:1 scale reduction. These were then projected through a modified microfilm reader-printer (3M brand, model 500R) with a 47X magnification factor. In effect, each 24-hour rain chart was thus stretched to more than 1.4 metres in length.

For scaling purposes, the regular viewing screen on the microfilm unit was replaced by a square digitizing tablet (Grafacon model 1010A, manufactured by Bolt Beranek and Newman Inc). This tablet consisted of a translucent Mylar plate with a perpendicular grid of wires embedded over the entire screen area. With a 0.01 inch spacing, the x- and y-axes each contained 1024 wires. Coded impulses transmitted along these wires permitted the unique identification of each of the 2^{20} grid intersections by means of a special, hand-held stylus. Figure 3 shows the digitizing tablet in operation.

Once the charts for a given station were digitized, collated and stored, the rainfall rates could be synthesized subject to any desired statistical processing, error correction, etc. The following sections outline some of these numerical manipulations.

2.2.1 Data Base Errors

Studies involving the application of rain gauge data to radio wave attenuation have sometimes been critical of the accuracy that can be obtained from tipping-bucket gauges. Since these gauges were not originally designed for such demanding applications, it is not surprising that difficulties are encountered when data from these gauges are employed without proper attention to possible sources of inaccuracy. The fact remains, however, that tipping-bucket rain gauges have been, and in the foreseeable future will continue to be, the most practical solution to the problem of obtaining the desired rainfall rate data with reasonably high resolution for a variety of locations. The task facing both the radio climatologist and the systems designer is therefore to relate propagation effects to rainfall statistics as they are routinely observed, recorded and reported. The following probably includes most of the important sources of rain gauge scaling errors.

2.2.1.1 Minor Rain Gauge Errors

Factors such as dew accumulation, evaporation from the gauge buckets prior to tipping, and wetting of the gauge surfaces are among the commonly recognized sources of error. These, fortunately, are important only at the very lowest rainfall rates and are of no immediate concern to us. One possible source of error at higher rain rates is the breakup and bounce of large drops following impact on the ground. Kurtyka (1953), quoting earlier observations, reported a large number of drops bouncing to heights of many tens of centimetres following impact (and disintegration into smaller droplets). Above bare soil, a significant number of drops would be expected to splash to a height of 45 cm or more for rainfall rates exceeding 10 mm/h. The standards for rain gauge installation in Canada call for the collector mouth to be positioned 12 inches (30.5 cm) above the earth's surface. In the presence of horizontal winds, one would expect a net increase in the number of raindrops trapped in the gauge. No measurements concerning the magnitude of this effect have been reported; however, it is unlikely to be a major consideration except under very unusual circumstances.

2.2.1.2 Rain Gauge Non-linearity

Among those sources of error that are more amenable to evaluation are several that relate to the physical chart-recording process. In a careful study of the various linkages within the stepping-pen recording unit used in conjunction with the tipping-bucket gauge, Bourke (1973) has detected errors in both linearity and symmetry in the pen position resulting from the finite dimensions of the stepping-cam follower and the pen pivot arm. Without going into unnecessary detail, it suffices to point out that except at the turning points on the chart, the actual pen trace is displaced slightly from its assumed position. Furthermore, this deviation depends upon the direction of pen travel. Figure 4 illustrates the deviations observed in a tipping-bucket recording unit as the

pen moves up and down the chart through a complete cycle. The most pronounced feature is the asymmetry in pen position, i.e., the position of the pen is different 'n' tips before and 'n' tips after reversal; the error being greater during the downward half of the cycle. While the absolute deviation in chart reading as a result of this characteristic is always less than 2%, the change in slope of the curve on the downward half cycle represents a periodic error of approximately ±5.5% in rainfall rate. This is not an insignificant error; however, as it is non-cumulative and smaller than several other factors, no action was taken to correct for this effect in this investigation.

2.2.1.3 Rain Chart Misalignment

Another potential source of error related to the recording process arose from occasional chart misalignment with respect to the recording pen. It is assumed that the paper chart is mounted circumferentially around the cylindrical drum which rotated about its axis of symmetry. If the chart were mounted so that the two ends were vertically displaced from one another, then the pen trace (in the absence of rain) would be inclined with respect to the horizontal chart axis. On the other hand, if the chart were mounted askew or if the drum rotated with a slight wobble, then the pen would trace a small amplitude cosinusoidal pattern. While these were not common occurrences, evidence of both types of misalignment were observed with regularity at certain stations. Figure 5 shows an example of a one hour rain event recorded on a chart displaying a moderate degree of misalignment. Since the rainfall rate is derived from the slope of the pen trace, this type of chart distortion may result in errors in the intensity distributions.

If, for the sake of analytical simplicity, we neglect the curvature of the rain coordinate, then it follows from the physical dimensions of the 24-hour rain chart that the rainfall rate, R, and the slope, θ, of the smoothed trace are related through

$$R_{mm/h} = 4.3683 \tan \theta \tag{1}$$

Hence

$$\frac{dR}{d\theta_{rad}} = 4.3683 \sec^2 \theta \tag{2a}$$

$$= 4.3683 + 0.22892 R^2_{mm/h} \tag{2b}$$

or

$$\frac{dR}{d\theta_{deg}} = 7.6241 \times 10^{-2} + 3.9954 \times 10^{-3} R^2 \tag{3}$$

Expression (3) may be interpreted as the error in measuring the rainfall rate per degree of chart misalignment at a true rate, R mm/h.

The minimum value of this error is approximately 3.5 percent/degree when R ~ 4.4 mm/h, but beyond about 15 mm/h the error may be taken as

$$\epsilon = 0.4R \text{ percent/degree} \tag{4}$$

That is, at R=50 mm/h a one degree misalignment would yield a 20% error. Fortunately, alignment errors seldom reached that magnitude. When observed, errors of 1/2 to 3/4 degree were typical.

This result may be expressed somewhat differently by substituting (1) into (3). Thus,

$$\epsilon_{\%} = 100 \times \frac{1}{R} \frac{dR}{d\theta_{deg}} = 3.490 \operatorname{cosec} 2\theta \tag{5}$$

Figure 6 illustrates this functional dependence of chart misalignment error on slope. We see that the rainfall rate error is small for chart traces inclined less than 75 or 80 degrees to the horizontal axis. During periods of intense rain, however (e.g., near 1740 hours in Figure 5), the error can become serious, and care was taken during the digitizing process to compensate for this effect by superimposing a new set of axes over the projected image of the rain trace.

2.2.1.4 Winds

Wind represents one of the major sources of error in the measurement of precipitation by means of conventional gauges. The normal, large-scale 3-dimensional wind fields associated with convective storms form an integral part of the precipitation process and do not, in themselves, contribute significantly to errors in the measurement of rainfall at the surface, or in applying these to predictions of radio-wave attenuation (at least with respect to terrestrial links). What concerns us, rather, are the winds flowing in the immediate vicinity of the gauge since these can seriously affect its operation.

The standard tipping-bucket rain gauge may be considered as representing a cylindrical obstacle, some 25 cm by 30 cm, to the free movement of air near the ground. As winds are deflected around and over the gauge, an updraft is produced above the orifice which tends to lift some of the drops and thus to reduce the catch efficiency of the gauge. In addition, the compression of streamlines flowing over the top of the gauge results in an increase in the horizontal component of the wind speed which serves to carry the rain drops beyond the gauge orifice, further increasing the deficiency in precipitation recorded by the gauge. The curves in Figure 7 are the averages of gauge efficiency as a function of wind speed based on a number of experimental observations (Wilson, 1954). It would be difficult to accurately relate the average wind speed in a given location to the rain intensity during storm conditions in order to correct for such gauge errors. However, we see that the rain catch deficiency can reach very large proportions under conditions of heavy winds. The effect is considerably greater for snow than for rain because these hydrometeors, being lighter and having a much lower vertical fall velocity, are more readily displaced by the wind. Black (1954) conducted a careful study of the precipitation at Barrow, Alaska. Various pieces of evidence led to the conclusion that the actual snowfall during winter was two to four times that recorded by means of the standard U.S. precipitation gauge. Winds at Barrow average in the vicinity of 20 or 25 km/h; during storms, they frequently exceeded 50 or 60 km/h. The results at Barrow are therefore consistent with the observations presented in Figure 7.

While the winds at more southerly latitudes are generally less extreme than those observed at Barrow, it is apparent that standard rain gauge measurements will sometimes seriously underestimate the true precipitation intensity. James (1964), for example, noted an 8% difference between the rain catch recorded on the windward side of a low, gently sloping hill from that on the leeward side. It was also noted that this difference increased with wind speed.

Fortunately, the magnitude of this induced gauge error is likely to be a little smaller in Canada than in many other countries under similar wind conditions. It is well known that the speed of low level winds increases with altitude. The vertical velocity gradient can be written in the form (Haltiner and Martin, 1957)

$$\frac{du}{dz} = az^{-\beta} \tag{6}$$

where a is a parameter combining both meteorological and surface roughness factors, and β is essentially a function of the temperature lapse rate. During unstable (superadiabatic) conditions, $\beta > 1$, while $\beta < 1$ during stable periods (temperature inversions). Under conditions of neutral equilibrium, $\beta = 1$ and the velocity increases logarithmically with height. Operating standards in Canada call for the gauge mouth to be positioned 30.5 cm (12 inches) from the ground. Other countries place their gauge orifices up to 2 m above the surface. In the U.S., the standard rain gauge is positioned approximately 79 cm (31 inches) from the ground, but the use of an Alter wind shield reduces the effect of the increased wind speed from what it otherwise would be (Sanderson, 1975).

The effect of wind on gauge catch is naturally greatest for drizzle and light rains where the droplets are small and are falling with a relatively low terminal velocity. The heavier drops that contribute significantly to thundershowers are less readily displaced by changes in wind speed in the vicinity of the gauge. Thus, the relative error in gauge measurement would not necessarily be expected to grow with storm intensity despite the increased winds that generally accompany severe events. It is estimated that surface winds account for an error of −5% to −15% under average storm conditions.

2.2.1.5 Missing Data

For many of the stations investigated, there were periods of varying duration for which normal rain data were lacking, for one reason or another. If such instances are simply ignored, then there is a distinct possibility that extraneous errors would be incorporated into the various statistical distributions. In order to reduce these errors, efforts were made to identify such intervals and to compensate for them, where possible, in a judicious fashion.

Periods of missing or poor quality records may be divided into several categories. The first of these consists of the relatively brief interludes —– ranging from minutes to days —– during which there was an equipment malfunction. Frequently, there were simply no rain charts available for such a period. Examination of other rainfall summaries indicated whether these periods could be overlooked, or whether they included a major portion of that month's precipitation. In at least one instance, it was found advisable to ignore the balance of the rain charts for that particular month and then to compensate for it as will be described shortly. Where chart quality suffered as a result of inking or pen stepping problems, efforts were made to reconstruct or otherwise correct the more significant portions of the records.

A second cause of data outage was more insidious since it tended to occur during major rain events. Intense rainfall events are of particular interest because of their rare occurrence and because of their importance in the estimation of radio-wave propagation conditions. Unfortunately, these events are frequently accompanied by the most severe winds for any given location. The power failures that sometimes result may lead to the loss of gauge records for a disproportionately large percentage of the high rainfall rate events (see Figure 8). Needless to say, there is no way of resurrecting the precipitation history for such periods. (There may be some slight consolation in the thought that many communications channels would also be disrupted during these periods by the same power failures!)

Occasionally, rain charts were simply missing from the AES archives, although records indicated that precipitation had occurred during that time. In Canada, a further loss of rain records frequently occurs during the winter months. Unless it is equipped with special heaters, the tipping bucket equipment is normally taken out of service once freezing temperatures set in. Over the years, the gauges at different locations have been out of operation for varying periods of time. As a result, the records available for analysis were seldom complete for the entire decade or so under study. As an example, during the 10-year record sample for Toronto International Airport, there were actually only 5,6,8,10,10,10,10,10,10,10,10, and 7 years' data covering the months January through December, respectively. Generally, stations at the more remote sites tended to have a greater number of months of missing data, at least during the winter period. The way in which this problem was treated was to apply to each month's rainfall accumulation, a correction factor inversely proportional to the number of times that calendar month appeared in the total record. Fortunately, at each of the stations studied, the heavy rainfall season was fairly complete, so that this correction for missing data had a relatively small overall effect.

At 26 of the 47 stations studied, data were completely lacking for one or more calendar months (i.e., only 21 stations had complete 12 month coverage on at least some occasions). Other climatological records, however, are available. These are based on observations taken with the standard, accumulating (i.e., non-recording) rain gauge rather than with the tipping-bucket gauge. From such records, it was possible to estimate the amount of rainfall that occurred during the period for which the tipping-bucket data were unavailable. For the 26 stations affected, the fraction of the total annual rainfall missed in this way varied widely. At Kentville, N.S., 23.6% of the mean annual rainfall occurs during the calendar months December

through March, for which records were never available. In general, the amount missed in this manner was far less, averaging only five percent for all 26 sites affected. Only three other locations (Caplan, Que., Carmacks, Y.T. and Central Patricia, Ont.) suffered more than a 10% loss of data due to non-operation of rain gauges during the winter months.

To compensate for these missing data, an adjustment factor was applied to the rainfall occurring during the month either immediately preceding or immediately following the missing interval. The size of this factor was calculated so as to increase the total observed precipitation by the amount deemed missing on the basis of the long-term climatological averages.

2.2.2 Rain Gauge Calibration

The tipping-bucket rain gauge in use today is a meteorological instrument of venerable ancestry(*). Over the years, it has successfully evolved to become the primary instrument throughout the world for measuring rainfall rates. Meteorological applications, however, do not generally require observations of the same intensity levels or with the same resolution that are in demand for radio-climatological predictions. Just as no experimental observation would be recorded without due attention being paid to the calibration of the associated equipment, so must we consider the measurement accuracy of the gauge over its complete range of operation, if these records are to be exploited to their ultimate limit. A number of errors related to the measurement of rainfall have been discussed in the preceding paragraphs. The concern now is with the tipping-bucket mechanism itself.

Although the tipping of the bucket assembly is a fairly simple and rapid operation, we are dealing with a purely mechanical system — — one influenced by such factors as bucket inertia, bounce, and friction at the pivots. One bucket does not instantaneously replace the other beneath the funnel. At very high rainfall rates, a modest amount of rain may be lost in this way. There will also be a certain amount of spilling or splashing of water over the edge of the buckets themselves, during rapid fill. In actual field operation, the tipping-bucket inaccuracies are called to account by applying a daily correction factor, derived by comparison with an AES standard (24-hour) rain gauge. These factors vary from day to day, presumably in response to the differences in rainfall intensity.

The Atmospheric Environment Service have performed a series of calibration tests on the tipping-bucket gauge (Bourke, 1963). Following the standard set-up procedure, the response of the gauge was measured by carefully releasing fixed quantities of water to simulate different (constant) precipitation rates. Figure 9 summarizes the results of several trials at rates of up to 330 mm/h. We see that the error is not negligible for rainfall beyond a few tens of mm/h. The error appears to stabilize near −9% over a broad range of (heavy) rain rates before growing once again as the rate moves beyond the range of normal experience. The curve adopted in this study consists of three analytically continuous, second degree segments, as shown. The slope of the error curve has been moderated somewhat beyond 300 mm/h since it is unlikely that the gauge error would continue to grow at as great a rate as suggested by the final portion of the experimental calibration. What was done, was to select a trend intermediate between that and the curve for the U.S. gauge. The trend at very low rain rates is somewhat uncertain, with evidence of a growing spread in the experimental results. The error curve was simply brought to a smooth termination at +2% at this end of the curve, which was of little importance to our present study. A correction factor corresponding to the inverse of the error curve shown in Figure 9 was applied to all of the rain rate data studied here.

(*) Kurtyka (1953) attributes the development of the first self-recording tipping-bucket rain gauge to Sir Christopher Wren in 1662. The oscillating, double bucket arrangement in use today was apparently introduced as long ago as 1829.

3. RAINFALL INHOMOGENEITY

Although precipitation events may sometimes extend over thousands of kilometres, rain storms are more frequently scattered and local in nature. This localization has given rise to the use of the term "rain cell" in connection with the precipitation process. The meaning and interpretation which might be associated with this term depends to a considerable extent upon the nature and intensity of the prevailing weather situation. It is the purpose of this section to touch upon some of the nuances implicit in any discussion of rain cell properties, and some of the uncertainties concomitant with their application.

In the absence of strong external turbulence or shear forces, a thin, unstable fluid layer tends to develop a regular pattern of small convective elements known as "Bénard cells" (Sutton, 1953). Fair-weather cumulus clouds frequently exhibit patterns suggestive of this type of cell development within the atmosphere. These patterns may, at times, cover very large areas of the earth's surface (Byers, 1965; Krishnamurti, 1975). Under the more complex and dynamic meteorological conditions encountered during precipitation, the term "cell" is used in different ways, frequently without a very precise, objective definition being applied. Perhaps the simplest situation under which precipitation may be associated with a distinct cellular atmospheric structure involves the "generating cell" (Marshall, 1953; Wexler and Atlas, 1959). These are typically found within stratiform cloud formations and result from the lifting above the freezing level of a shallow layer of potentially unstable air in association with an advancing warm front or an occluded trough of warm air. Generating cells are relatively shallow (about 1 km deep) and several kilometres in horizontal extent, with light to moderate precipitation extending to the ground.

Another instance where precipitation originates from within a more or less identifiable, self-contained turbulent element is in association with the so-called "convective cell". Of greater interest to the radio engineer, these vertical structures develop in conjunction with strong cumulus formations and are much deeper than the generating cell. The convective cell typically extends to altitudes of 6–10 km but may reach well above 12 km under severe frontal or pre-frontal squall conditions (Crowe, 1971).

The total rainfall observed at any location inevitably includes some of decidedly non-cellular origin. Houze (1973), for example, has shown that no more than 74% of the observed monthly precipitation at a site in New England was cellular (and only 31% during the month that recorded the greatest precipitation). For a location on the west coast, the maximum monthly contribution resulting from cellular precipitation was only 25%. The most intense rainfall, however, almost always originates within convective-type cells, although these intense rain centres may well be contained within very much larger areas of non-cellular type precipitation.

Attempts have been made at estimating both the rainfall and the precipitation attenuation distributions from presumed properties of rain cells (Lefrançois, 1971; Misme and Fimbel, 1975). Such predictions, of course, are more soundly based on detailed rainfall statistics as presented here. However, a thorough understanding of the small-scale spatial structure of rainfall remains a matter of considerable importance, since the separation and orientation of stations in a site-diversity radio system, whether terrestrial or earth-space, are ideally based upon known characteristics of the precipitation inhomogeneities for a given region.

3.1 PROBING OF PRECIPITATION STRUCTURE

The introduction of weather radar equipment has played an important role in adding to the basic understanding of cloud physics and storm meteorology. For wavelengths that are large compared with the diameters of individual rain drops, incident electromagnetic energy will be backscattered by the precipitating particles, roughly independent of frequency. The magnitude of the returned signal is then determined by the characteristics of the radar, the distance to the scattering particles, and the number and size distribution of the rain drops. Although the rain drop-size distributions show considerable variation for different rain types and from one event to another, we may, for the present discussion, approximate the radar reflectivity factor by the relation

$$Z(\mathrm{mm}^6/\mathrm{m}^3) = 200\ R^{1.6}(\mathrm{mm/h}) \qquad (7)$$

The observed radar echo intensity thus permits the mapping of equivalent precipitation intensities in three dimensions. Results are generally quoted in terms of received signal strength (dBZ=10logZ) relative to that which would be produced by an assemblage of uniform 1 mm diameter drops having an average spatial density of 1 drop per cubic metre. Figure 10 shows how this factor varies with R. The observed echo is extremely sensitive — — at least in the high intensity region — — to the effective rainfall rate. A calibration error of only a few dB would correspond to a very significant error in equivalent precipitation intensity, particularly in the area of greatest concern in radio propagation predictions.

3.1.1 Internal Organization

Numerous radar investigations have been conducted into rain storm structure and movement. In a perceptive study of the structural composition of precipitation events, Austin and Houze (1972) analyzed basic rainfall patterns for a number of severe storms passing through the New England region of the U.S. Within the broad ranges of basic meteorological size classifications, they were able to detect a tendency toward preferred sub-sizes, the precipitation within each size group exhibiting particular attributes (e.g., persistence, intensity, motion), and each structure in turn containing elements of the next smaller category (Austin, 1973). The basic results are summarized in Table 2. The cells, here defined as small, intense radar echoes and assumed to represent individual cumulus convective elements, were nearly always observed within the small mesoscale areas (as many as 10 cells to one SMSA), while 3–6 SMSA's were generally found within each LMSA. The column listing equivalent diameters was obtained by assuming circular cross-sections.

3.2 CELL SIZE OBSERVATIONS

3.2.1 Global Summary

Figure 11 illustrates one of the most frequently used models of rain cell sizes in radio propagation applications, viz., that adopted by the International Radio Consultative Committee (CCIR, 1975). The curve summarizes independent measurements made variously in Japan, France, Switzerland and Malaysia. Conveying no information on the distribution of cell diameters for any given rain intensity, the curve expresses a simple inverse relationship between average cell size and intensity. It has been suggested that this reflects the (assumed) fact that intense outbursts of rain are generally more confined and of shorter duration than are moderate or light rain showers. Whether applied to entire rain storms or to the actual cells themselves, such arguments represent a specious over-simplification of reality. Radar images of major precipitation events are highly variable with respect to overall size, shape (both horizontally and in vertical extent) and internal organization (i.e., fine-scale structure). New areas of intense precipitation are continually being formed within the larger, undulating, convective region. For the most severe multi-cell storms studied, individual cells grow until — — at their peak of activity — — they merge and can no longer be resolved with respect to one another (Marwitz, 1972). For most locations, some of the most intense rainfall will originate with cells (or cell complexes) of major proportions. What should nevertheless be noted is the basic agreement between the observations presented in Table 2 and the cell sizes reported for precipitation rates in the range 25–100 mm/h.

TABLE 2

Characteristics of Basic Precipitation Structures (After Austin, 1973)

Feature Definition	Characteristic Area (km^2)	Equivalent Diameter (km)	Typical Lifetime (hr)
Large mesoscale area (LMSA)	2000–5000	50–80	1.5–4.0
Small mesoscale area (SMSA)	100–500	11–25	0.5–2.5
Cell	3–10	2–3.5	<0.7

3.2.2 Slant-Path Observations

In a scheme designed to obviate some of the calibration difficulties associated with the use of radar probes, Strickland (1974) took advantage of a 15.3 GHz beacon operating aboard the Applications Technology Satellite, ATS-5. An S-band (2.86 GHz) radar equipped with a 3 metre antenna was used to probe rain structure in the region, while a separate receiving system was used to monitor the 15 GHz beacon. Whenever rain attenuation was detected on the beacon signal, the weather radar was diverted to that position and the echo calibrated in terms of the equivalent slant-path 15 GHz attenuation.

Approximately 750 cells were observed in the Ottawa region during most of the 1970 precipitation season. The horizontal size of the observed rain cells was defined by the azimuthal range within which a given attenuation level would be exceeded (at a fixed elevation angle). For a given attenuation level and elevation angle, the distribution of cell sizes was found to be approximately log-normal. Mean values are shown in Figure 12 for a 5° beam elevation angle (which was the closest approximation to horizontal propagation). The standard deviation about these mean values was 0.8 km at 3 dB attenuation, dropping rapidly to about 0.55 km at 5 dB and then remaining close to this value. Of particular interest here is the shape of the distribution, for while one cannot readily translate the observed slant-path, 15 GHz attenuation to rainfall intensity within the cell area, the two are nonetheless monotonically related. The low-attenuation cells which diminish in size with increasing attenuation are possibly shallow "generating cells", while the high attenuation portion represents the deeper, high-intensity convective cells. We note in this instance that the more intense rain cells increase in size with increasing attenuation level. We also note that, in general, the sizes indicated are larger than of those shown in Figure 11 and intermediate between those for cells and SMSA's reported in Table 2. While Austin and Houze (1972) were unable to adequately resolve the horizontal extent of many of the rain cells in their study, they nevertheless noted a direct relationship between the rainfall intensity from a cell and its overall dimensions. Altman (1973) has likewise presented data suggesting that the area of a rain cell increases as the logarithm of the reflectivity of the cell core.

3.2.3 Low Elevation-Angle Measurements

Another important radar investigation of rain cells was the detailed study conducted during the summer of 1973 at Wallops Island, Va. (Katz, 1975,1976; Konrad and Kropfli, 1975). In this case, a 10 centimetre radar was linked to a 60 foot diameter antenna to yield a beam having a 0.4 degree angular resolution, compared with one nearly six times as broad in the Ottawa study. Azimuthal scans were possible down to an elevation angle as low as 0.5 degrees, thus permitting the probing of rain cells close to the ground, even at extreme ranges. Careful attention to equipment claibration yielded final data to an estimated accuracy of better than 2 dB over a 90 dB dynamic range. Shifting the transmitter frequency between successive pulses ensured that statistically reliable averaging was obtained for each of the 1141 discrete cells analyzed.

The spatial extent of the rain cells was somewhat arbitrarily — — although consistently — — defined by the contour having a radar reflectivity 10 dB below the peak value observed within the cell. Figure 13 presents some of the results of this study for all cells observed below the atmospheric freezing layer (approximately 4 km altitude). The curve seems to combine some of the characteristics of both Figures 11 and 12 but the net result is one of decreasing diameter with increasing intensity after a brief inflection. The median cell size for the entire population ranged from approximately 5.3 km (equivalent diameter) near the surface, to 5.0 km at 3 km altitude. While the procedure employed in this study gave a clear, objective definition of the cell boundary, this boundary may not relate closely to other meteorologically meaningful dimensions. Because of the non-linearity noted in Figure 10, the rain intensity at the assumed boundary of a 60 dBZ cell, for example, significantly exceeds that at the very core of a 40 dBZ cell. The former would certainly be producing significant rainfall at considerably greater distances than suggested by Figure 13. On the other hand, it is only the most intense cells in Figure 13 that exhibit diameters as small as those displayed in Figure 11.

3.2.4 Surface Rainfall Patterns

Of course, it is also possible to study surface rainfall patterns directly, without the use of radar probes. Thus, a rain cell might be defined by means of a contour (such as a suitably chosen isohyet) enclosing an area

of significantly enhanced precipitation. The detailed rainfall pattern would be observed by means of a dense network of rain gauges on the ground. In principle, such observations could be of greater validity to the study of terrestrial radio-wave propagation than radar echoes from elevated raindrops.

Huff (1973) has presented the results of such a hydrological study of more than 1400 rain "cells" observed at St. Louis, Missouri. Figure 14 illustrates the properties of these cells during their most intense five minute interval. There are two significant points to be noted. First, the observed cell size increases monotonically with average rainfall intensity, in sharp contrast with the results presented in Figures 11 and 13. Secondly, the equivalent cell diameters are considerably larger than those discussed above. While the inevitability of this result was dictated by the relatively wide spacing (approximately 12 km) of the elements in the rain gauge network, it raises serious questions with regards to the interpretation of the observations. Although referred to as cells, the structures more likely correspond to Austin's SMSA's than to fundamental rain cells aloft, as detected by the radar studies described earlier.

Because rain storms move with considerable speed, it is possible to gain some insights into the internal structure by observing the rainfall pattern from a fixed point on the surface as a storm passes overhead. The complexity in defining and summarizing rain cells is illustrated in Figure 15 which contains three examples of time-varying rainfall rates as recorded and synthesized with a 1-minute resolution. Very similar variations in rainfall rate have been reported using rapid response rain gauges with resolution times of several seconds (Hogg, 1968; Bodtmann and Ruthroff, 1974).

Figure 15(a), depicting what might be considered a "text-book" example of intense precipitation from an isolated rain cell, was recorded during a springtime shower at Ottawa. Reaching a peak of nearly 200 mm/hr, the entire event was over in a matter of minutes, although it was followed several hours later by a smaller rain shower. In Figure 15(b) we again have a classic example of smooth growth and decay of rain intensity from a clearly defined cell during a late summer event in central Canada. Attaining a peak rainfall rate even greater than for 15(a), the single event in this case (at approximately 2200 h) lasted for more than a half hour.

Neither of these instances, however, is typical. What is generally observed is an event displaying a great deal of poorly-resolved structure. Figure 15(c) shows evidence of a maritime rainfall event of longer duration than either (a) or (b) above. Despite several peaks of fairly heavy rainfall, (three instances of rainfall rates greater than 50 mm/h and one exceeding 100 mm/h), it would be extremely difficult, in this case, to extract a simple rain cell model with any degree of confidence. Using high-resolution tipping-bucket rain gauges, Hobbs and Locatelli (1978) have observed similar fine-scale precipitation structure.

3.3 RAIN CELL SPACING

Both Strickland (1974) and Konrad and Kropfli (1975) have also analyzed the distribution of inter-cell spacing from their respective observations. For cells exhibiting a 15 GHz slant-path attenuation greater than 3 dB, Strickland's published distribution of inter-cell separation displays a remarkably precise fit to a Rayleigh distribution with median value of about 28.8 km. The implications of this result warrant further examination.

It can be shown that if a distribution of points is purely random (Poisson distributed) in two dimensions, then the distances between adjacent points (i.e., nearest neighbours) will exhibit a Rayleigh type density function. The fact that the distribution of inter-cell spacing for *all* cells (and not merely adjacent ones) was an excellent fit to the Rayleigh function implies that the individual cells were not, in fact, positioned in purely random fashion, but maintained some form of collective structure. An azimuthally symmetric Rayleigh function expressed in polar coordinates as

$$P(r) = \frac{r}{\sigma^2} \exp\left(\frac{-r^2}{2\sigma^2}\right), \quad r \geqslant 0 \tag{8}$$

transforms into the symmetrical, two-dimensional Gaussian distribution in Cartesian coordinates:

$$P(x,y) = \frac{1}{2\pi\sigma^2} \exp\left(-\frac{x^2+y^2}{2\sigma^2}\right) \quad (9)$$

In this form, it is clear that attenuating rain cells tend to cluster somewhat about a central core — — a result that is consistent with the observations of Austin and Houze (1972) discussed above.

However, in the design of a microwave route-diversity system the parameter of prime interest is not the overall two dimensional distribution of inter-cell spacing, but rather the distribution in the direction perpendicular to the transmission paths. Along an axis so defined, (9) reduces to the normal density function

$$P(d) = \frac{1}{\sigma\sqrt{2\pi}} \exp\left(\frac{-d^2}{2\sigma^2}\right) \quad (10)$$

Accordingly, the median absolute value of the inter-cell separation in one dimension is given by

$$|d|_m = 0.675\ \sigma \quad (11)$$

Because d may assume negative as well as positive values, the conditional probability that attenuating rain cells might simultaneously be positioned over two circuits will not exceed 25% for parallel paths more widely spaced than $|d|_m$. Figure 16 shows how this maximum conditional probability varies as a function of path separation. By way of comparison, the median of the Rayleigh distribution (8) is

$$r_m = \sigma\sqrt{2 \ln 2} = 1.177\ \sigma \quad (12)$$

The median value of 28.8 km for inter-cell spacing noted above may thus be translated into a path separation of $|d|_m$ = (0.675/1.177)x28.8 = 16.5 km, approximately, for a significant diversity improvement.

By contrast, despite a careful investigation of the inter-cell spacing statistics, no simple mathematical relationship (such as a Rayleigh, exponential or log-normal distribution) could be found consistent with the observed data, in the Wallops Island study. The median distance between cells was found to be approximately 33.3 km, more than 15% greater than the 28.8 km reported above for the Canadian study. Since we may accept both sets of observations as valid, we are forced to conclude that the morphology of rain storms varies significantly with geographic location.

3.4 CELL-PAIR ORIENTATION

Severe storms frequently occur along or ahead of the weather fronts separating competing air masses. As a result, the areas of heavy precipitation are often banded (Browning et al., 1973), with cells clustered close to one another along the band but separated by greater distances from cells outside the band. Hobbs and Houze (1976) have identified rainbands occurring under six meteorologically different situations. In the design of a path-diversity system, the orientation of such rainbands represents the worst possible alignment for pairs of stations, since it is quite likely that both would be subjected to severe rain at the same time during squall-line or multi-cell conditions.

These rainbands are generally reported to be aligned perpendicular to the direction of the winds in the upper atmosphere; however, close examination of the available charts suggests that they are, in fact, more often oriented approximately 10° to 45° clockwise with respect to this perpendicular (Harrold, 1973; MacKenzie and Allnutt, 1977; Marwitz, 1972). The direction of the winds may therefore provide some guidance as to the optimum geometry for stations in a route-diversity system. Figure 17 shows the azimuthal distribution of winds recorded at a typical cloud-level altitude of approximately 3 km (700 mbar pressure level) over Edmonton

(Stony Plain), Alberta. Nearly 4200 rawinsonde observations taken over a 10-year period are plotted, covering the calendar months April to October, inclusive(*). A striking feature of this distribution is its obvious peakedness (coefficient of kurtosis = 0.59). The mean wind direction during this period was from 279° with an inter-quartile spread of only 71° (50% of all values lie between 240° and 311°).

Figure 18 shows the mean 700 mbar wind speed and direction for locations across the entire country and for neighbouring portions of the U.S. As in the above example, data were included for the calendar months April to October only, for most locations, since no heavy rains are expected during the balance of the year (see Seasonal and Diurnal Characterisitcs, Section 4.2.2). Along the coasts, the full 12-month data base was included. Examining the wind vector for Maniwaki, Quebec (situated due north of the eastern tip of Lake Ontario, and approximately 100 km from Ottawa), we see that the mean upper-level wind direction is 283° (i.e., originating approximately west by north). Adding an additional 10° to 45° one would conclude from the preceding discussion that rainbands in this area would tend to be oriented in the range 23° to 58° east of north (i.e., 40.5° ± 17.5°).

In his study of rain cells in the Ottawa area, Strickland (1974) reported a minimum in the probability of cell pairs occurring at an orientation of −50° (i.e., 310°) and a maximum near +35°. Actually, for the 275 cells producing slant-path attenuation greater than 5 dB, the minimum extended roughly over the range −47° ± 25° with a broader maximum over the range +37° ± 45°, approximately. These results are in good agreement with the deduction made above on the basis of the upper-level winds. It is thus reasonable to assume — — in the absence of any conflicting observational evidence — — that pairs of severe rain cells are least likely to occur with orientations from 10° to 45° clockwise with respect to the mean wind directions indicated in Figure 18. Over most of eastern and central Canada, this implies a generally NW–SE configuration. For terrestrial path-diversity circuits, parallel links directed within this range are most likely to suffer simultaneous fades and should be avoided, if possible. Similarly, for earth-space links, sites separated along a line at right angles to this are likely to offer the smallest diversity improvement.

The observations described in this section, while differing in many details, should not be interpreted as necessarily indicating a lack of agreement over the fundamental characteristics of rain cells. Rather, they illustrate the fact that only very inadequate descriptions and statistics regarding the morphology of rain structures are available at this time. Since there is no universally accepted, objective definition of a rain cell, different workers produce results of differing form. The fact that cells are born, grow, mature and decay as they move irregularly through space and time means that a more complex description than a mere 'diameter versus rainfall rate' distribution is required. The definitive study on which a comprehensive rain cell model of radio wave attenuation can be based has clearly not yet been completed. Nevertheless, various heuristic rain-cell methods have been developed that may be useful in certain climatic regions and/or over a limited frequency range. The discussion presented above should help to alert the user to some of the limitations inherent in such methods.

4. TEMPORAL VARIABILITY

The bulk of this report is directed towards the presentation of long-term cumulative rainfall-rate distributions for locations from coast to coast. An understanding of the geographical trends in the precipitation climate is, of course, essential to the judicious design of many microwave systems. Of equal or perhaps greater import is a knowledge of the variation of intense rainfall as a function of time. Despite its importance, however, this area of radio-climatology has received little attention in the literature, largely due to a paucity of

---

(*) The results would scarcely be altered if we were to consider the distributions for the full 12 month period. For the case being considered here, the mean wind direction shifts by only 5° and the distribution becomes even more leptokurtic.

appropriate data. Although interest in this aspect of the meteorological environment is growing, there is little agreement as to how such temporal variability might best be expressed. Indeed, different situations may call for different descriptions of the time-varying character of intense rain. For example, circuits designed to carry low-priority traffic may need to allow only for year to year variation; on the other hand, outages of several minutes on the diverse links of a vital telecontrol circuit may be of crucial significance. This section addresses the subject of temporal rainfall variability in broad fashion. Summaries of the hourly, monthly and yearly changes in rainfall behaviour are presented for a sampling of stations in different climatic regions. Additional analyses of this type may be carried out in future, as the nature of the requirements in this area become more clearly defined.

4.1 INTER-ANNUAL VARIATION

This section takes up the subject of year-to-year variation in the probability of occurrence of intense rainfall. This subject has never been thoroughly treated before. The need for better understanding in this area has two complementary facets. On the one hand, it may be necessary to anticipate and allow for large annual departures from average conditions. What is the likelihood, for example, of encountering a year in which the incidence of intense rain is two or three times greater than average? On the other hand, it is important, when dealing with limited experimental or observational data, to be able to estimate how close the mean of these data is likely to be to the long-term average. Several papers have made rudimentary approaches to this question (Lin, 1976b,1977; CCIR, 1978c). These suggest that intense rainfall probabilities may not be fully stabilized even when 10 or 20 years of data are averaged. These observations, however, do not allow one to determine the probable error in the estimate of the mean.

Several of the stations selected for this study were chosen on the basis of the length of continuous record available. These include London, in a moderately high precipitation area of southern Ontario (mean annual rainfall = 737 mm, average number of thunderstorm days = 28.1) and Regina, in the much dryer plain (21.4 thunderstorm days, but only 292 mm rain). Each of these stations provided 20 years' data, while Halifax, which yielded 18 years of record, enjoys a climate typical of the east coast (1177 mm rain with only 9.0 days of thunderstorm activity).

In order to study the inter-annual rainfall characteristics referred to above, the probabilities of exceeding various rainfall rate levels were derived, year by year. These were then analysed to establish the statistical nature of the variation. At very low rain rates, the ensemble of annual probabilities was found to approximate reasonably well to a Gaussian (normal) distribution. As the rate is increased, however, the distribution becomes more and more positively skew. This behaviour is expected in the case of meteorological observables such as rainfall which are bounded in one direction but are unlimited in the other (Brooks and Carruthers, 1953). On the other hand, the distributions occasionally exhibited a strong negative skew with respect to the log-normal form. On the basis of the three extended-duration stations, it was concluded that the cube-root normal distribution provides the optimum fit to the data. That is, if we let $y(R) \equiv t^{1/3}(R)$, where $t(R)$ represents the number of minutes in any year that a given rain rate is exceeded, then $y(R)$ will be normally distributed. An explanation of the mechanism giving rise to such a distribution is left as a problem for the physical meteorologist. Its significance here is simply to permit numerical predictions and assessments to be made, relevant to radio-wave propagation conditions within Canada.

Displayed on Gaussian probability paper in Figure 19 is a distribution of yearly cube root exceedance intervals for London, Ontario. The mean value, $\bar{y}(R)$, is simply the 50% probability intercept, while the slope of such a distribution provides a measure of the standard deviation, $\sigma_y(R)$, relative to the mean. Thus, one can derive both the mean and variance for different rainfall rates. This has been done for the stations discussed above(*), and in Figure 20 the ratio $\sigma_y/\bar{y}$ is plotted as a function of the long-term exceedance probability,

---

(*) For purposes of geographical completeness, Figure 20 also contains results for Comox, B.C. for which only 10 years of data were available. Comox receives some 1100 mm of rainfall annually, but only 3.1 days per year with thunder.

$\overline{P(R)}$, for a wide range of rainfall rates. The relative variation in y may then be translated into corresponding variations in real time, t, through the relation

$$\xi \approx \eta^3 + 3\eta^2 + 3\eta \tag{13}$$

where $\eta=\delta y/(\overline{y})$ and $\xi=\delta t/(\overline{t^{1/3}})^3$.

Since y is normally distributed, we may employ standard statistical procedures to predict the degree of variation from the mean likely to occur with a given probability. For example, the probability that a value $\overline{y}+n\sigma_y$ will be exceeded once in N years is

$$p(N) = 0.5x(1-\Phi(n)) \tag{14}$$

where $\Phi(n)$ is the normal probability integral for agrument n. Deviations, of course, are equally likely above and below the mean, so that (14) also expresses the probability of occurrence of a value y less than $\overline{y}-n\sigma_y$.

A numerical example may help to clarify the procedure. Suppose we are interested in rainfall at Halifax having an intensity of 75 mm/h. Figure 57 shows that the average annual exceedance for this rate is approximately 9.5 mins, or $P(R)=1.8x10^{-5}$ yr. For this value of P(R), Figure 20 indicates a relative dispersion $\sigma_y(R)/(\overline{y})=0.38$. Suppose we want to estimate the maximum exceedance occurring one year in five, that is, p(N)=0.20. From equation (14), $\Phi(n)=0.60$, for which n=0.84 (Dwight, 1947). Substituting a value of $\eta=0.84x0.38$ into (13), we find $\xi=1.30$. The maximum expected rainfall exceedence is therefore $t+\delta t = (1+\xi)\overline{t}$ or 2.3 times the long-term average. This value may also be obtained by means of Figure 21 which illustrates, graphically, the relationship between the dispersion, $\sigma_y/\overline{y}$, and the expected range of variation in rainfall probability for various observation periods. We also see from Figure 21 that during another one year out of five, the 75 mm/h rainfall duration at Halifax would fail to reach even one-third of the average value — a total range over five years of some 7.2:1. Over a decade, the ratio of upper to lower limits likely to be surpassed is approximately 24:1. Imagine the consequences of a design relying heavily on observations made during one or two years of relatively low occurrence of heavy rainfall!

Let us now turn our attention to the second question posed at the start of this section, namely, to determining the total length of time needed for reliably stable statistics to hold. If the standard deviation of the annual exceedance times for a rainfall rate R is given by $\sigma_t(R)$, then a set of mean values of N-yearly observations will itself form a distribution about the "true" mean with a standard deviation

$$\sigma_N(R) = \frac{\sigma_t(R)}{\sqrt{N}} \tag{15}$$

In order to obtain an estimate of this deviation from the mean, we may consider as a rough average of the four curves in Figure 20, the following values:

TABLE 3

Average Relative Dispersion of Cube Root of Annual Exceedance Time for Several Rain Probability Levels

Rain Probability Level P(R)	Coefficient of Variation $\sigma_y(R)/(\overline{y})$
$1x10^{-3}$	0.125
$3x10^{-5}$	0.275
$1x10^{-6}$	0.750

For these values, Figure 22 presents the average probability limits about the mean that could be expected for data samples up to 20 years in duration. For events occurring with a probability of approximately $1.0x10^{-3}$ (i.e., 0.1% of year), three years will suffice for a confident estimate to be made of the mean duration to within

20 or 25%. At the 3×10^{-5} probability level (0.003%) the variations are somewhat larger, and a period of between 8 and 15 years would be required before the same 20% deviation from the mean could be assumed (a decade would suffice for 25% accuracy). As we move to the rarest cases ($P=10^{-6}$, or 0.0001%) the accuracy to be expected, from even a 20-year data average, is becoming small. For a 10-year sample, as is the case for most of the stations analyzed in this report, there will be a 2/3 probability that the computed mean exceedance will lie within about ± 80% of the true mean(*).

4.2 INTRA-ANNUAL VARIATION

4.2.1 Worst-Month Conditions

The microwave system designer must frequently take into consideration the fact that propagation conditions are not stable throughout the year and that precipitation attenuation may be far more severe over short periods of time than is indicated by long-term averages. The CCIR has recommended the use of a "worst-month" concept as a means of dealing with this matter. The annual mean condition is generally better known — — or more readily predicted — — than the statistics for shorter intervals. It would be desirable, in the absence of more detailed information, to be able to relate, in a statistical sense, the "worst month" to the long-term average situation.

In several recent publications (Brussaard, 1977; Brussaard and Watson, 1978; Crane and Debrunner, 1978; Morita, 1978), attempts have been made to derive numerical factors to convert annual into worst-month statistics. Detailed intercomparison of the various results and possible application to practical design problems are difficult, however, since the character of intense rain is dependent on geographic location, and the available data have so far been very sparse. The subject is further complicated by the fact that no single definition has been accepted for the term "worst month" (Brussaard and Watson, 1978; CCIR, 1978c). Four of the definitions that have been proposed are discussed below. Many other formulations are possible.

4.2.1.1 The Majorant Distribution Method

Perhaps the most direct approach to the question of monthly extremes is to use the "majorant" of all monthly distributions(**) to define a hypothetical worst month. The use of this definition has been proposed in a submission to the CCIR (1977a). Results of three years' rainfall data taken in Europe suggest that the majorant monthly probability, P(R), of rainfall at a rate R, ranges from about twice the average probability at very low rates (~1 mm/h) to approximately 12 times average for R=100 mm/h. Because this approach deals with absolute extreme values, the majorant distribution will be dependent upon the duration interval for the complete data sample. In fact, if very large samples were involved, then the worst case values could be expected to increase as the logarithm of the number of months under consideration (Gumbel, 1954). Over brief periods, however, extreme values are highly variable and a statistical approach is more likely to prove satisfactory.

Various versions may be considered, each resulting in somewhat different numerical values, even with respect to the same data base. Fundamentally, we may categorize all of these analytical methods according to

---

(*) *Actually, the deviation limits are asymmetrical with respect to positive and negative excursions and are closer to +100%/–60%, in this case.*

(**) *Defined as the greatest monthly probability of exceeding any particular rainfall rate without regard to the situation at any other rate. That is, for a set of k monthly distributions the majorant probability is*

$$P_m(R) = \max \{P_1(R), P_2(R), \ldots P_k(R)\}$$

for all values of R.

whether they consider a) the amount of time that a given meteorological (or propagation) parameter is exceeded, or b) the greatest value of that parameter attained for a specified period of time. The latter category (Brussaard, 1977) has merit in the area of system design, where the maximum allowable outage due to precipitation may be specified in advance. This basic approach has also been suggested by CCIR (1977c). Methods based on category (a) have received greater attention (Crane and Debrunner, 1978; Brussaard and Watson, 1978; Morita, 1978) largely due to the fact that it adapts more readily to electronic data processing of experimental records.

4.2.1.2 The One-Year Return Period Formulation

Crane and Debrunner (1978; CCIR, 1977b) base their "worst month" definition on the monthly exceedance of a specified threshold that exhibits a one-year return period(*).

Let χ_j be the critical value under consideration. In this case, χ represents some observable parameter such as attenuation or rainfall rate, while j corresponds to a particular threshold level, e.g., 35 dB, 60 mm/h, etc. Let x_{ij} be the probability of exceeding the critical value χ_j during any month i, and P_j the cumulative probability that a monthly value will exceed x_{ij}. Gumbel (1958) shows that the asymptotic distribution of extreme values for a large class of natural phenomena is of an exponential form. Thus, for large x_{ij} we may write

$$P_j \sim C_{oj} \exp(-x_{ij}/C_{1j}) \tag{16}$$

For a one-year return period, $P_j = 1/12$, yielding a value of the worst month exceedance probability of

$$x_{wm,j} = C_{1j} \ln(12\, C_{oj}) \tag{17}$$

If we denote the probability density function by

$$p_j(x) = -\frac{dP_j}{dx} \tag{18}$$

then the long-term average monthly occurrence will be

$$x_{y,j} = \int x_{ij}\, p_j(x)\, dx \tag{19}$$

Integrating by parts yields

$$x_{y,j} = C_{oj} C_{1j} \tag{20}$$

so that the ratio of worst-month to annual exceedance from the asymptotic approximation is

$$Q_j = x_{wm,j}/x_{y,j} = \frac{\ln(12C_{oj})}{C_{1j}} \tag{21}$$

This approach was readily applicable to the rainfall data base studied in this investigation. Figure 23 illustrates the behaviour of P_j with respect to x_{ij} for a rainfall rate threshold of 80 mm/h at London, Ontario. The x_{ij} are here expressed in terms of minutes/month rather than as a probability in order to reduce confusion with the ordinate scale. On a logarithmic plot as employed here, the asymptotic approximation takes the form

---

(*) The return period for an event is the time interval corresponding to the reciprocal of its probability. A one-year return period thus implies a monthly probability of occurrence of 1/12.

of a straight line with the vertical and horizontal intercepts yielding the desired values of C_{oj} and C_{1j}. However, since this approximation is valid only over a limited range, there is some error resulting from the use of (21) to compute Q_j; the average exceedance may be either greater or less than that given by (20). Because the records analyzed here have resulted in accurate long-term average values, we may proceed from (17) to obtain the ratio

$$Q_j = C_{1j} \ln(12C_{oj})/\overline{x_{y,j}} \tag{22}$$

This was done for a number of different threshold rain rates at selected stations across Canada. Figure 24 shows the resulting behaviour of Q_j. The values are seen to lie below the limiting value of 4.41 based on (21). The variation of Q_j with respect to R and the range of values for different stations is reminiscent of the results reported by Brussaard (1977) for locations in western Europe. Comox, in particular, appears to exhibit anomalous behaviour, but one must bear in mind that rainfall rates of 50 mm/h and larger are extremely rare on the West coast. Only during two months out of the 10 years of record investigated were even brief instances of rainfall reaching 100 mm/h recorded at Comox.

The worst month exceedance computed in this manner is the value having a return period of one year. This is not to be interpreted, however, as meaning that the value so derived will necessarily be observed in any particular year. In fact, the likelihood that this "worst month" value will be seen in any year depends to a large extent upon the seasonal variation in intense rainfall. Let p_{ij} be the *a priori* probability of exceeding χ_j during each of $N_i \leqslant 12$ calendar months where $i = 1,2 \ldots i_{max} \leqslant 12$ as appropriate, with

$$\sum_i N_i = 12 \tag{23a}$$

and

$$\sum_i p_{ij} N_i = 1 \tag{23b}$$

It can readily be shown that under these conditions, the combined probability of exceeding χ_j during a 12-month interval is

$$p_j = 1 - \prod_i (1 - p_{ij})^{N_i} \tag{24}$$

On the other hand, if intense rainfall were likely to occur with equal probability during any one of N_1 months but had no significant probability of occurrence during the remaining $N_2 = 12 - N_1$ months, then

$$p_{1j} = 1/N_1 \quad , \quad p_{2j} = 0 \tag{25a}$$

and

$$p_j = 1 - (1 - p_{1j})^{N_1,} \tag{25b}$$

The dependence on p_j on N_1 under these idealized conditions is shown in Figure 25.

The second half of this section on intra-annual variability will examine the seasonal variation in rainfall probability. For maritime locations such as Halifax, we may reasonably assume that heavy rain is likely to occur only during seven months of the year; for most of the other locations examined, intense rainfall is restricted to only four or five months. It follows that for most of Canada there would be only a 2/3 probability that the "worst-month" value would occur in any given year. Even at Calgary, which exhibits an extremely peaked seasonal pattern, this probability is only about 75%.

4.2.1.3 The Worst Calendar Month Approach

Morita (1978) has examined the relationship between the "worst month" and annual probability as a function of rainfall rate for six locations in Japan. The worst month, in this case was defined simply as the

calendar month having the greatest average rainfall. Morita perceptively deduced a single power-law relationship for all stations, despite their different meteorological regimes. In terms of absolute rainfall probability rather than percentage time, the Japanese results may be written

$$P_{wm}(R) = 0.483 \times P_{yr}^{0.74}(R) \tag{26}$$

The section dealing with seasonal rainfall patterns presents a summary of data for six Canadian stations which permit precisely this type of relationship to be investigated (see Figures 27b to 32b). These stations represent a fair cross-section of low-latitude Canadian climatic environments.

In Figure 26 we relate the average "worst-month" rainfall probability with the average annual probability at the same rainfall rate for all six locations. Included here are data for rain rates of 0.25, 10, 25, 50, 80 and 100 mm/h at each station. Equation (26) was found not to apply to these Canadian results — — generally overestimating the worst-month condition — — but the form of the relation, viz.,

$$P_{wm}(R) = A \cdot P_{yr}^{B}(R) \tag{27}$$

holds very well, yielding regression coefficients

$$A = 0.73, \quad B = 0.84 \tag{28}$$

These constants would naturally be expected to vary with climatic conditions. A complete study of the geographic dependence of A and B has not been performed; however, A appears to be more strongly linked to differences in location (i.e., climate). For the six stations analyzed here, the relative variation in A was more than 10 times greater than the variation in B. The relatively small change observed in B when going from Japan to Canada also suggests a more subtle climatic dependence for this parameter. Nonetheless, the fact that the functional form (27) holds so well over such a wide range of precipitation rates and for locations separated by many thousands of kilometres, is strongly suggestive of a fundamental relationship in precipitation climatology.

In general, the calendar month exhibiting the greatest rainfall probability is a function of the rainfall rate that is adopted as the threshold level. In preparing Figure 26, that month exhibiting the greatest likelihood of exceeding a 50 mm/h rainfall rate was employed. This corresponds to a moderately intense precipitation event and one which will generally result in propagation difficulties. Because the exponential factor B is less than unity, there is an upper bound to the range over which (27) is valid. This bound occurs when

$$P_{wm}(R) = P_{yr}(R) = 10^{[\log A/(1-B)]} \tag{29}$$

For the values of A and B indicated in (28), this occurs for P(R)=0.137. Beyond this point, we have the apparently absurd situation of the average annual condition being worse than the "worst month", that is $P_{wm}(R) < P_{yr}(R)$. This situation arises because of the above mentioned changes in the rainiest month of the year, especially as we move toward very low rainfall rates. The curves for Comox, B.C. exhibit this phenomenon most dramatically (see Figure 32b), since the "worst month" at the 25 mm/h or 50 mm/h rate becomes the "best month" when judged by the 0.25 mm/h condition.

4.2.1.4 The Worst Annual Occurrence Method

Brussaard and Watson (1978) used a different formulation to analyze microwave radiometer observations from 8 sites in Western Europe. The results of only 19 station-years of pooled data were presented, with a range of cumulative probability levels of little more than 1-1/2 decades (cf. Figure 26). Their approach closely parallels the one considered in 4.2.1.3, above. Instead of the worst calendar month, however, these authors consider the average of the worst monthly condition occurring in the course of each calendar year. Like the procedure described in Section 4.2.1.1, and in constrast to the method of 4.2.1.2, this approach includes in the

averaging process not only those events corresponding to a 1-year return period, but also to the 2-year, 3-year, ... N-year expectation values. It is not surprising therefore, that the ratio of "worst month" to yearly average by this means is greater than that obtained using the method of 4.2.1.2.

This difference in the numerical value of Q_j is merely a consequence of having adopted an alternate definition of the "worst month", and brings into focus the need for a clear understanding of what is implied by a "worst-case" statistic. We have already seen that approach 4.2.1.2 yields the "worst month" condition having a one-year "expectation value". Over the long term, this condition will be equalled or exceeded, on average, every 12 months. We have also noted, that despite this expectation, the likelihood is only 65% to 75% that it will be satisfied in any particular year.

In the present section, we are dealing with averages rather than expectation values, so that the "worst month" does not relate immediately to the condition likely to occur during any one year. This definition is perhaps best suited to the type of situation considered by Brussaard and Watson (1978), viz., the averaging of data for a large number of propagation circuits operating simultaneously, under climatically identical conditions. For a single link, it represents the average of many years' propagation conditions and tells us little about any specific year.

Unless the ultimate in link reliability over a statistically long period is demanded, then the technique described in 4.2.1.1 is not relevant. The return-period approach, represents an attractive methodology, but the numerical factor relating "worst month" to annual conditions exhibits a complex behaviour with respect to location and rainfall intensity. Failing a more precise description of the nature of this variation, then seasonal averages such as described in 4.2.1.3, or in the immediately following segment, may represent a reasonable and acceptable approach to the problem of temporal variability and system design.

4.2.2 Seasonal and Diurnal Characteristics

The design reliability levels of a radio relay system are established on the basis of a complex compromise between service requirements, availability of sites and equipment, precedence, and economics. Due in part to the sparse nature of the radio-climatological data that are normally available, design has traditionally been based on long-term average conditions. Because of the intensity of the various climatic cycles that exist, it is important to investigate precipitation trends that may occur within the annual period. In some regions of the country severe rainfall is restricted to only a few months of the year. The performance of a microwave system in a location of this sort would likely be considerably worse than anticipated for certain months of the year, while still meeting the design performance on an annual basis. If a system is to provide consistent, year-round reliability, even on a statistical basis, it must be governed by conditions during the worst period of the year. Figures 27(b) to 32(b) illustrate the mean seasonal variation in rainfall probability at six locations, fairly evenly spaced across the country. Except for Comox, B.C., each graph shows the statistical variation in rainfall of 50 mm/h and 100 mm/h intensities as well as the overall probability regardless of intensity level. At Comox, where the orographically-induced rainfall is of generally lower intensity than elsewhere, the corresponding curves are at the 25 mm/h and 50 mm/h levels. While intense rain is generally seen to be 3 to 5 times more prevalent than average during peak calendar months, the distribution is even more non-uniform in western Canada. Table 4 summarizes these results in greater detail.

In addition to illustrating the variations in rainfall that occur on a seasonal basis, Figures 27 to 32 also display the ways in which the statistical occurrence of rain might be expected to change diurnally. For some applications, such variation may be of no consequence. It is not too difficult, however, to conceive of situations in which it would have some import. In the transmission of TV programming material along microwave links, for example, it might be of interest to know whether severe rain storms are likely to occur during peak viewing hours with significantly higher than normal probability. Conversely, during heavy rainfall seasons (as indicated by the high rainfall rate curves of Figures 27(b) to 32(b)), it might be possible to schedule services to take advantage of the fact that in some regions of the country there are periods during the day that remain statistically dry. In summarizing these diurnal patterns, Table 4 shows that the range of variation, averaged over two-hour intervals, may be several orders of magnitude.

TABLE 4

Summary of Seasonal and Diurnal Variation in Intense Rainfall at Selected Locations Across Canada

Location	Diurnal Behaviour	Seasonal Characteristics
Halifax	Essentially constant. Slight variation with 3 cycles/day. Ratio of maximum to minimum 2–hr rainfall probability approximately 4:1.	A maximum in heavy rains follows the minimum during Winter and early Spring. Ratio of intense monthly rainfall probabilities ~45:1, ranging from approx. 2.6 to 0.06 times annual average.
Montreal	Total rainfall probability nearly constant. Broad minimum in intense rainfall probability is followed by a sharp peak between 14–16 hrs. Ratio of 2–hr max to min probabilities is approximately 25:1, ranging from more than four times average to less than 1/6 average!	Very pronounced maximum in intense rainfall probability during Summer and early Autumn. Probability of heavy rainfall during August is 4.9 times annual average. Almost negligible incidence of intense rain October to April, inclusive.
Sault Ste. Marie	A semi-diurnal pattern with minima between 04–12 hrs and 18–22 hrs. The overall ratio of max/min 2–hr probabilities is only ~4:1.	Heavy rains occur from late Spring through Summer, decaying during October. Average probability of intense rain for May to September, inclusive is 2.5 times annual, while for June only, it is 3.7 times the annual average.
Winnipeg	Pattern suggests onset of an 8–hour periodicity (becoming very clear at Regina). Only slight variation throughout day with 6.5:1 ratio of maximum to minimum probability at the 100 mm/h rain rate.	Heavy rainfall takes place during late Spring and Summer, as at Sault Ste. Marie, with even sharper cutoff for remaining months. Probability of intense rain during July and August is equal to 3.5 times annual average.
Calgary	The 3–cycle per day pattern is now extremely pronounced. During the 10–year period studied, no case of rainfall exceeding 50 mm/hr was ever detected between 10–12 hrs! Ignoring this interval, diurnal variation still covers two orders of magnitude. The overall probability of rain remains remarkably constant, considering. (The variation becomes even greater at Edmonton, with the null now appearing between 08 and 10 hrs.)	Occurrence of rain severely restricted. Intense rainfall confined entirely to June, July and August with probability during peak month equal to 7.4 times value averaged over the entire year!
Comox	Typically heavy maritime precipitation, but orographically-influenced rainfall generally much less intense than on East coast. A null in heavy rainfall observed for 00–02 hrs period. Diurnal pattern shows large fluctuations not evident on East coast. Variation of 10 or 20:1 between successive two hour periods.	Seasonal patterns show interesting, inverse correlation between the probability of having any rain during a given month, and the probability of heavy rain. For the first five months of the year, probability of rainfall >25 mm/hr less than 1/5 annual average. Virtually no rain >50 mm/hr during February to June. July and August only months during which significant precip attenuation is likely. Contrasts sharply with situation on East coast where intense rain probability was above average for six months and less than average for another six.

4.3 CLIMATIC TRENDS

Recent years have seen a growing interest and concern over the nature of possible changes in world climate in the coming decades. While this topic extends far beyond the bounds of this report, it behoves us to consider whether the data so carefully assembled and analyzed might prove to be more of historical than of current interest. Among the various theories and predictions of climatic change, we find the suggestion of global warming due to increased atmospheric levels of carbon dioxide, alongside predictions of net cooling as a result of the scattering of incoming solar radiation by increased atmospheric dust concentration. Others predict reduced solar output due to long-period oscillations in sunspot activity. It is perhaps not too surprising that predictions for the next half century range over a wide spectrum (Miles, 1978).

Disregarding future predictions for the moment, what information can be derived from past records? Climate is highly variable; attempts at extracting weak, incipient trends from the accompanying "noise" is fraught with considerable risk. It is only by gauging the consistency of trends prevailing among many stations that meaningful conclusions can be reached. Thomas (1975) has surveyed the climatic records of a sampling of stations in Canada for the 35 year period starting with 1940. Except for the Pacific coast where the variation is difficult to interpret clearly, the general trend across Canada since the mid 1950s has been clearly towards lower temperatures. On a national basis the decrease averaged slightly less than 0.5°C. This trend is in reasonable agreement with the observed drop in temperatures over the entire Northern Hemisphere since about 1940. (This follows an overall increase that had been in progress since the first half of the 19th century).

Changes in global temperatures might be expected to produce, indirectly, changes in the precipitation climate (for example through changes in atmospheric moisture or circulation patterns). Thomas (ibid) also summarized precipitation records for a number of stations for periods ranging from 25 to 35 years. Bearing in mind that these records include frozen as well as liquid precipitation and further, that we are primarily interested in the intense rainfall component, the significance of any observed precipitation trend would be diminished accordingly. The observed changes in precipitation climate, however, are far less conclusive than the temperature trends. Small increases in precipitation recorded in eastern Canada and the western Arctic since 1950 are not in harmony with the behaviour in the central and western provinces, where various trends that had been observed during 1950s have been reversed during the 60s and early 70s. Neither does the year to year variability in total recorded precipitation reveal any significant trend during the past 35 years. It would therefore appear safe to conclude that regardless of the direction of the overall temperature trends during the next few decades, its effect on the intense rainfall climatology as presented here is likely to be of minor significance.

5. RAINFALL REGIMES

5.1 GLOBAL CLASSIFICATIONS

The earliest attempts by geographers at systematically classifying the world into climatic zones were based on the long-term averages of temperature and total precipitation. Agricultural crops and naturally occurring vegetation represent both vital economic factors and readily recognized identifiers of the trends in both temperature and precipitation. Accordingly, these identifiers have strongly influenced the identification of different climatic regions and the selection of zonal boundaries. Since more detailed rainfall data have been largely unavailable until now, this approach has dominated the many climatic classification schemes developed over more than half a century. Thus, the boundaries between the rainfall climatic regions adopted by the CCIR (1975) for propagation modelling generally resembled those of earlier schemes, employing only five distinct classifications to cover the entire world land mass.

Barry and Chorley (1971) modified these climatic regions for the North American continent. The zones and boundaries in this case were based largely on the different seasonal precipitation patterns. A total of 10

zones was employed for all of North America, while six regions were required to cover Canada. The National Atlas of Canada (Fremlin, 1974) divided the country in similar fashion, but by employing more detailed Canadian meteorological data it was able to identify 11 distinct precipitation regions across the country.

A recent submission to the CCIR (1978b) offers a more refined set of rainfall climate classifications. But while the objective is to identify global rainfall rate regimes, the different zones were nonetheless selected on the basis of other climatological criteria. Average rain rate distributions were then assigned to the various zones. This was done using the Rice-Holmberg (1973) prediction model and modified, where necessary, on the basis of whatever experimental data were available. Although a total of 8 global rainfall regimes were now recognized, only four suffice to classify all of Canada. These are illustrated in Figure 33; the cumulative distributions corresponding to these zones appear in Figure 34. The variation in rainfall behaviour within a given region is claimed to be bounded by the distribution curves for the adjacent regions. Even if this were so, the designer would be left with a very large uncertainty to contend with. At the 10^{-5} probability level for example, the range of rainfall rates for zone C (i.e., between curves B and D) is approximately ±30%. For zone B the acceptable range would be ±50%, while for zone A it is of the order of 100%. What is perhaps more important, for a given rain rate (corresponding to a fixed propagation fade level), the range of probabilities within a given zone is generally more than an order of magnitude.

Despite this large spread, the proposed regional distributions generally fail to encompass the complete range of variation observed over the large areas involved. Curve 'A' (Polar Tundra) of Figure 34, for example, significantly overestimates the rainfall rate probabilities in the high Arctic, while grossly underestimating others in Newfoundland. Similarly, for locations in Region 'B' (Polar Taiga), the actual spread in rainfall probability greatly exceeds the suggested range. (Compare, for example, the distributions for Carmacks, Figure 46, with that for Halifax, Figure 57). Of equal importance, the scheme, as delineated in Figure 33, overlooks the semi-desert conditions prevailing at locations along the Interior System of the western Cordilleran Region (see distribution for Summerland, B.C., Figure 78).

In addition, a careful comparison between the distributions deduced for the various Canadian locations and the CCIR (1975, 1978b) curves reveals not only that the latter inadequately predict specific rainfall probabilities, but that they frequently do not exhibit the proper variation with respect to rain intensity. In view of the vastness of the area covered and the limited amount of rain rate data incorporated into these models, it is not surprising that such discrepancies should exist. In view of the unique data base available here, however, it would clearly be appropriate to attempt a description of the Canadian rain climate based directly on the rainfall rate distributions themselves.

5.2 RAINFALL-RATE MODEL FOR CANADA

As the various precipitation generating processes combine differently in different areas, so also might the ratio of light to heavy rainfall be expected to vary. A complete description of the rainfall climate would thus require a minimum of two more-or-less independent parameters; at least one to depict the shape or spectrum of the distribution, and another to specify its magnitude. Rice and Holmberg (1973) first recognized the need for more than one parameter to characterize global rainfall climates. In their work they divided (conceptually) the range of rainfall intensities into heavy (classified as thunderstorm rain) and light (non-thunderstorm) segments with exponential type functions to approximate each. The two parameters required to uniquely designate a distribution in this scheme were β, which expressed the fraction of total rain accumulation due to thunderstorm type activity and M, the total annual rainfall. After converting a large amount of available data into equivalent clock-minute rain rates, they derived world-wide contours of M and β.

A complete description of the various mathematical models that have been proposed for fitting rainfall rate distributions is beyond the scope of this document. Suffice to say that all of these various expressions provide a reasonable fit to the majority of distributions, particularly if these include a limited range of intensities, a relatively brief period (statistically) and/or a low time resolution. The present work is perhaps unique in the amount of data analyzed: in the number of stations investigated as well as the length of record

at these stations which could be analyzed with high resolution. It was therefore possible to carefully examine how various mathematical models might be fitted to these data. The distributions to be presented in Figures 43 to 89 are based on a 60-second minimum sampling interval. Section 7 discusses the way in which the rainfall rate probabilities appear to vary with changes in resolution time. When the data for all 47 stations were analyzed with no additional integration imposed (i.e., with the ultimate resolution contained in the tipping-bucket records as digitized), it was found, without exception, that a power law relationship of the form

$$P = P_0 \cdot (R/R_0)^{\gamma} \tag{30}$$

provided the best fit except in the very low-intensity (drizzle) region. The quantity R_0 in expression (30) is a suitable reference rain rate and $P_0 \equiv P(R_0)$ is the probability of exceeding R_0. The fit provided by (30) was generally excellent for R greater than about 2 or 3 mm/h. One example of such a power law fit is shown in Figure 35. The excellence of the approximation in this example is typical; in many instances the approximating line virtually obscures the data curve. Figure 35 also shows a log-normal approximation to the same distribution.

The parameters P_0 and γ may thus be used to define accurately the high-resolution rainfall distributions above about 2.5 mm/h. Figures 36 and 37 illustrate the way in which these parameters vary throughout the country for $R_0=100$ mm/h. The dashed lines in the central and western portions of British Columbia are indicative of the uncertainty and rapid variation in precipitation characteristics in the mountainous region. To a first approximation, the isopleths of these parameters would lie parallel to successive mountain ridges and valleys. Table 5 lists the values of P_0 and γ for all of the stations situated in B.C. The problem of interpolating rainfall data in Western Canada recurs in the section on Terrain Effects in the following section.

6. PRECIPITATION-MODIFYING INFLUENCES

In Figures 43 to 89, the complementary distribution functions are presented for 47 fixed locations across the country. Inasmuch as the user will frequently be called upon to consider locations more or less removed from those studied, it is important to look into some of the problems that are involved in extrapolating rainfall data from one site to another. The parametric representation of the rainfall climate for different regions is the first step in establishing a rational basis for interpolating or extending data to new locations. Frequently, however, there are forces acting that severely distort the precipitation pattern within relatively short distances. Little attention appears to have been paid to this problem, particularly within the context of radio system design. As a result, there are few data in appropriate form and little guidance as to

TABLE 5

Values of the Parameters P_0 and γ for Stations Situated in British Columbia and Yukon Territory

STATION	P_0	γ
CARMACKS	6.03×10^{-7}	−2.110
COMOX	4.66×10^{-7}	−2.720
HOPE	2.76×10^{-7}	−3.045
MISSION	1.90×10^{-6}	−2.400
PRINCE GEORGE	2.85×10^{-6}	−1.875
SUMMERLAND	3.29×10^{-7}	−2.290
VANCOUVER	4.82×10^{-7}	−2.713

how best to proceed. The immediately following sections examine several of the more significant areas with a view to providing a qualitative awareness of these factors and also some broad quantitative guidelines as to their importance. As additional climatological and propagation data become available, a more accurate assessment of these items will be possible.

6.1 TERRAIN EFFECTS

In section 2.2.1, dealing with data base errors, we discussed briefly the influence of rain gauge location relative to wind-shielding hills and of elevation with respect to earth's surface on the rainfall catch efficiency. Of equal or greater importance in many instances is the dependence of rainfall on the variation in altitude of the terrain itself, i.e., on topographic factors. Because air cools adiabatically when it is forced to rise (by approximately 0.65°C/100m for saturated air), major terrain irregularities tend to be reflected in differences in the total rainfall received. In some instances, the influence of orographic features is manifest up to several hundred kilometres downstream from its inception.

In Canada, the major topographic effects, quite naturally, take place in the western cordillera region. Figure 38 shows the overall trend in total precipitation along an East-West "slice" through southern British Columbia. The general correlation that exists with respect to altitude is evident. (Although the amount of recorded precipitation falls dramatically as we pass over the plateau east of the Fraser River, the rainfall pattern continues to reflect the general topographic contour). Fairbridge (1967) shows a very similar example of orographic control of precipitation in Europe along a section through Switzerland and Northern Italy. Since all six of the British Columbia stations for which data are presented in this report are situated at relatively low altitudes, one must proceed cautiously when attempting to extrapolate conditions to higher-elevation sites.

The predominantly North-South alignment of the western mountain ranges together with the prevailing westerly air flow result in a precipitation pattern that varies primarily in the East-West direction. Major precipitation trends, however, can and do take place at other orientations as well. Figure 39 illustrates the variation in total annual precipitation observed at stations situated along a narrow strip on the 123°W meridian and extending a total of 50 kilometres from Delta, B.C. through Burnaby to North Vancouver. There is a 4:1 ratio in total precipitation over this distance with 50% of this variation occurring in the final 15 km alone. Vancouver International Airport is the closest station for which detailed rainfall data are presented in this report. The mean annual rainfall accumulation at this station is 1018 mm. Annual rainfall statistics for other locations in the vicinity can be obtained from climatological publications such as those of the Atmospheric Environment Service (AES, 1975) or the British Columbia Department of Agriculture (Anon., 1976). The approach suggested here is to estimate the distributions for these locations by multiplying the Vancouver probability corresponding to any particular rainfall rate by the ratio of total rainfall for that location to the Vancouver value. The assumption implicit in this procedure is that the "shape factor" (as discussed in section 5.2 dealing with rainfall rate models) for the rainfall distribution function does not change over short distances as a result of orographic effects alone. This is consistent with the observation that convective rainfall is not appreciably intensified by orographic lifting but that the duration of intense rain events is prolonged (Sporns, 1964).

While the general trends in average precipitation values resemble the corresponding topographic contours the reader is cautioned against using altitude alone as an interpolation parameter in any detailed numerical application. In Figure 39 for example, the maximum rainfall occurs at the northern extremity of the chart. Some 8 km to the south of this point, at an elevation more than 600 m greater, the annual rainfall is only 74% of the maximum. Spreen (1947) has shown that the slope of the terrain in the vicinity of a given site, the absence of sizeable barriers within a 30 km radius and the direction of greatest freedom from obstruction are all vital for accurate correlation of precipitation in mountainous regions.

Although the orographic influence on precipitation in the western provinces is dramatically evident, the uplift produced by air flowing over much more modest hills and terrain irregularities may result in locally significant changes in rainfall statistics. Bellon and Austin (1978) have studied in detail the precipitation

climatology within a 200 km radius of the McGill University weather radar. Situated at Ste. Anne de Bellevue, Quebec, the radar coverage area includes the confluence of the Ottawa and St. Lawrence Rivers. With the Laurentian, the Gatineau and the Adirondack Mountains additionally cut by numerous lakes and smaller river valleys, the area contains many distinct, small-scale topographic features. Although these might justifiably be considered slight by comparison with the major orographic structures in the West, areas were found where the rainfall intensity is statistically augmented or diminished. Furthermore, these areas were found to be associated with changes in local terrain. This association was sufficiently secure as to result in a significant improvement in the reliability of local weather prediction services.

As an interesting extension to these instances of terrain-influenced precipitation effects, it should be noted that Bergeron (1960) has shown that under certain circumstances, topographic irregularities are unnecessary. The banded rainfall pattern observed in the flat, coastal region of Holland suggest atmospheric waves set up as a result of differences in friction at the boundary layers above land and above water surfaces, respectively. Over a distance of 75 km, a variation in total rainfall of 5:1 was noted with changes of 2:1 occurring within the space of only a few kilometres (Crowe, 1971).

6.2 ANTHROPOGENIC EFFECTS

6.2.1 Urban Influences

Man's continued activities on Earth serve, both directly and indirectly, to modify the climatic environment in which we live. These changes occur on several geographic scales which we may describe as global, urban or metropolitan, and local. (Perhaps the most profound changes of all are the microscale effects that take place close to the earth's surface. These, however, are outside the range of our present concerns). The overall influences on the weather of such activities as the consumption of fossil fuels, the deforestation of extended regions of the globe and the tilling of soil are long-term in nature. They tend to merge with the natural trends that are occurring, and thus form part of the general background climatology observed over areas of continental or global magnitude.

Weather modification that is more readily evident and identifiable over a smaller scale is sometimes referred to as being anthropogenic, thus reflecting its human (although generally inadvertent) origin. It has long been known, for example, that the large metropolitan conglomeration exerts a profound modifying influence upon the surrounding atmosphere (Landsberg, 1956). The general increase in temperature and atmospheric turbidity together with changes in air turbulence, wind and water vapour are all components of what is commonly referred to as the urban "heat island". Recent studies indicate, as well, that the nature of the precipitation climate is modified as a consequence of urban activity (Harnack and Landsberg, 1975). Detwiller and Chagnon (1976) have studied the records of precipitation measurements spanning 80–100 years at St. Louis, Missouri; Chicago, Illinois; and Paris, France. Over this long time interval, they noted increases of 19–38% in the summertime maximum daily precipitation. While these increases in themselves represent a very small rate of growth (averaging only 1/4% to 1/3% per year when compounded over the entire period), they do indicate, at least partially, the consequences of growth in urbanization and/or industrial development — — conditions that are far more prevalent today than ever before and likely to continue accelerating.

Atkinson (1969) investigated the rainfall yield during thunderstorm showers and found this to be approximately 30% greater within metropolitan London (England) than in the countryside. Landsberg (1970) suggests that a bias of perhaps 10% is closer to reality in the majority of cases. While a simple comparison of rainfall accumulations at different locations without adequate statistical and meteorological analyses is open to serious criticism, it is nonetheless interesting to observe, in passing, a few of the climatological records for major Canadian metropolitan areas. Thus, we note that the long-term annual rainfall recorded at the Montreal International Airport, southwest (i.e., predominantly upwind) of the city, is 707 mm compared with 757 mm at the McGill University observatory, close to the commercial centre of the city. While farther east, at the Botanical Gardens, nestled peacefully between the industrial core and the oil refineries, an average annual rainfall of 785 mm is recorded, 11% greater than at the airport less than 20 km away. Similarly, at Toronto,

the annual rainfall in the Downsview-Glenview area averages approximately 665 mm or nearly 8% greater than the 622 mm recorded at the International Airport, some 20 km to the west.

6.2.2 Industrial Influences

In related investigations that are of more serious concern to the radio meteorologist and systems designer, Chagnon (1968) studied the patterns of precipitation values, thunderstorm occurrence, etc. that have taken place over 40 years in the Chicago area. The analysis of records at 30 weather stations in the area led to the unexpected discovery that the maximum in warm season precipitation took place not within the core of the urban area (i.e., within the "heat island" itself) but at a location some 55 km downwind from the major industrial complex surrounding Hammond and Gary, Indiana. Increases in annaul precipitation of up to 30% compared with neighbouring regions, with a 38% increase in frequency of occurrence of thunderstorms were observed. The pattern of changing precipitation correlated reasonably well with the atmospheric pollution index at Chicago. Huff and Chagnon (1972) and Semonin and Chagon (1974) have noted similar, though less pronounced, effects downwind of the city of St. Louis, lending support to their conclusion that the phenonmenon is an example of inadvertent weather modification. (In this case, increases of only 8–10% in summer rainfall were recorded, being confined predominantly to distances of 15–40 km downwind from the industrial centre). Although the complex interaction of factors giving rise to the increased precipitation is not fully understood, it is likely that thermal updrafts combined with many of the common industrial effluents serve to increase the development of larger rain cells, and to increase the convective instability leading, subsequently, to more intense rainfall.

In a study highly pertinent to the Canadian situation, Hobbs, et al. (1970) investigated the concentration of cloud condensation nuclei(*) and annual precipitation throughout Washington State and southern British Columbia during the 37 year period, 1929–1966. The observed changes were attributed to the large growth in size and number of industrial smelters and pulp and paper mills in the region during the post war period. Over so large an area, it was possible to clearly identify industrial effects well removed from any competing urban influences. Pulp mills are prolific generators of CCN. They also emit copious amounts of heat and water vapour, thus providing the major essentials for cloud formation; in some instances, isolated precipitating clouds were observed to originate directly with industrial smoke plumes. Two of the three areas experiencing the greatest rainfall increases in this study were situated in Canada. The first was located north of Victoria, B.C., and had a mean annual precipitation over the 20 year period 1947–1966 more than 30% greater than for the preceding two decades. The causative factors in this case were unclear due to the proximity of the city itself. The most statistically significant increase in precipitation for the entire region, however, took place approximately 45 km up the Columbia-Kootenay valley (i.e., downwind) from the large metal smelters at Trail, B.C.

Warren (1968) and Allee (1970), on the other hand, have shown that the injection of extremely high levels of CCN may serve to increase cloud stability and actually reduce precipitation (by increasing the number of small droplets and thus limiting the number drops of precipitable size). The overall effects may thus prove to be self-limiting to a certain extent.

Regardless of the processes involved, however, the observed magnitude of these inadvertent, man-made changes to the precipitation climate are large enough to serve as a caution when extending the statistics contained in this report to large urban or industrial areas. The widespread experiences outlined in this section would suggest an increase in overall rainfall probability of 5% to 10% when applying data from suburban or rural areas to nearby metropolitan centres. A 20% to 30% increase in assumed precipitation rate probabilities appears to be reasonable for sites located several tens of kilometres downwind of those industrial activities producing large quantities of CCN. (It should be noted in this regard that the particulate effluent of oil refineries is largely non-hygroscopic and thus is not an efficient precipitation producing agent).

(*) Cloud condensation nuclei, or CCN, are hygroscopic particles in the atmosphere that serve as centres of preferred rain drop growth within a cloud.

7. RAINFALL RATE DISTRIBUTIONS

The preceding sections have described, in some detail, the nature of the precipitation data used in the course of this investigation and the methods employed in their analysis. They have also presented various observations regarding the spatial and temporal characteristics of intense rain for different parts of the country. In addition, an effort has been made to discuss the various instrumental errors and uncertainties, as well as the geographic and man-made influences that serve to distort real-life climatology from simple statistical averages. It is hoped that these discussions will serve to extend the usefulness of this monograph beyond that of a mere set of statistical distributions.

In the final 47 pages of this document, the rainfall rate exceedance probabilities are presented for locations across Canada in the same order (i.e., alphabetical) as they appear in Table 1. To adequately permit examination of the all-important probability regime below 10^{-4} or 10^{-5}, the distributions in Figures 43 to 89 have been limited to covering only the range 10–300 mm/h, although the statistics have been computed for the larger range 0.25 mm/h to 1000 mm/h. Of course, the cumulative probabilities continue to increase below the 10 mm/h cutoff; however, on a log-log plot as employed here, the gradients gradually decrease, as was seen in Figure 35.

Most of the rainfall statistics and attenuation models published recently are based on one minute or longer sampling intervals (e.g., Sims and Jones, 1973). An effective integration time of one minute was therefore employed in deriving the present curves. However, since rain is a time-varying phenomenon (recall Figure 15) any temporal integration of the data, whether inherent in the instrumentation or analytically imposed, will influence the resultant distributions and eliminate information regarding events of briefer duration than the basic resolution period. In one study employing an experimental, rapid-response rain gauge, Bodmann and Ruthroff (1974) presented results of two years' observation at a site in New Jersey. Cumulative rain rate distributions for this location were compared for integration times ranging from 1.5 seconds to two minutes.

The present data base permitted a limited study of the effects of integration time on the resultant distributions. Figure 40 shows the intrinsic relationship between the time required to fill one of the rain gauge buckets (i.e., the minimum time per tip) and the rainfall rate. We see, for example, that it is impossible even in theory, to observe and determine a rain rate of 100 mm/h in less than ϵ_1=0.15 minutes (9 sec) using the present tipping-bucket rain gauge data. Beyond this fundamental limitation we were able, in this study, to synthesize any desired integration time. Figure 41 shows how the computed distribution for Kingston, Ontario, changes progressively as this integration time, ϵ_2, is changed.

The effect we are looking at here is not one of gauge sensitivity or accuracy; those are accounted for by suitable instrument calibration. Rather, we are looking at one aspect of the rainfall intensity-duration relationship for this location. In general, the more intense the rainfall event, the more likely it is to occur for only a very brief period, and thus to lose its identity when ϵ_2 is large. If P_t represents the cumulative rainfall probability for ϵ_2=t and P_0 the "instantaneous" probability for ϵ_2=0, then there will be an apparent error due to the finite integration time, of

$$\text{err}(\%) = 100\text{x}(^{P}t/P_0 - 1) \tag{31}$$

Unfortunately, the ratio of rainfall exceedance probability for different values of ϵ_2 does not vary smoothly for the large values of R that are of interest, due to the diminishing number of samples in even a 10-year data base. Furthermore, the behaviour was found to vary considerably from one location to another. In Figure 42, the form of this integration-time error is shown for different values of ϵ_2 for two sites, one typical of the west coast maritime climate and the other representing the heavy rainfall region of eastern Canada. At Comox, where very heavy rainfall rates are exceedingly rare, the duration times are very small. Less than 40% of the sparse rainfall at 100 mm/h is likely to last one full minute, while at Kingston, 70% of these events exceed one minute in duration. Because of the large fluctuations that occur in the ratio P_t/P_0 at the higher rain rates, these curves are merely indicative of the trends that take place. Where statistics of short duration rain events are required for design purposes, it is recommended that the parameters of the power-law rainfall model presented in Figures 36 and 37 be employed.

8. REFERENCES

AES, *Canadian Normals,* **Vol. 2-SI**, Precipitation 1941–1970, Fisheries and Environment Canada, Downsview, (1975).

Allee, P.A., *Air Pollution and the Cloud Droplet Condensation Nuclei Concentration*, Second Conference on Weather Modification, (Santa Barbara), Preprint Volume, American Geophysical Union, Boston, (1970).

Altman, F.J., *Storm Cell Models from Digital Radar Data*, in: Propagation of Radio Waves at Frequencies above 10 GHz, IEE Conference Publication No. 98, London, (1973).

Anon., *Climate of British Columbia*, British Columbia Ministry of Agriculture, Victoria, (1976).

Atkinson, B.W., *A Further Examination of the Urban Maximum of Thunder Rainfall in London*, 1951–1960, Publication No. 48, Inst. Brit. Geogr., London, (1969).

Austin, P.M., *Spatial Characteristics of Precipitation on the Subsynoptic Scale*, Proceedings of IUCRM Colloquium on Fine Scale Structure of Precipitation and EM Propagation (Nice), Centre National d'Etudes des Telecommunications, Issy-les-Moulineaux, (Oct. 1973).

Austin, P.M. and R.A. Houze, Jr., *Analysis of Precipitation Patterns in New England*, J. Appl. Meteor., 11, 926–935, (Sept. 1972).

Barry, R.G. and R.J. Chorley, *Atmosphere, Weather and Climate*, Second Edition, Methuen & Co., Ltd., London, (1971).

Bellon, A. and G.L. Austin, *The Real-Time Test and Evaluation of a Short Term Precipitation Forecasting Procedure*, Proceedings of the 18th Conference on Radar Meteorology (Atlanta), American Meteorological Society, Boston, (1978).

Bergeron, T., *Problems and Methods of Rainfall Investigation*, in: Physics of Precipitation, H. Weickmann, editor, Geophysics Monograph No. 5, American Geophysical Union, Washington, (1960).

Black, R.F., *Precipitation at Barrow, Alaska, Greater than Recorded*, Trans. A.G.U., 35, 203–206, (April 1954).

Bodtmann, W.F. and C.L. Ruthroff, *Rain Attenuation on Short Radio Paths: Theory, Experiment, and Design*, Bell Syst. Tech. J., 53, 1329–1349, (Sept. 1974).

Bourke, R.S., *M.S.C. Tipping Bucket Rain Gauge*, (Unpublished Report), I/C Calibration Laboratory, AES, Downsview, (Dec. 1963).

Bourke, R.S., *Redesign of Anemograph Cam*, Report on Project 8092, (Unpublished), I/C Calibration Lab, AES, Downsview, (Jan. 1973).

Brooks, C.E.P. and N. Carruthers, *Handbook of Statistical Methods in Meteorology*, Her Majesty's Stationery Office, London, (1953).

Browning, K.A., M.E. Hardman, T.W. Harrold and C.W. Pardoe, *The Structure of Rain Bands Within a Mid-Latitude Depression*, Quart. J. Roy. Meteor, Soc., 99, 215–231, (1973).

Bruce, J.P. and R.H. Clark, *Introduction to Hydrometeorology*, Pergamon Press, Oxford, (1960).

Brussaard, G., *Rain Attenuation on Satellite-Earth Paths at 11.4 and 14 GHz*, Ann. Telecomm., 32, 514–518, (Nov.–Dec. 1977).

Brussaard, G. and P.A. Watson, *Annual and Annual-Worst-Month Statistics of Fading on Earth Satellite Paths at 11.5 GHz*, Electron. Lett., 14, 278–280, (Apr. 1978).

Byers, H.R., *Elements of Cloud Physics*, University of Chicago Press, Chicago, (1965).

CCIR, *Radiometeorological Data*, Report 563, 13th Plenary Assembly (Geneva, 1974), International Telecommunications Union, Geneva, (1975).

CCIR, *Rain Data for the Prediction of the Attenuation Statistics in the Most Unfavourable Month*, Document 5/230-E, [1974–1978], International Telecommunications Union, Geneva, (July 1977a).

CCIR, *Worst-Month Statistics*, Document 5/302-E, (Switzerland),[1974–1978], International Telecommunications Union, Geneva, (Sept. 1977b).

CCIR, *Draft Reply From Study Group 4 to the Chairman of Study Group 5 With Respect to the Definition of the term "Worst Month"*, Document 4/388-E, [1974–1978], International Telecommunications Union, Geneva, (October, 1977c).

CCIR, *Radiometeorological Data*, Report 563-1. 14th Plenary Assembly (Kyoto), International Telecommunications Union, Geneva, (1978a).

CCIR, *Rain Attenuation Prediction*, Document P/105-E, Special Preparatory Meeting, International Telecommunications Union, Geneva, (1978b).

CCIR, *Relationship Between Point Rain Rate Distribution in the Worst-Month and that in the Year*, Document P/259-E, Special Preparatory Meeting, International Telecommunications Union, Geneva, (1978c).

Chagnon, S.A., Jr., *The Laporte Weather Anomaly – Fact or Fiction*, Bull. Amer. Meteor. Soc., 49, 4–11, (Jan. 1968).

Chapman, J.D., D.B. Turner, A.L. Farley, and R.I. Ruggles, Editors, *British Columbia Atlas of Resources*, First Edition, B.C. Natural Resources Conference, Vancouver, (1956).

Chen, W.Y.S., *A Simple Method for Estimating Five-Minute Point Rain-Rate Distributions Based on Available Climatological Data*, Bell Syst. Tech. J., 55, 129–134, (Jan. 1976).

Crane, R.K. and W.E. Debrunner, *Worst Month Statistics*, Electron. Lett., 14, 38–40, (Jan. 1978).

Crowe, P.R., *Concepts in Climatology*, St. Martin's Press, New York, (1971).

Detwiller, J. and S.A. Chagnon, Jr., *Possible Urban Effects on Maximum Daily Rainfall at Paris, St. Louis and Chicago*, J. Appl. Meteor., 15, 517–519, (May 1976).

Dwight, H.B., *Tables of Integrals and Other Mathematical Data*, The Macmillan Co., New York, (1947).

Fairbridge, R.W., Editor, *The Encyclopedia of Atmospheric Sciences and Astrogeology*, Reinhold Publishing Corp., New York, (1967).

Fremlin, G., Editor in Chief, *The National Atlas of Canada*, Fourth Edition, The Macmillan Co. of Canada, Ltd., Toronto, (1974).

Gumbel, E.J., *Statistical Theory of Extreme Values and Some Practical Applications*, Monograph No. 33, NBS Applied Math Series, U.S. Dept. of Commerce, Washington, (Feb. 1954).

Gumbel, E.J., *Statistics of Extremes*, Columbia University Press, New York, (1958).

Haltiner, G.J. and F.L. Martin, *Dynamical and Physical Meteorology*, McGraw-Hill Book Co., New York, (1957).

Harnack, R.P. and H.E. Landsberg, *Selected Cases of Convective Precipitation Caused by the Metropolitan Area of Washington, D.C.*, J. Appl. Meteor., 14, 1050–1060, (Sept. 1975).

Harrold, T.W., *The Structure of Precipitation Systems*, Proceedings of IUCRM Colloquium on Fine Scale Structure of Precipitation and EM Propagation (Nice), Centre National d'Etudes des Telecommunications, Issy-les-Moulineaux, (Oct. 1973).

Hobbs, P.V. and R.A. Houze, Jr., *Mesoscale Structure of Precipitation in Extratropical Cyclones*, Proceedings of the International Conference on Cloud Physics (Boulder), American Meteorological Society, Boston, (1976).

Hobbs, P.V. and J.D. Locatelli, *Rainbands, Precipitation Cores and Generating Cells in a Cyclonic Storm*, J. Atmos. Sci., 35, 230–241, (Feb. 1978).

Hobbs, P.V., L.F. Radke and S.E. Shumway, *Cloud Condensation Nuclei from Industrial Sources and Their Apparent Influence on Precipitation in Washington State*, J. Atmos. Sci., 27, 81–89, (Jan. 1970).

Hogg, D.C., *Millimeter-Wave Communication Through the Atmosphere*, Science, 159, 39–46, (Jan. 1968).

Houze, R.A., Jr., *A Climatological Study of Vertical Transports by Cumulus-Scale Convection*, J. Atmos. Sci., 30, 1112–1123, (Sept. 1973).

Huff, F.A., *Statistics of Precipitation*, Proceedings of IUCRM Colloquium on Fine Scale Structure of Precipitation and EM Propagation (Nice), Centre National d'Etudes des Telecommunications, Issy-les-Moulineaux, (Oct. 1973).

Huff, F.A. and S.A. Chagnon, Jr., *Climatological Assessment of Urban Effects on Precipitation at St. Louis*, J. Appl. Meteor., 11, 823–842, (Aug. 1972).

James, J.W., *The Effect of Wind on Precipitation Catch over a Small Hill*, J. Geophys. Res., 69, 2521–2524, (June 1964).

Katz, I., *Rain Cell Statistics Experiment*, Proceedings of the 16th Radar Meteorology Conference (Houston), American Meteorological Society, Boston, (1975).

Katz, I., *A Rain Cell Model*, Proceedings of the 17th Conference on Radio Meteorology (Seattle), American Meteorological Society, Boston, (1976).

Konrad, T.G. and R.A. Kropfli, *Statistical Models of Rain Cells Derived from Radar Observations*, Proceedings of the 16th Radar Meteorology Conference (Houston), American Meteorological Society, Boston, (1975).

Krishnamurti, R., *On Cellular Cloud Patterns, Part 1: Mathematical Model*, J. Atmos. Sci., 32, 1353–1363, (July 1975).

Kurtyka, J.C., *Precipitation Measurements Study*, Report of Investigation No. 20, Illinois State Water Survey, Urbana, Ill., (Feb. 1953).

Landsberg, H.E., *The Climate of Towns*, in: Man's Role in Changing the Face of the Earth, Edited by W.L. Thomas, Jr., University of Chicago Press, Chicago, (1956).

Landsberg, H.E., *Man-Made Climatic Changes*, Science, 170, 1265–1274, (Dec. 1970).

Lefrançois, G., *Modèle théorique de précipitation équivalente sur un trajet radioélectrique*, Ann. Télécomm., 26, 445–453, (Nov–Dec. 1971).

Lin, S.H., *Dependence of Rain-Rate Distribution on Rain-Gauge Integration Time*, Bell Syst. Tech. J., 55, 135–141, (Jan. 1976a).

Lin, S.H., *Rain-Rate Distributions and Extreme-Value Statistics*, Bell Syst. Tech. J., 55, 1111–1124, (Oct. 1976b).

Lin, S.H., *From Rain to Attenuation: Application to 11 GHz Radio*, 1977 International Conference on Communications, Chicago, (1977).

MacKenzie, E.C., and J.E. Allnutt, *Effect of Squall-Line Direction on Space-Diversity Improvement Obtainable with Millimetre-Wave Satellite Radiocommunication Systems*, Electron. Lett., 13, 571–573, (Sept. 1977).

Marshall, J.S., *Precipitation Trajectories and Patterns*, J. Meteor., 10, 25–29, (Feb. 1953).

Marwitz, J.D., *The Structure and Motion of Severe Hailstorms, Part II: Multi-Cell Storms*, J. Appl. Meteor., 11, 180–188, (Feb. 1972).

Miles, M.K., *Predicting Temperature Trends in the Northern Hemisphere to the Year 2000*, Nature, 276, 356–359, (23 Nov. 1978).

Misme, P. and J. Fimbel, *Détermination théorique et expérimentale de l'affaiblissement par la pluie sur un trajet radioélectrique*, Ann. Télécomm., 30, 149–158, (May–June 1975).

Morita, K., *A Method for Estimating Year and Worst-Month Rain Rate Distributions*, Trans. Inst. Electr. Comm. Eng. Japan, E-61, 618–624, (Aug. 1978).

Rice, P.L. and N.R. Holmberg, *Cumulative Time Statistics of Surface-Point Rainfall Rates*, Trans. IEEE, COM-21, 1131–1136, (Oct. 1973).

Sanderson, M., *A Comparison of Canadian and United States Standard Methods of Measuring Precipitation*, J. Appl. Meteor., 14, (Sept. 1975).

Segal, B., *High-Resolution Rainfall Data Distributions at Locations Across Canada*, Preliminary Report, Communications Research Centre, Ottawa, (May 1977).

Semonin, R.G. and S.A. Chagnon, Jr., *METROMEX: Summary of 1971–1972 Results*, Bull. Amer. Meteor. Soc., 55, 95–100, (Feb. 1974).

Sims, A.L. and D.M.A. Jones, *Climatology of Instantaneous Precipitation Rates*, Report No. TR-73-0171, Air Force Cambridge Research Laboratory, Bedford, Mass., (March, 1973).

Sporns, U., *On the Transposition of Short-Duration Rainfall Intensity Data in Mountainous Regions*, Tech. Publ. No. TEC-519, Atmospheric Environment Service, Downsview, Ont., (1964).

Spreen, W.C., *A Determination of the Effect of Topography upon Precipitation*, Trans. A.G.U., 28, 285–290, (April 1947).

Strickland, J.I., *Radar Measurements of Site-Diversity Improvement During Precipitation*, J. Recherches Atmos., 8, 451–464, (Jan–June 1974).

Sutton, Sir O.G., *Micrometeorology*, McGraw-Hill Book, Co., New York, (1953).

Thomas, M.K., *Recent Climatic Fluctuations in Canada*, Climatological Studies, No. 28, Atmospheric Environment Service, Toronto, (1975).

Trewartha, G.T., *An Introduction to Climate*, Fourth Edition, McGraw-Hill Book Co., New York, (1968).

Warner, J., *A Reduction in Rainfall Associated with Smoke from Sugar-Cane Fires – An Inadvertent Weather Modification?* , J. Appl. Meteor., 7, 247-251, (1968).

Wexler, R. and D. Atlas, *Precipitation Generating Cells*, J. Meteor., 16, 327–332, (June 1959).

Wilson, W.T., Discussion of paper, *Precipitation at Barrow, Alaska, Greater than Recorded*, by R.F. Black, Trans. A.G.U., 35, 206–207, (April 1954).

Wright, J.B. and C.H. Trenholm, *Greater Vancouver Precipitation*, Tech. Memo TEC 722, Atmospheric Environment Service, Downsview, (Sept. 1969).

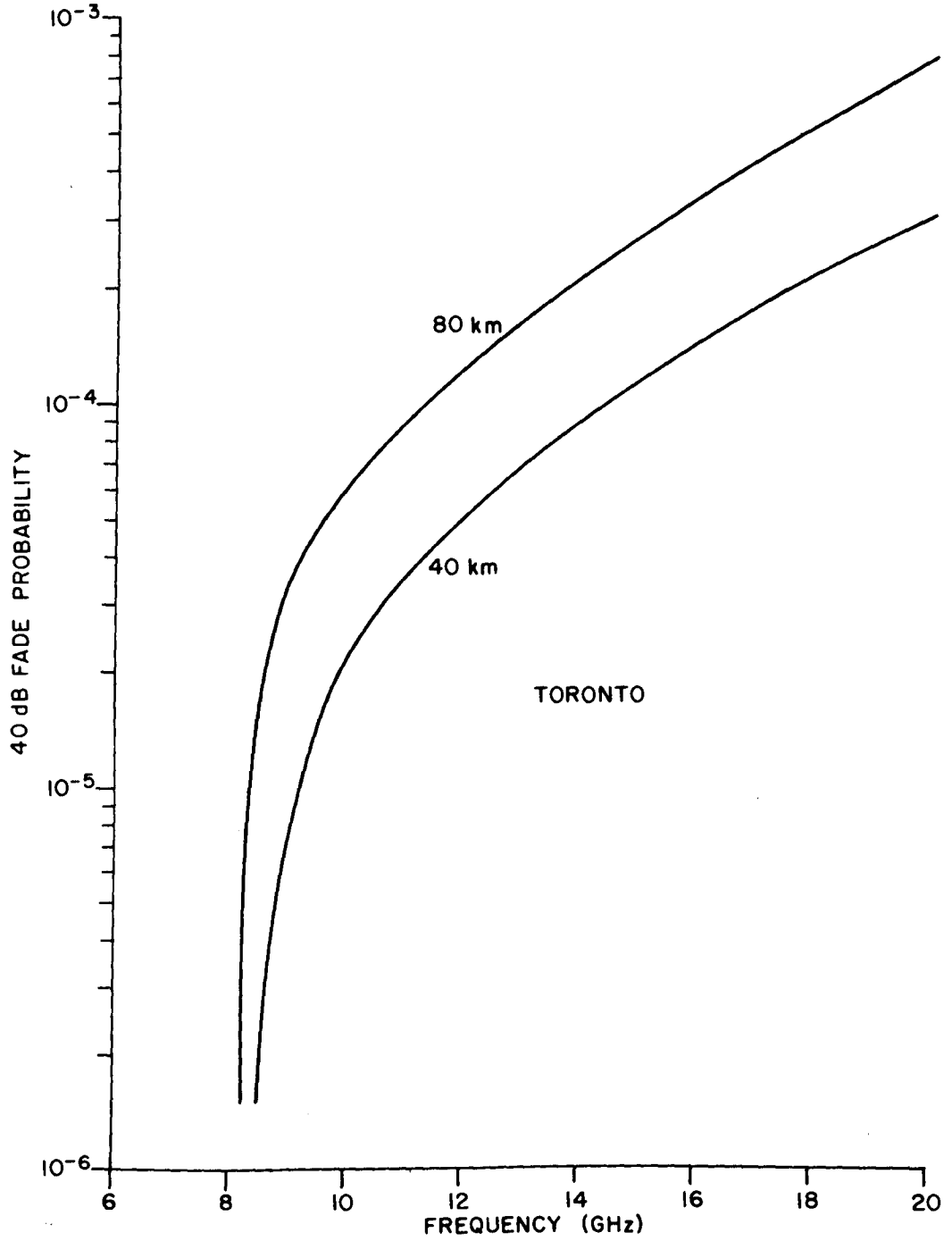

Figure 1. Probability of severe rain attenuation occurring over terrestrial microwave links of 40 and 80 km at Toronto, Ontario

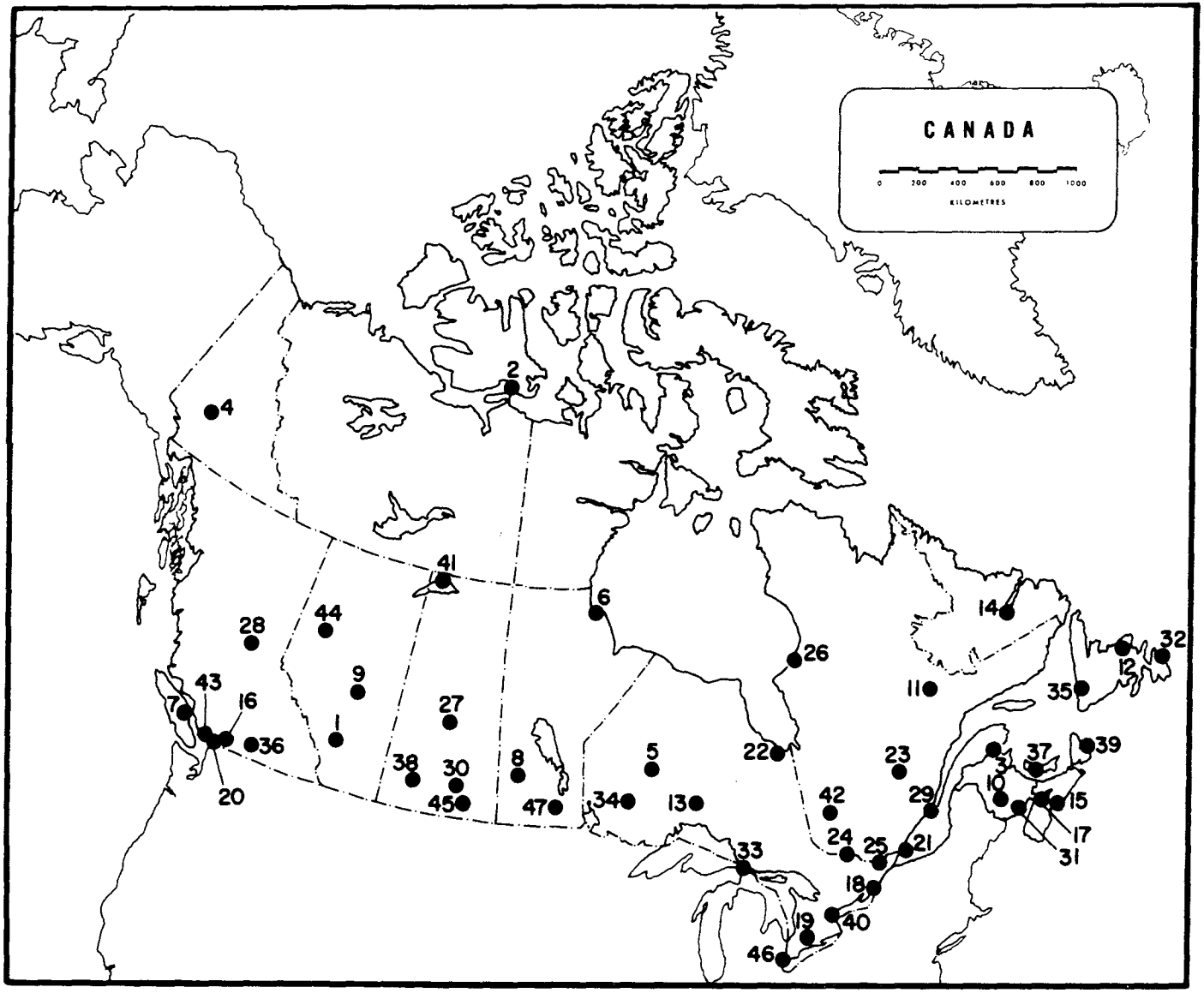

Figure 2. Map indicating the location of precipitation recording stations from which rain gauge data have been analyzed. The numerals correspond to the station listing in Table 1.

Figure 3. Digitizing the enlarged trace of a tipping-bucket rain chart

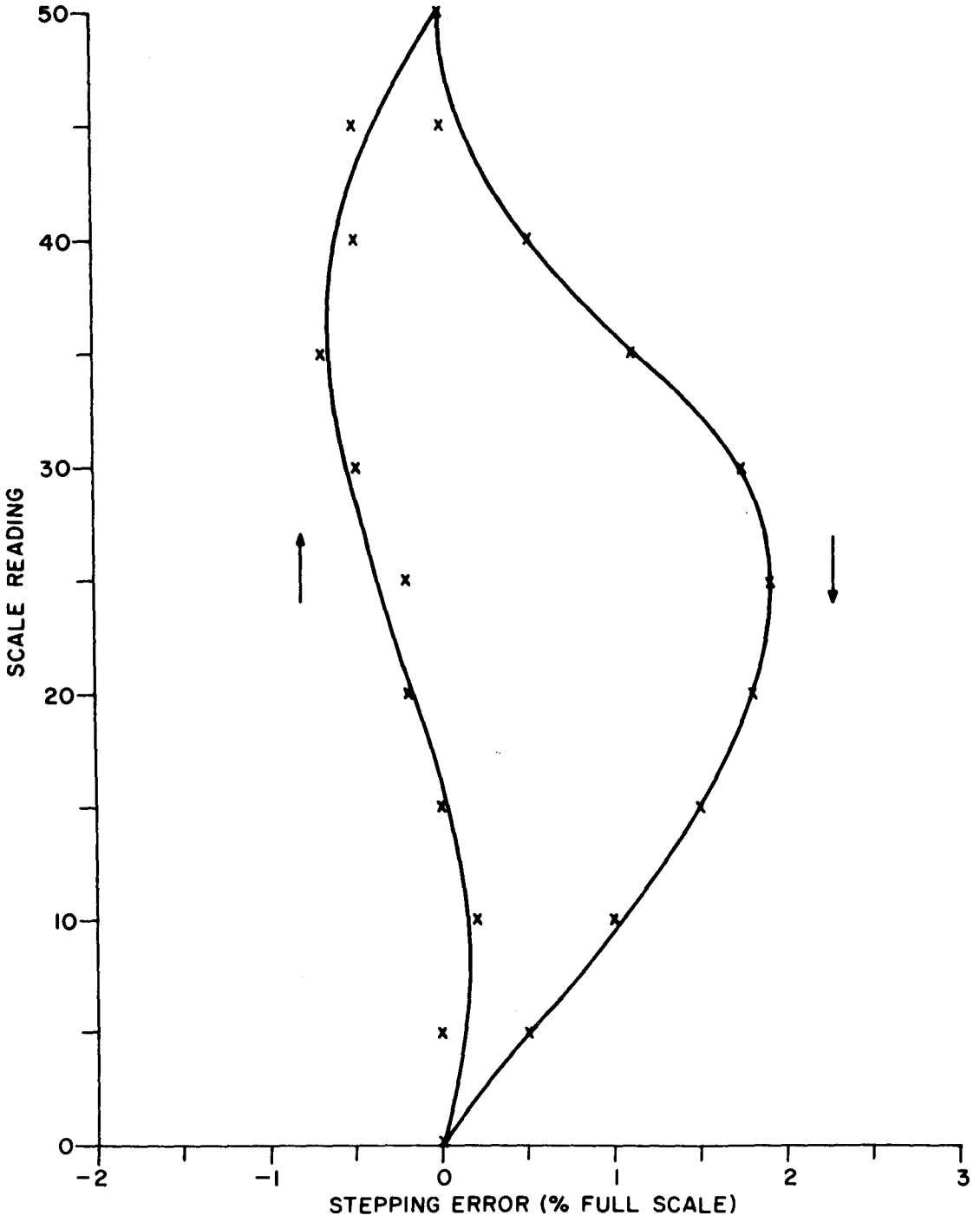

Figure 4. Positional error of tipping-bucket graph trace. The indicated scale reading is in units of 0.01 inch rain accumulation, increasing from the bottom of the paper chart. The arrows indicate the direction of pen movement.

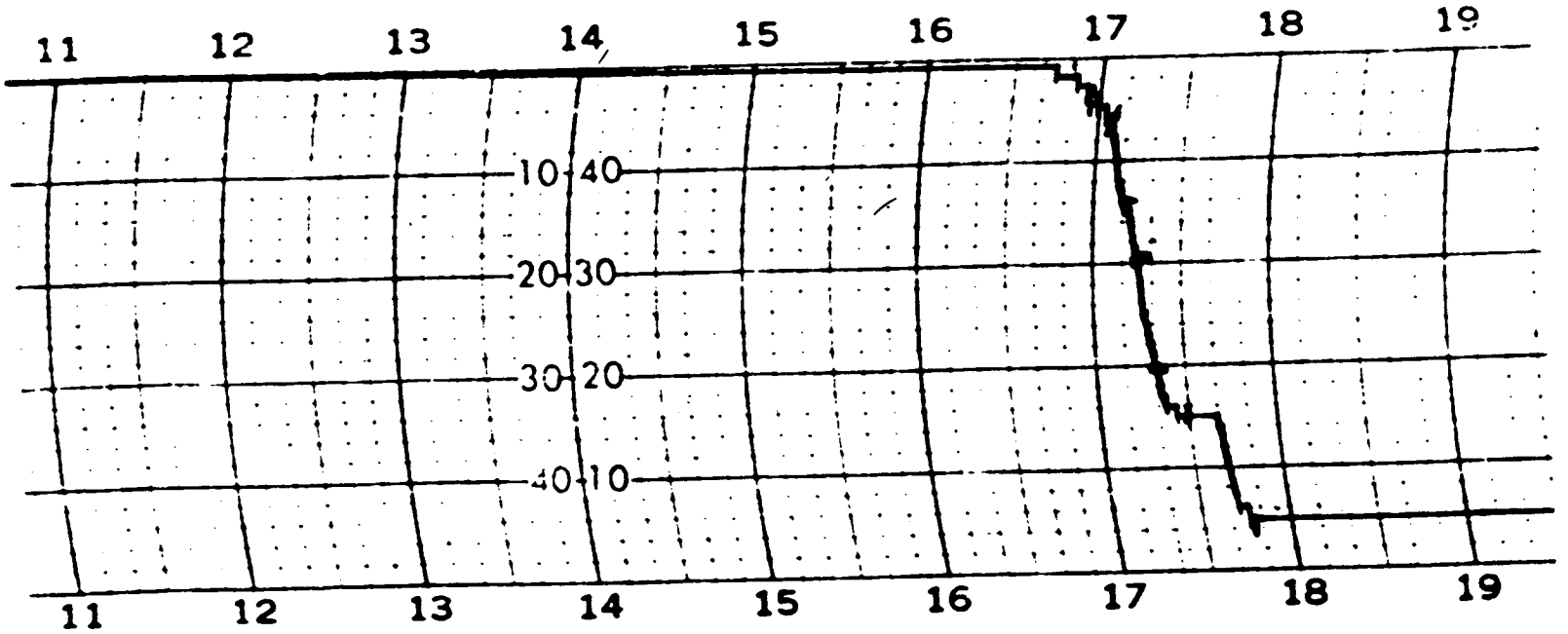

Figure 5. Portion of a rain chart with moderate misalignment error. The peak in precipitation rate near 1740 hours briefly exceeds 50 mm/h. Inclination of horizontal trace with respect to time axis is approximately 3/4° in this example.

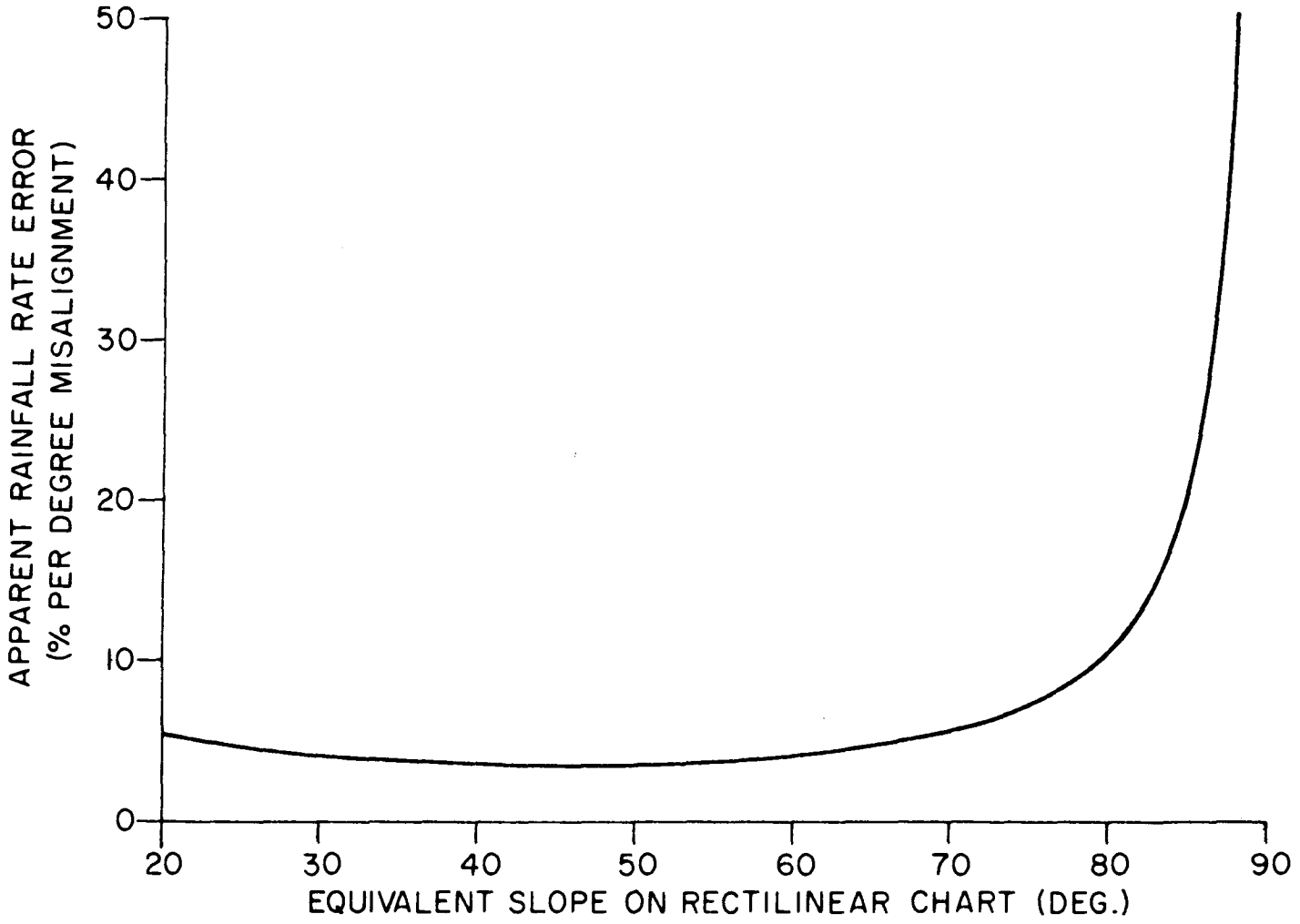

Figure 6. Error resulting from misalignment of chart registration versus trace slope

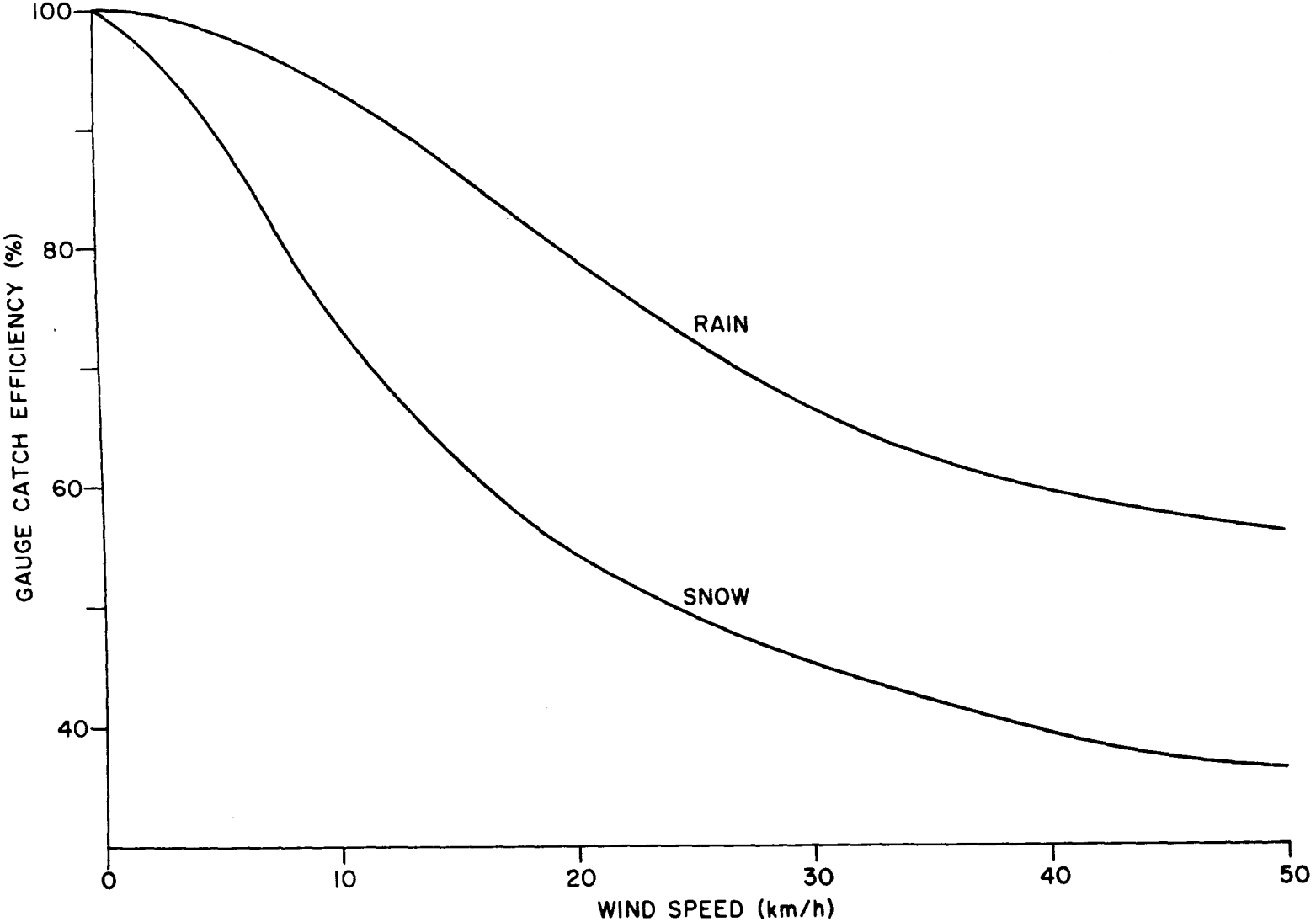

Figure 7. Precipitation gauge efficiency as a function of horizontal wind speed

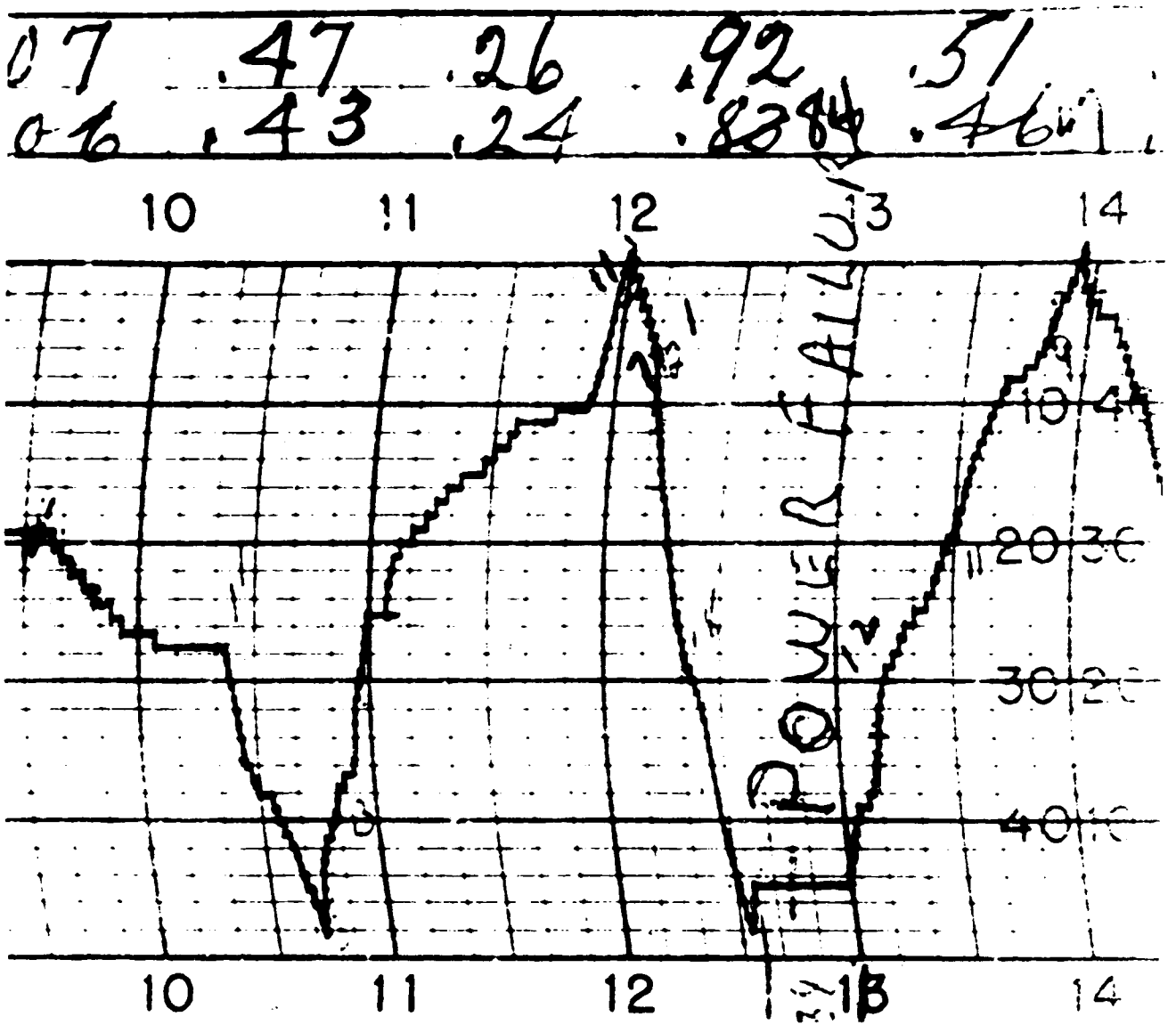

Figure 8. Example of a loss of rain gauge data during a moderate storm as a result of a power failure. This event was recorded at the Montreal International Airport station shortly after noon on 12 Sept. 1963. The break followed a 10-year record for 30-minute rainfall during September.

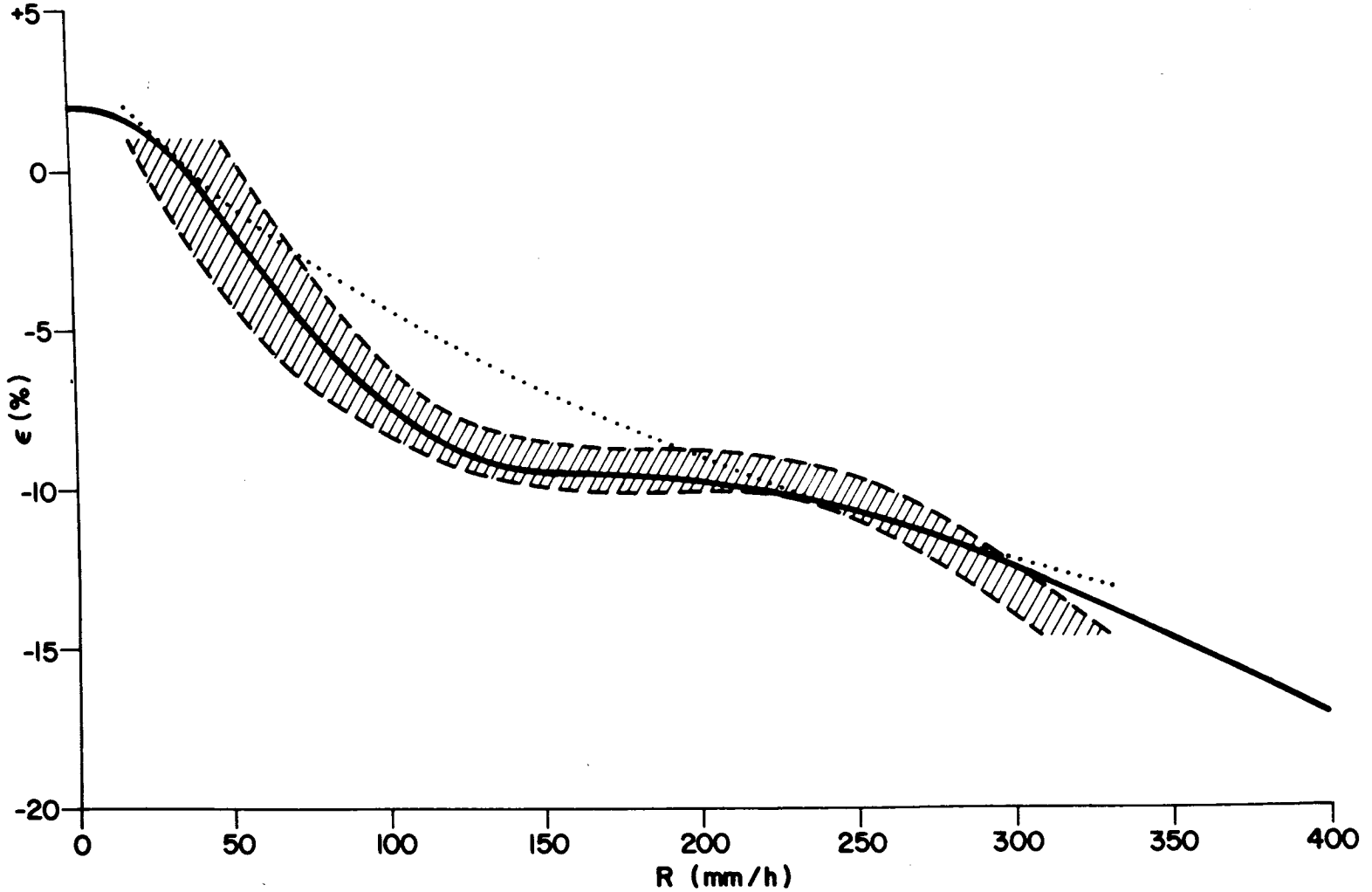

Figure 9. Inaccuracy of the tipping bucket gauge in measuring rainfall rate. The hatched area brackets a number of experimental observations carried out by the A.E.S. Also shown (dotted) is a calibration of the U.S. Weather Bureau tipping bucket gauge. The heavy line indicates the gauge error assumed in the present work.

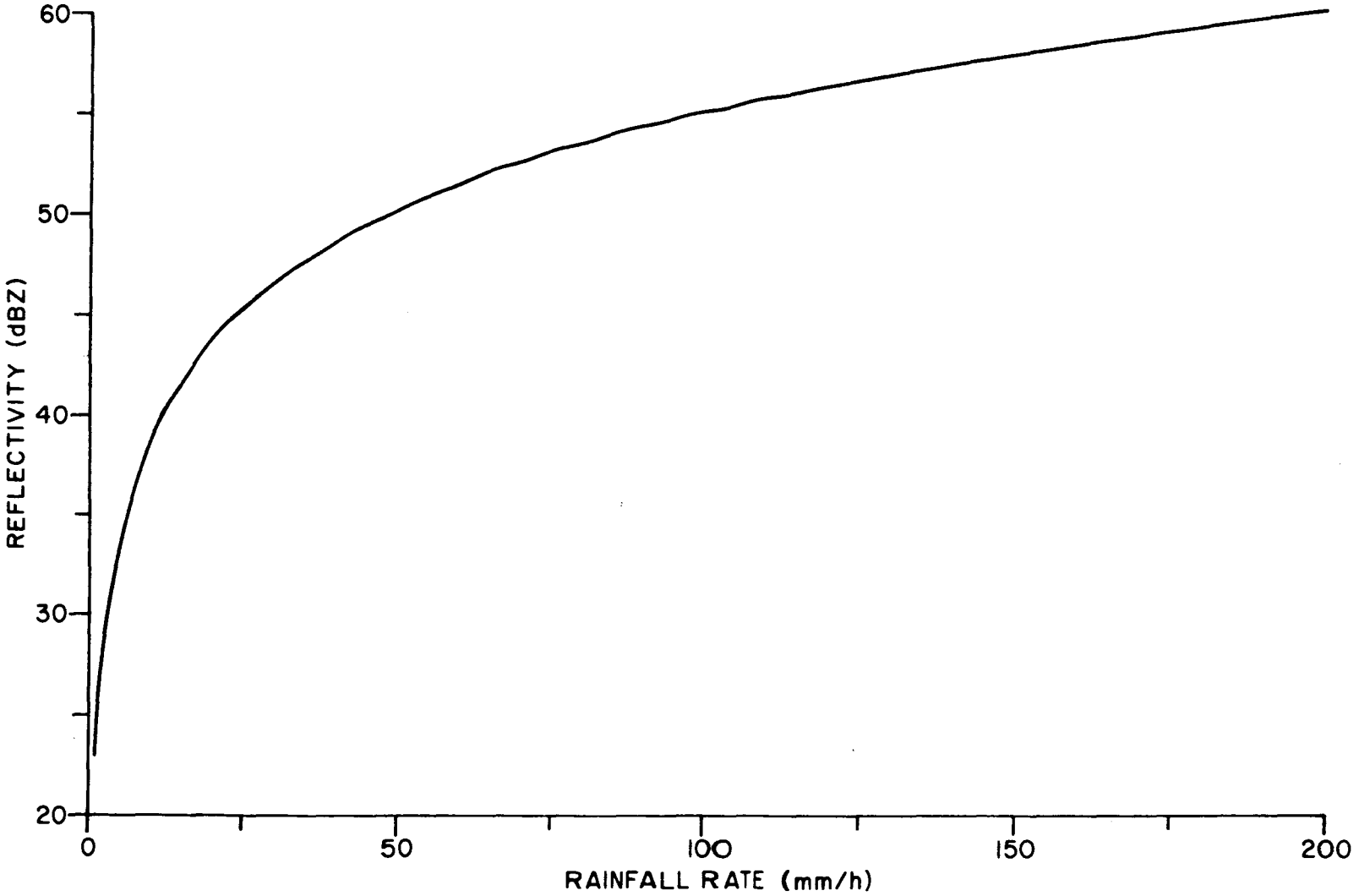

Figure 10. Approximate relationship between the observed rainfall rate at the ground and the radar reflectivity factor (referred to $Z=1\ mm^6/m^3$).

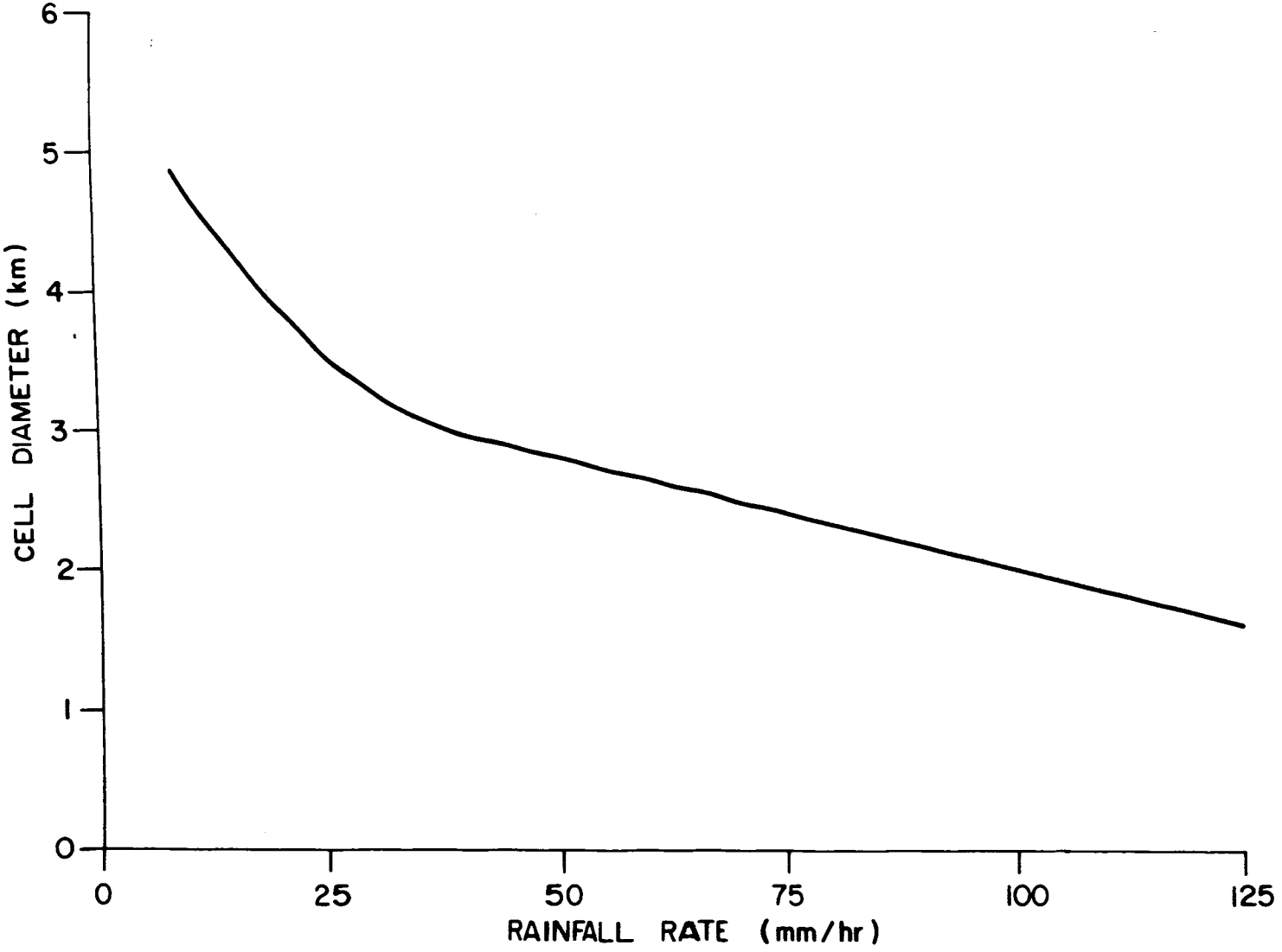

Figure 11. CCIR (1974) model of average rain cell size as a function of rainfall rate, based on data from various geographic locations.

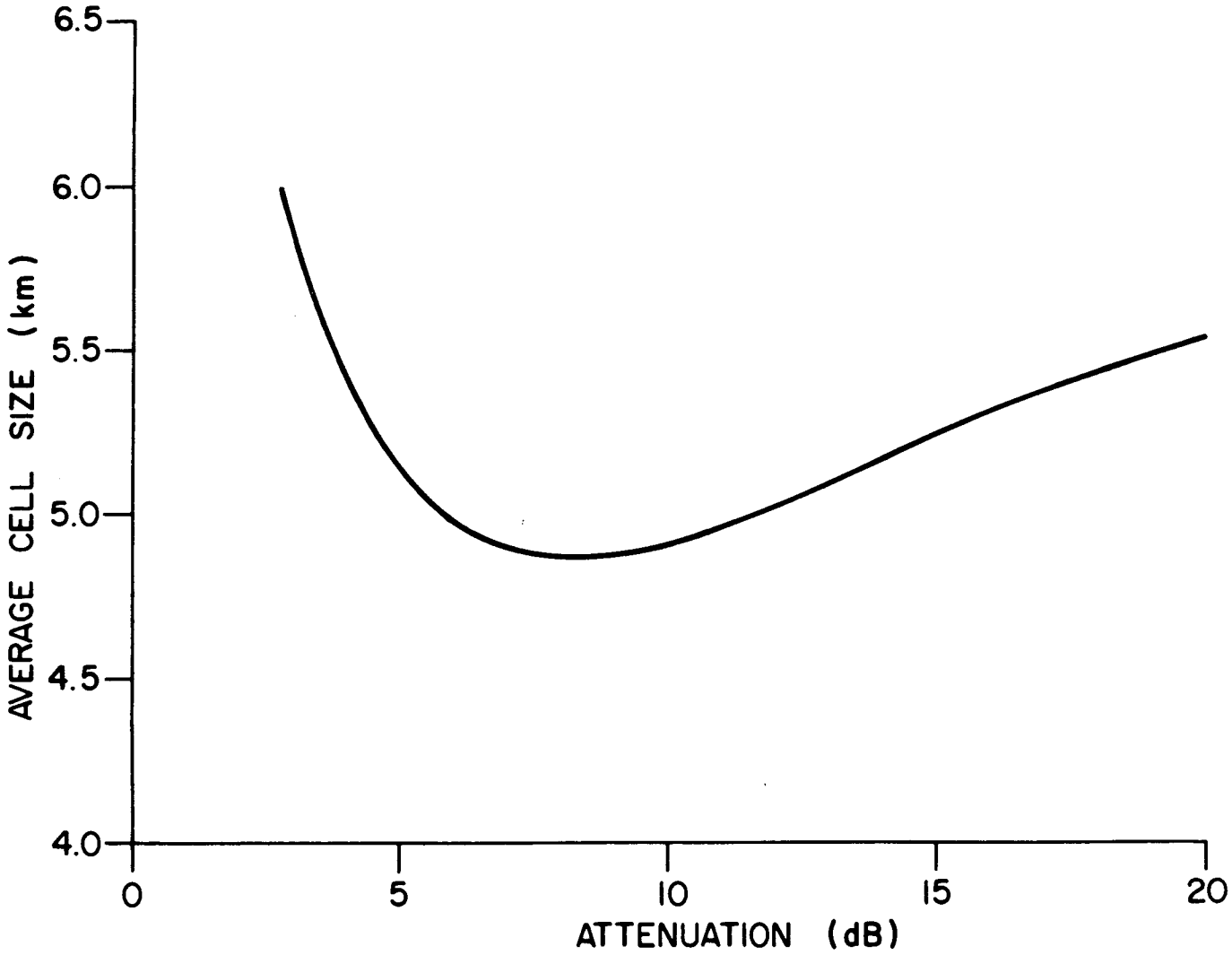

Figure 12. Mean horizontal dimension of rain cells observed at Ottawa versus slant-path attenuation for a 5° elevation angle. (Strickland, 1974).

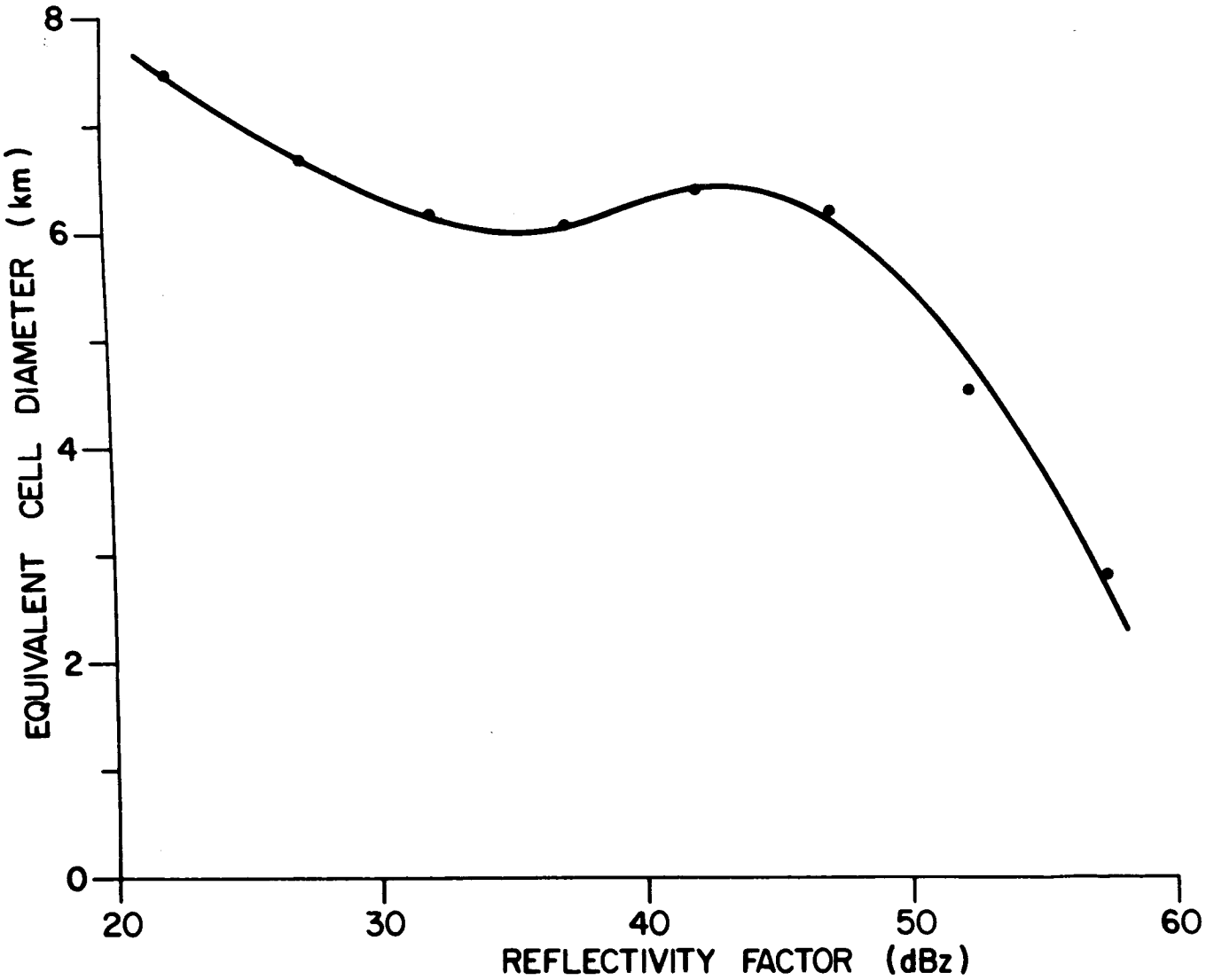

Figure 13. Rain cell size versus radar reflectivity observed at Wallops Island, Va. (Konrad and Kropfli, 1975).

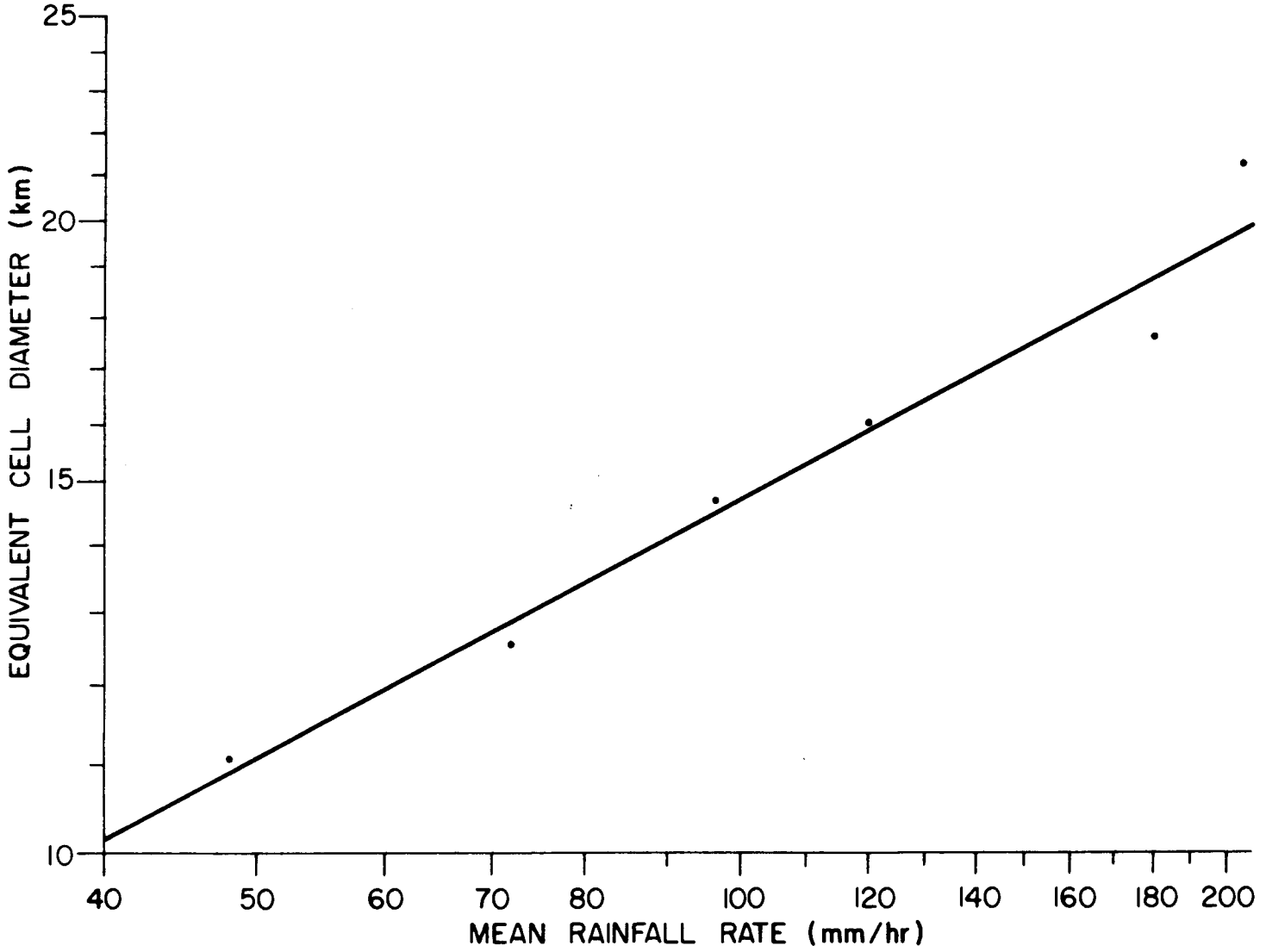

Figure 14. Equivalent rain "cell" diameter versus mean rainfall rate observed at the surface in the area of St. Louis, Mo. (Huff, 1973).

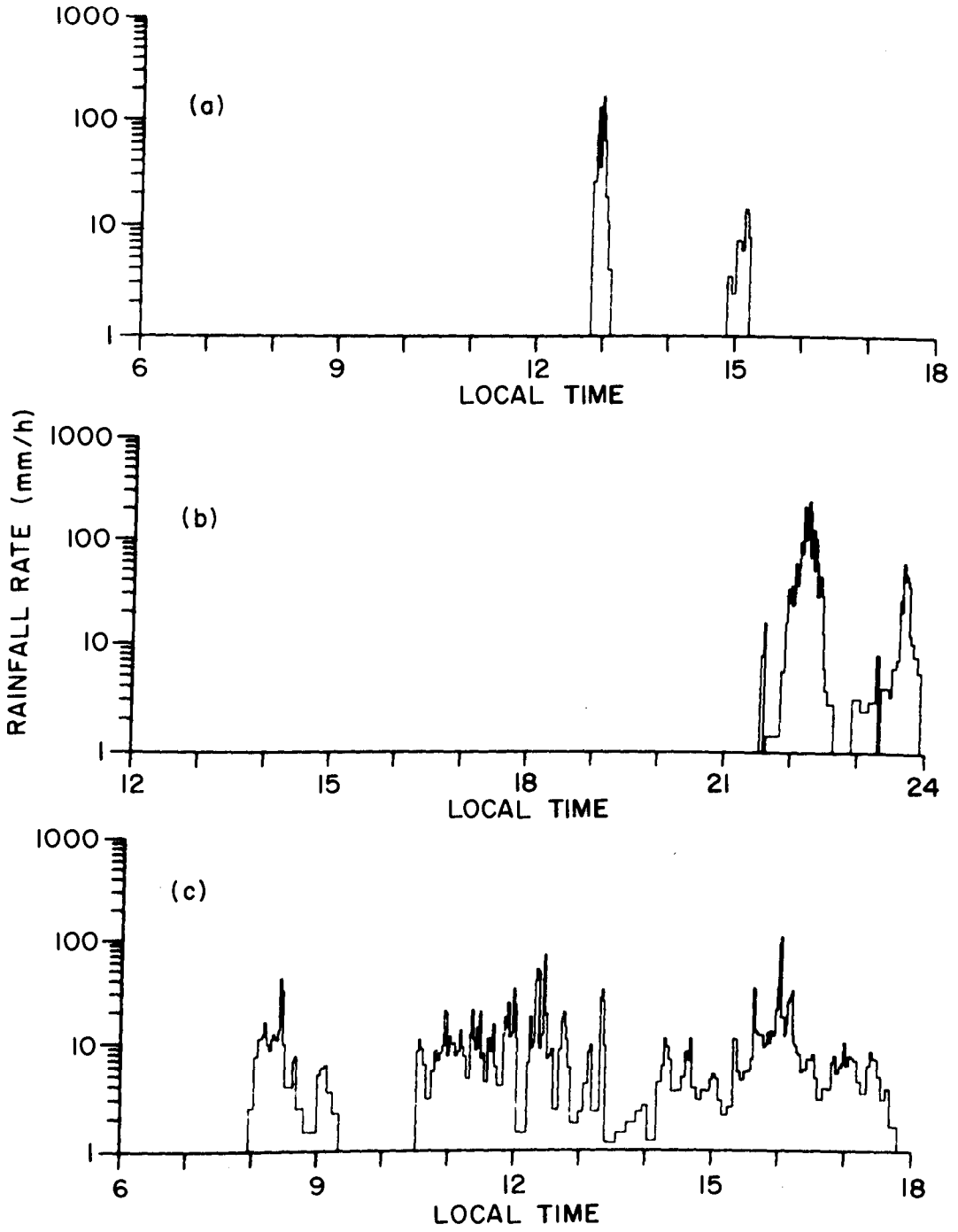

Figure 15. Examples of precipitation events as observed from a fixed location on the ground. Three distinctly different time-varying characteristics are illustrated.

(a) very, brief, intense cell observed at Ottawa, May 14, 1963.

(b) large isolated rain cells observed at Winnipeg, September 20, 1970.

(c) diffuse, complex rain structure observed at Halifax, August 24, 1963.

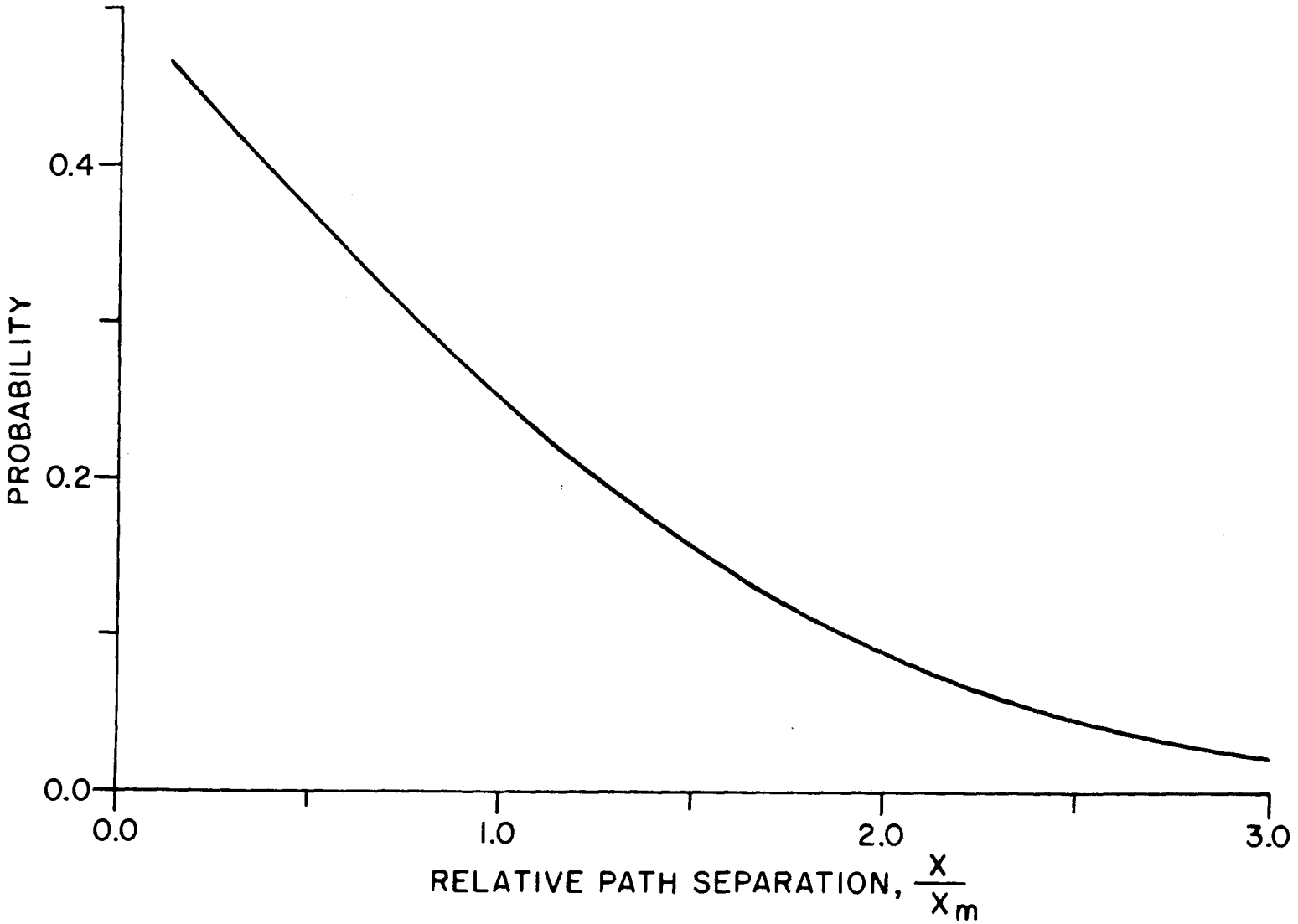

Figure 16. Maximum conditional probability that attenuating rain cells will occur simultaneously on parallel paths for the Ottawa area. $X_m = 0.675\ \sigma$ is the median of the absolute value of cell-pair separation in one dimension. Relationship breaks down for small separations due to finite size of individual rain cells.

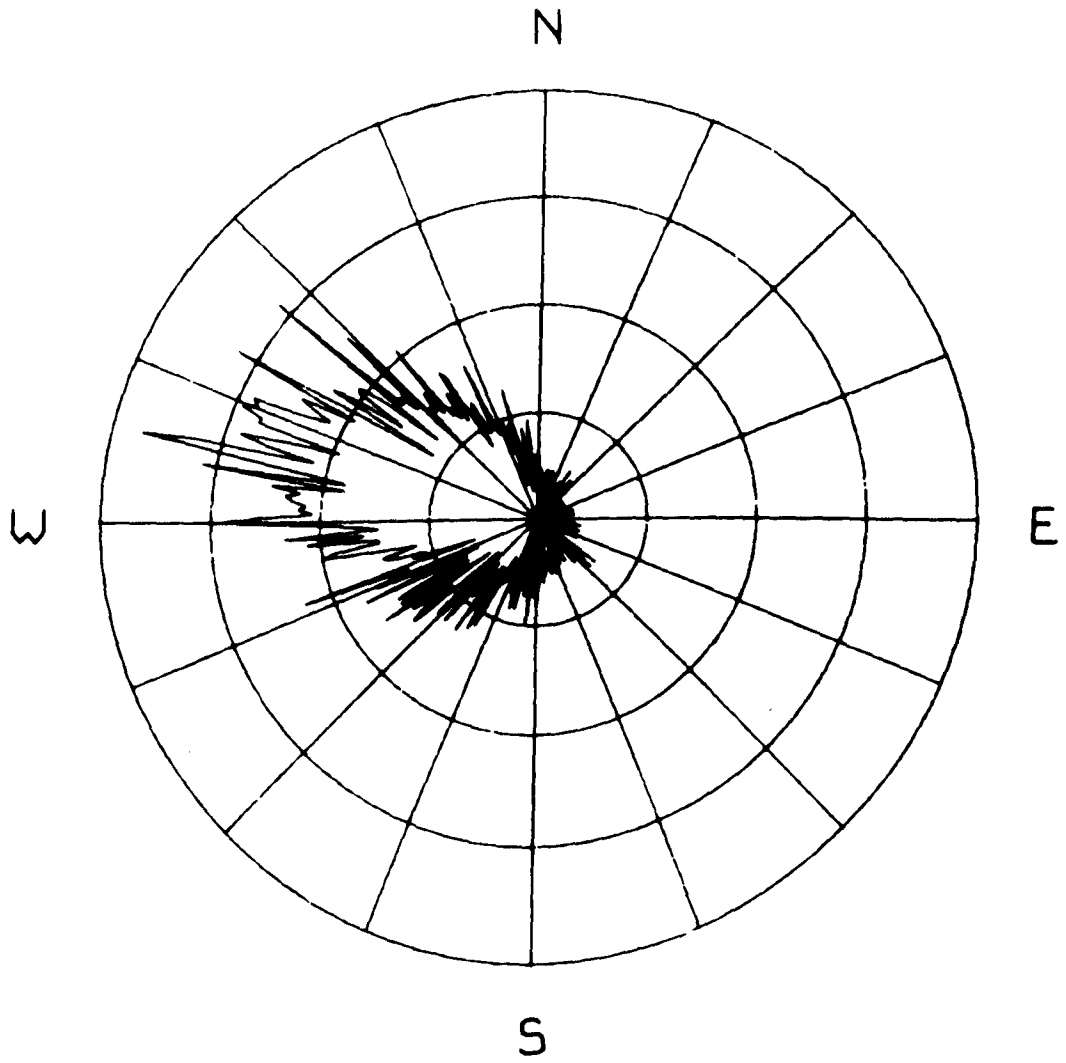

Figure 17. Distribution of wind source direction at the 700-mbar pressure level recorded at Edmonton, Alberta over a ten-year period (1961–1970).

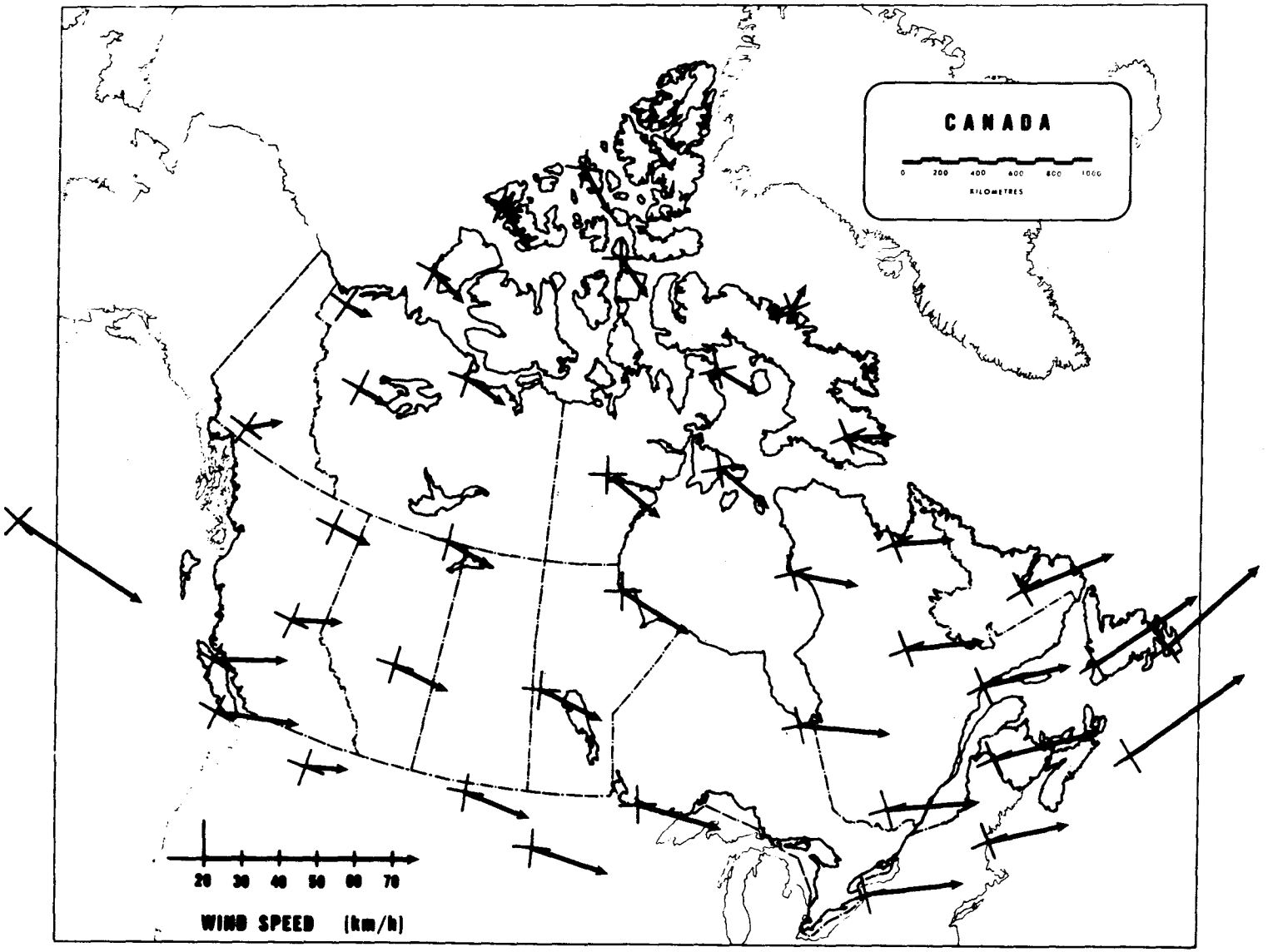

Figure 18. Mean upper atmosphere wind speed and direction for locations across Canada. Data cover the months April–October only, except along the east and west coasts. The crossed lines at the origin of each wind vector indicates the cardinal points of the compass at that location.

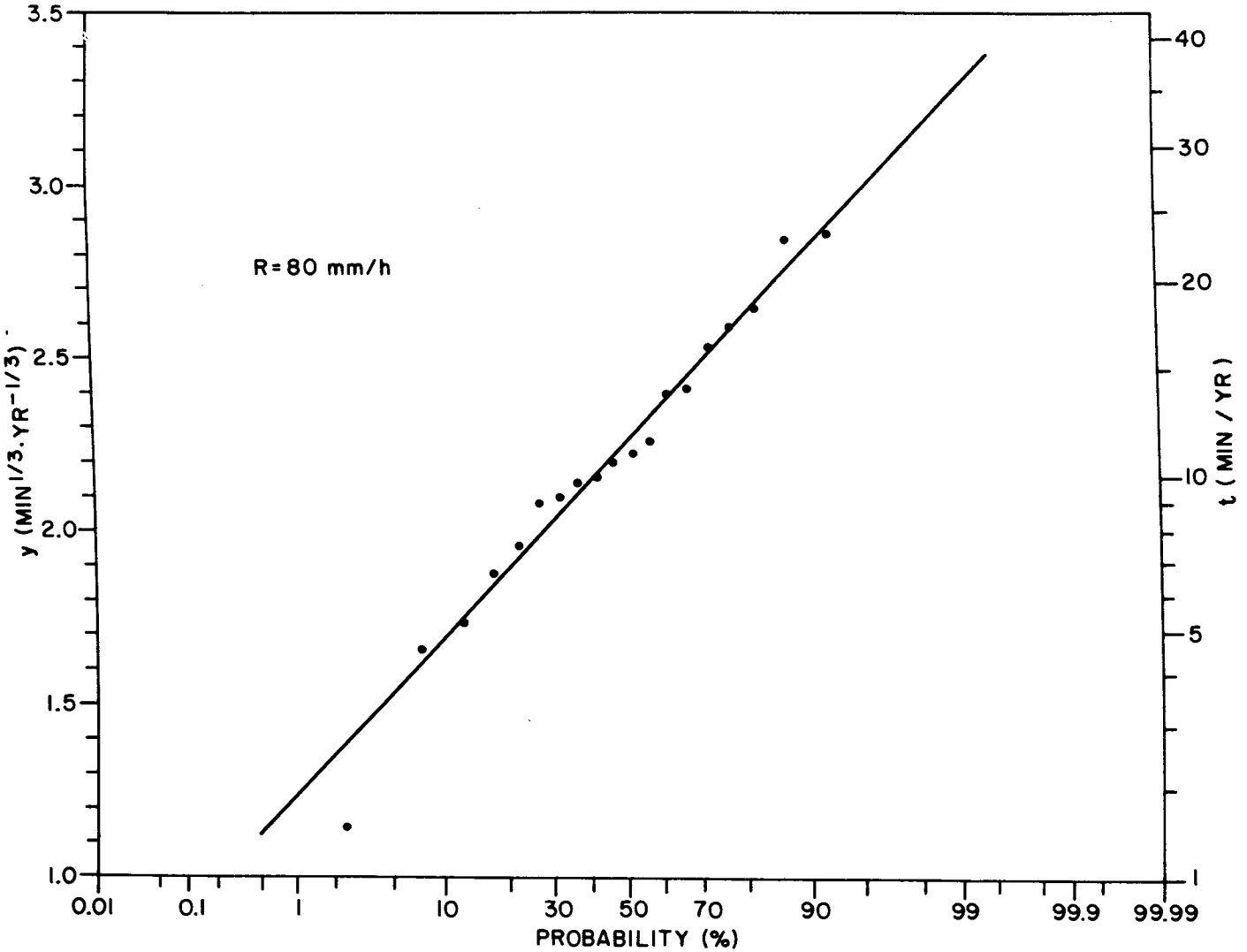

Figure 19. Cumulative distribution of the time during a calendar year that the rainfall rate exceeded a threshold of 80 mm/h at London, Ontario. The left hand ordinate is the cube root of the observed time, in minutes per year, shown on the right.

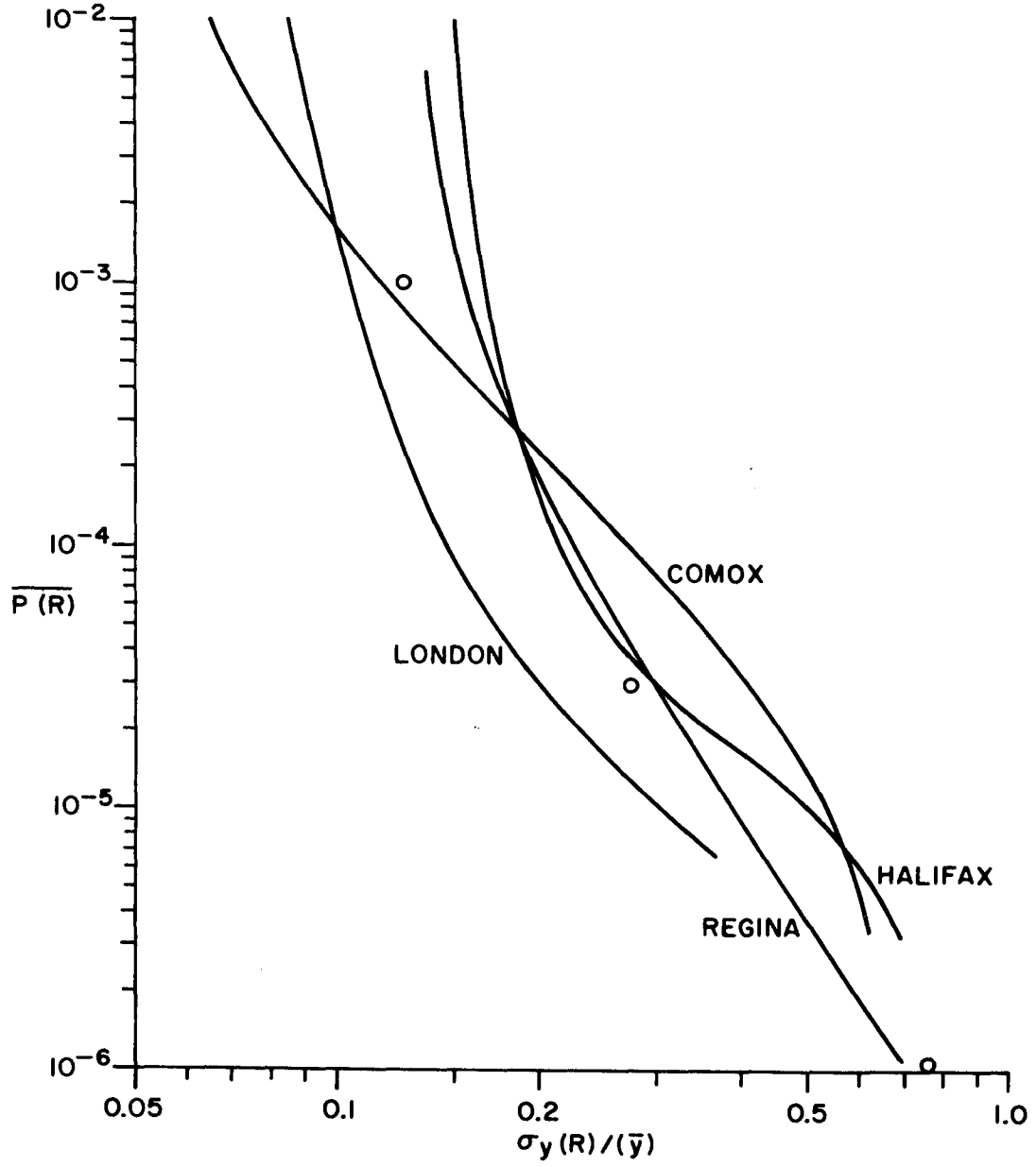

Figure 20. Mean probability of rainfall at any rate versus relative dispersion of the cube-root annual exceedance for that rate. The open circles indicate the "typical" values selected for further consideration (see text).

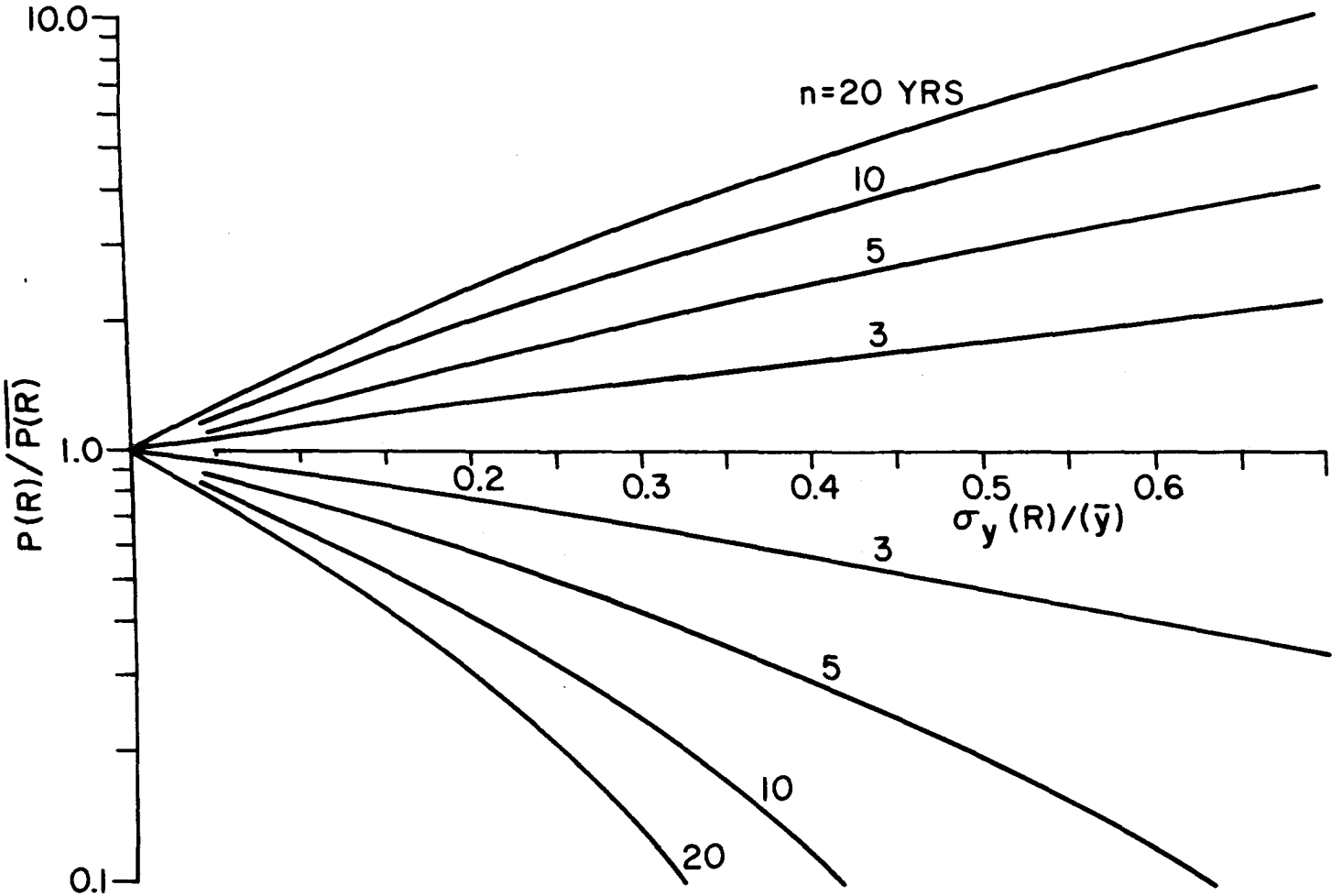

Figure 21. Range of variation in yearly rainfall likely to be exceeded once in several years as a function of the relative dispersion in y(R).

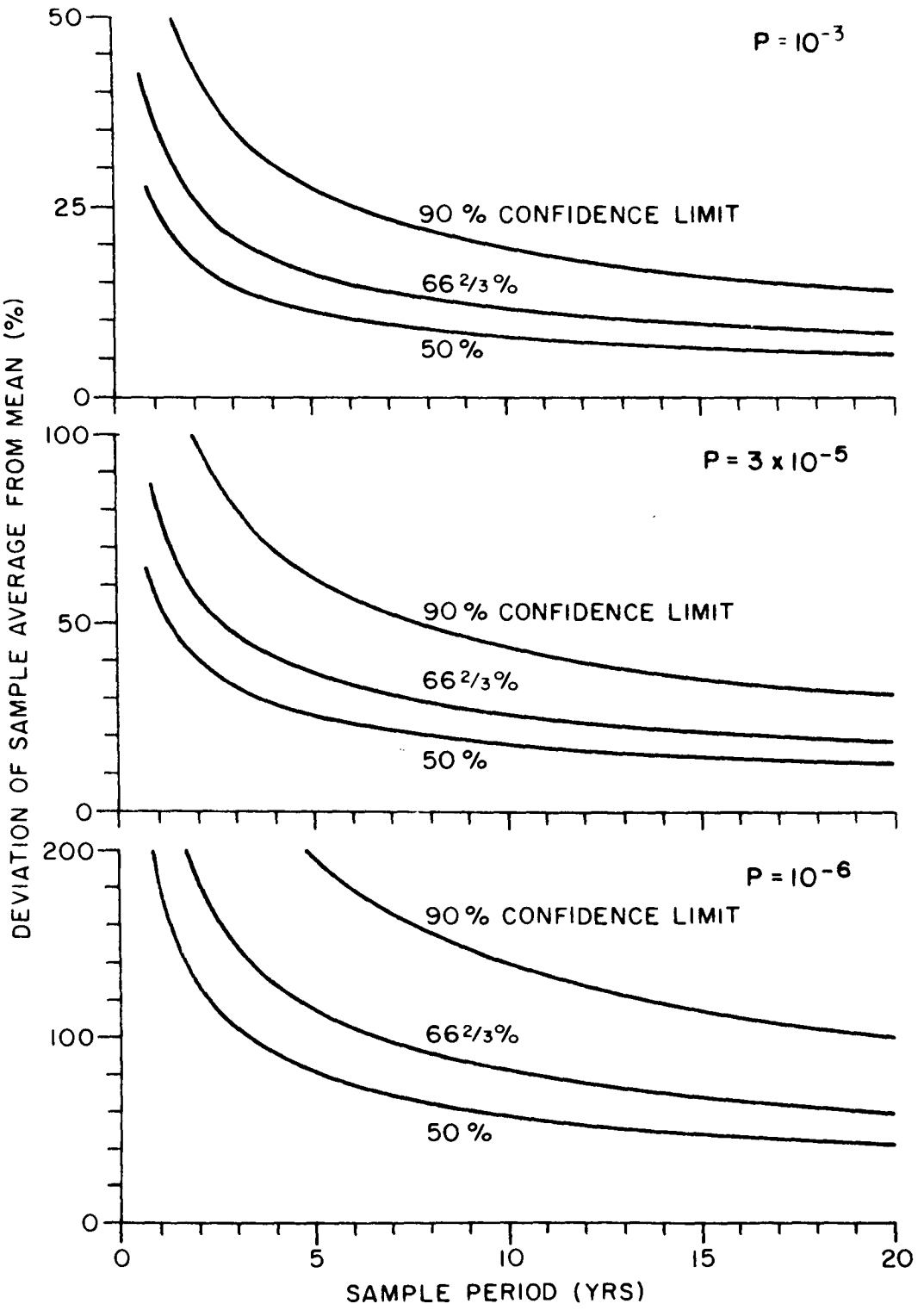

Figure 22. Deviation of average of yearly exceedances from long-term mean as a function of data sample length for three rainfall rate exceedance probability levels

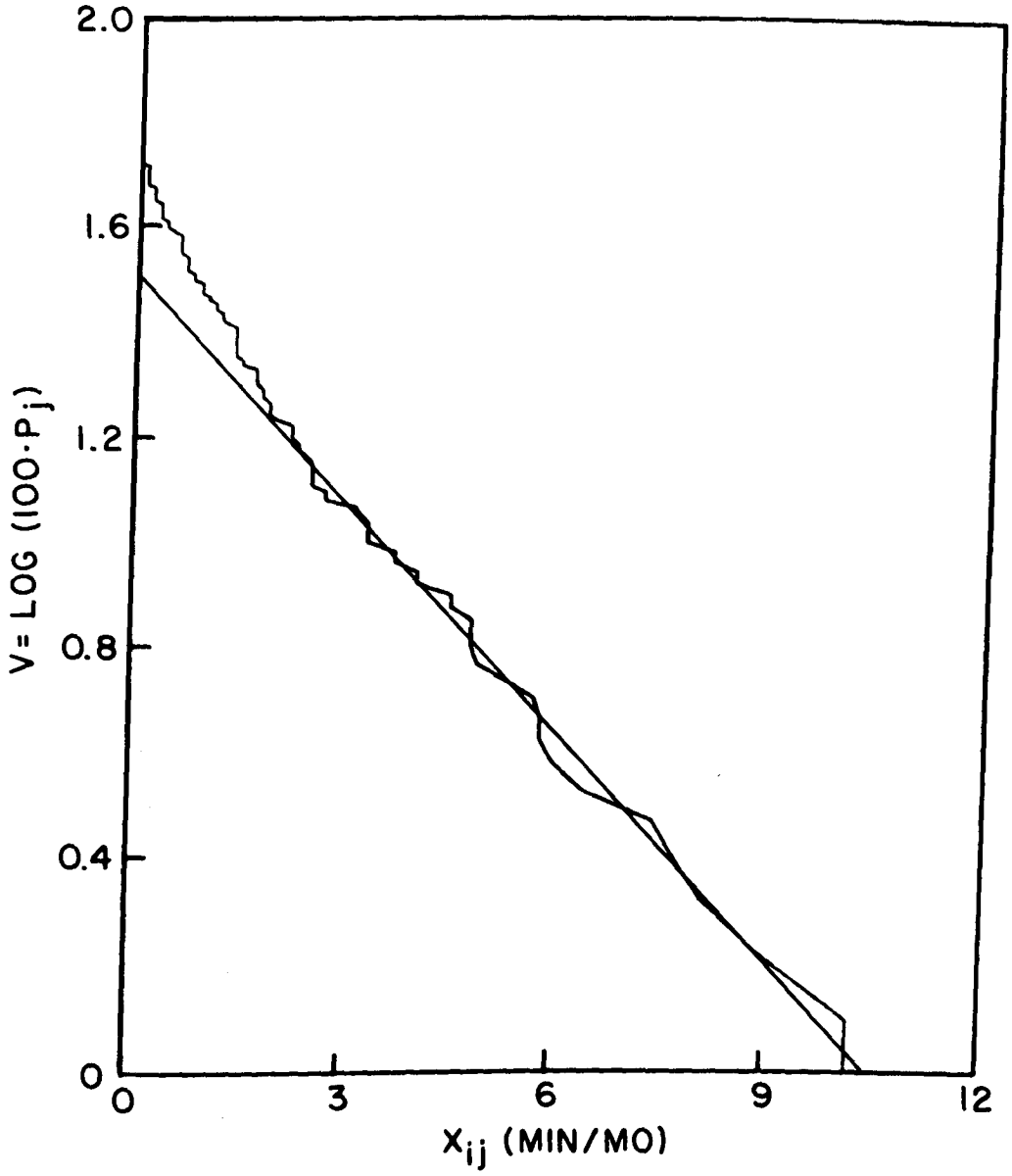

Figure 23. Cumulative probability, P_j, versus monthly exceedance with respect to 80 mm/h threshold at London, Ontario. Data for this plot totalled 240 months; the two points having probabilities less than 1% (i.e., V<0.0) have been omitted for the sake of clarity.

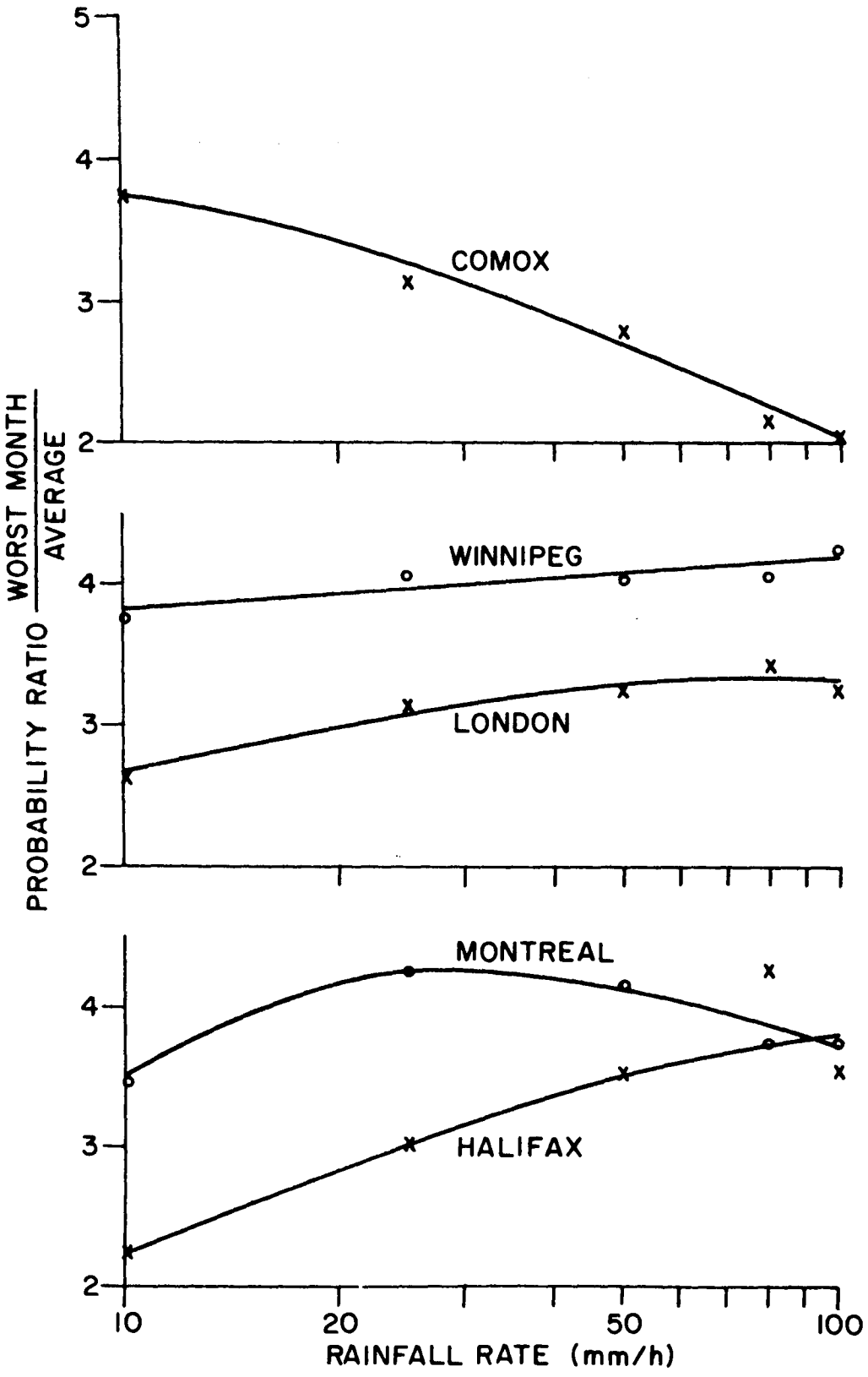

Figure 24. Ratio of monthly exceedance probability (having a one-year return period) to average annual probability as a function of rainfall rate for various locations across Canada

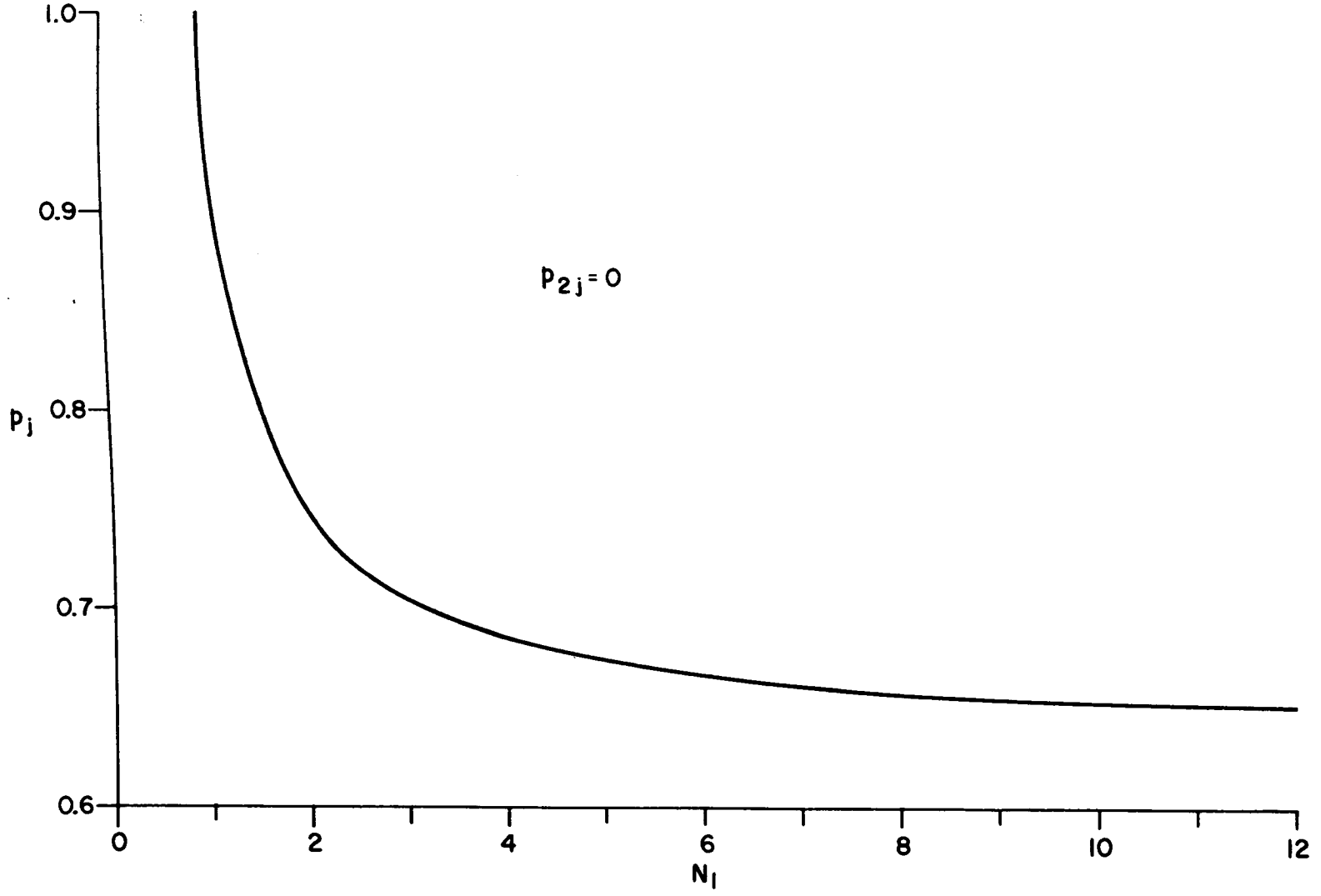

Figure 25. Probability that a "worst-month" value, as predicted by curves in Figure 24, will occur in any given year. N_1 is the number of calendar months during the year that rainfall corresponding to the selected threshold may be expected to occur.

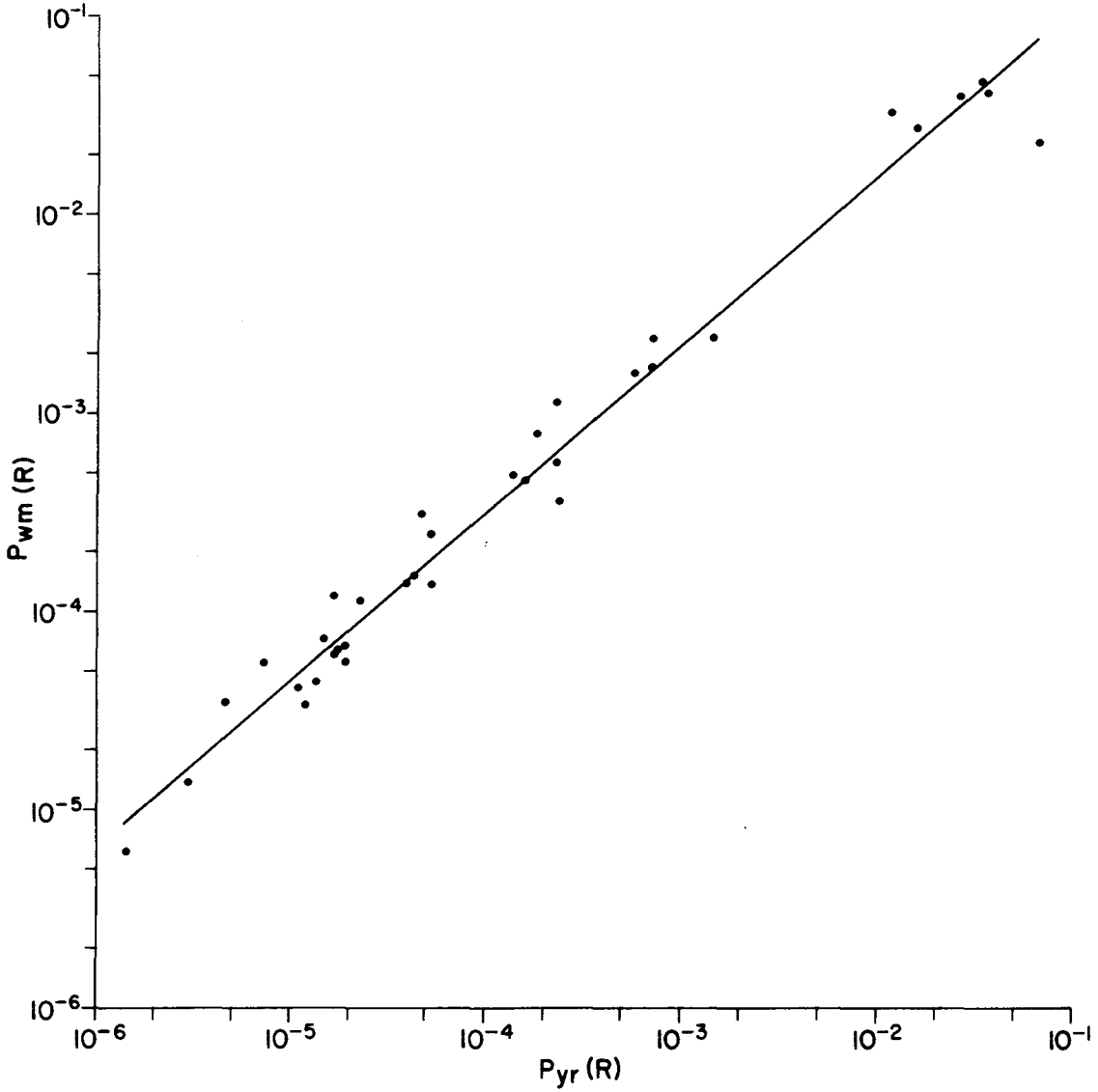

Figure 26. Worst calendar month rainfall probability versus annual probability for the same rain rate. Combined data are from six stations variously located across Canada.

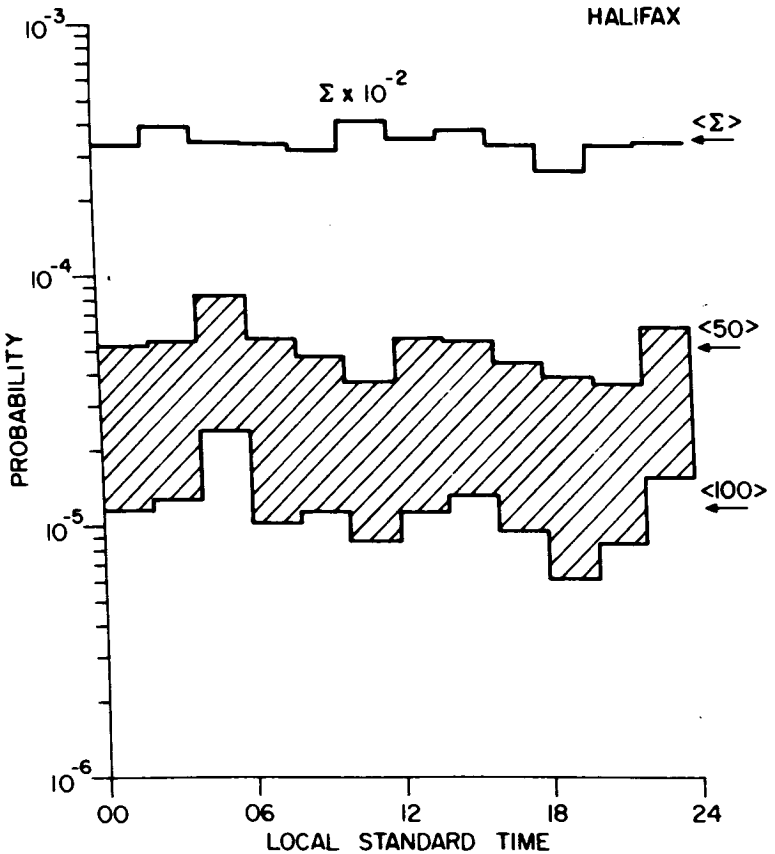

Figure 27(a). Mean diurnal variation in total and intense rainfall probabilities for Halifax, N.S. The uppermost curve has been multiplied by a factor of 10^{-2} in order to permit plotting on the existing scale. The arrows to the right of the graph indicate the mean probability of rainfall exceeding 50 mm/h and 100 mm/h as well as the total rainfall probability.

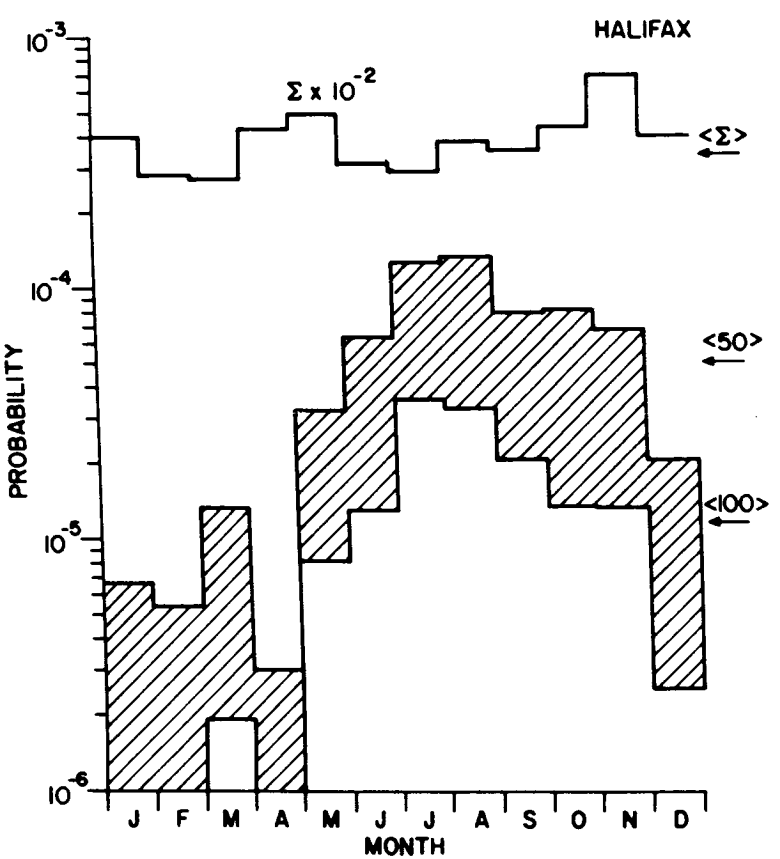

Figure 27(b). Mean seasonal variation in total and intense rainfall probabilities for Halifax, N.S. The uppermost curve has been multiplied by a factor of 10^{-2} in order to permit plotting on the existing scale. The arrows to the right of the graph indicate the mean probability of rainfall exceeding 50 mm/h and 100 mm/h as well as the total rainfall probability;

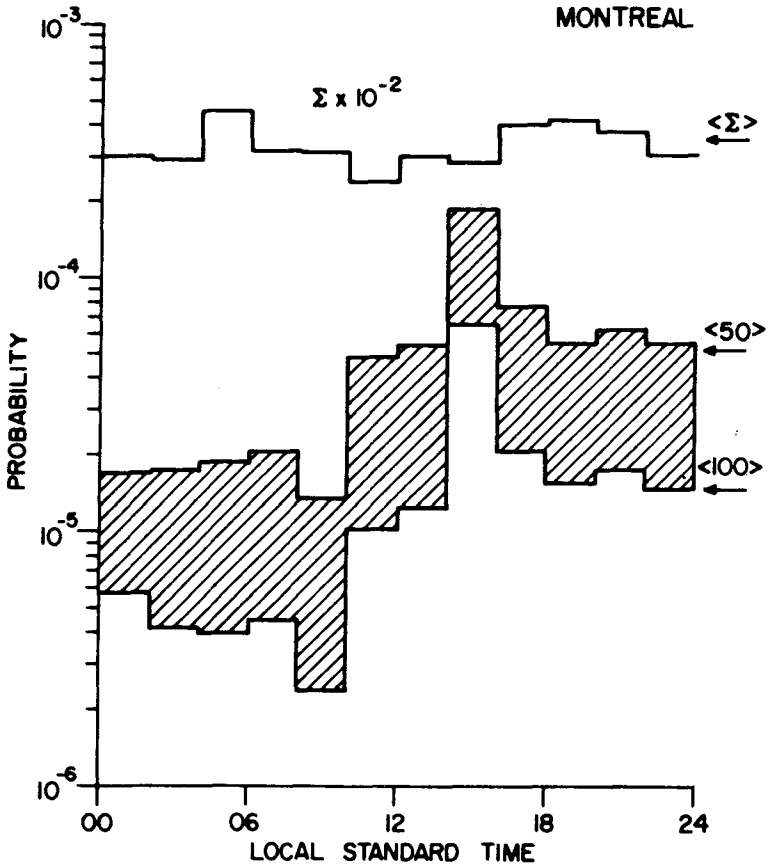

Figure 28(a). Mean diurnal variation in total and intense rainfall probabilities for Montreal, Que. The uppermost curve has been multiplied by a factor of 10^{-2} in order to permit plotting on the existing scale. The arrows to the right of the graph indicate the mean probability of rainfall exceeding 50 mm/h and 100 mm/h as well as the total rainfall probability.

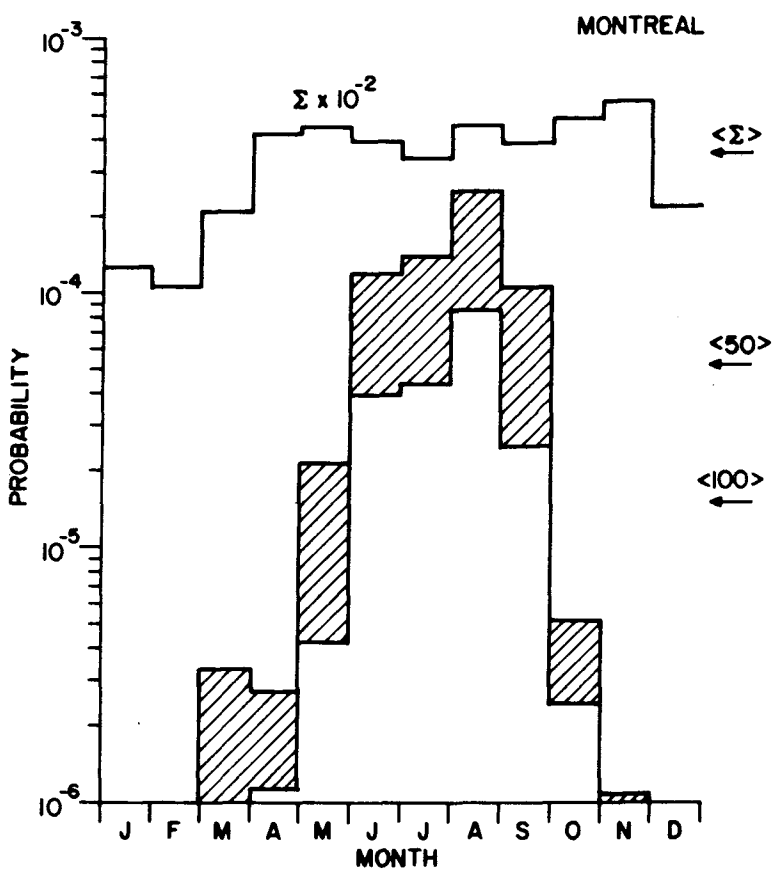

Figure 28(b). Mean seasonal variation in total and intense rainfall probabilities for Montreal, Que. The uppermost curve has been multiplied by a factor of 10^{-2} in order to permit plotting on the existing scale. The arrows to the right of the graph indicate the mean probability of rainfall exceeding 50 mm/h and 100 mm/h as well as the total rainfall probability.

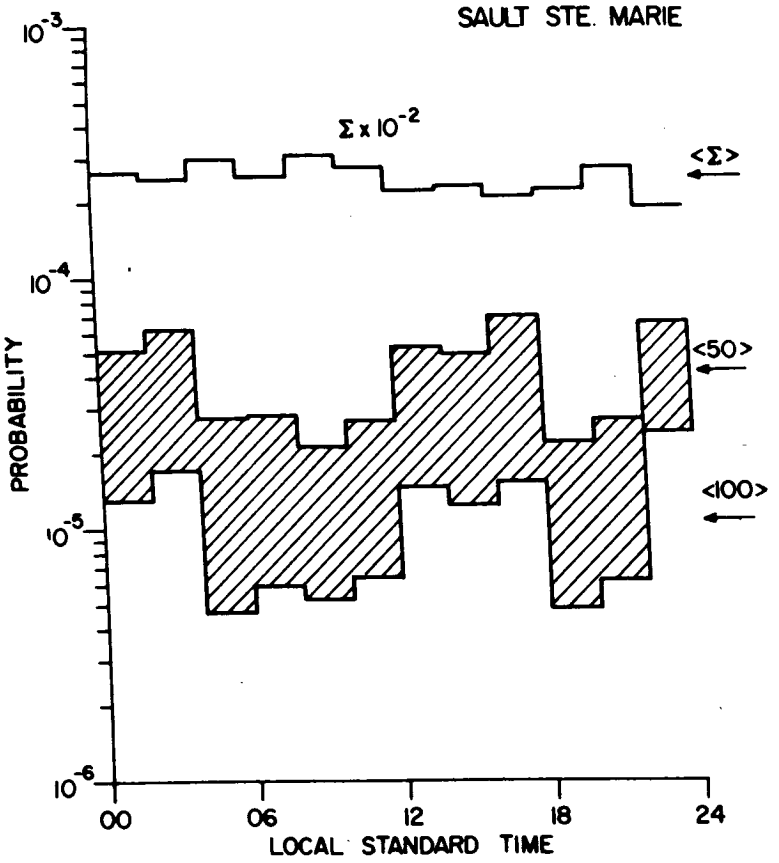

Figure 29(a). Mean diurnal variation in total and intense rainfall probabilities for Sault Ste. Marie, Ont. The uppermost curve has been multiplied by a factor of 10^{-2} in order to permit plotting on the existing scale. The arrows to the right of the graph indicate the mean probability of rainfall exceeding 50 mm/h and 100 mm/h as well as the total rainfall probability.

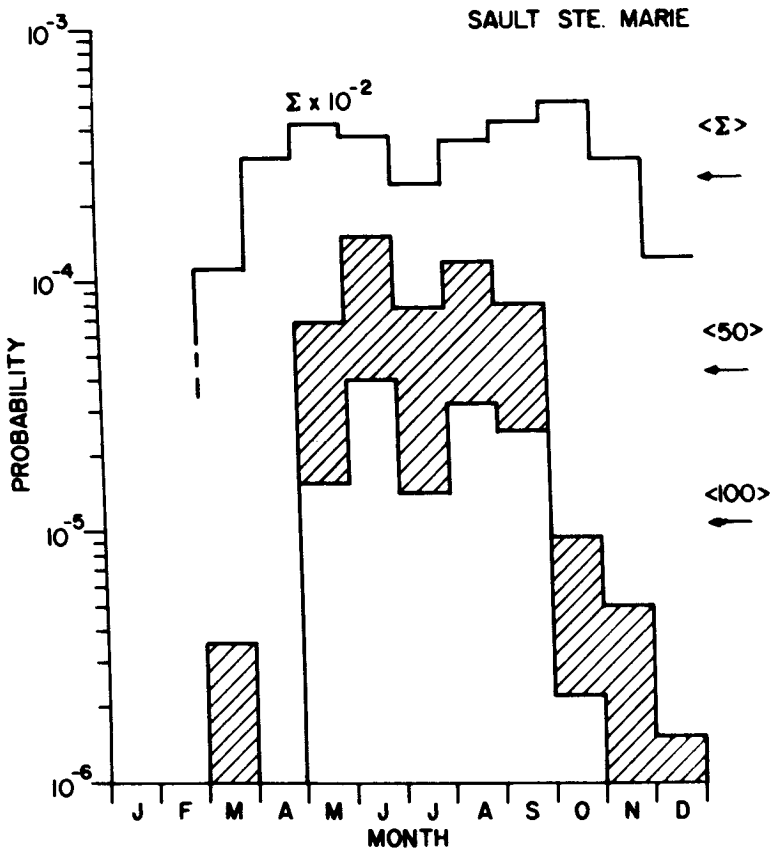

Figure 29(b). Mean seasonal variation in total and intense rainfall probabilities for Sault Ste. Marie, Ont. The uppermost curve has been multiplied by a factor of 10^{-2} in order to permit plotting on the existing scale. The arrows to the right of the graph indicate the mean probability of rainfall exceeding 50 mm/h and 100 mm/h as well as the total rainfall probability.

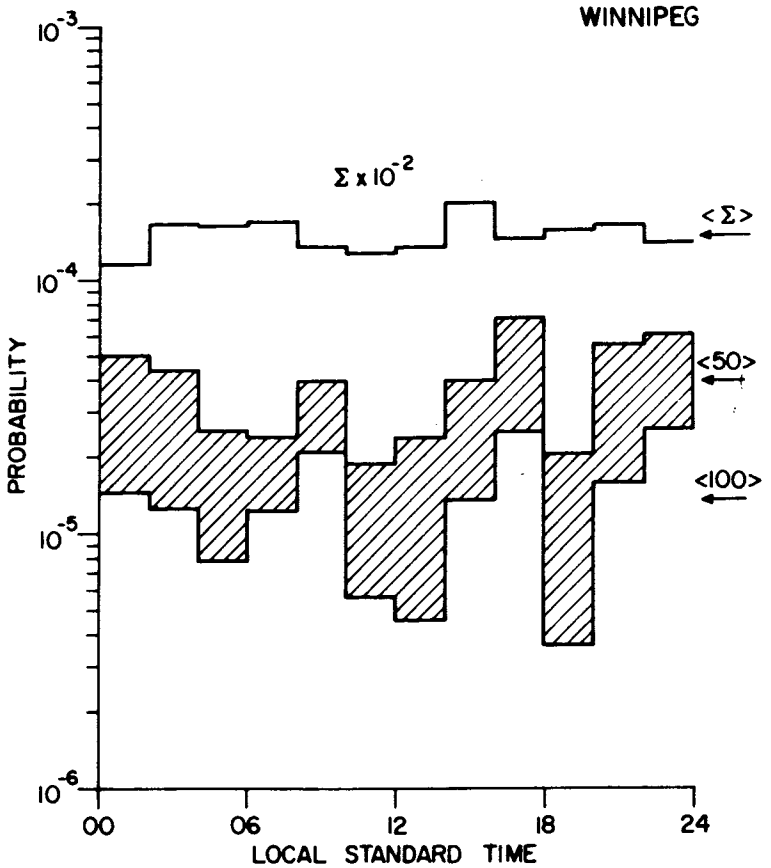

Figure 30(a). Mean diurnal variation in total and intense rainfall probabilities for Winnipeg, Man. The uppermost curve has been multiplied by a factor of 10^{-2} in order to permit plotting on the existing scale. The arrows to the right of the graph indicate the mean probability of rainfall exceeding 50 mm/h and 100 mm/h as well as the total rainfall probability.

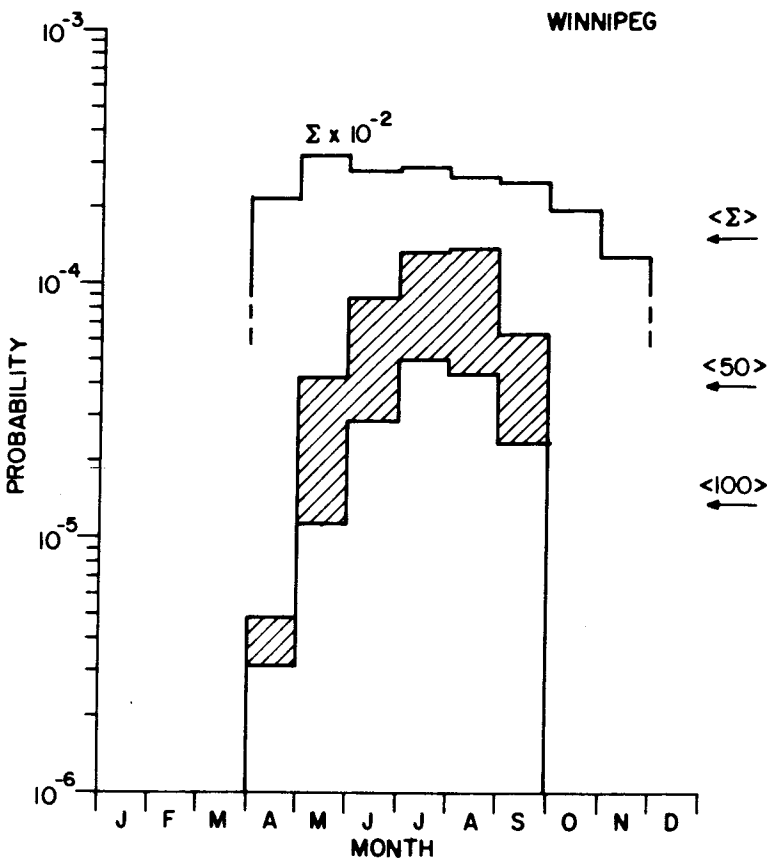

Figure 30(b). Mean seasonal variation in total and intense rainfall probabilities for Winnipeg, Man. The uppermost curve has been multiplied by a factor of 10^{-2} in order to permit plotting on the existing scale. The arrows to the right of the graph indicate the mean probability of rainfall exceeding 50 mm/h and 100 mm/h as well as the total rainfall probability.

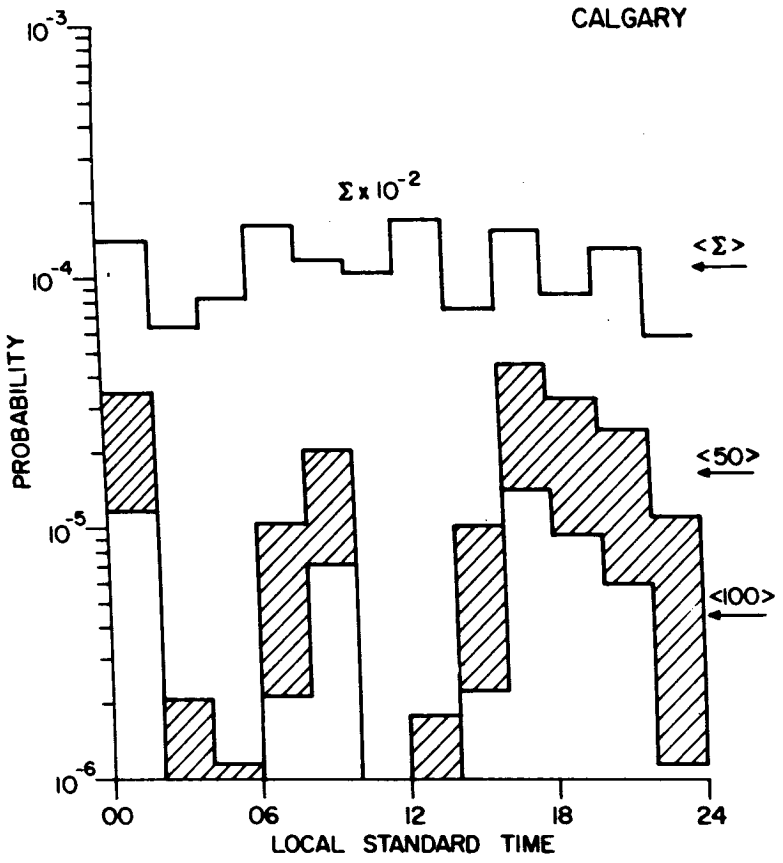

Figure 31(a). Mean diurnal variation in total and intense rainfall probabilities for Calgary, Alta. The uppermost curve has been multiplied by a factor of 10^{-2} in order to permit plotting on the existing scale. The arrows to the right of the graph indicate the mean probability of rainfall exceeding 50 mm/h and 100 mm/h as well as the total rainfall probability.

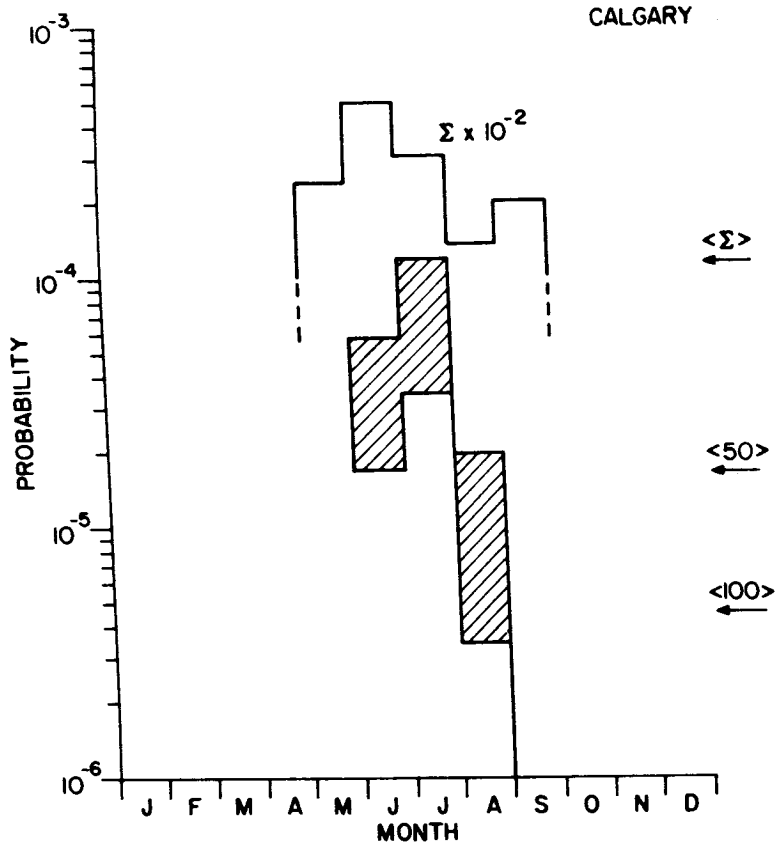

Figure 31(b). Mean seasonal variation in total and intense rainfall probabilities for Calgary, Alta. The uppermost curve has been multiplied by a factor of 10^{-2} in order to permit plotting on the existing scale. The arrows to the right of the graph indicate the mean probability of rainfall exceeding 50 mm/h and 100 mm/h as well as the total rainfall probability.

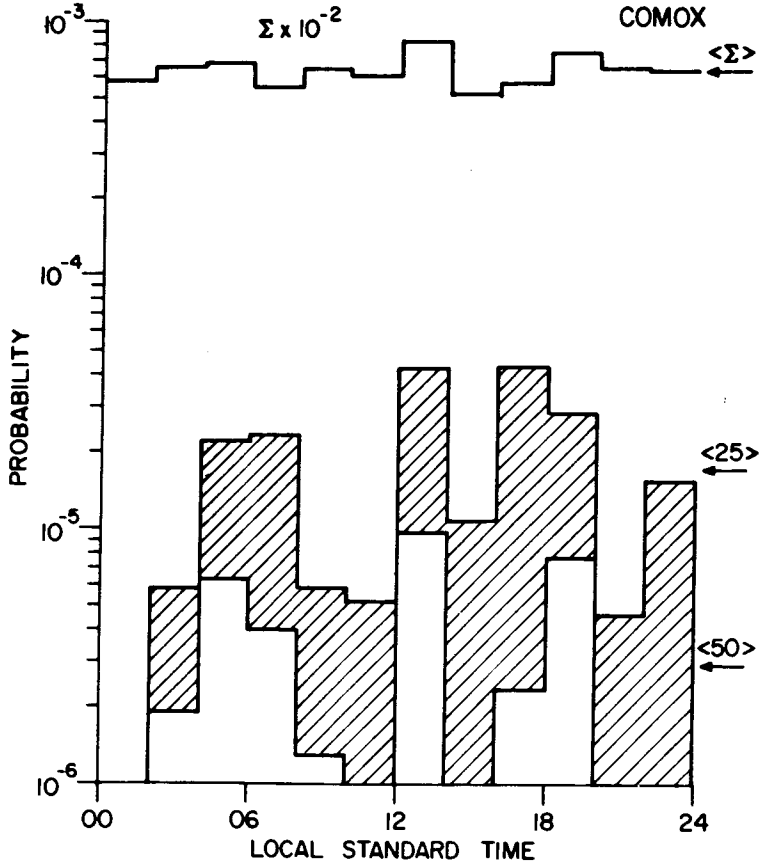

Figure 32(a). Mean diurnal variation in total and intense rainfall probabilities for Comox, B.C. The arrows to the right of the graph indicate the mean probability of rainfall exceeding 25 mm/h and 50 mm/h (c.f. 50 mm/h and 100 mm/h for preceding examples) as well as total rainfall probability x 10^{-2}.

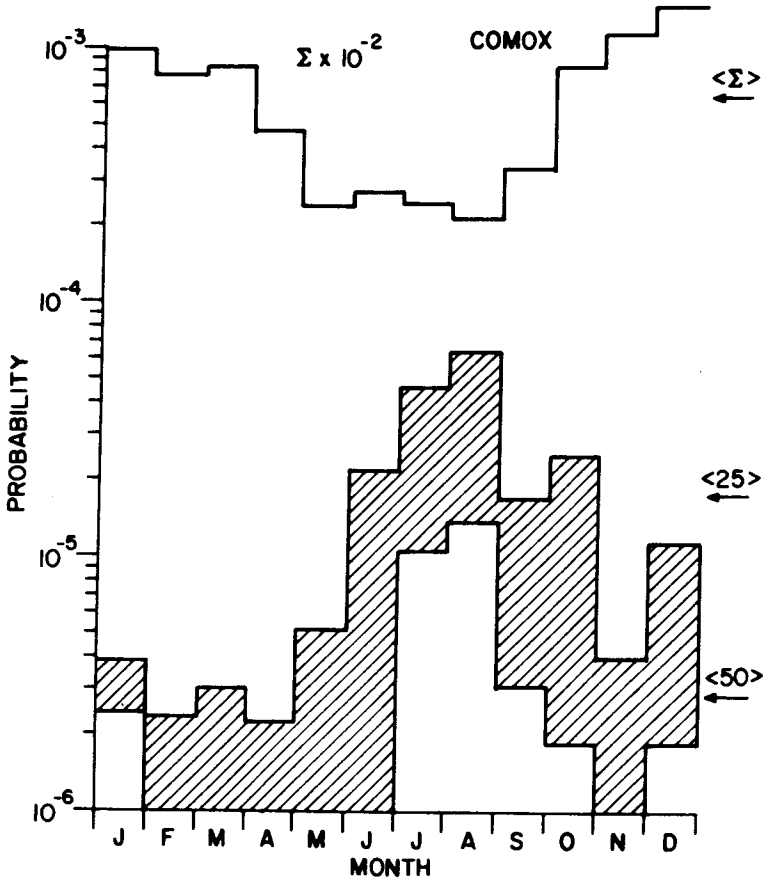

Figure 32(b). Mean seasonal variation in total and intense rainfall probabilities for Comox, B.C. The arrows to the right of the graph indicate the mean probability of rainfall exceeding 25 mm/h and 50 mm/h (c.f. 50 mm/h and 100 mm/h for preceding examples) as well as total rainfall probability x 10^{-2}.

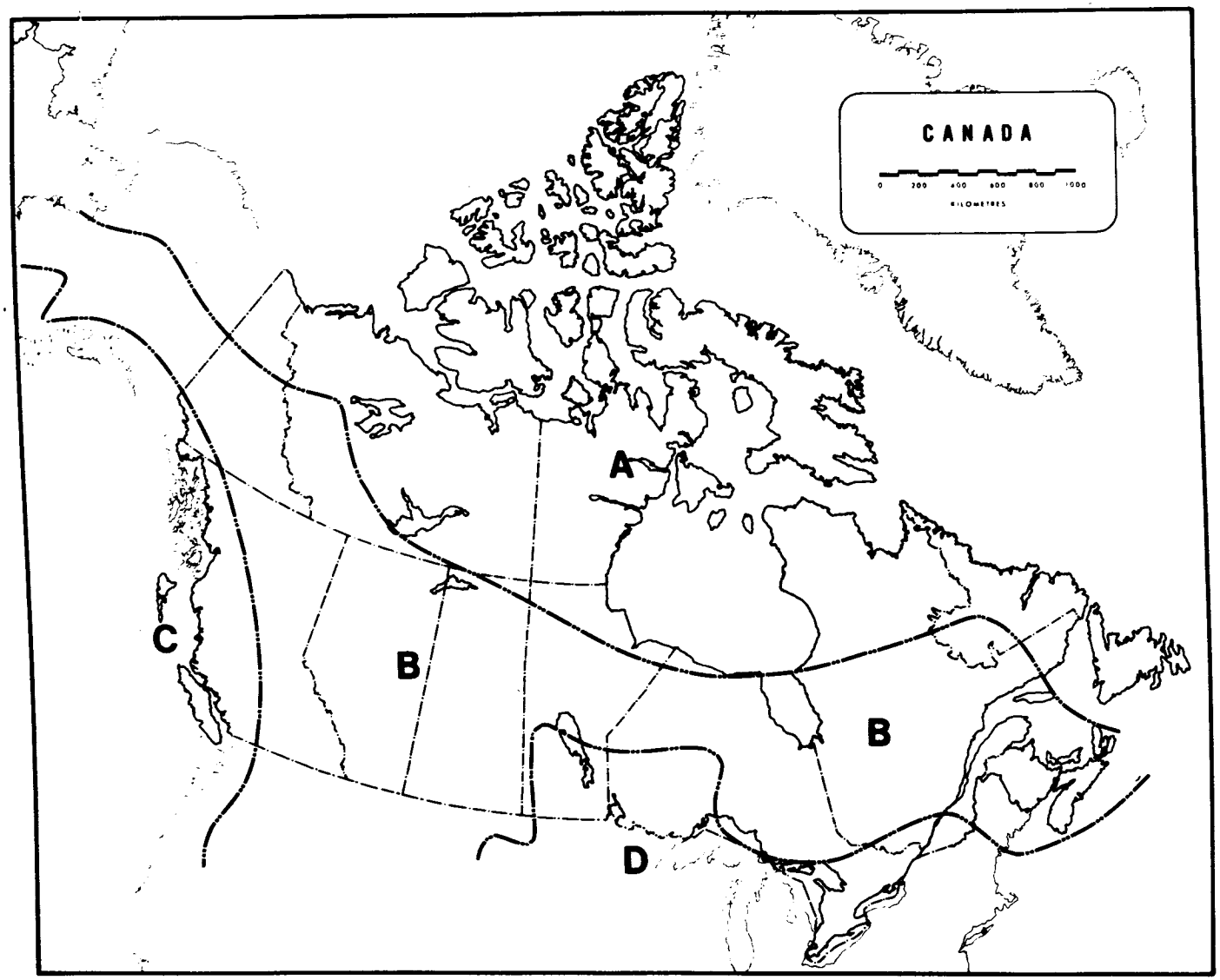

Figure 33. Rainfall regions within Canada according to the CCIR (1978b) classification

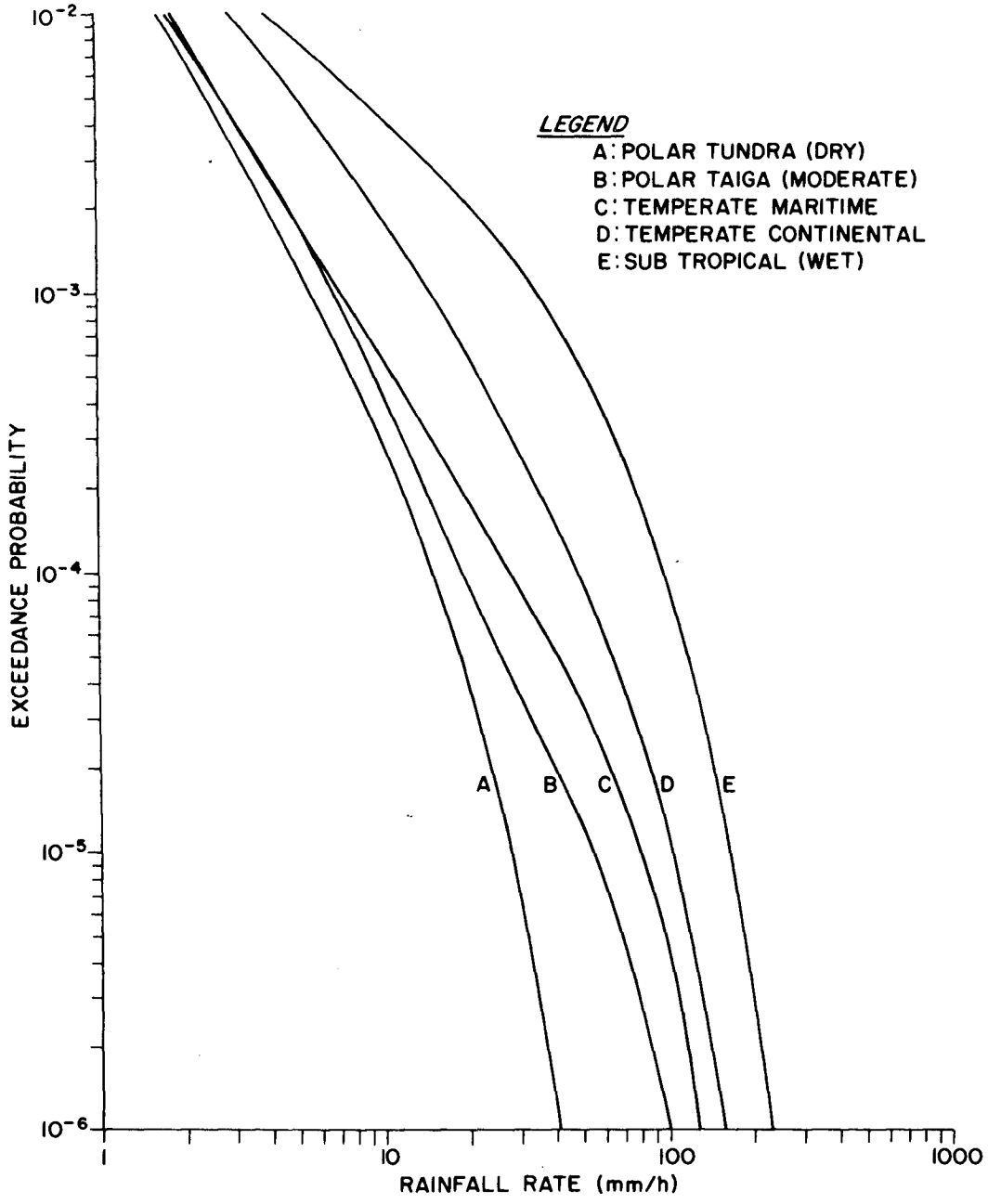

Figure 34. Complementary distribution functions for CCIR (1978b) rainfall rate climatic zones. Curves have been extrapolated to the 10^{-6} probability level for comparison with results presented in Figures 43 to 89.

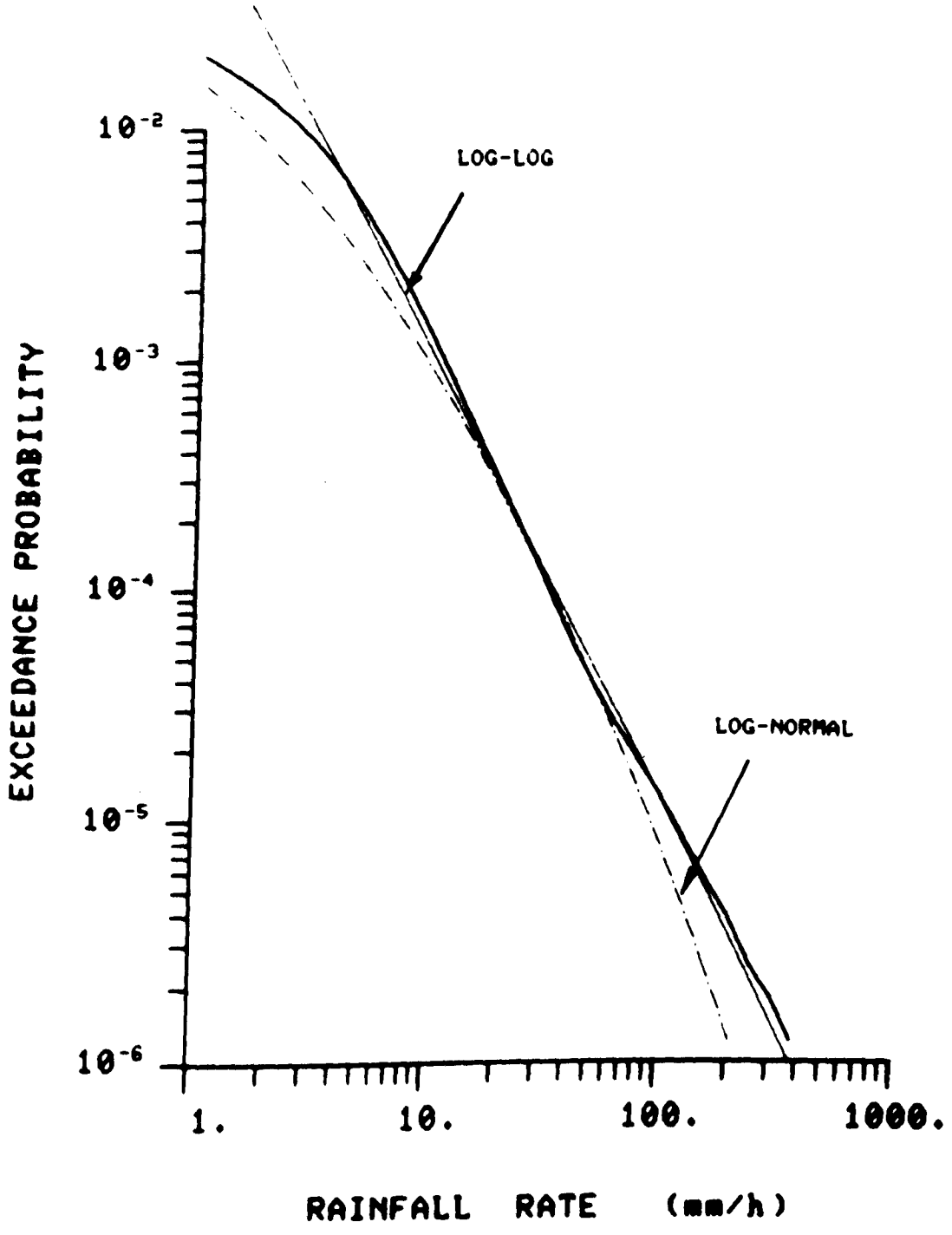

Figure 35. High-resolution rainfall distribution curve for Saint Joh, N.B. with both log-log (solid line) and log-normal (broken line) approximations. The latter was derived by constraining the curve to fit the analytical data at R=0.25 mm/h and at R=50 mm/h.

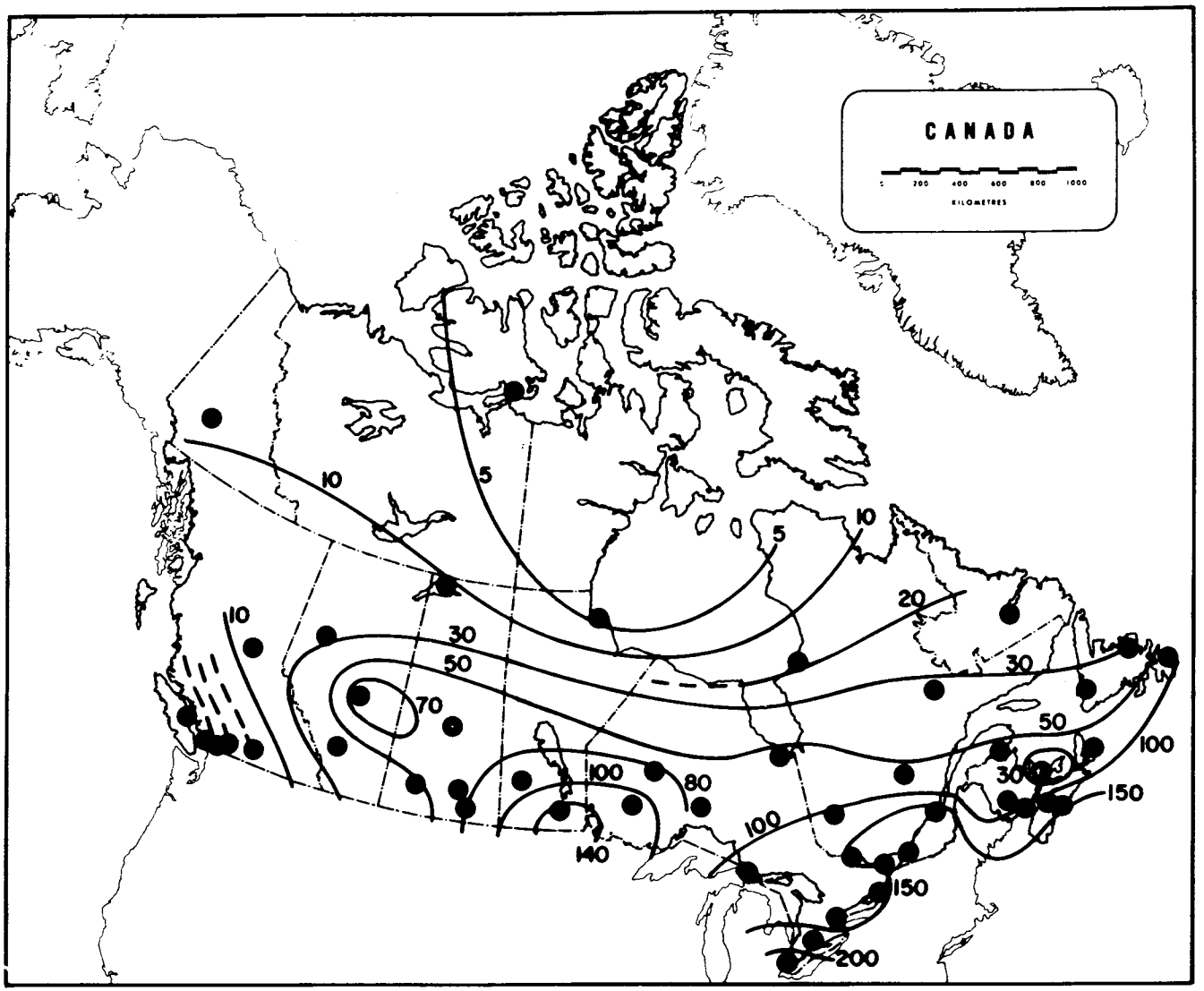

Figure 36. Contours of constant P_o against a background showing the location of all stations employed in this study. The numerical values shown beside the isopleths correspond to $10^7 P_o$.

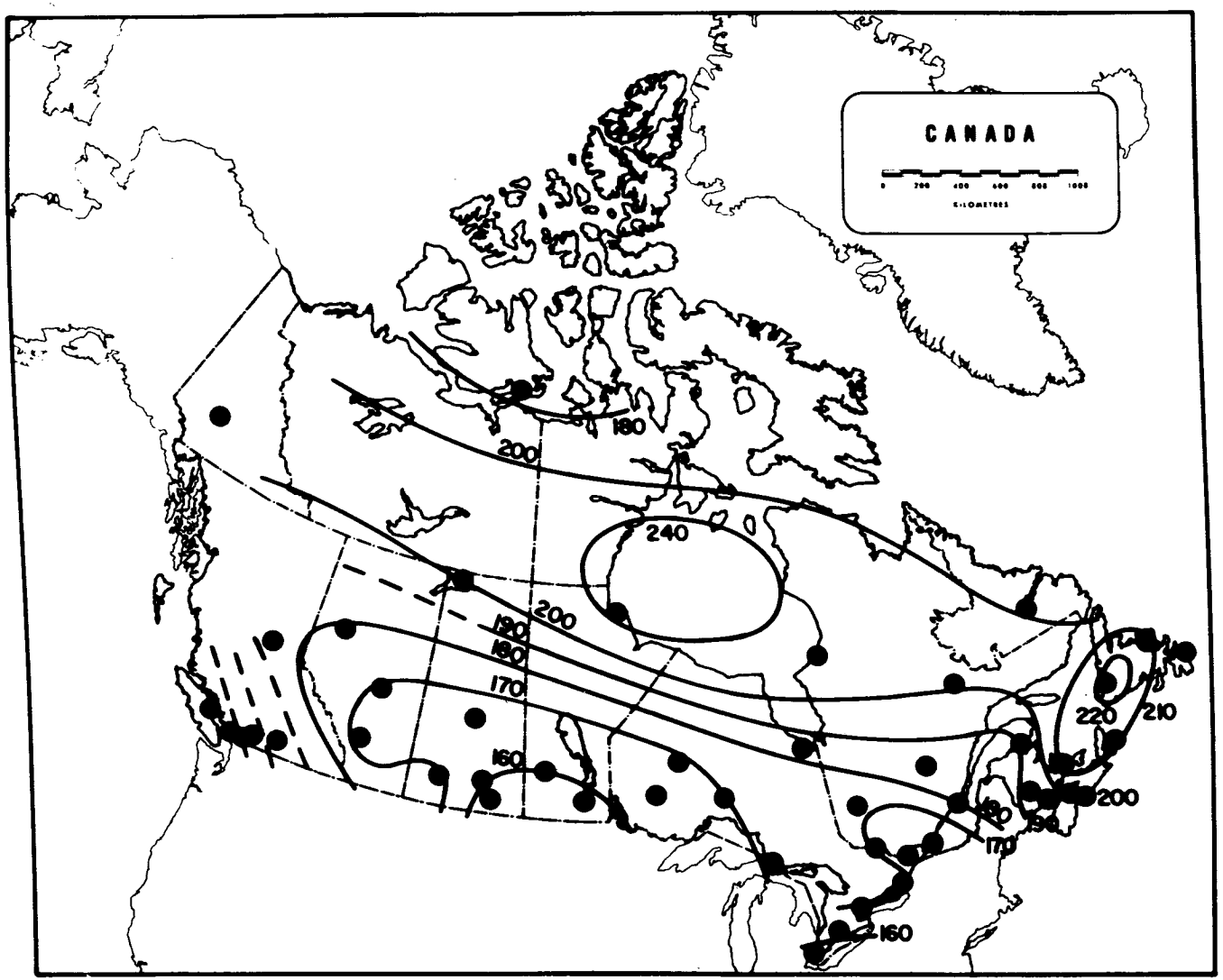

Figure 37. Contours of constant γ. The numerical values shown beside the isopleths correspond to −100 γ.

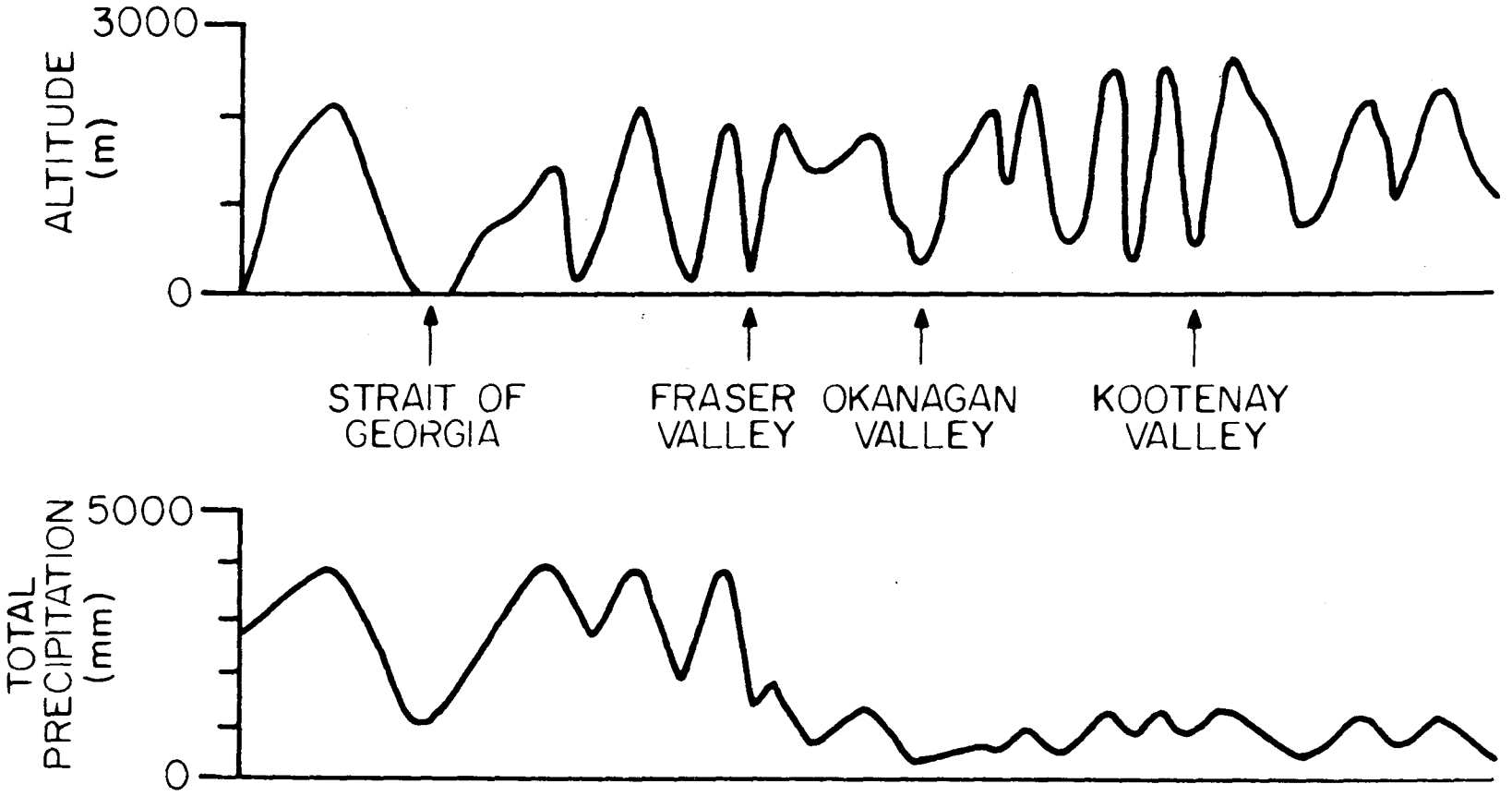

Figure 38. Topographic contour and precipitation trends along an East–West section through southern British Columbia. (Chapman, et. al., 1956).

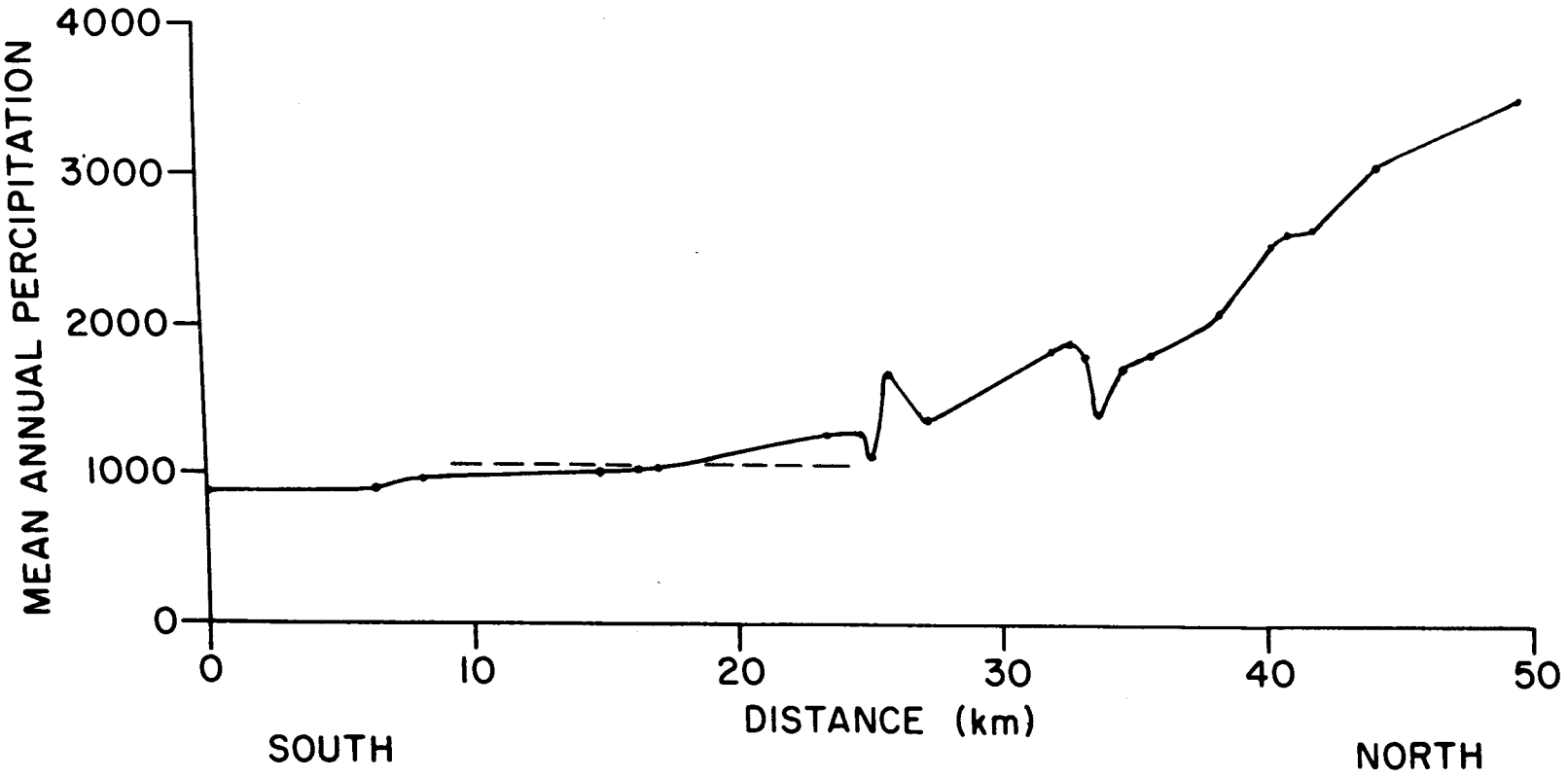

Figure 39. Annual rainfall occurring along a North–South strip in the greater Vancouver area. For reference, the dashed line indicates the average recorded rainfall for Vancouver International Airport which is located slightly west of the stations considered here (Wright and Trenholm, 1969; Anon., 1976).

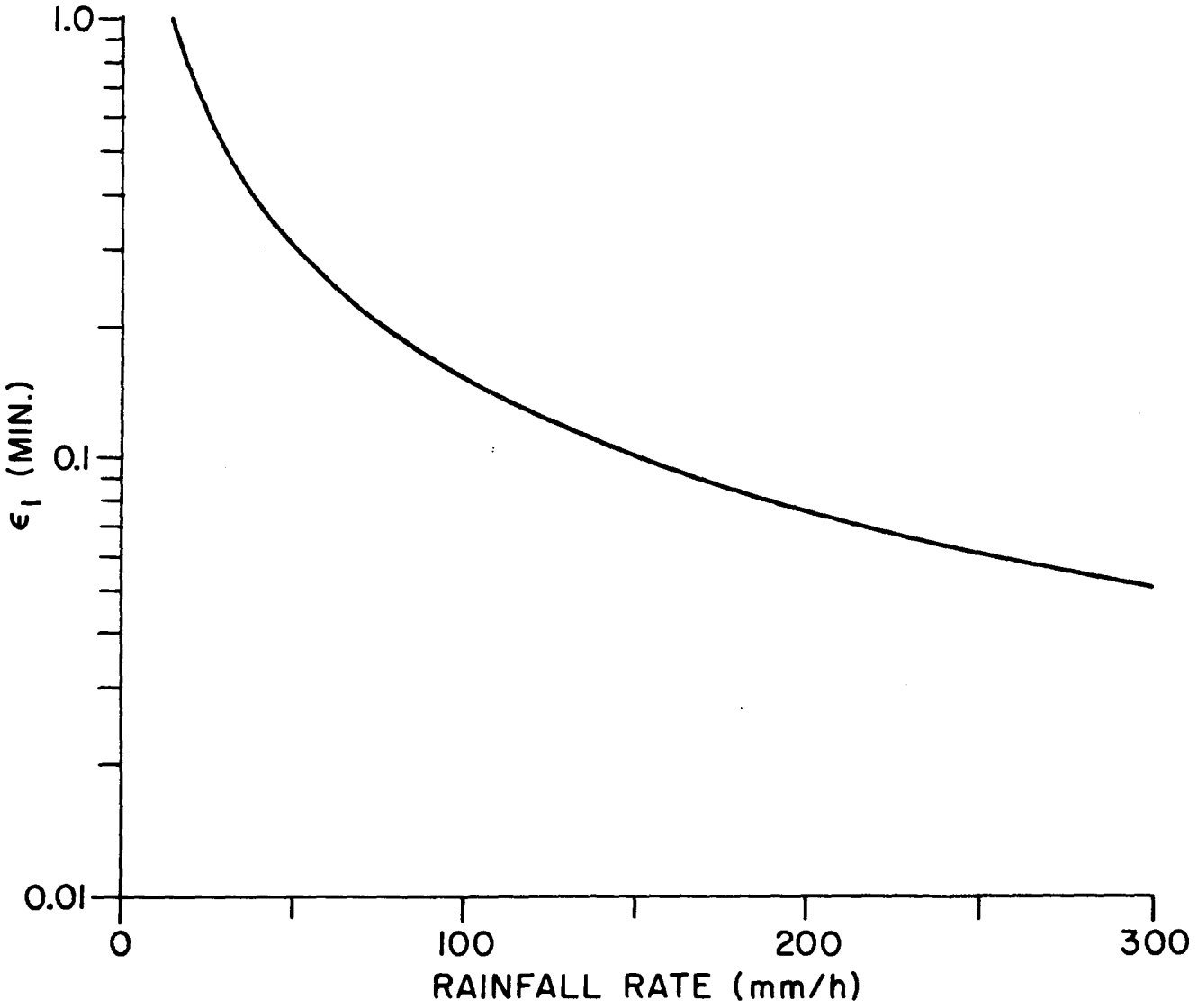

Figure 40. Time required to fill one bucket of a tipping-bucket rain gauge

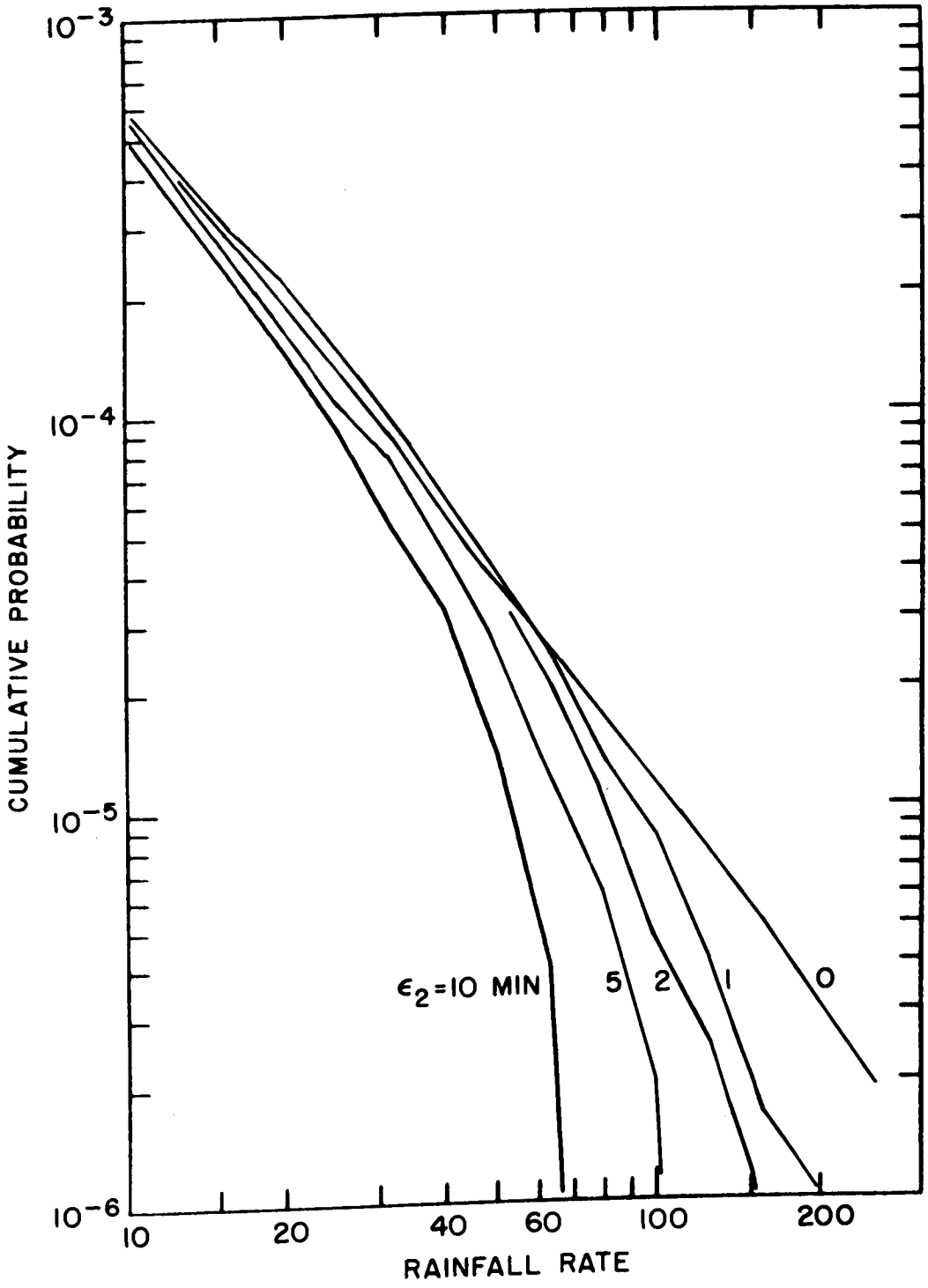

Figure 41. Changes in the cumulative rain rate distribution as a function of integration time for Kingston, Ontario

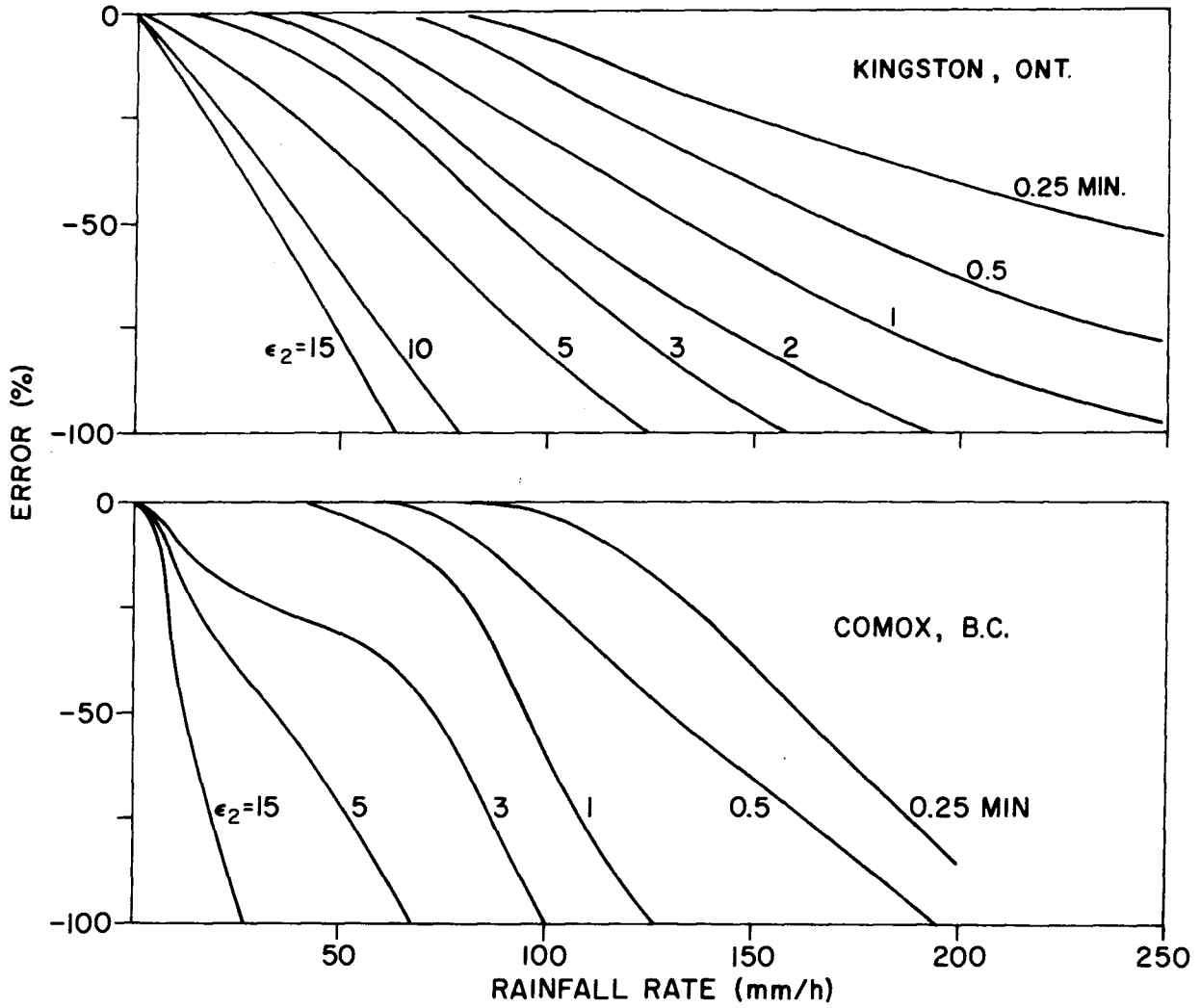

Figure 42. Error in rainfall exceedance probability resulting from finite resolution time of measuring system, relative to "instantaneous" response.

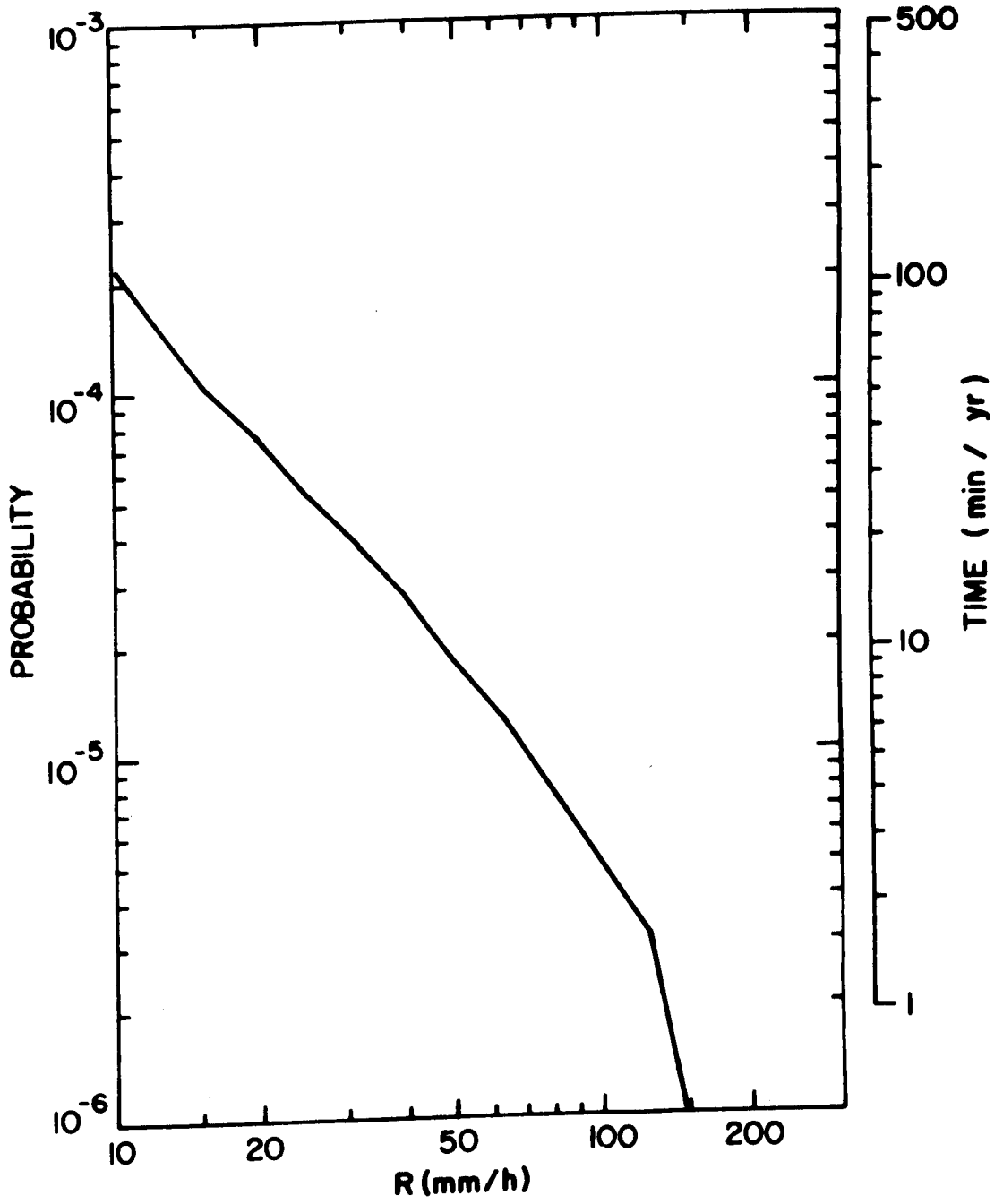

Figure 43. Long term average probability of exceeding a given rainfall rate at Calgary, Alta.

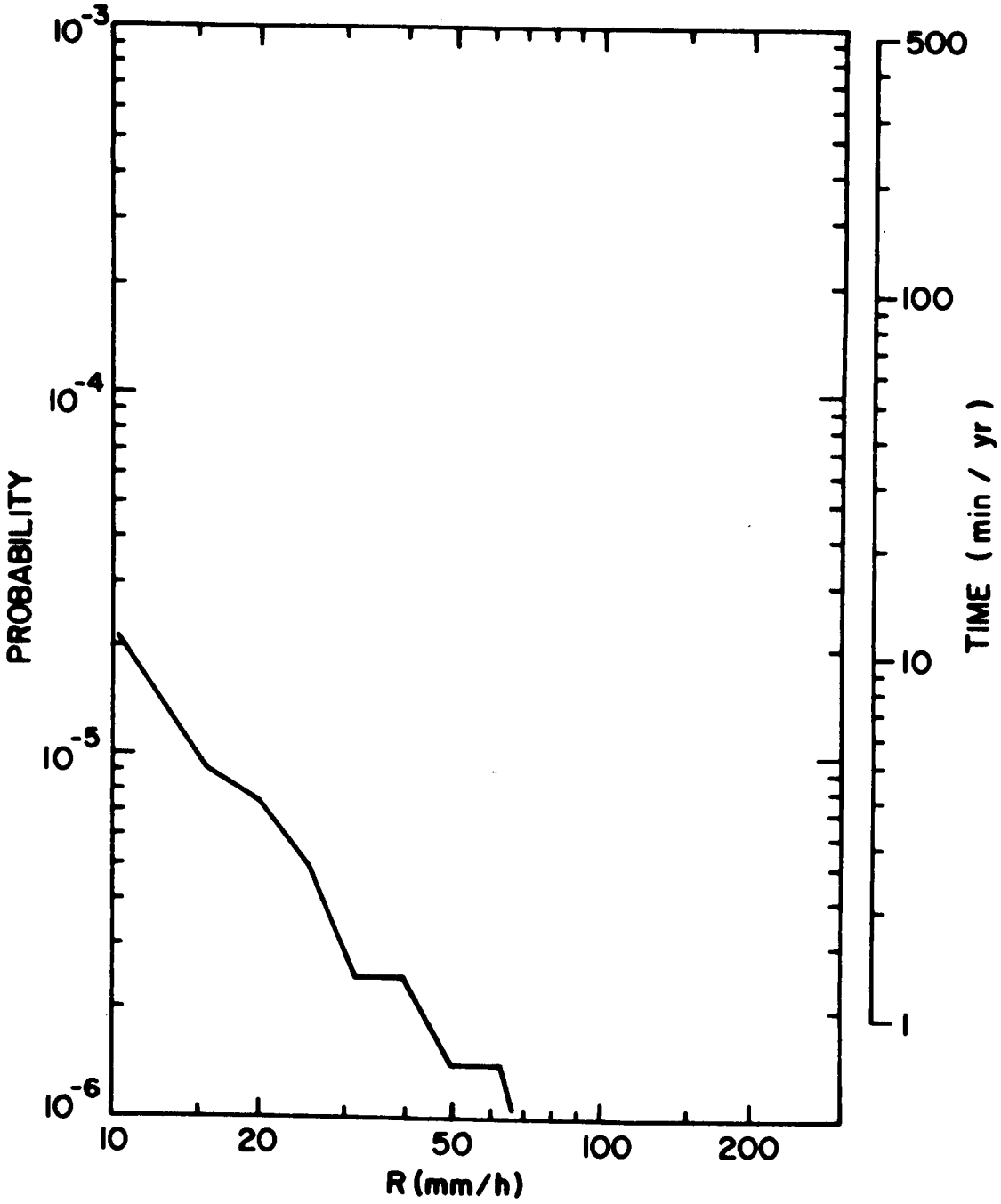

Figure 44. Long term average probability of exceeding a given rainfall rate at Cambridge Bay, N.W.T.

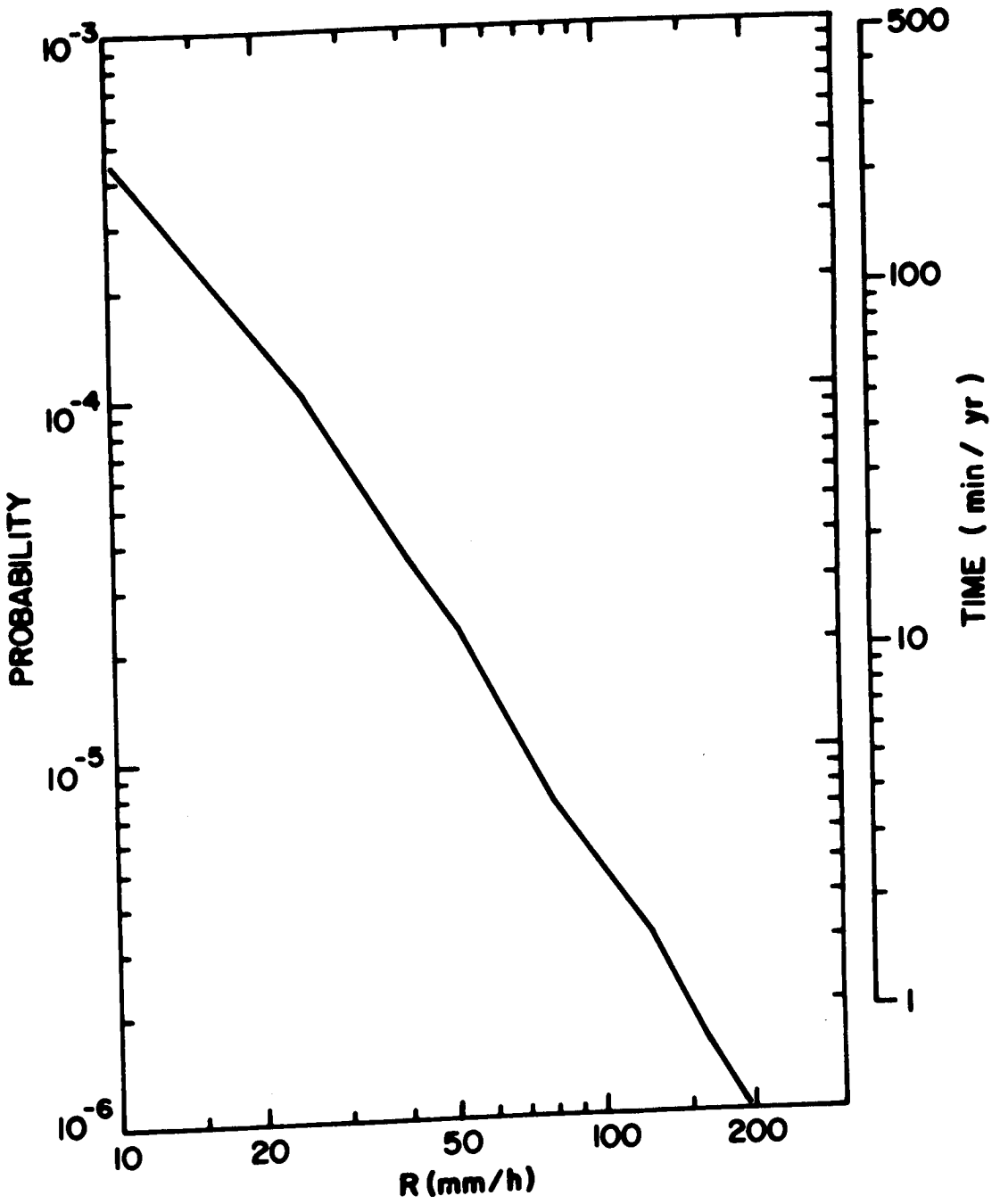

Figure 45. Long term average probability of exceeding a given rainfall rate at Caplan, Que.

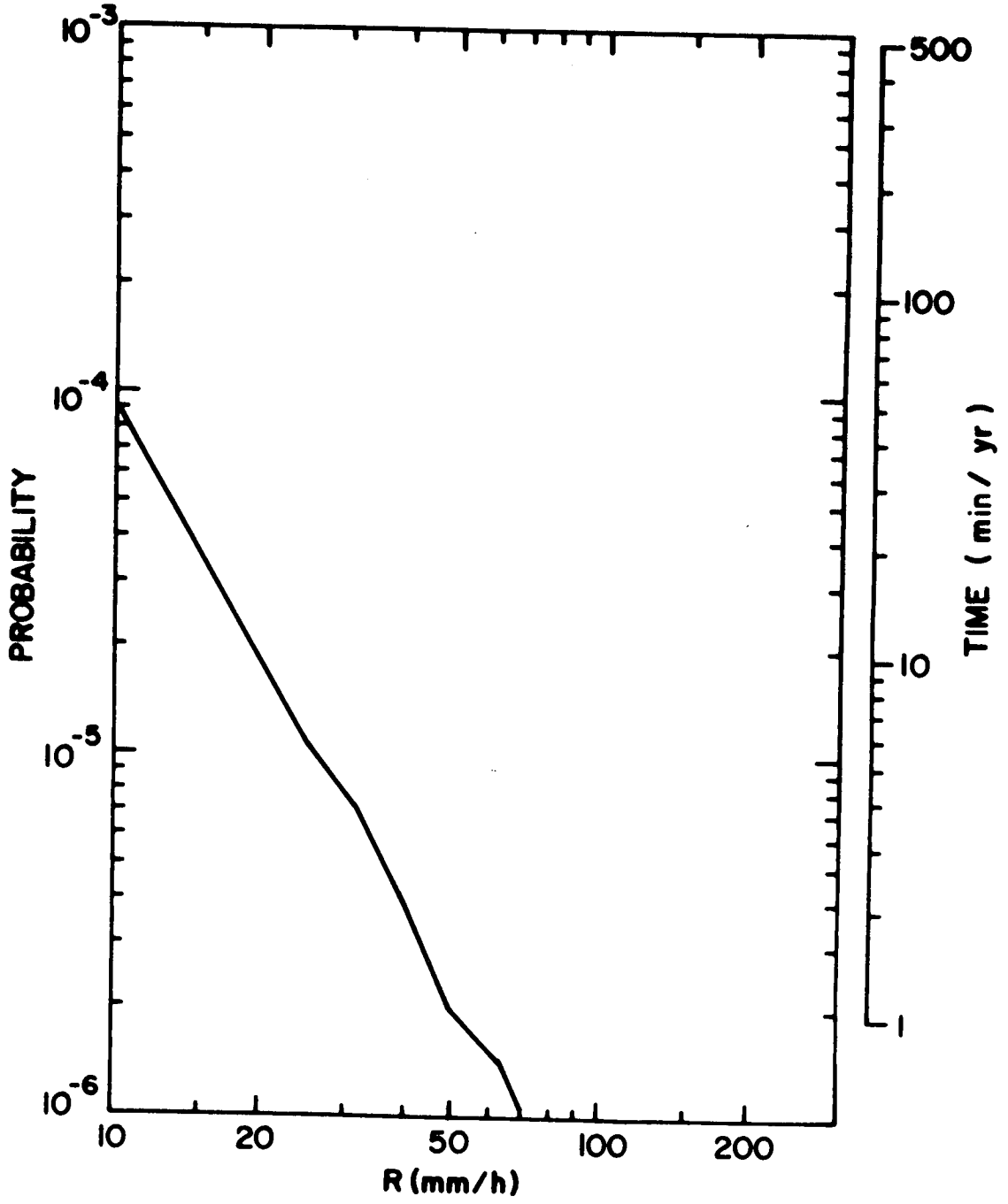

Figure 46. Long term average probability of exceeding a given rainfall rate at Carmacks, Y.T.

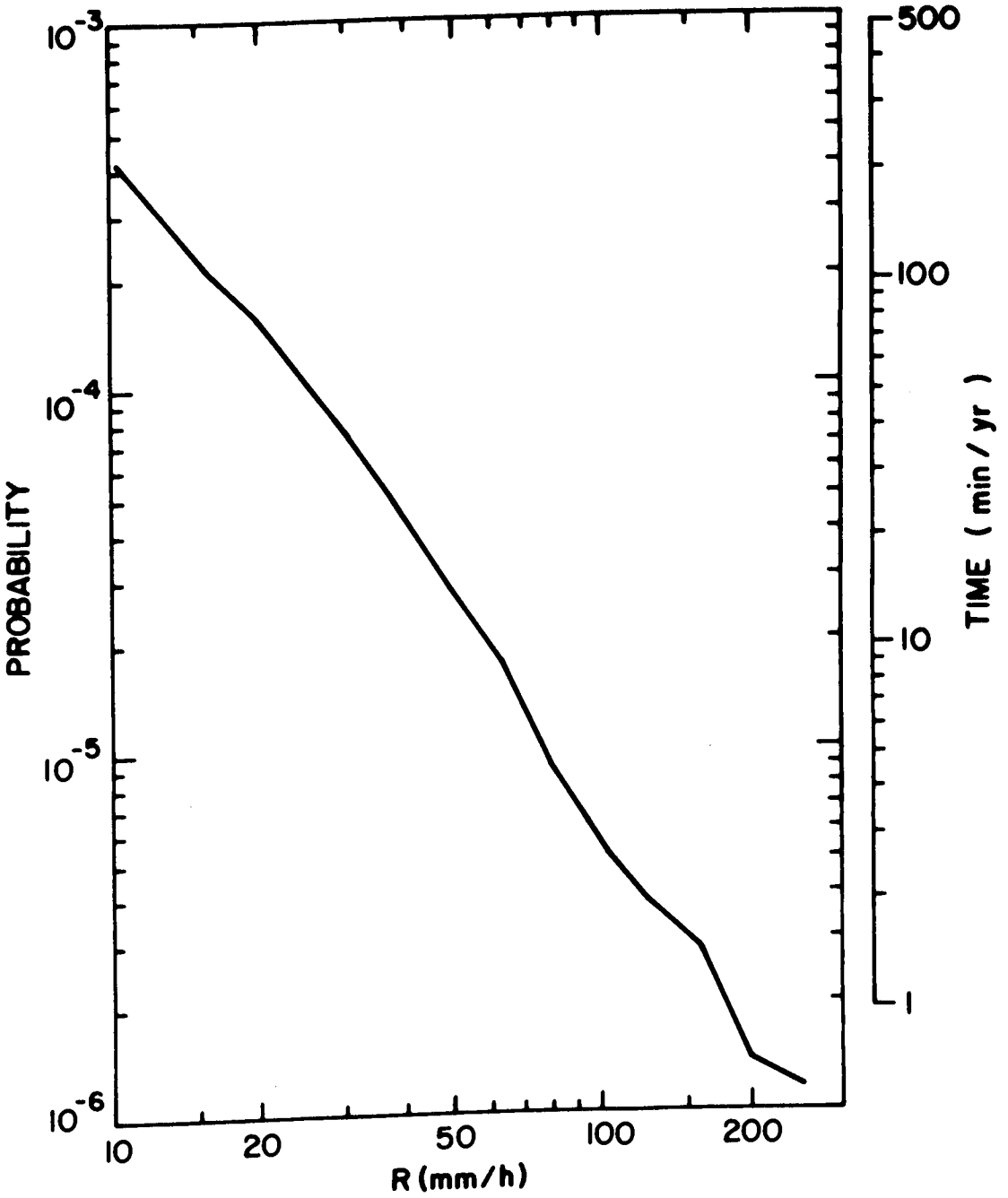

Figure 47. Long term average probability of exceeding a given rainfall rate at Central Patricia, Ont.

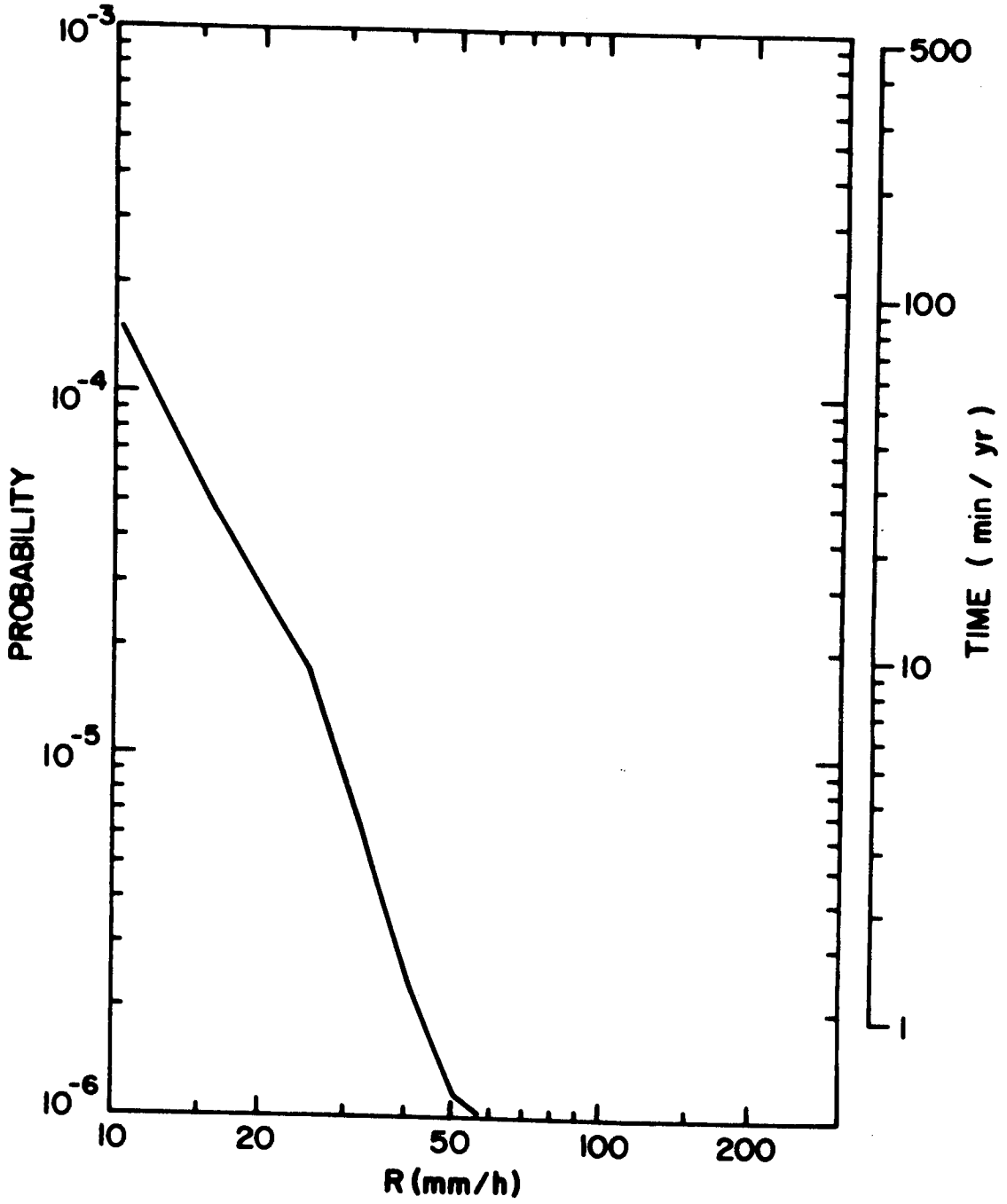

Figure 48. Long term average probability of exceeding a given rainfall rate at Churchill, Man.

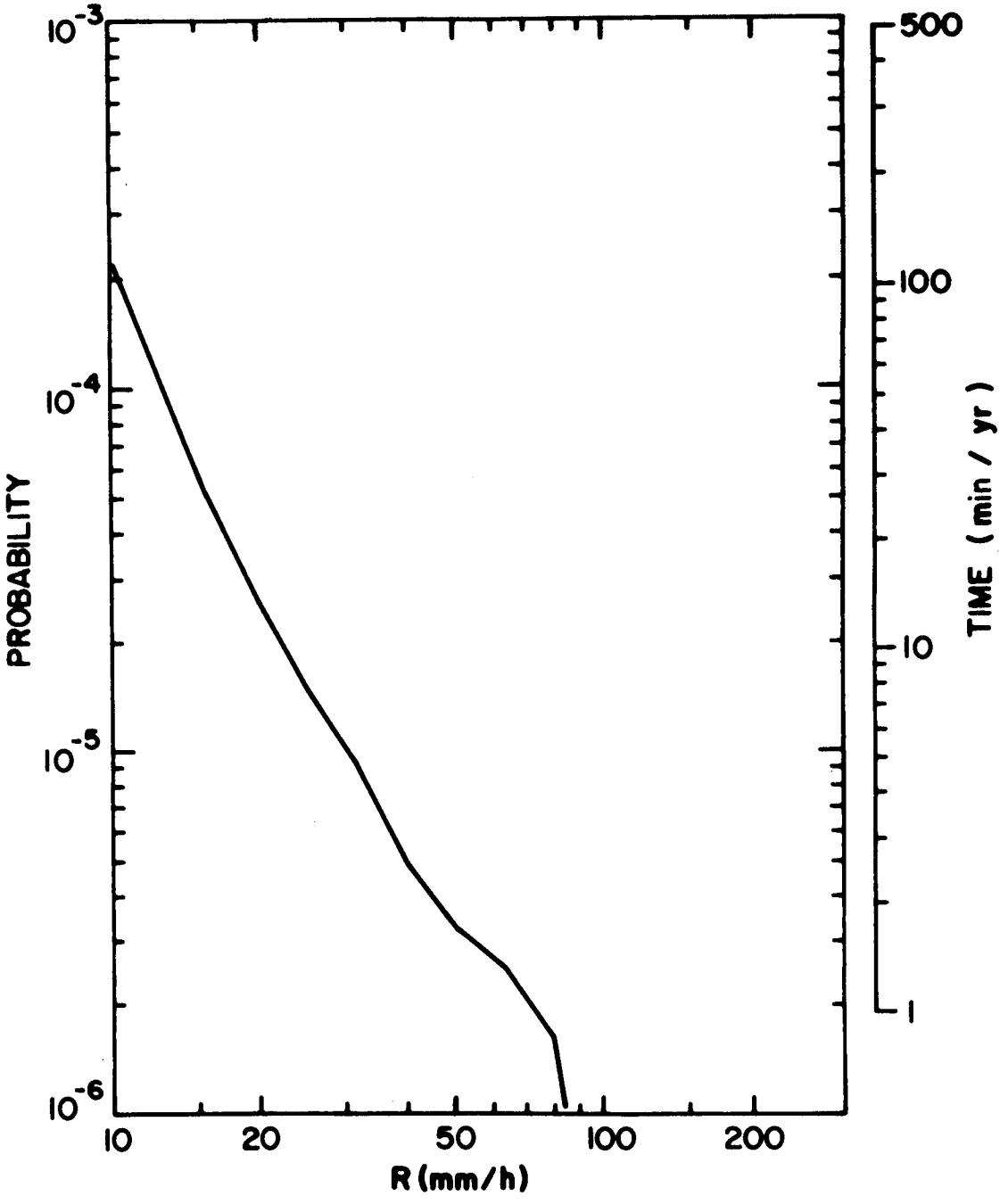

Figure 49. Long term average probability of exceeding a given rainfall rate at Comox, B.C.

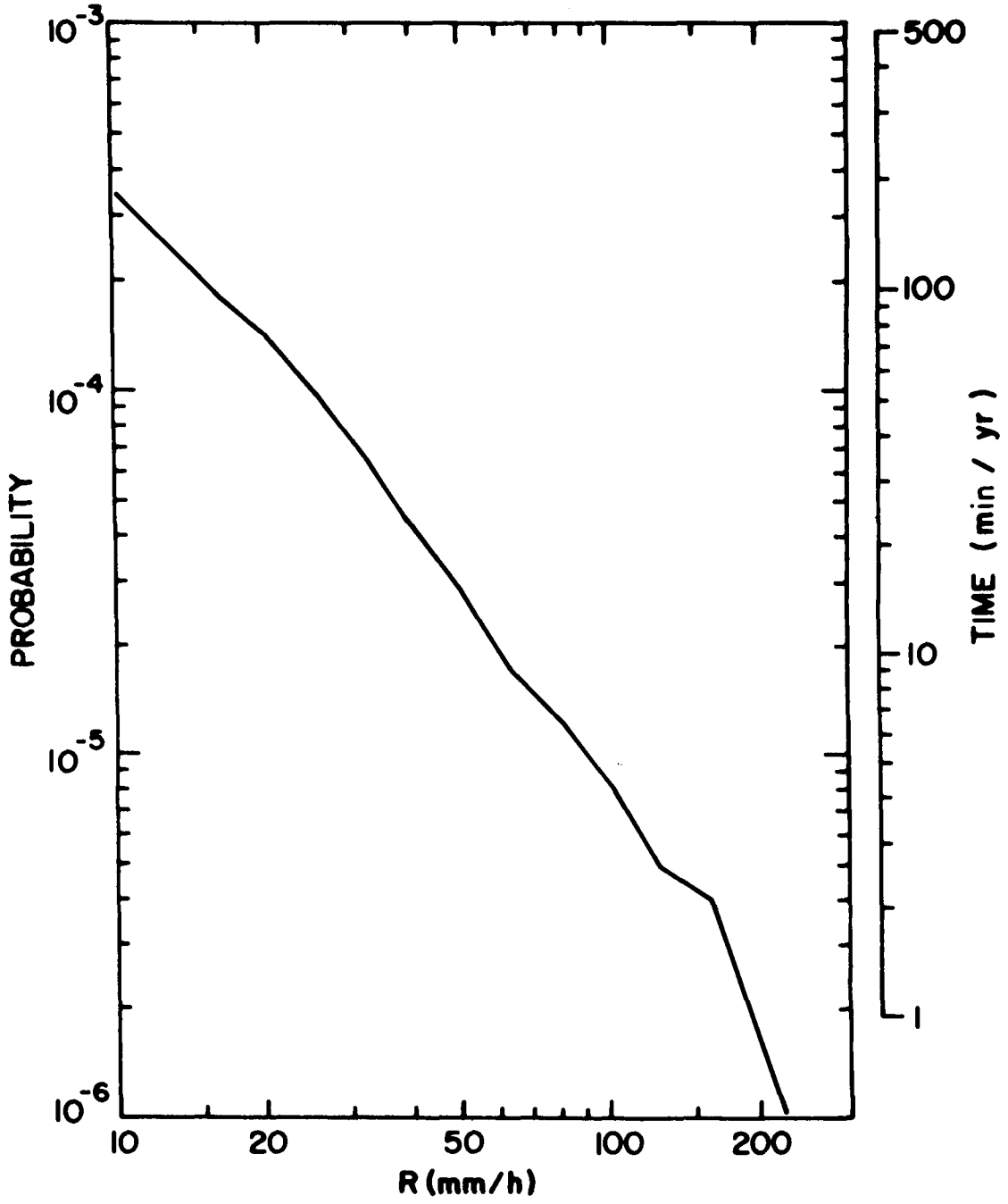

Figure 50. Long term average probability of exceeding a given rainfall rate at Dauphin, Man.

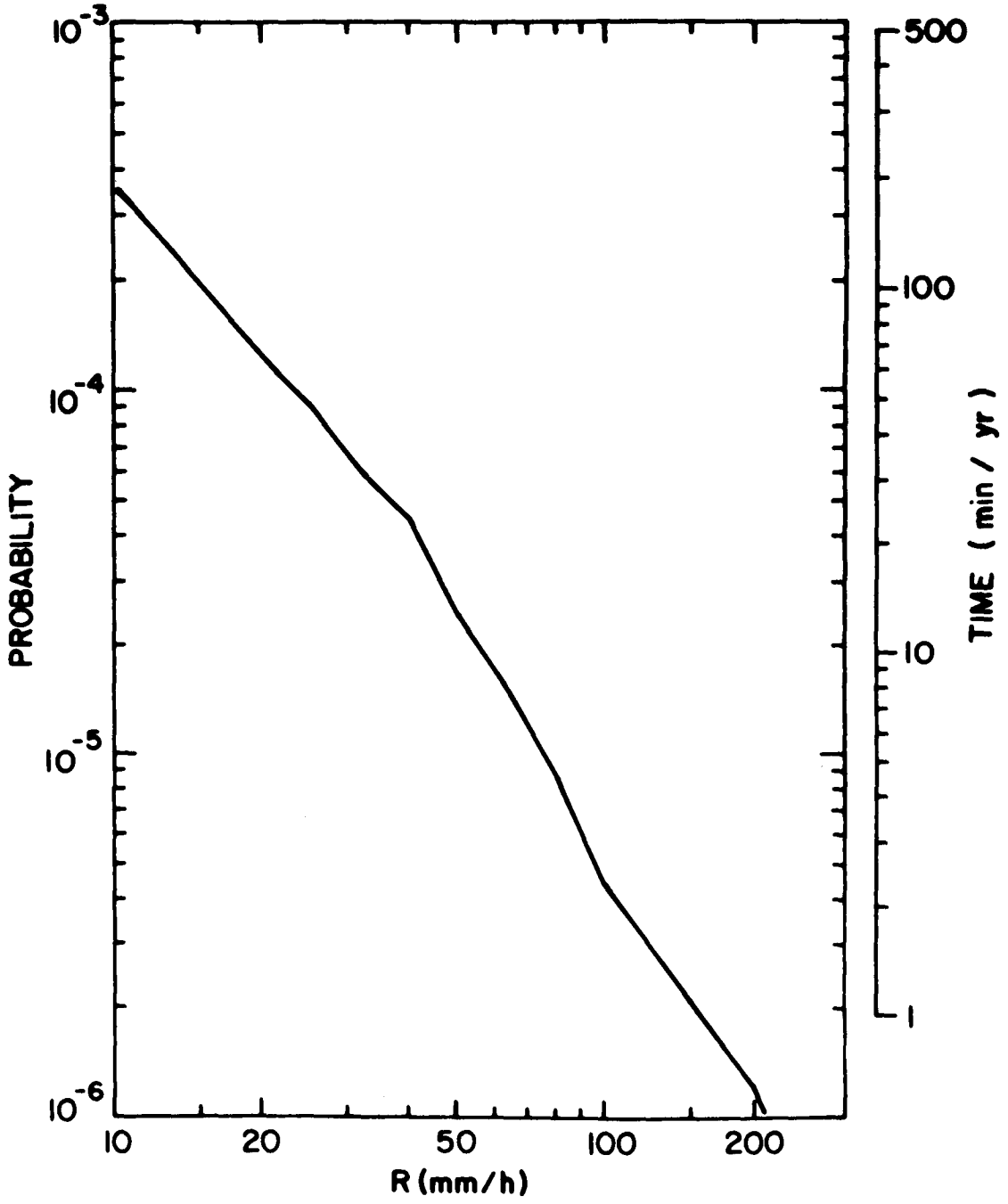

Figure 51. Long term average probability of exceeding a given rainfall rate at Edmonton, Alta.

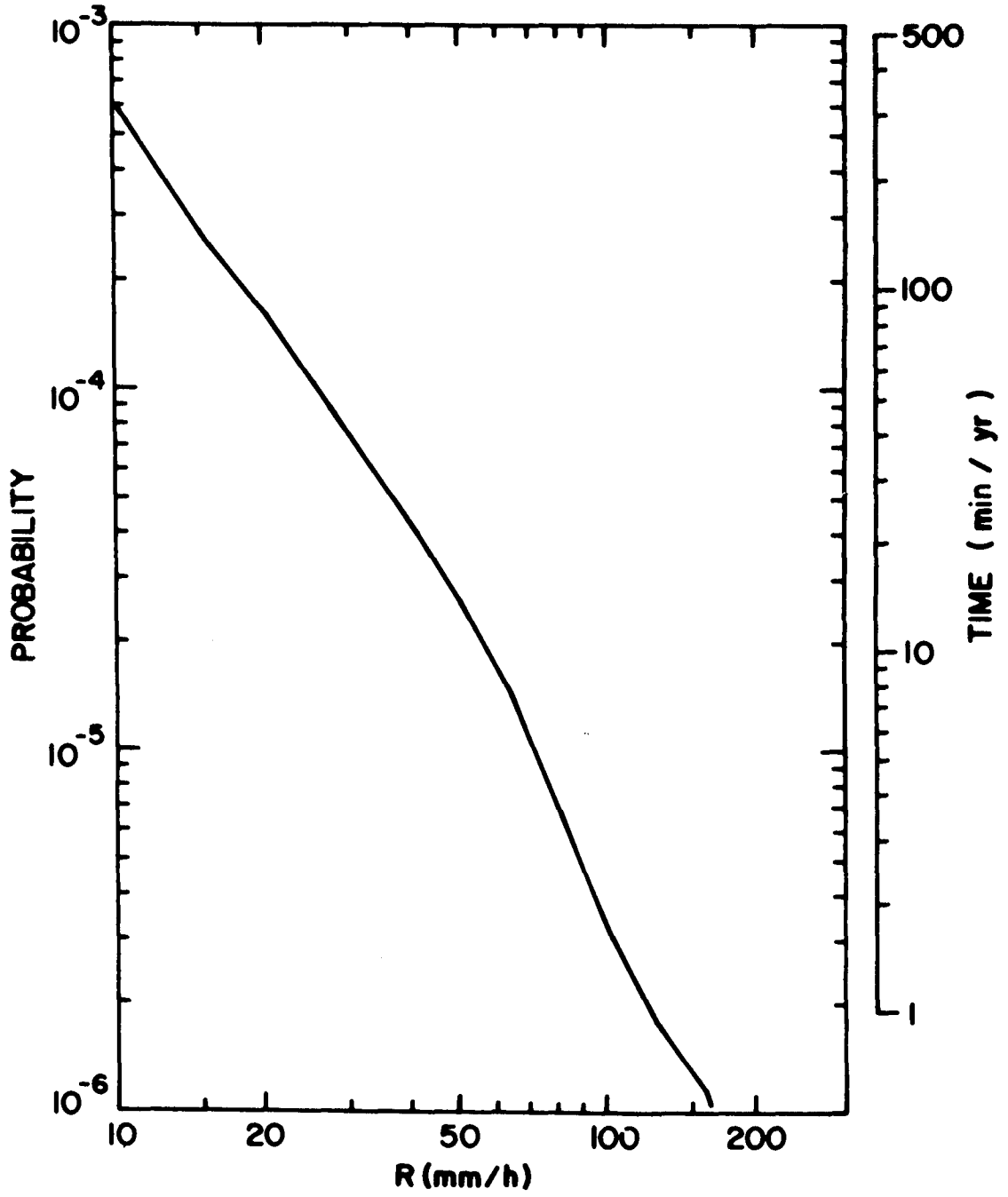

Figure 52. Long term average probability of exceeding a given rainfall rate at Fredericton, N.B.

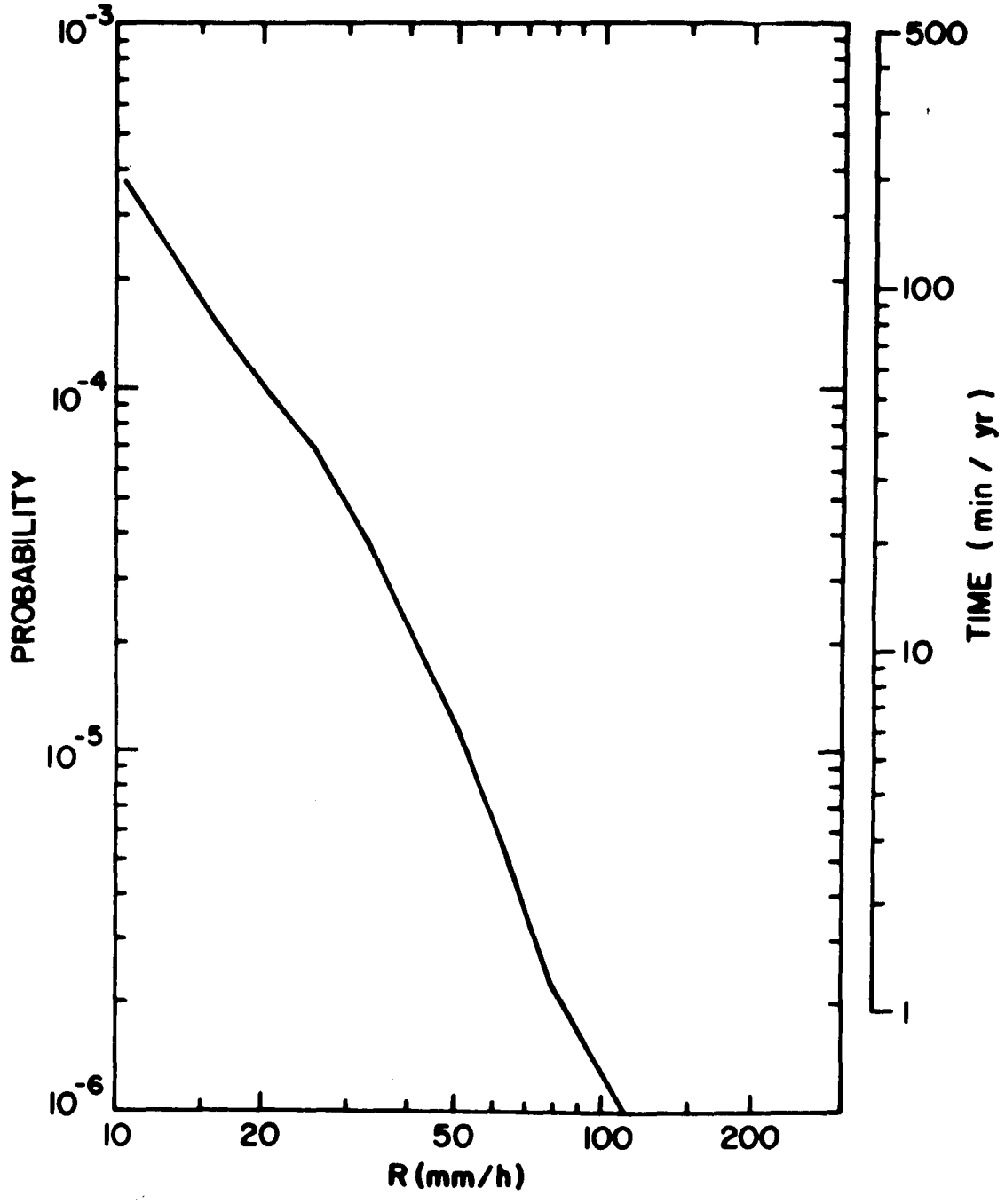

Figure 53. Long term average probability of exceeding a given rainfall rate at Gagnon, Que.

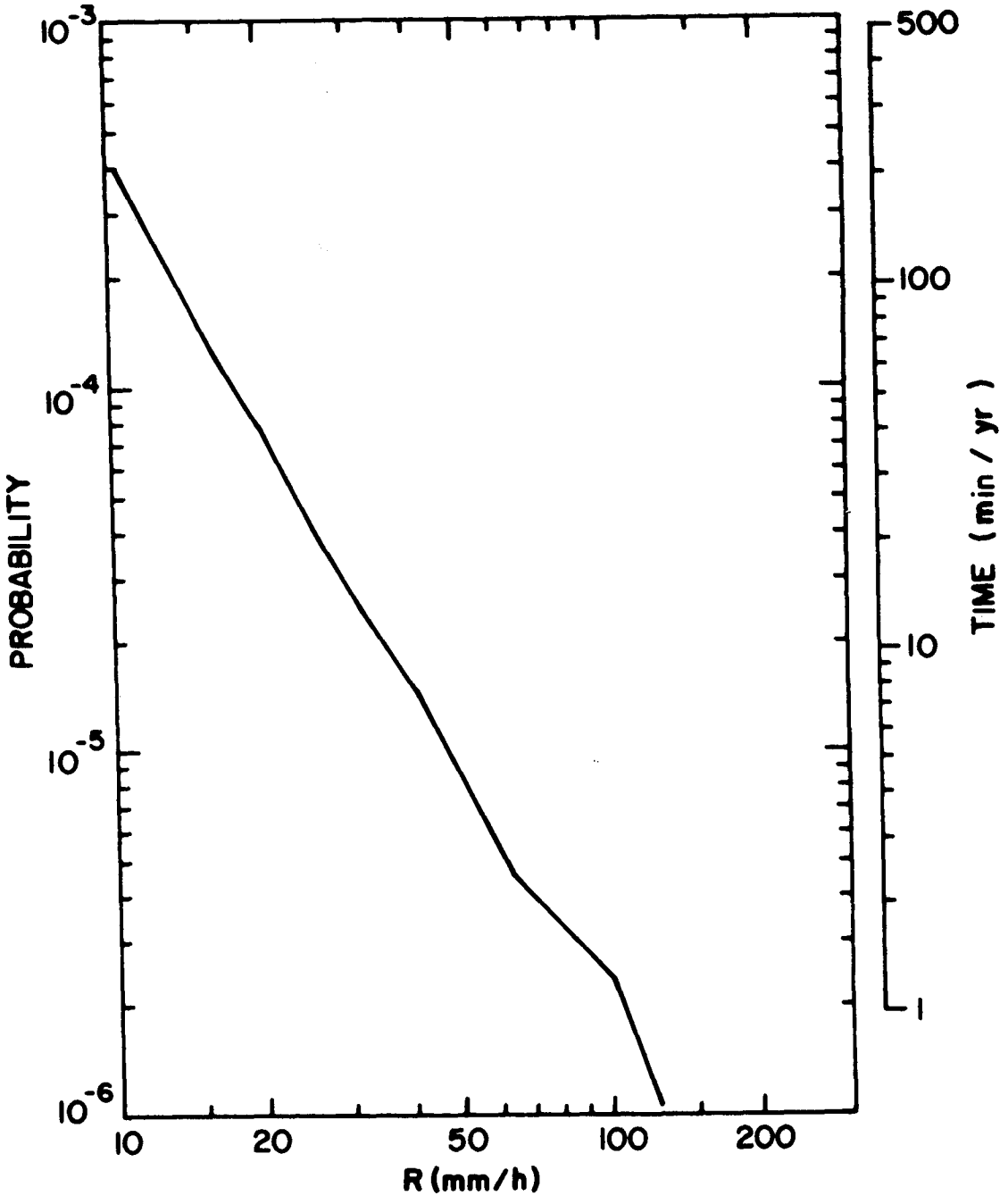

Figure 54. Long term average probability of exceeding a given rainfall rate at Gander, Nfld.

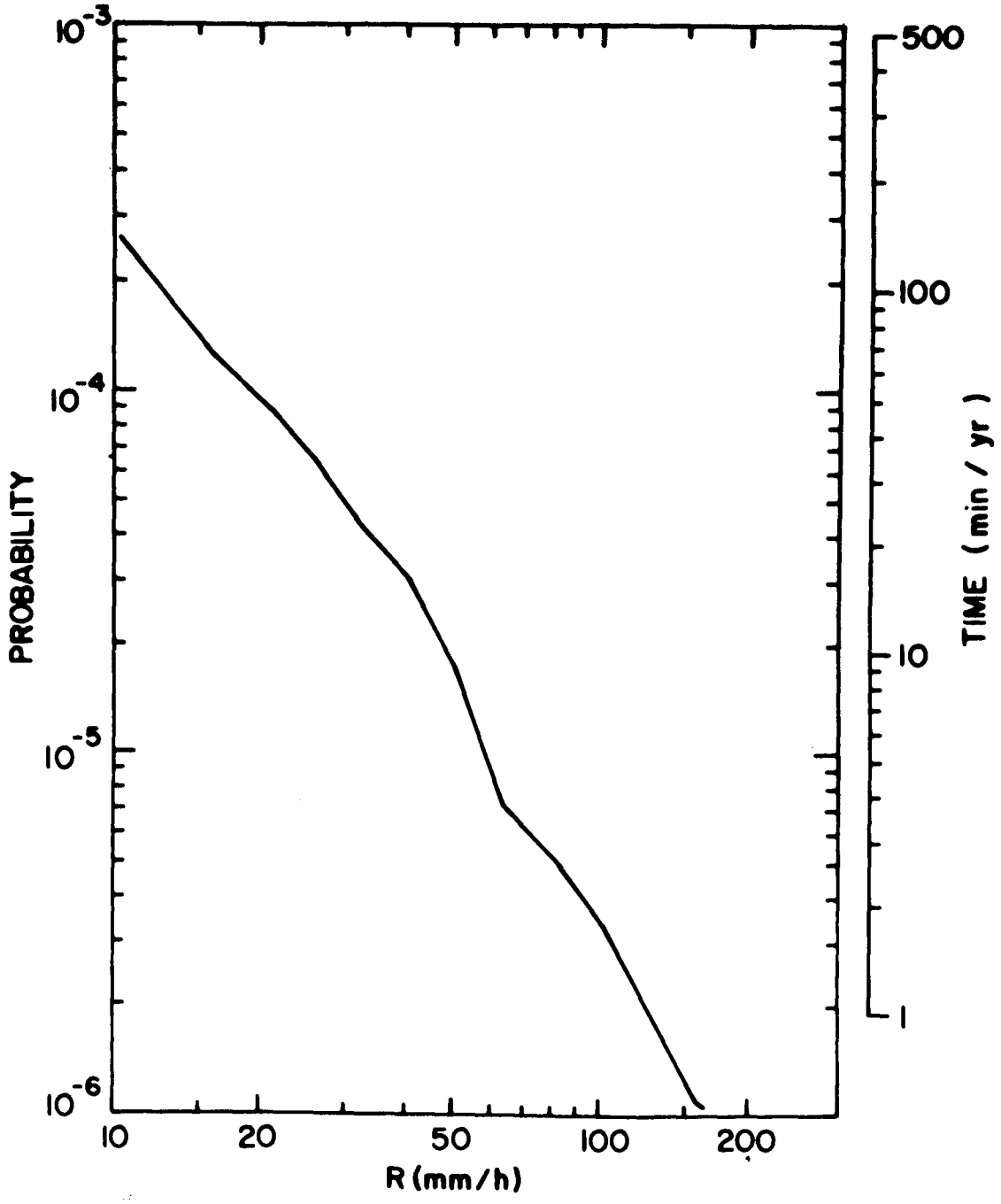

Figure 55. Long term average probability of exceeding a given rainfall rate at Geraldton, Ont.

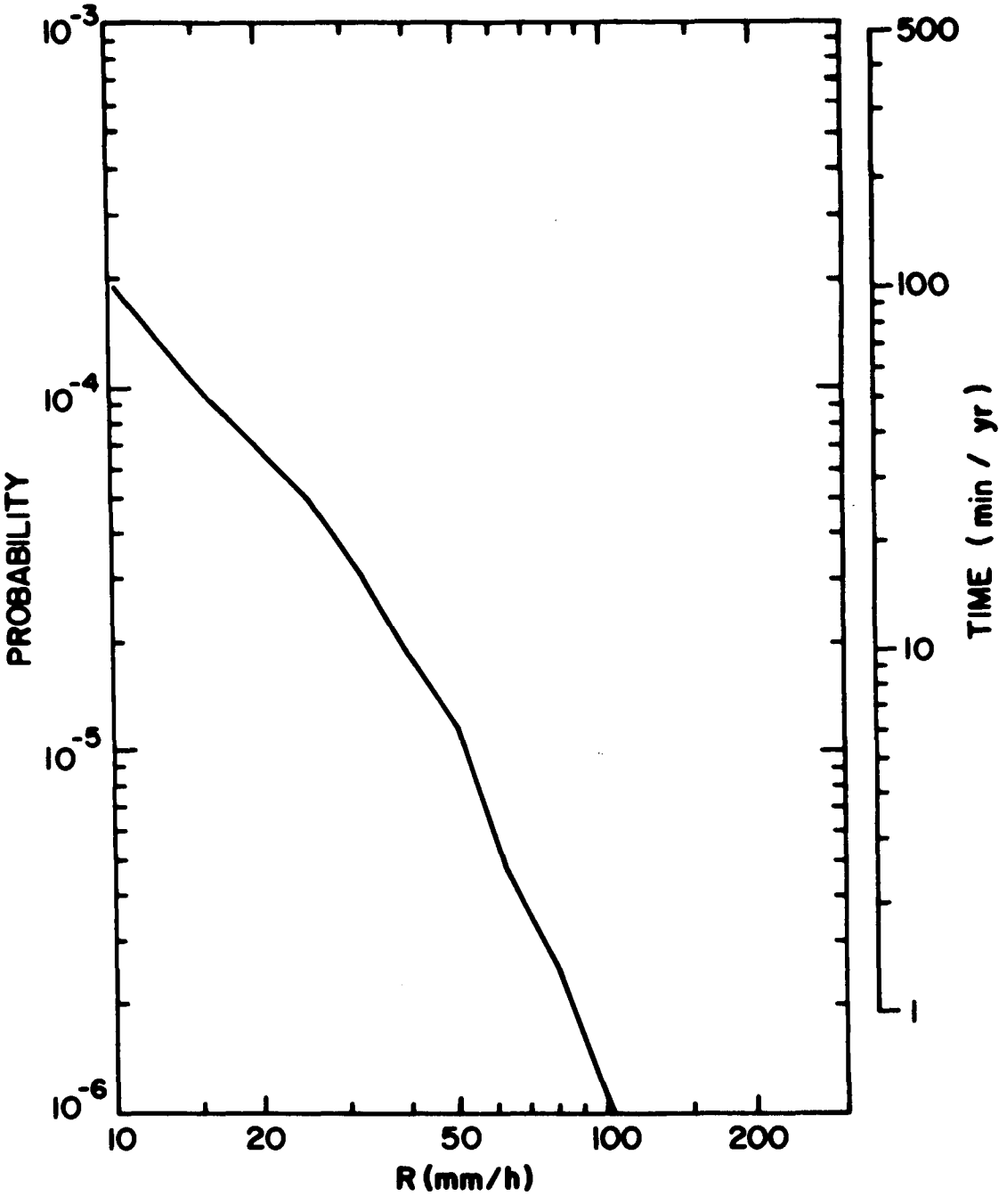

Figure 56. Long term average probability of exceeding a given rainfall rate at Goose Bay, Nfld.

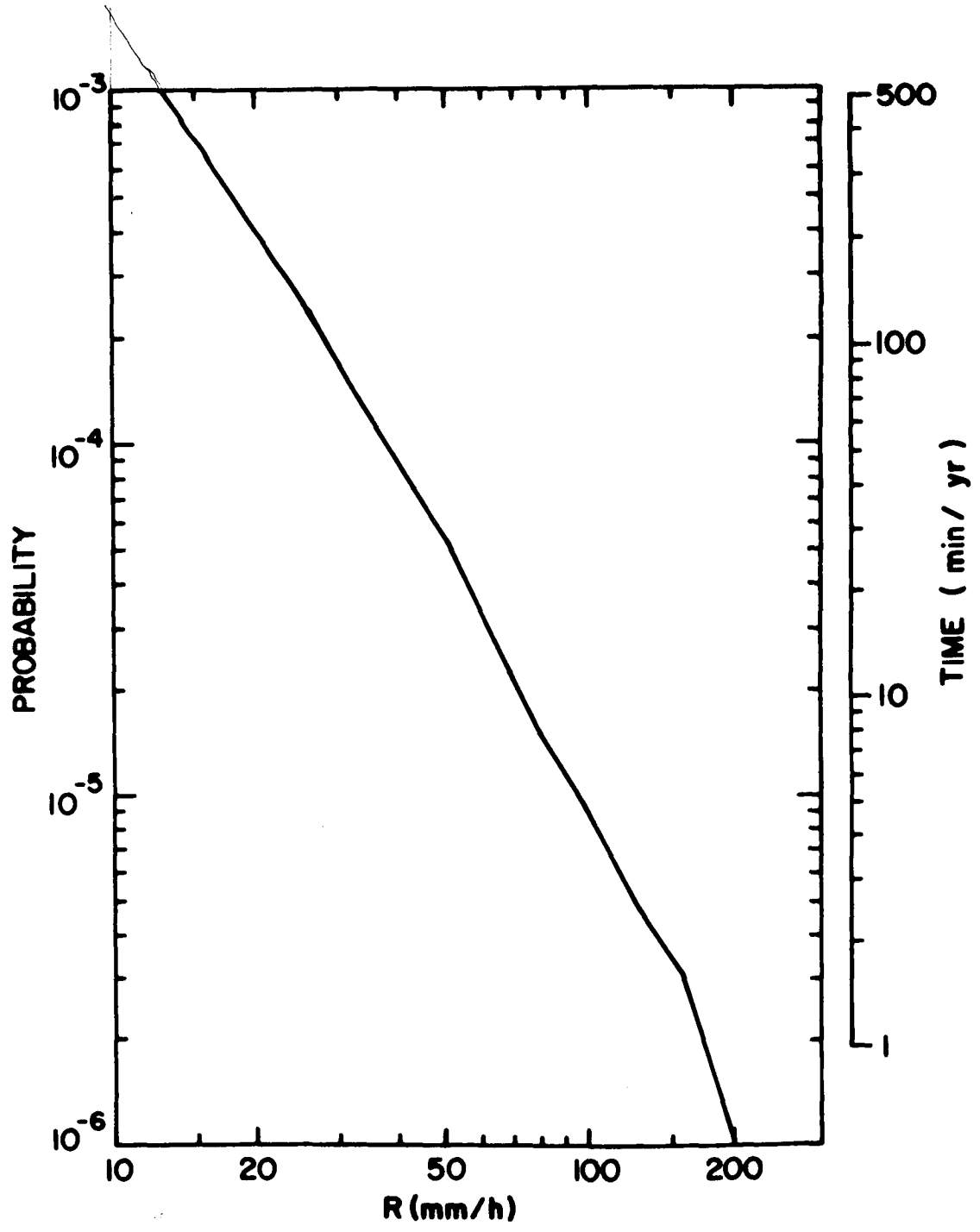

Figure 57. Long term average probability of exceeding a given rainfall rate at Halifax, N.S.

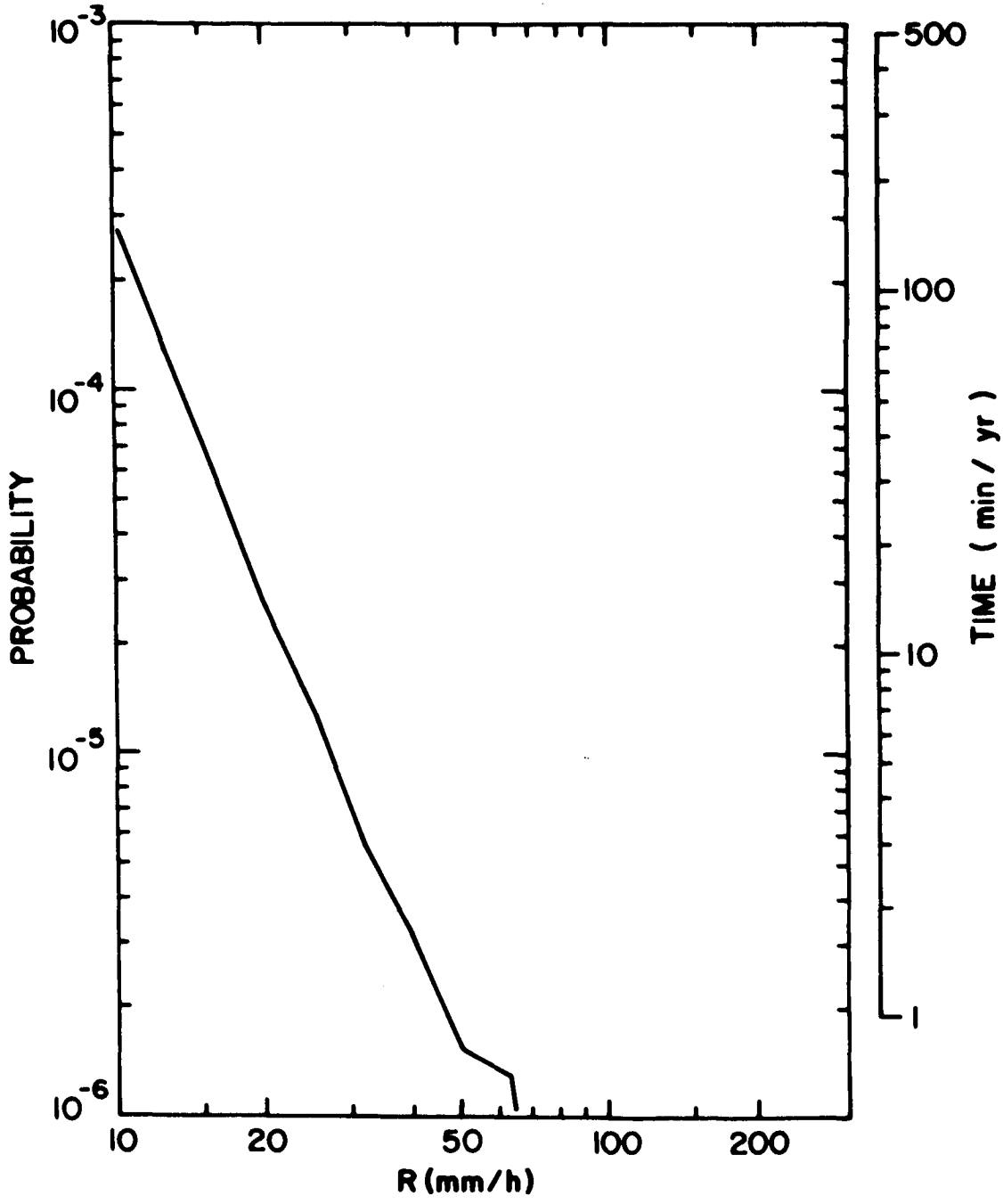

Figure 58. Long term average probability of exceeding a given rainfall rate at Hope, B.C.

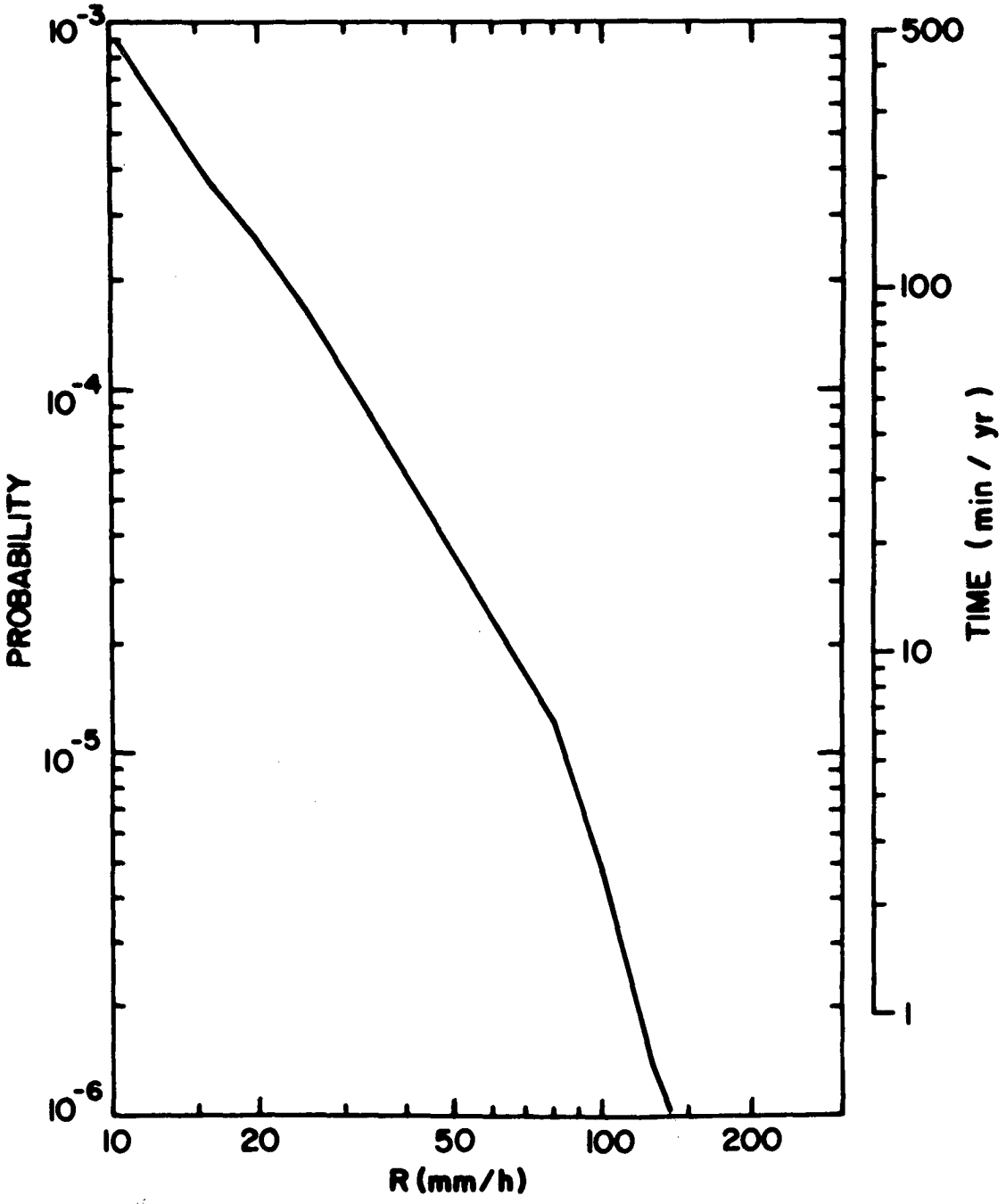

Figure 59. Long term average probability of exceeding a given rainfall rate at Kentville, N.S.

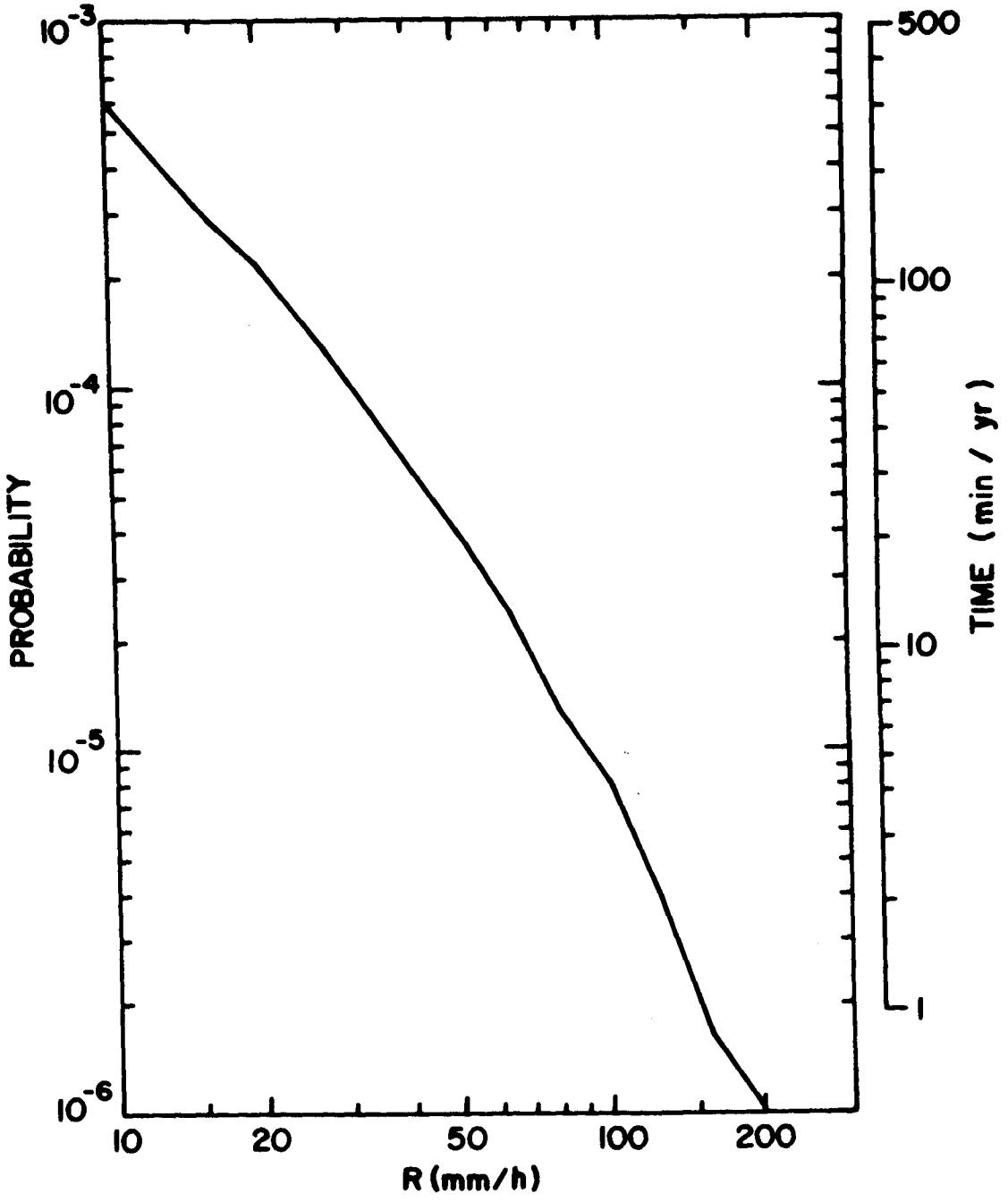

Figure 60. Long term average probability of exceeding a given rainfall rate at Kingston, Ont.

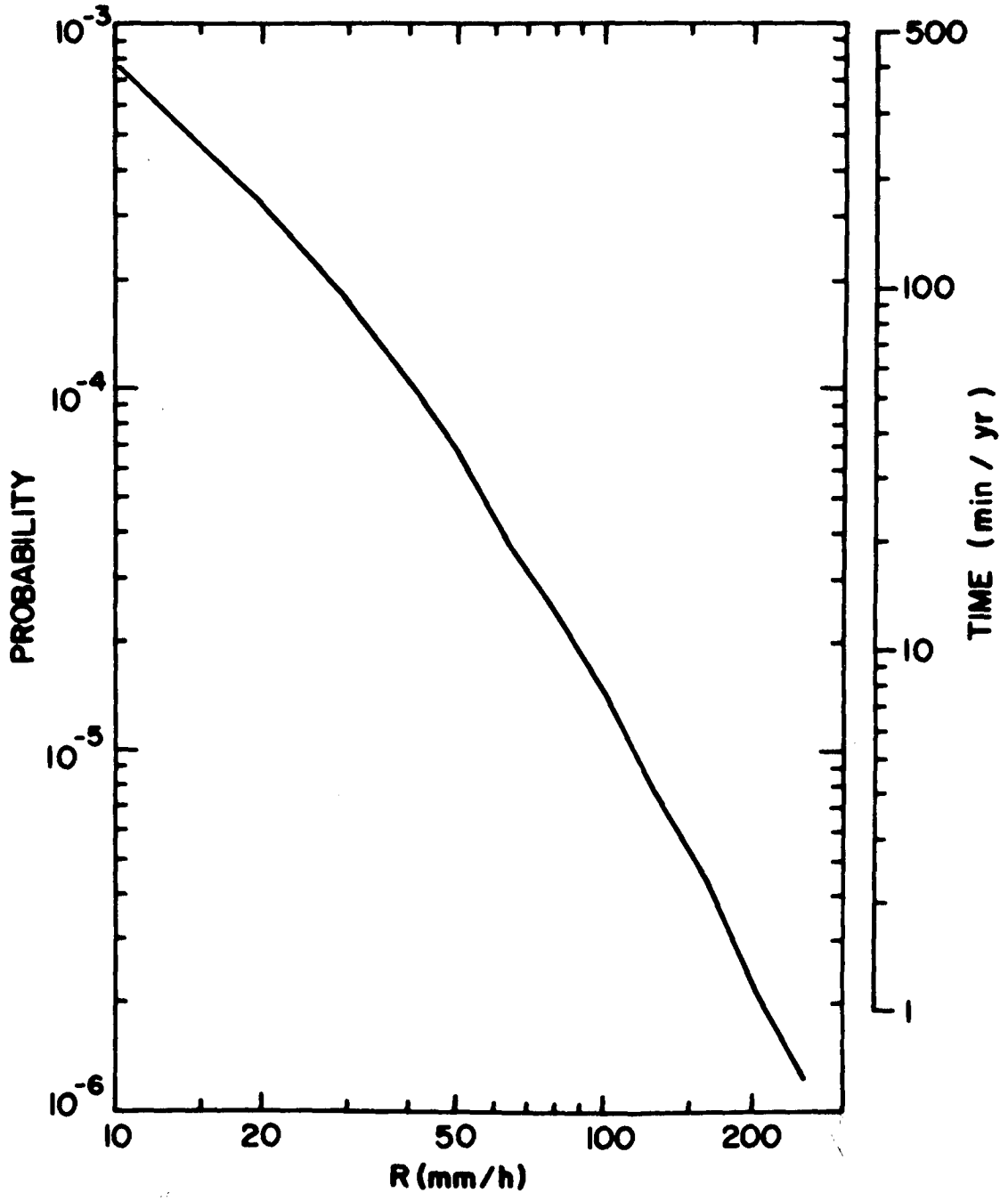

Figure 61. Long term average probability of exceeding a given rainfall rate at London, Ont.

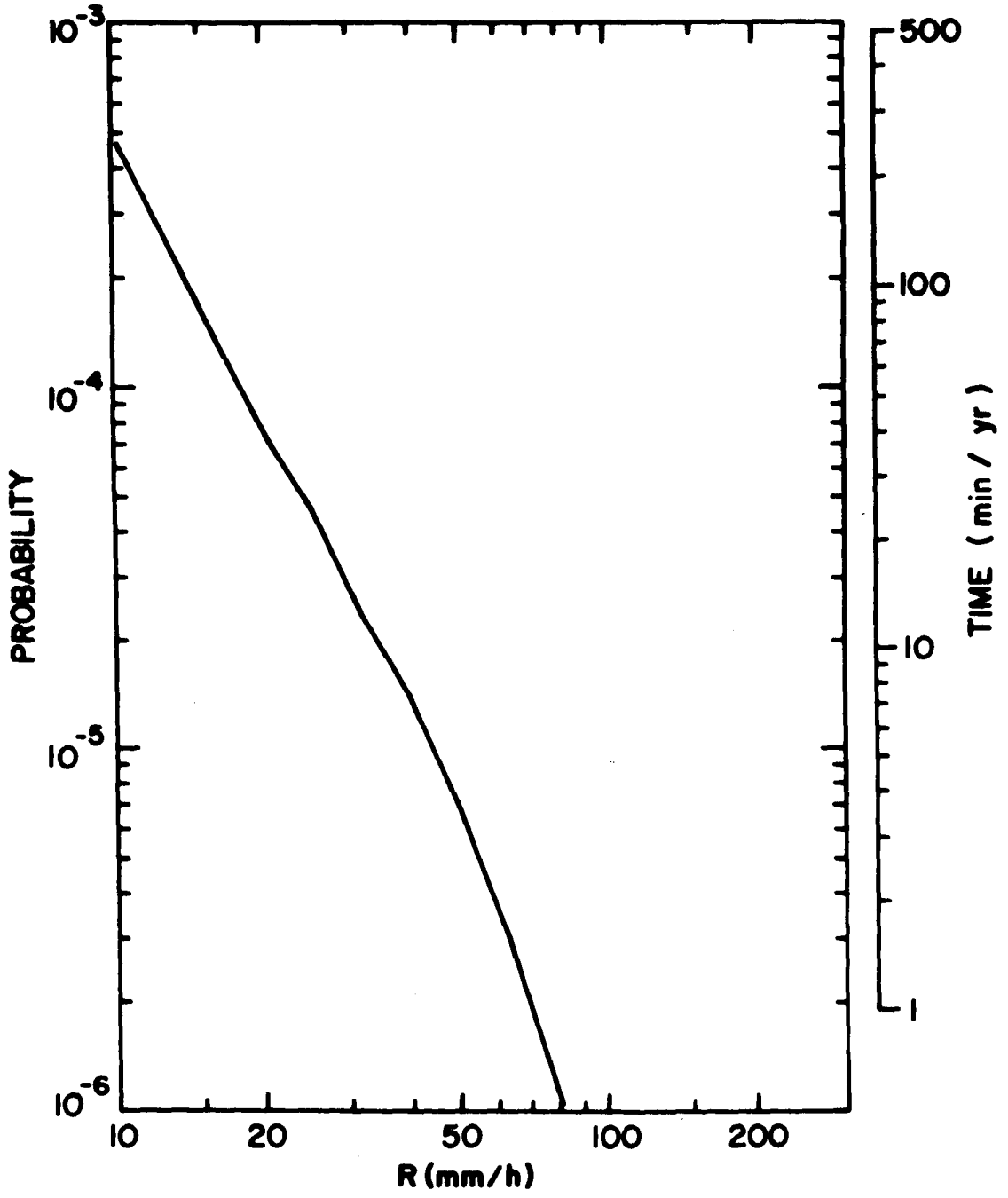

Figure 62. Long term average probability of exceeding a given rainfall rate at Mission, B.C.

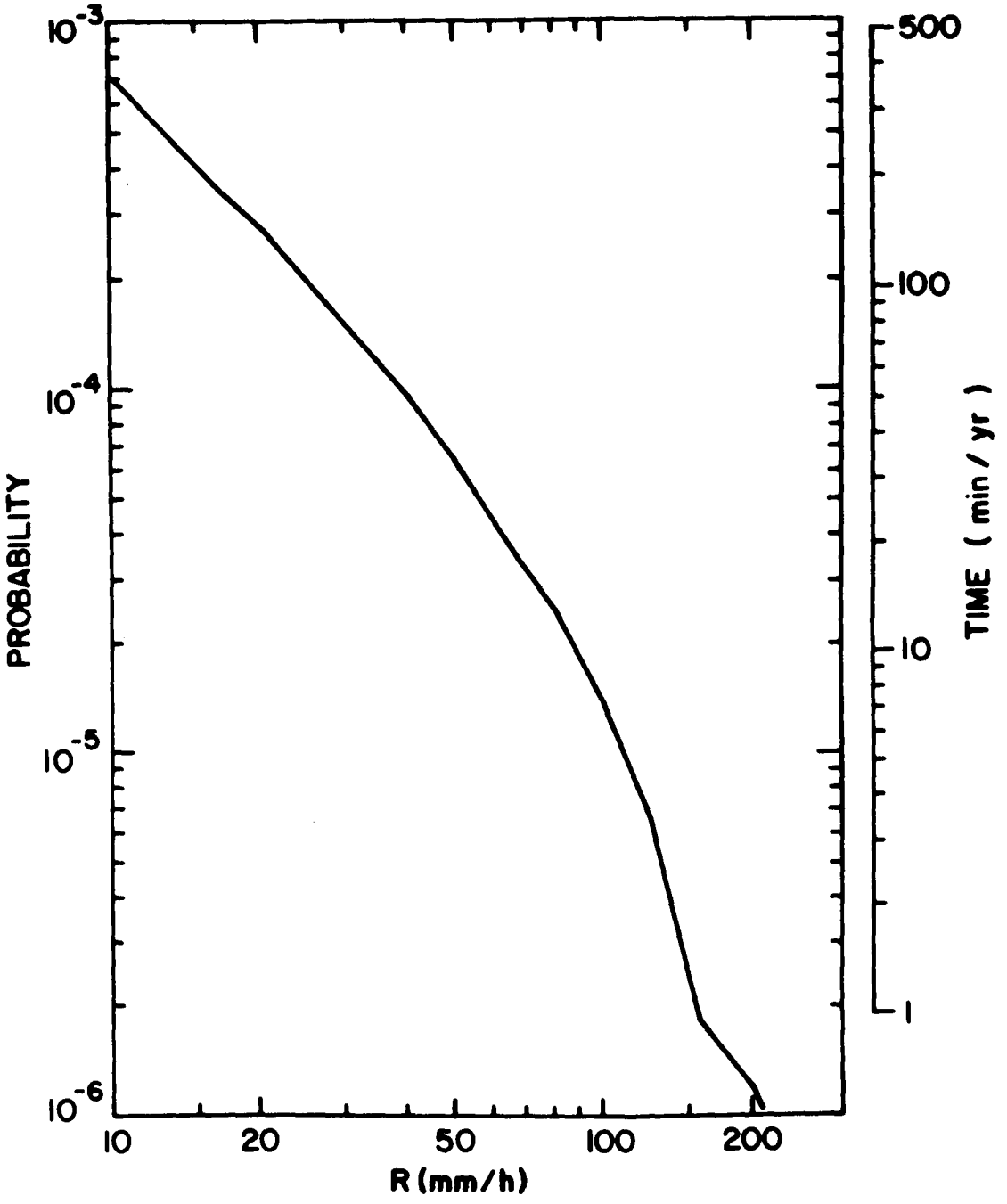

Figure 63. Long term average probability of exceeding a given rainfall rate at Montreal, Que.

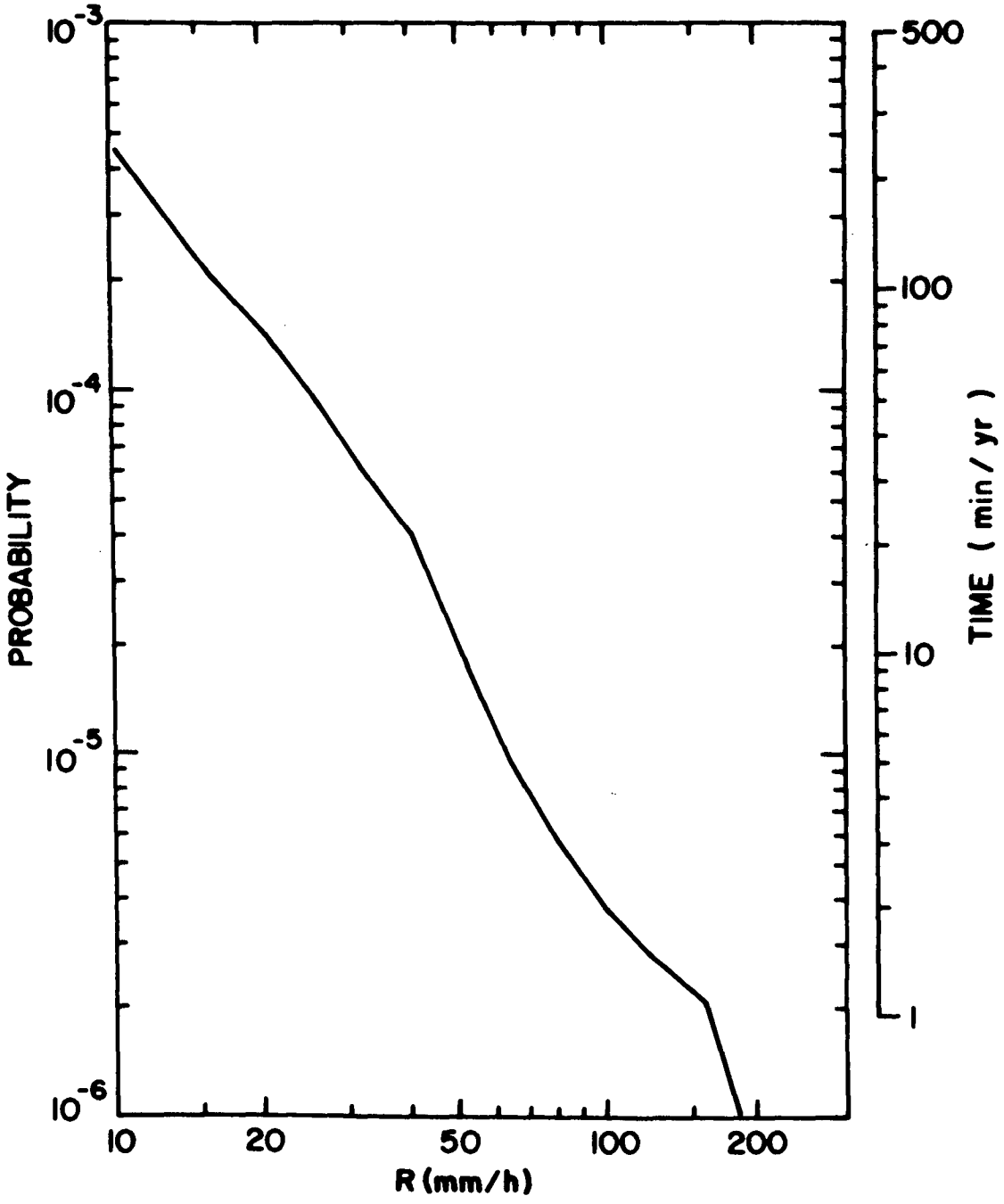

Figure 64. Long term average probability of exceeding a given rainfall rate at Moosonee, Ont.

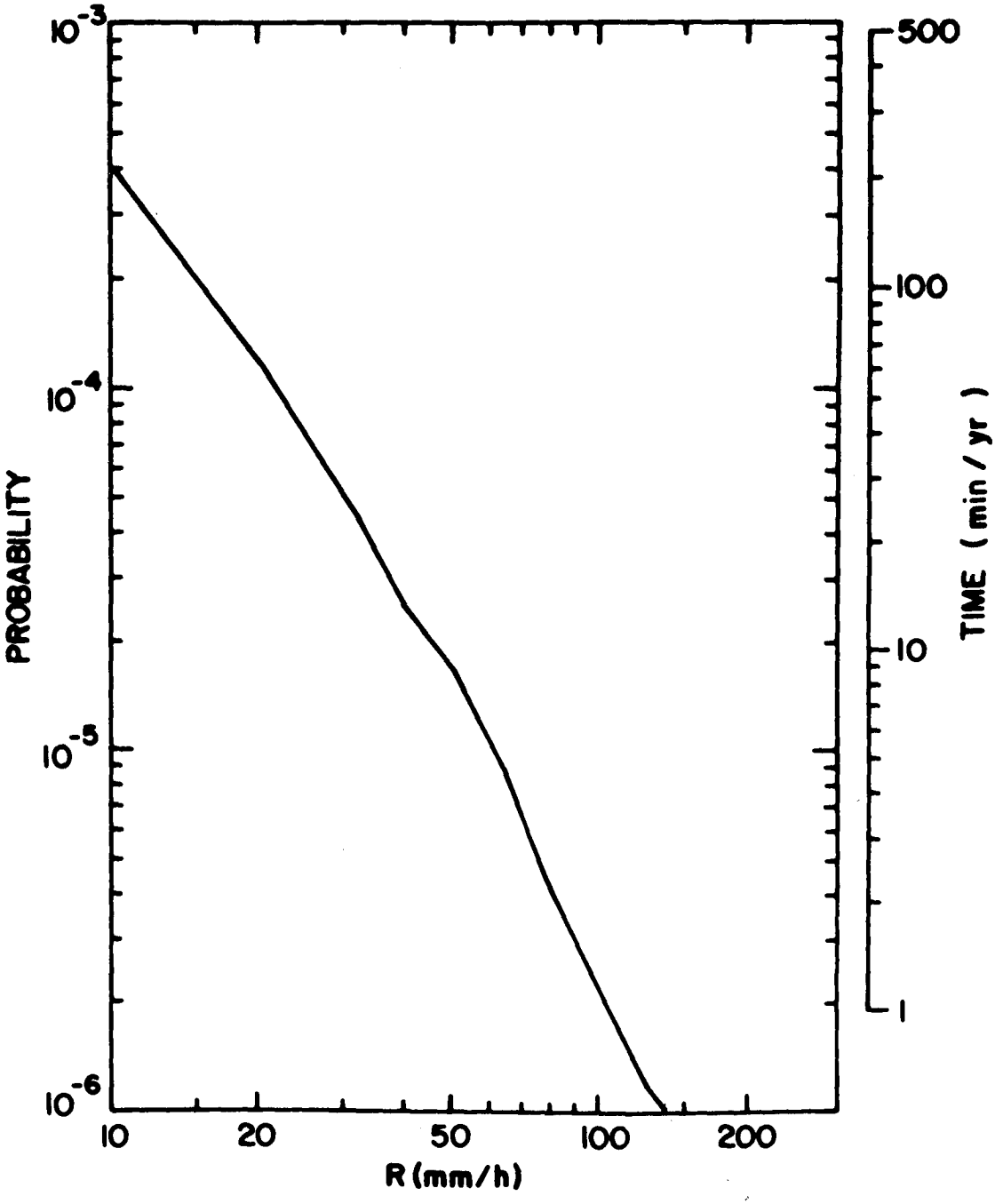

Figure 65. Long term average probability of exceeding a given rainfall rate at Normandin, Que.

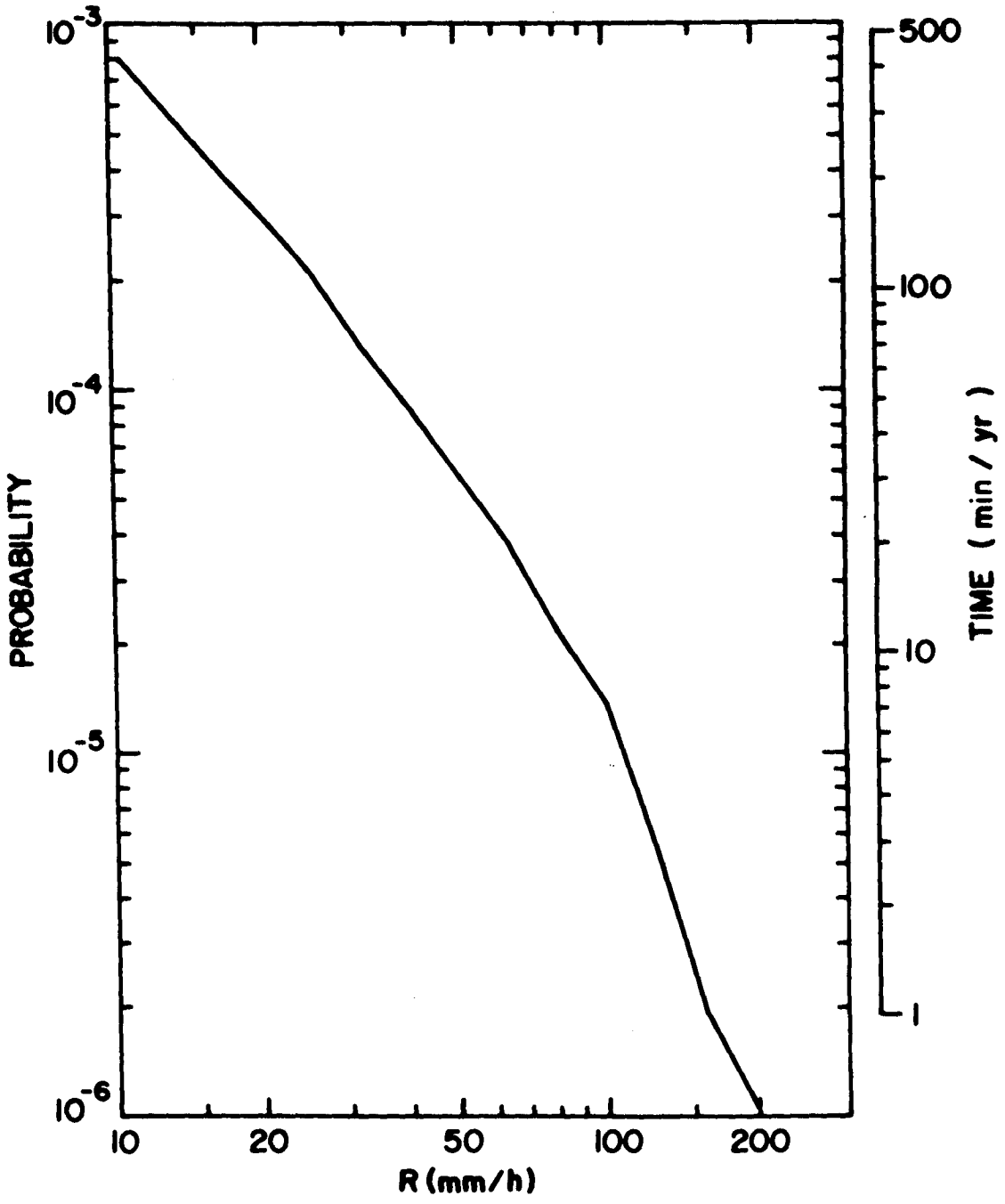

Figure 66. Long term average probability of exceeding a given rainfall rate at North Bay, Ont.

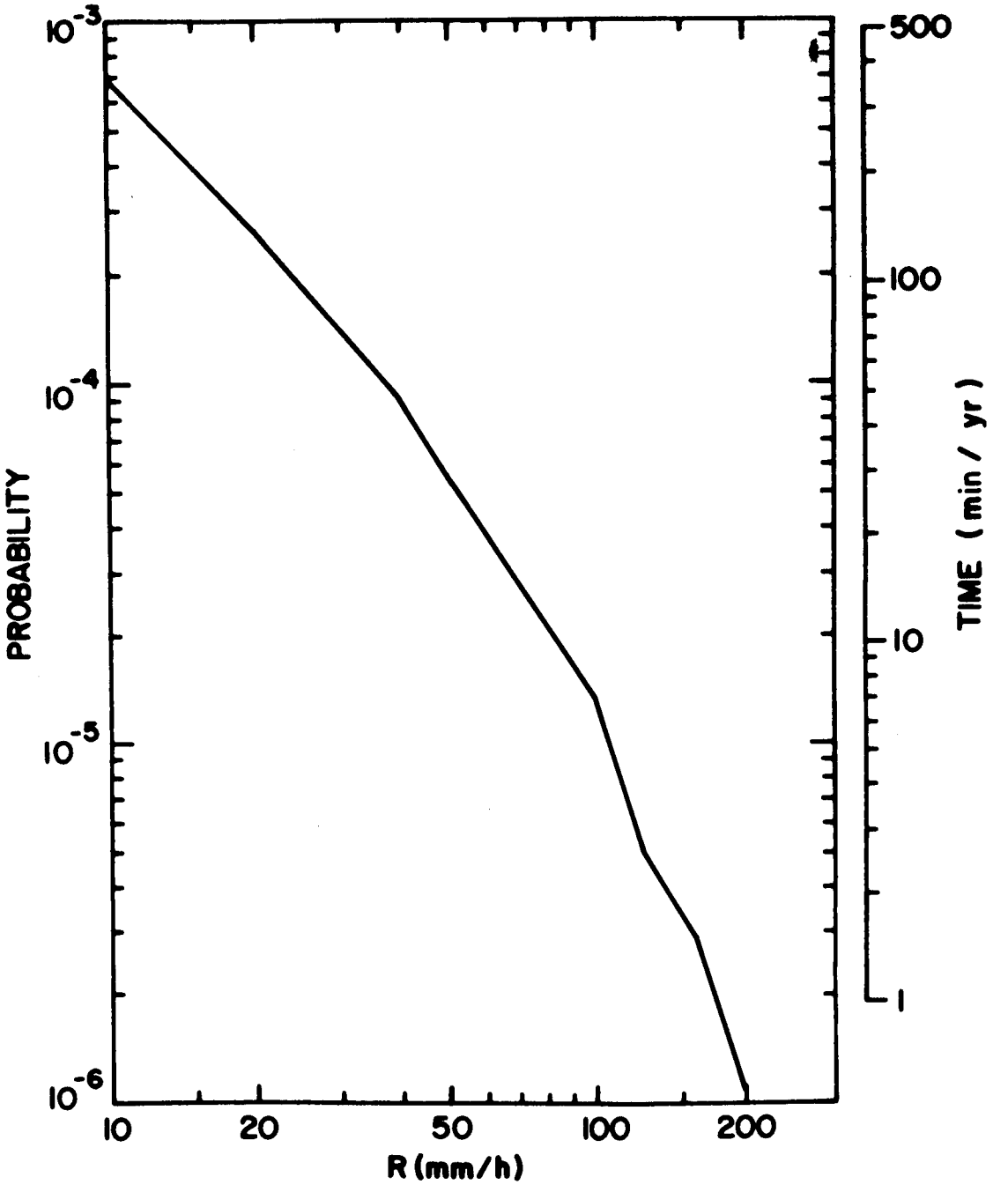

Figure 67. Long term average probability of exceeding a given rainfall rate at Ottawa, Ont.

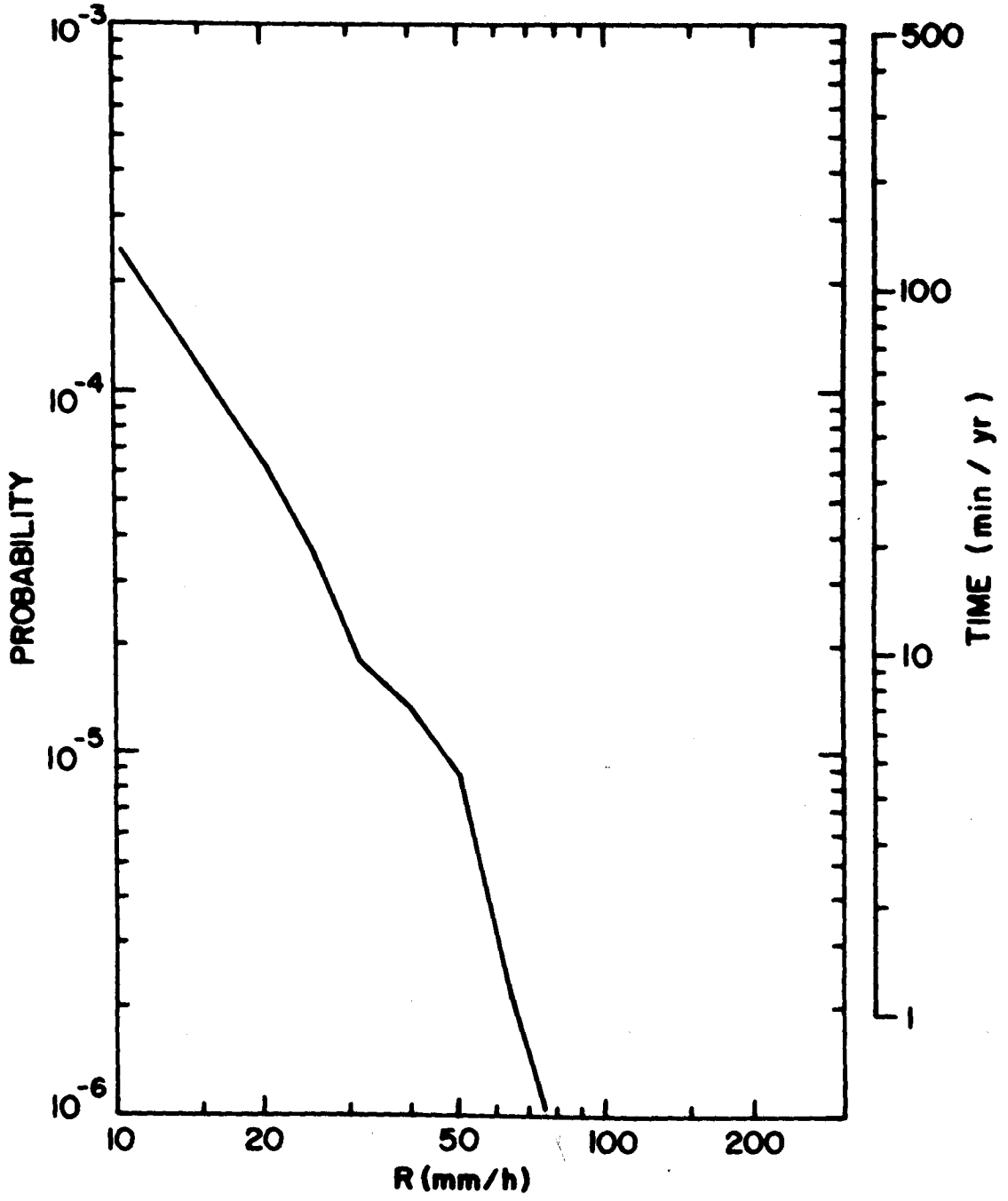

Figure 68. Long term average probability of exceeding a given rainfall rate at Post de la Baleine, Que.

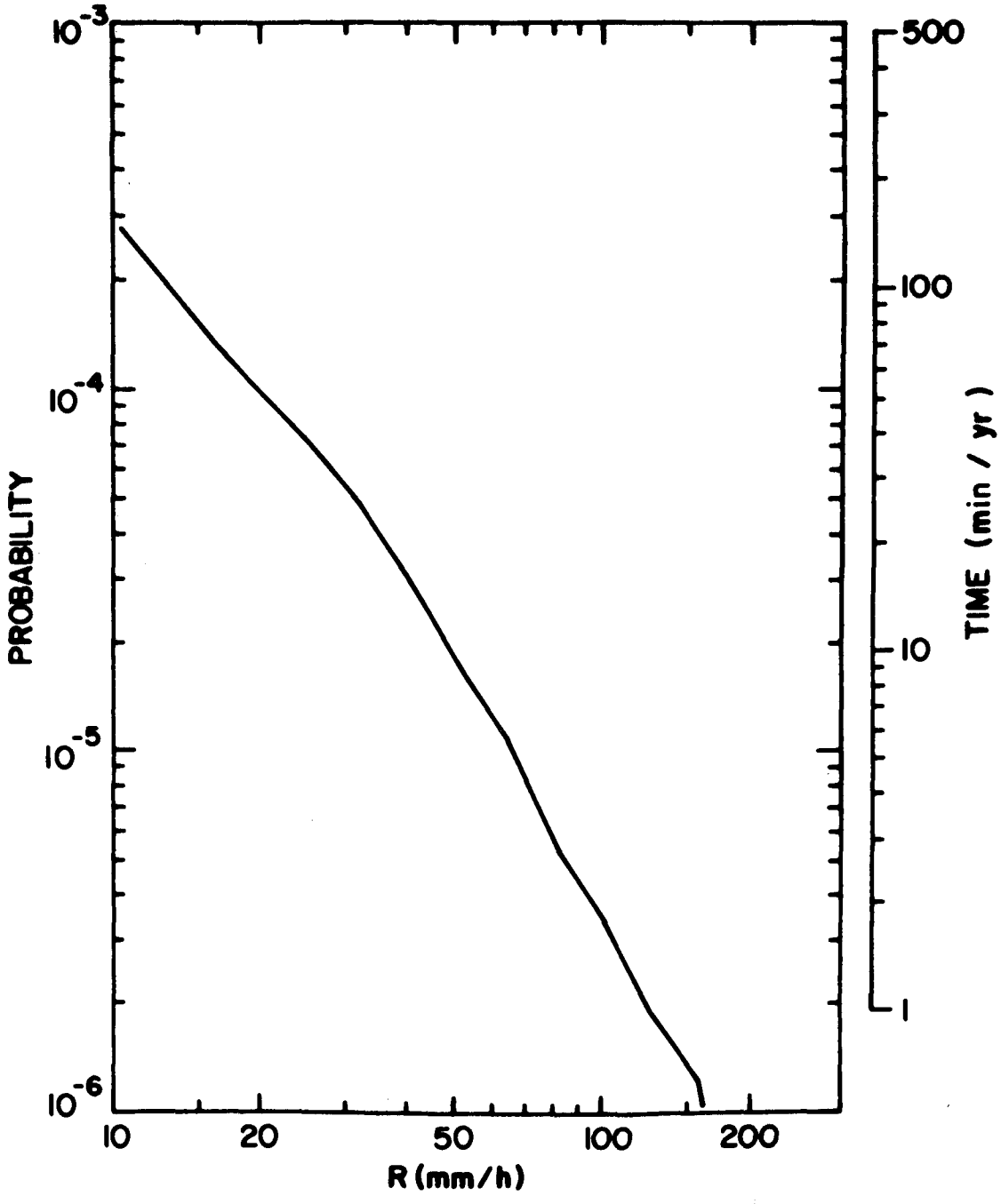

Figure 69. Long term average probability of exceeding a given rainfall rate at Prince Albert, Sask.

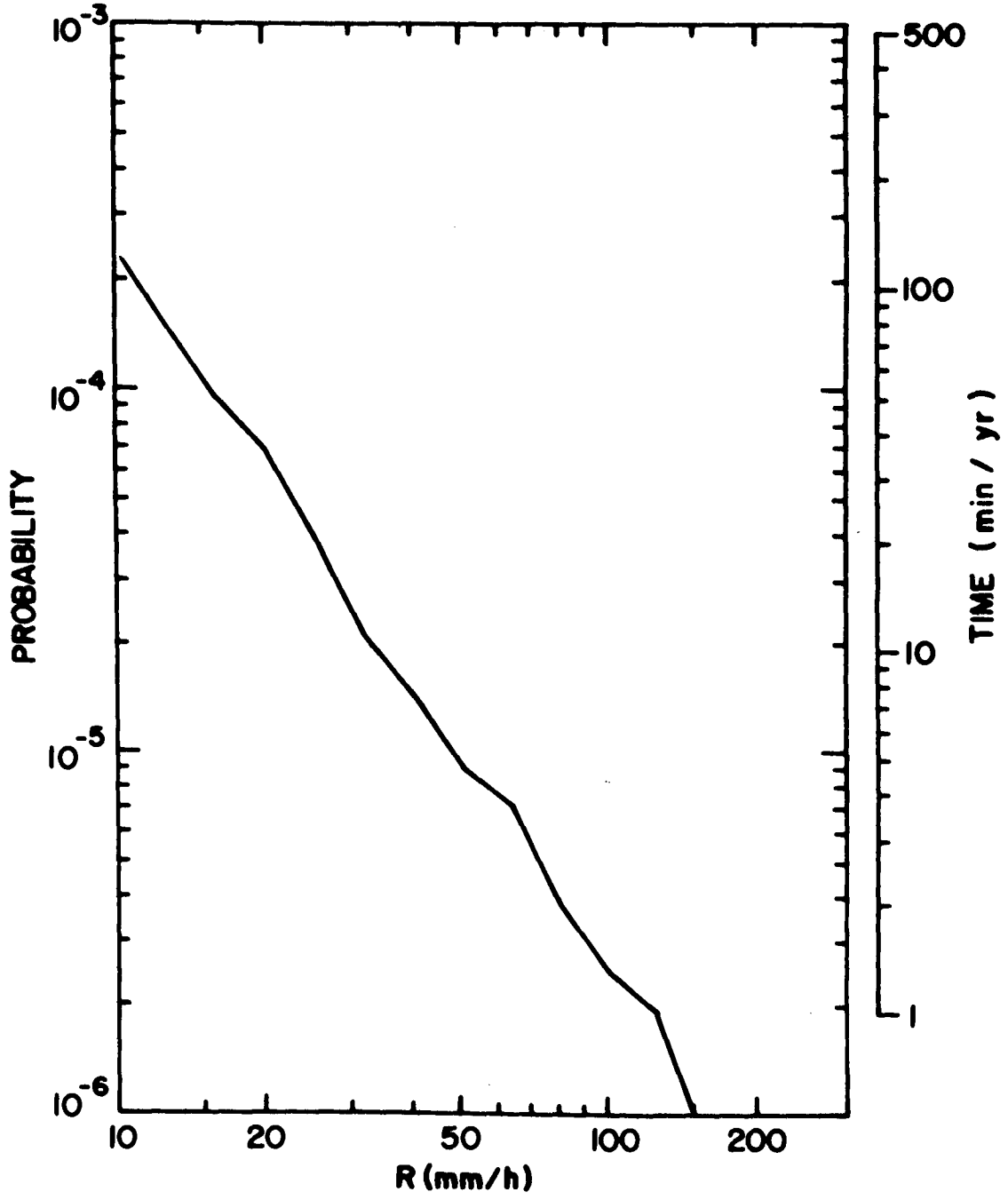

Figure 70. Long term average probability of exceeding a given rainfall rate at Prince George, B.C.

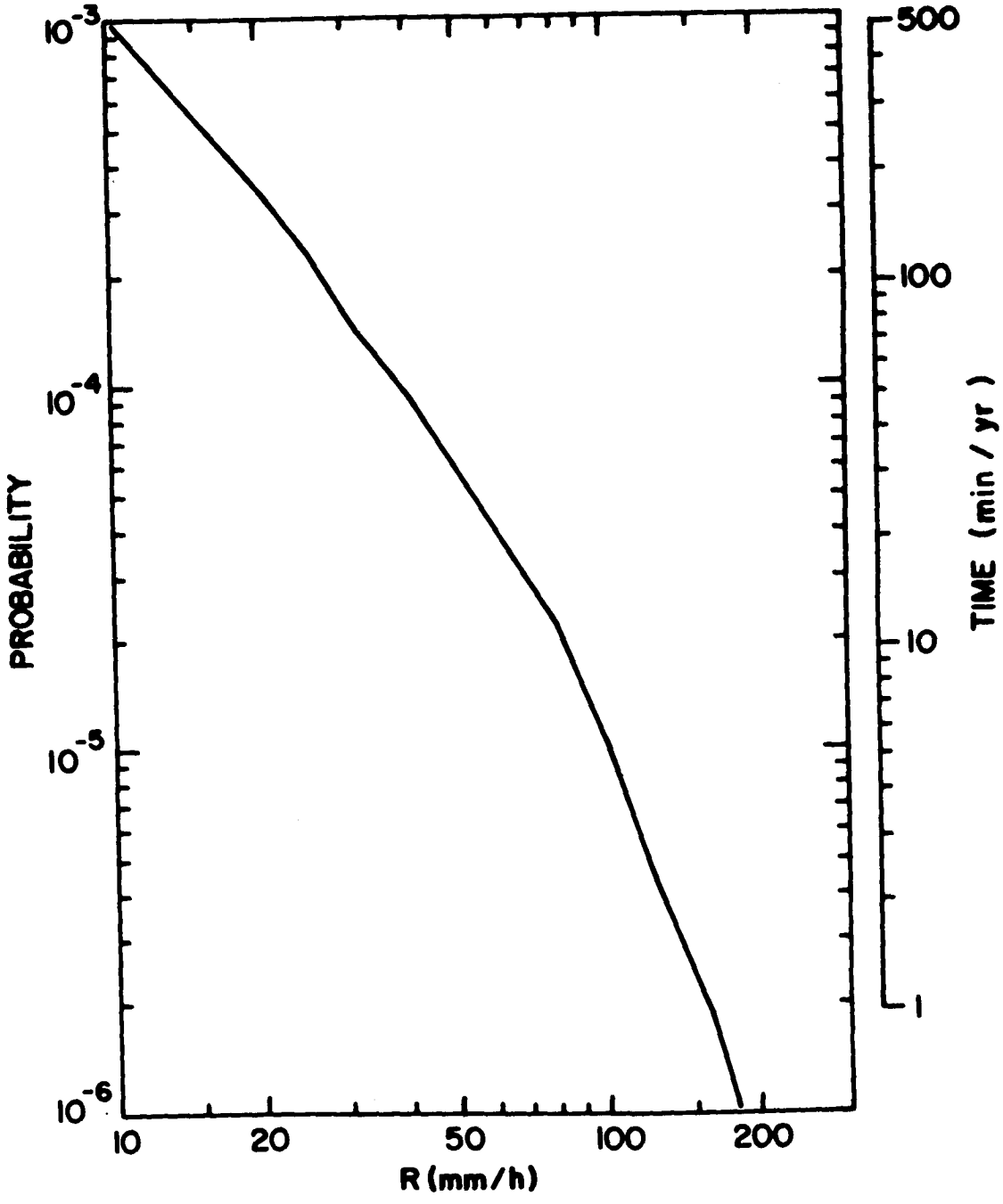

Figure 71. Long term average probability of exceeding a given rainfall rate at Quebec, Que.

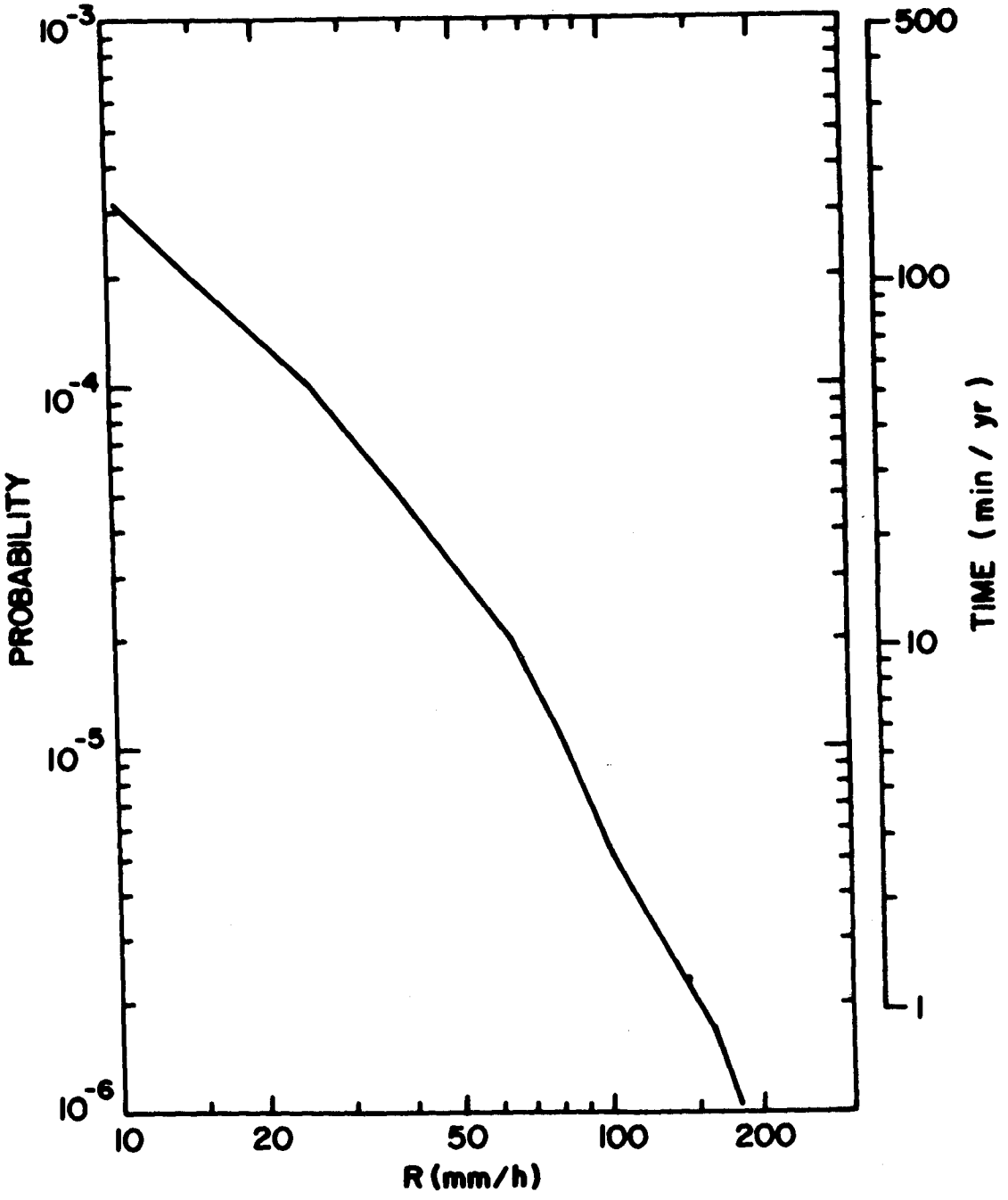

Figure 72. Long term average probability of exceeding a given rainfall rate at Regina, Sask.

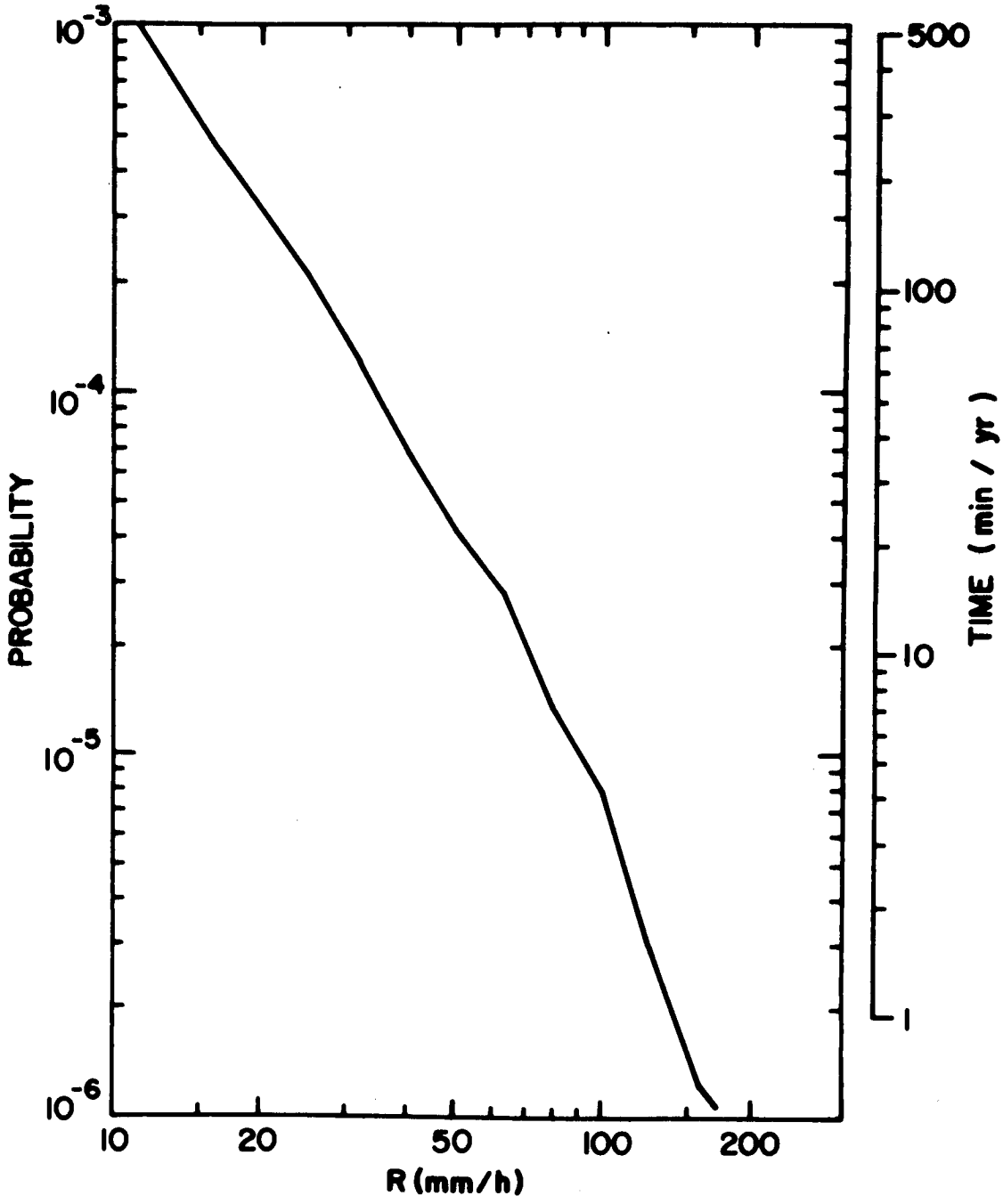

Figure 73. Long term average probability of exceeding a given rainfall rate at Saint John, N.B.

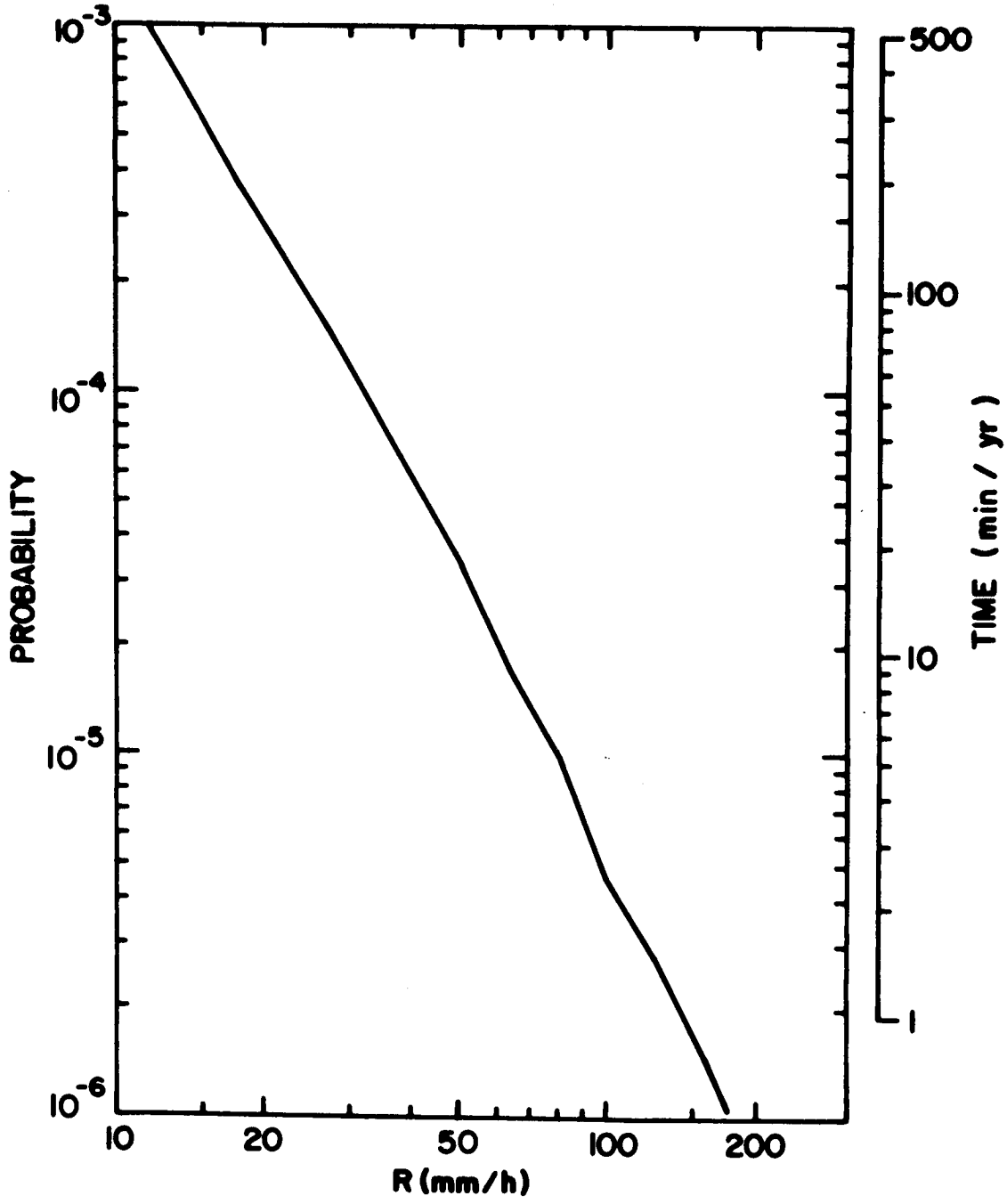

Figure 74. Long term average probability of exceeding a given rainfall rate at St. John's, Nfld.

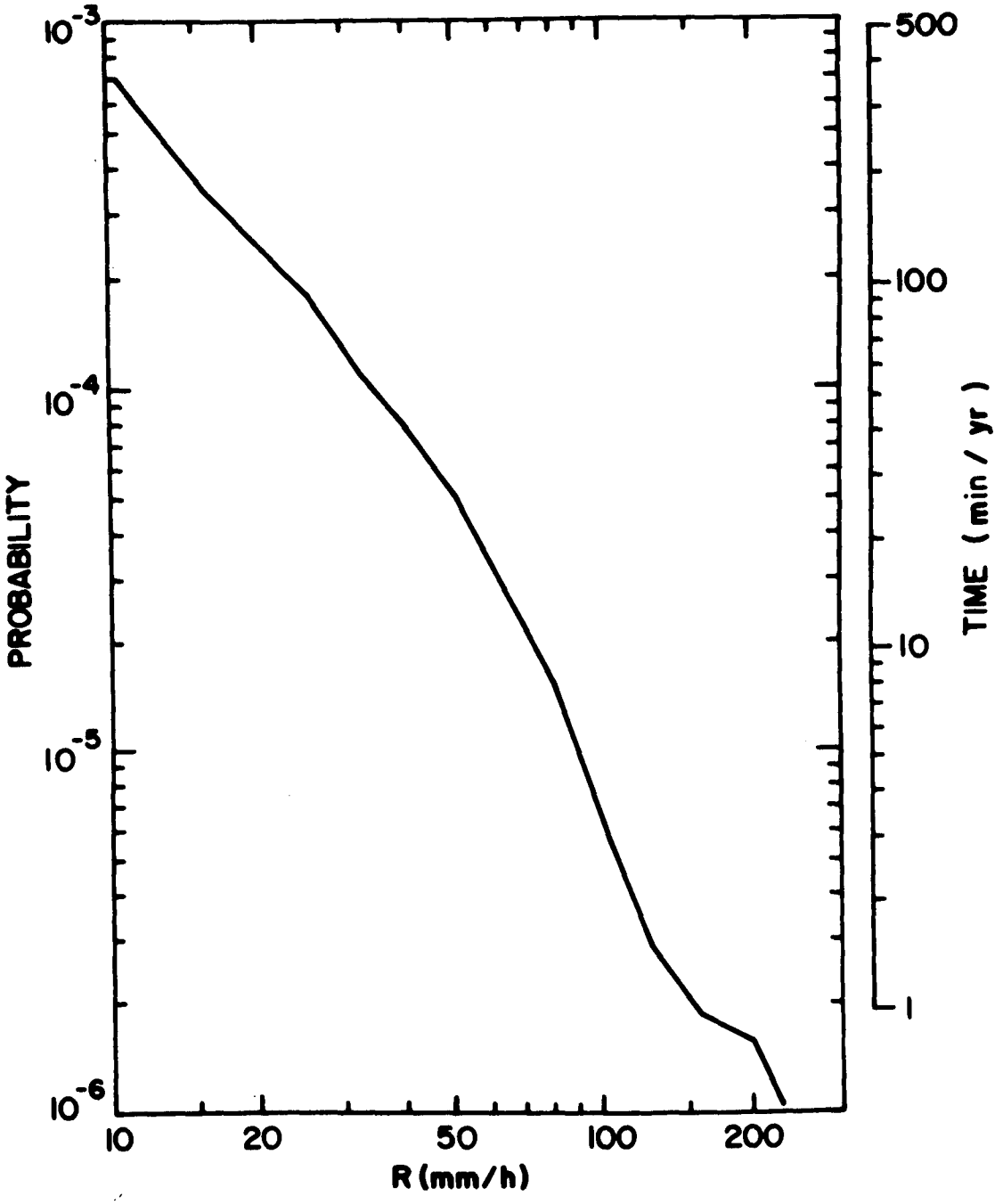

Figure 75. Long term average probability of exceeding a given rainfall rate at Sault Ste. Marie, Ont.

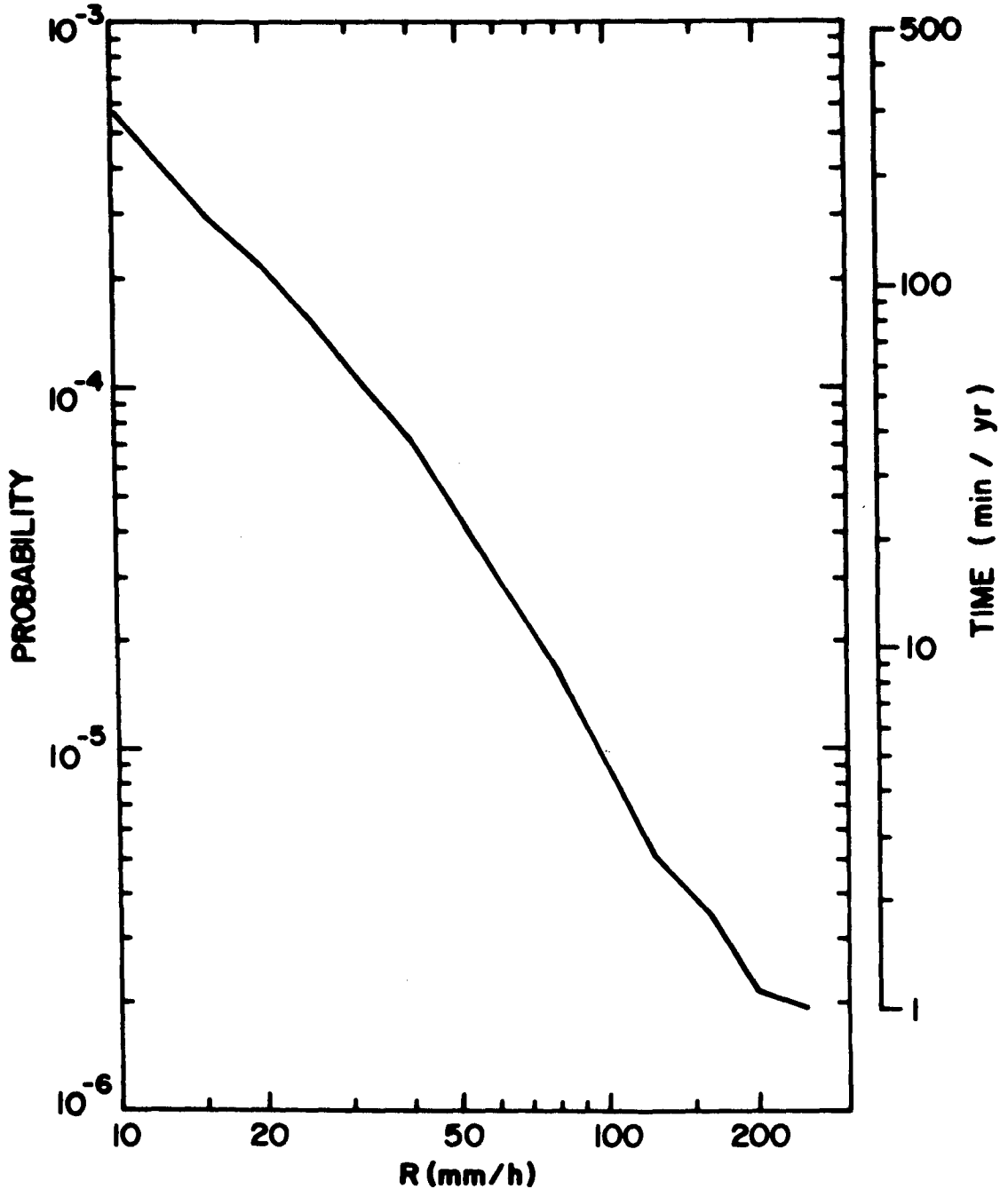

Figure 76. Long term average probability of exceeding a given rainfall rate at Sioux Lookout, Ont.

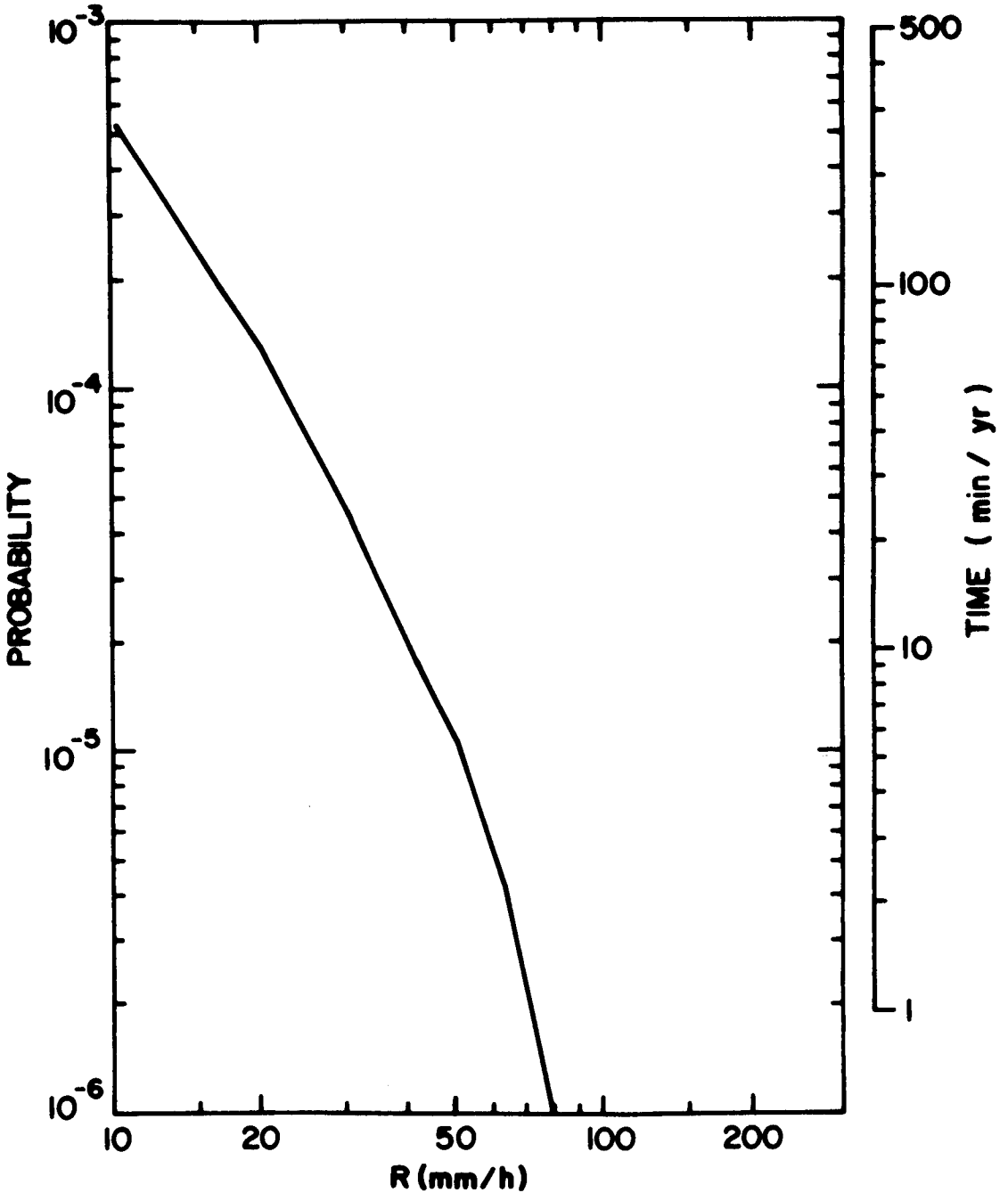

Figure 77. Long term average probability of exceeding a given rainfall rate at Stephenville, Nfld.

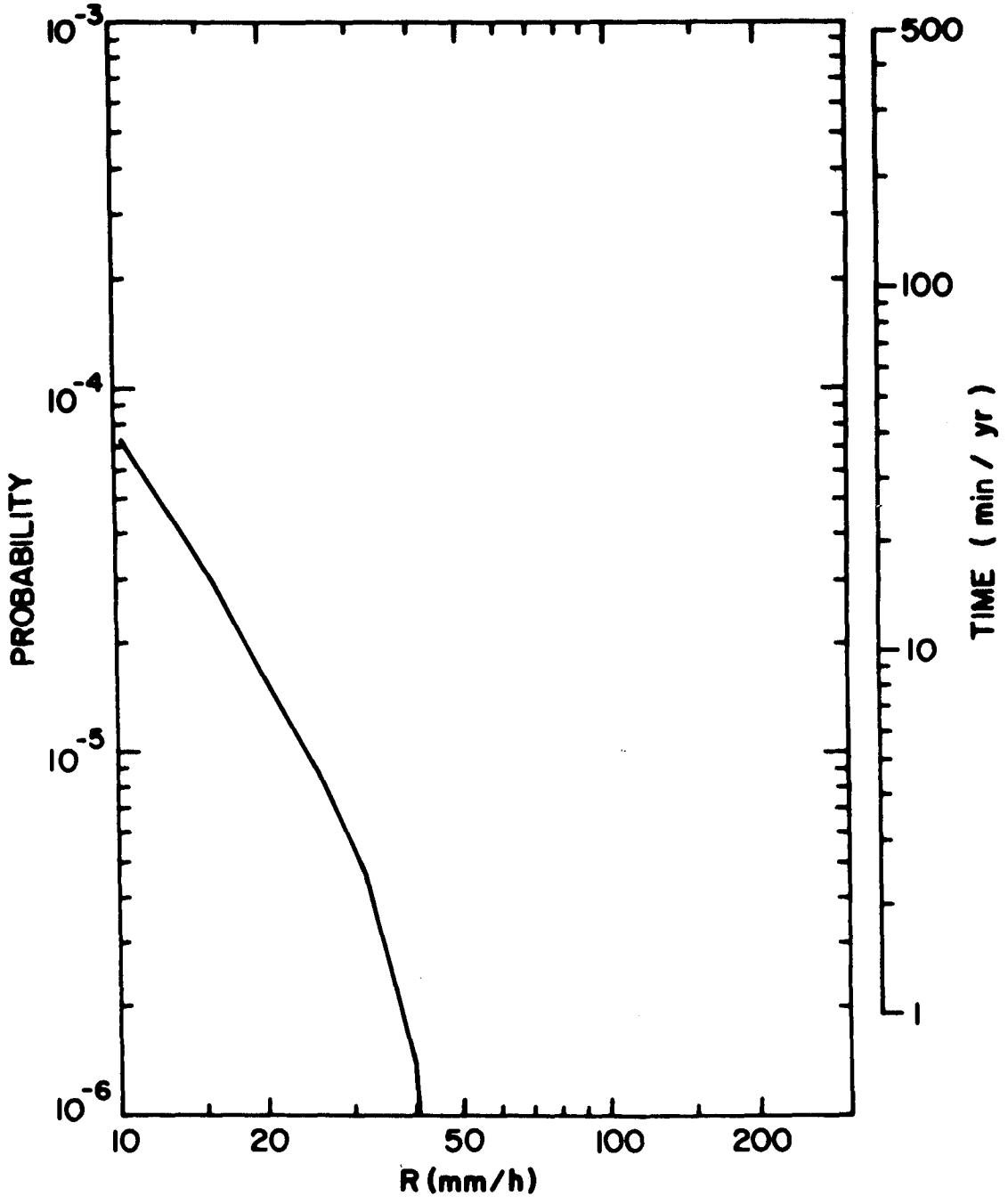

Figure 78. Long term average probability of exceeding a given rainfall rate at Summerland, B.C.

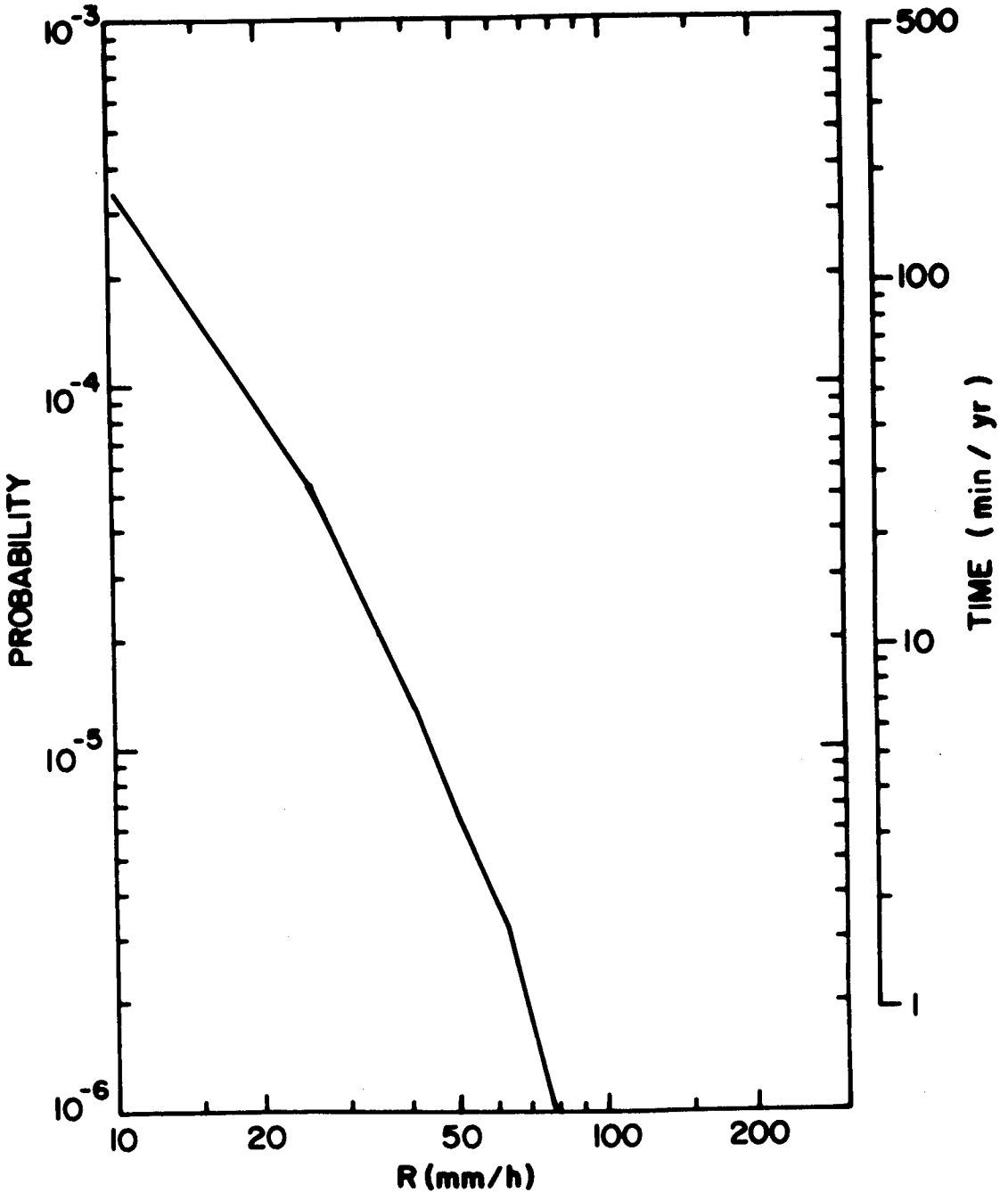

Figure 79. Long term average probability of exceeding a given rainfall rate at Summerside, P.E.I.

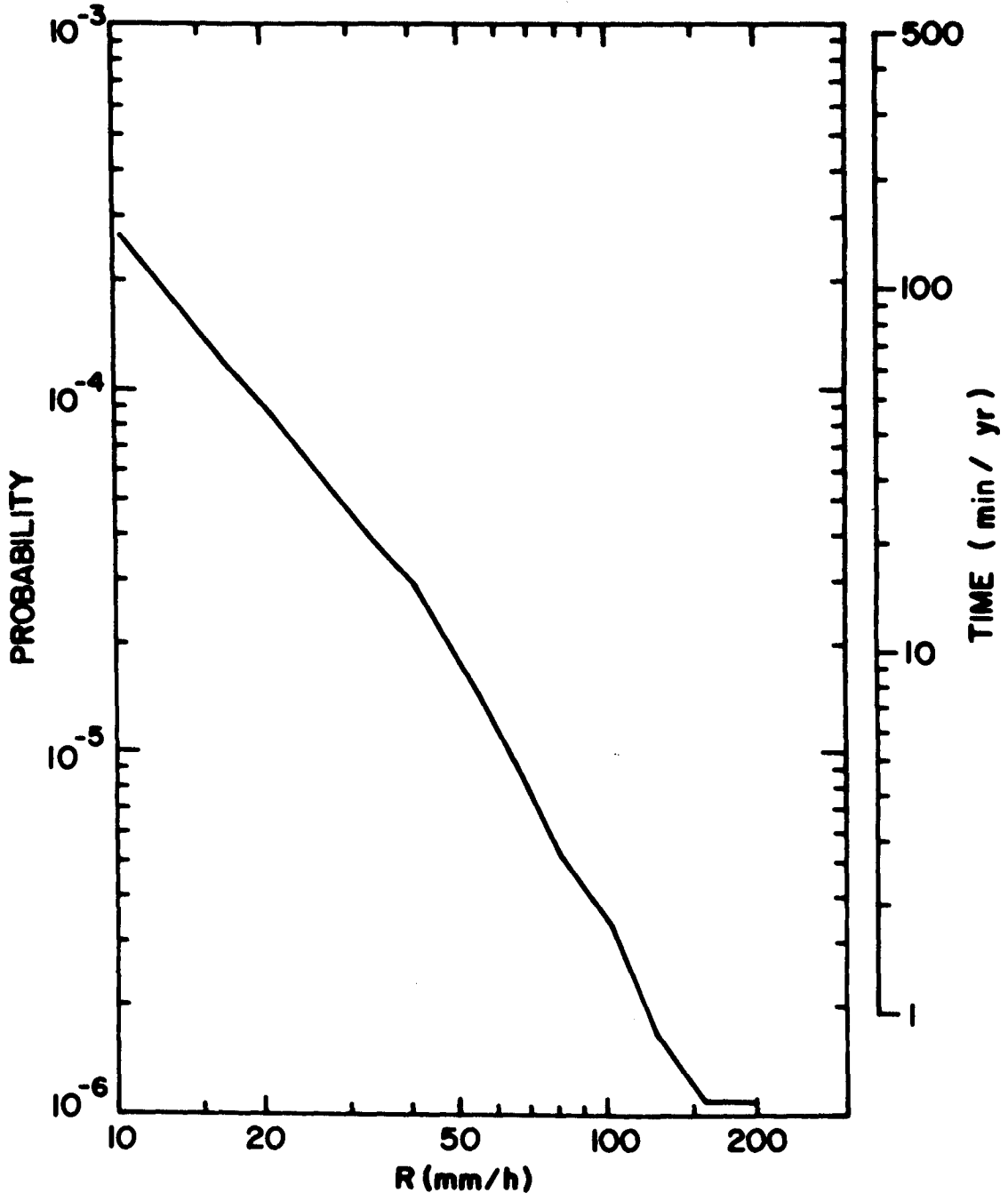

Figure 80. Long term average probability of exceeding a given rainfall rate at Swift Current, Sask.

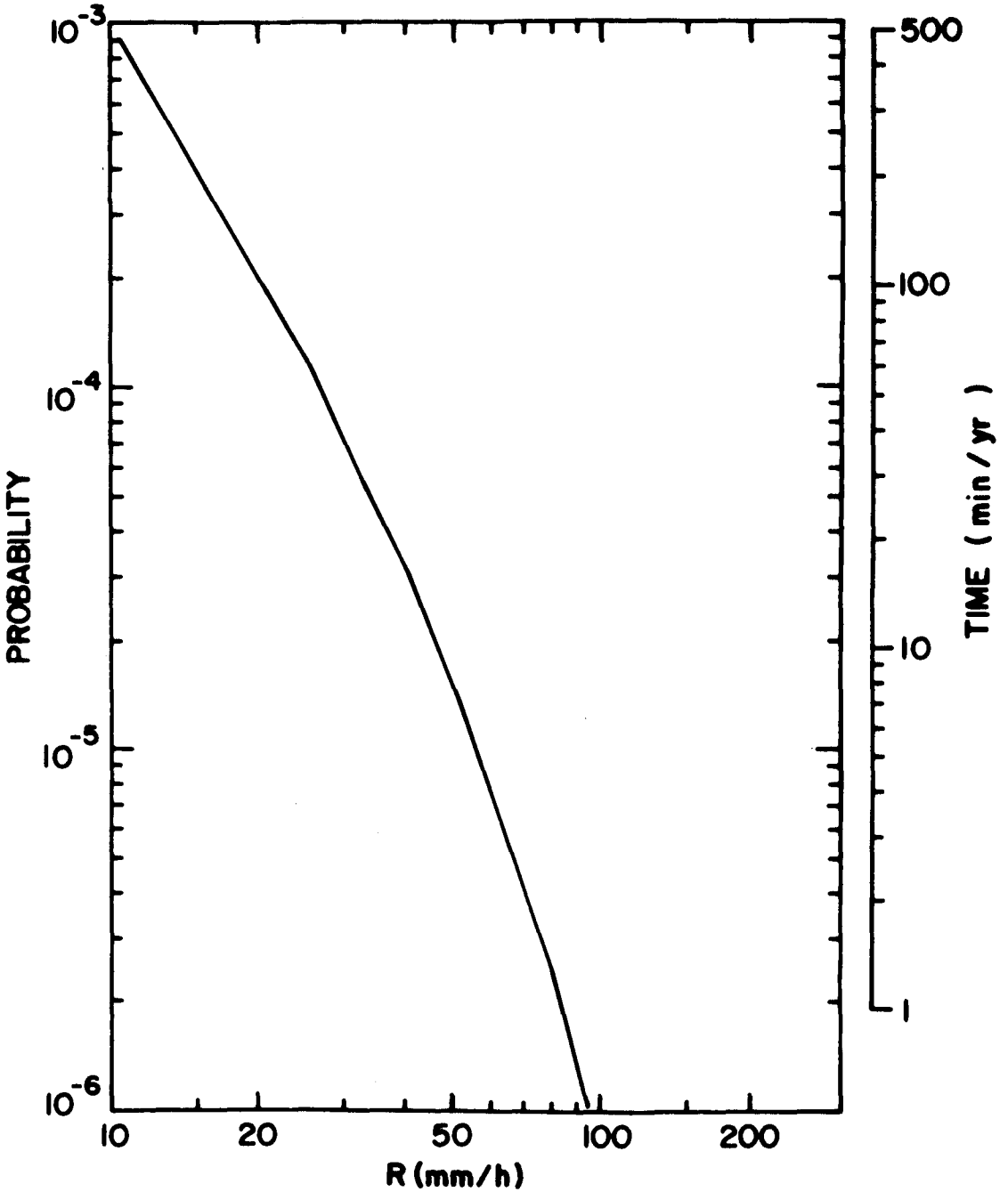

Figure 81. Long term average probability of exceeding a given rainfall rate at Sydney, N.S.

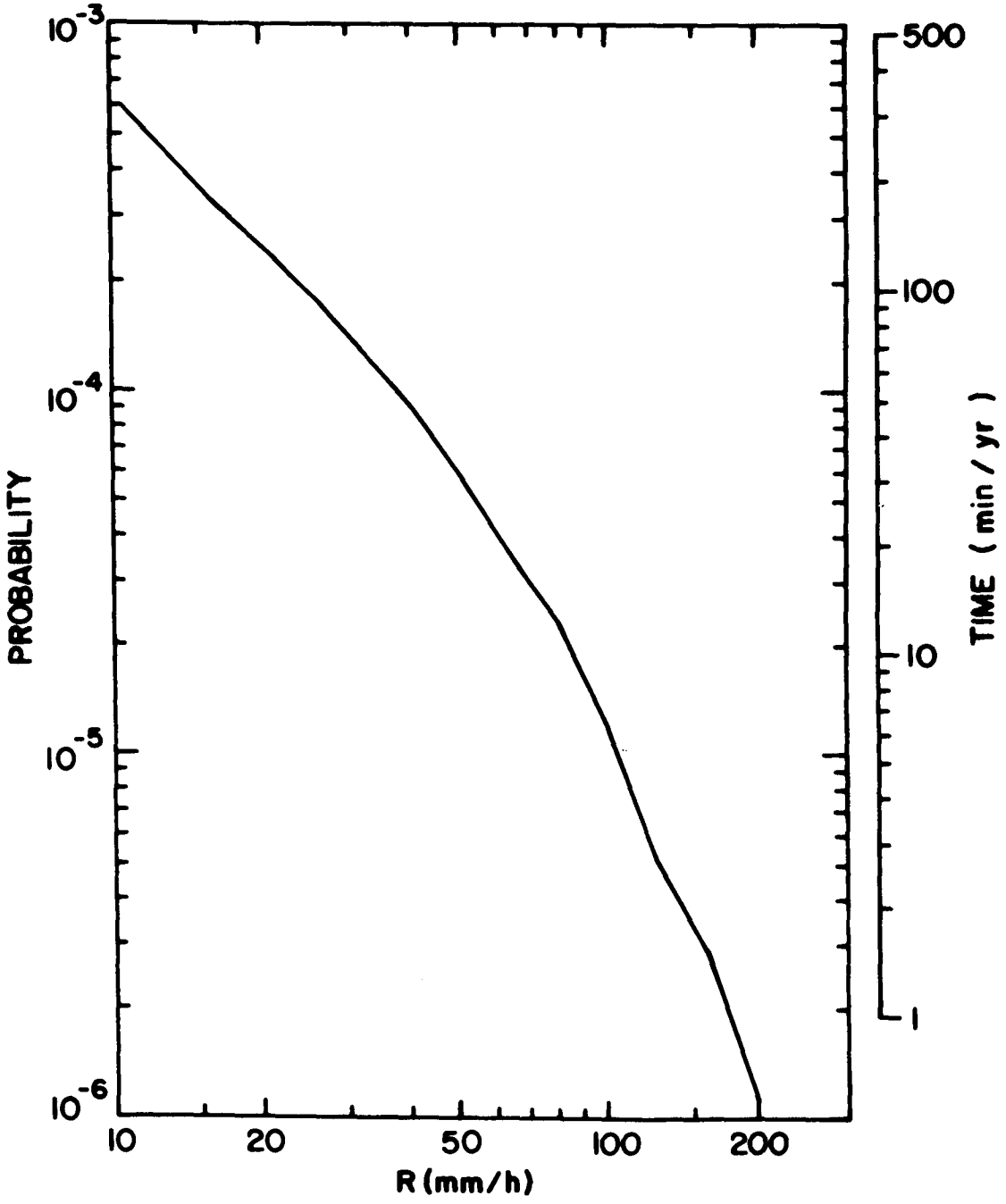

Figure 82. Long term average probability of exceeding a given rainfall rate at Toronto, Ont.

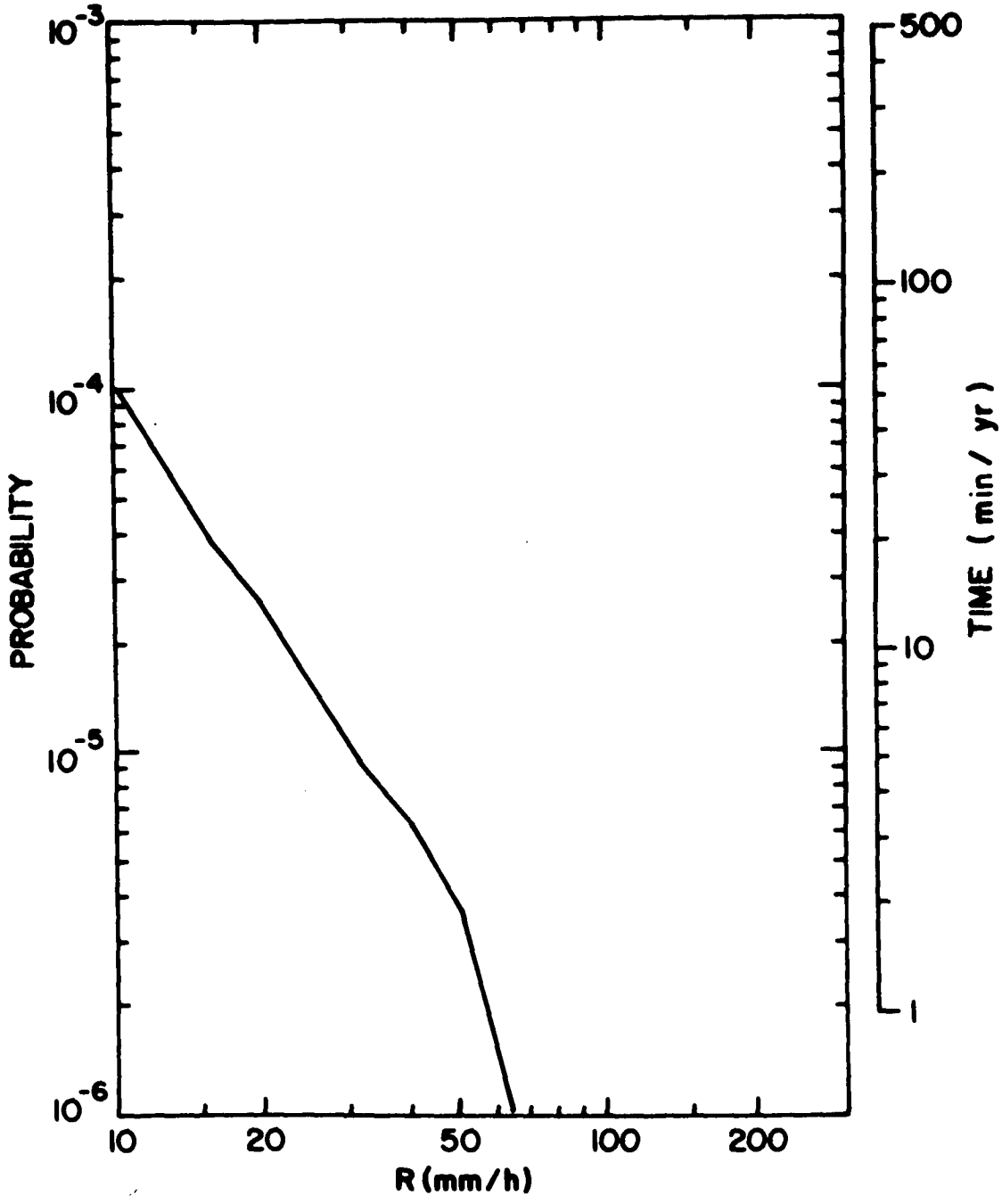

Figure 83. Long term average probability of exceeding a given rainfall rate at Uranium City, Sask.

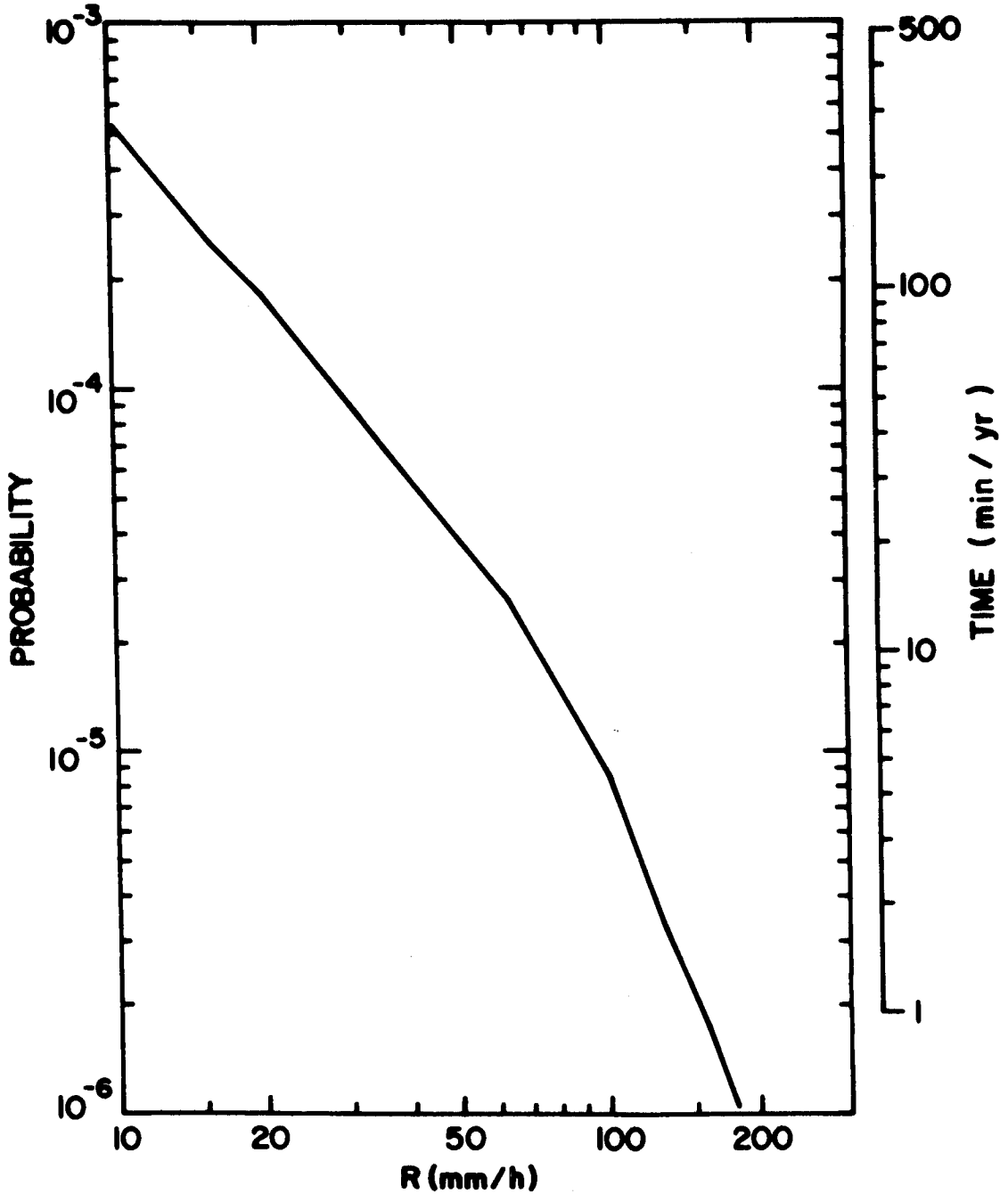

Figure 84. Long term average probability of exceeding a given rainfall rate at Val d'Or, Que.

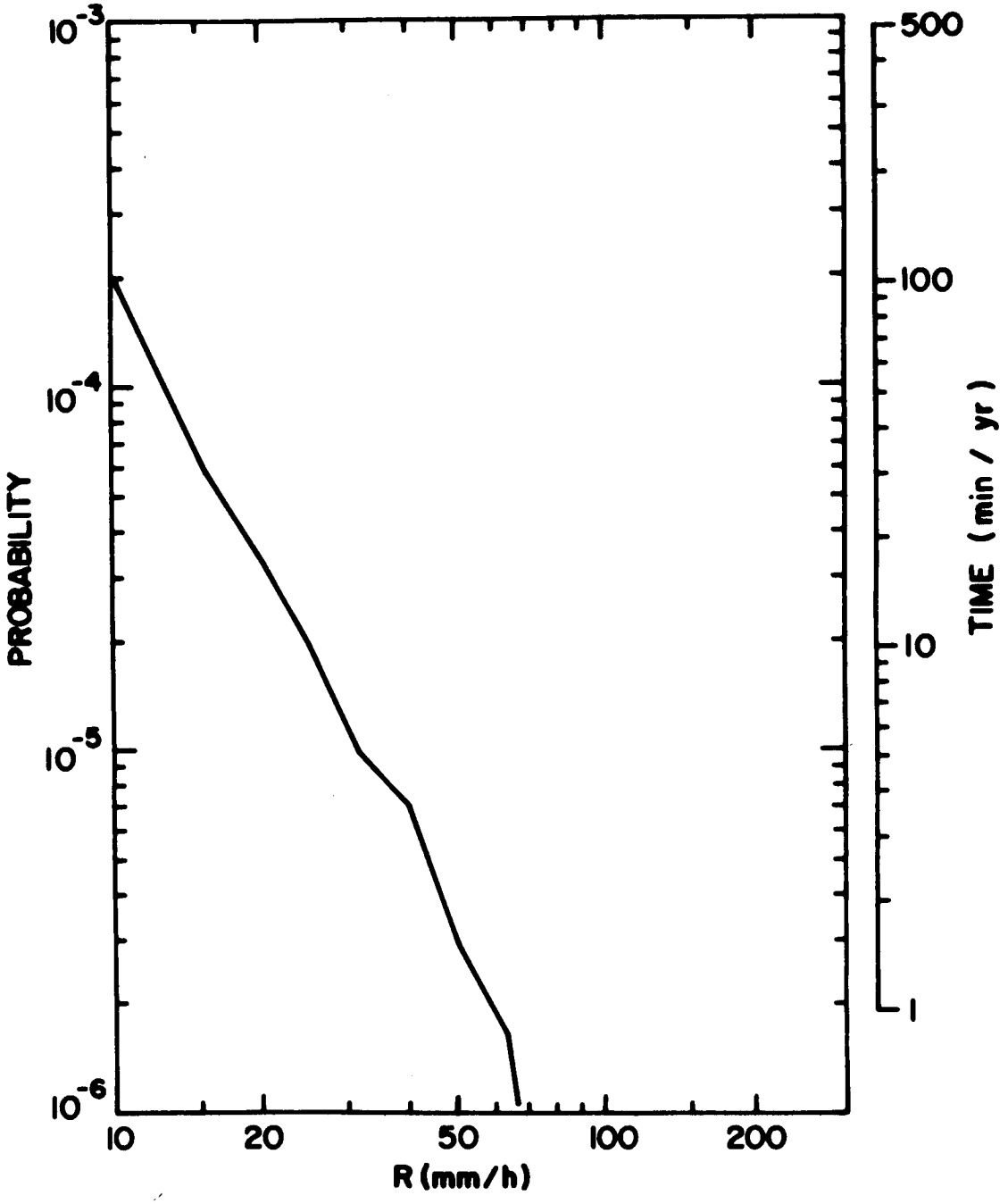

Figure 85. Long term average probability of exceeding a given rainfall rate at Vancouver, B.C.

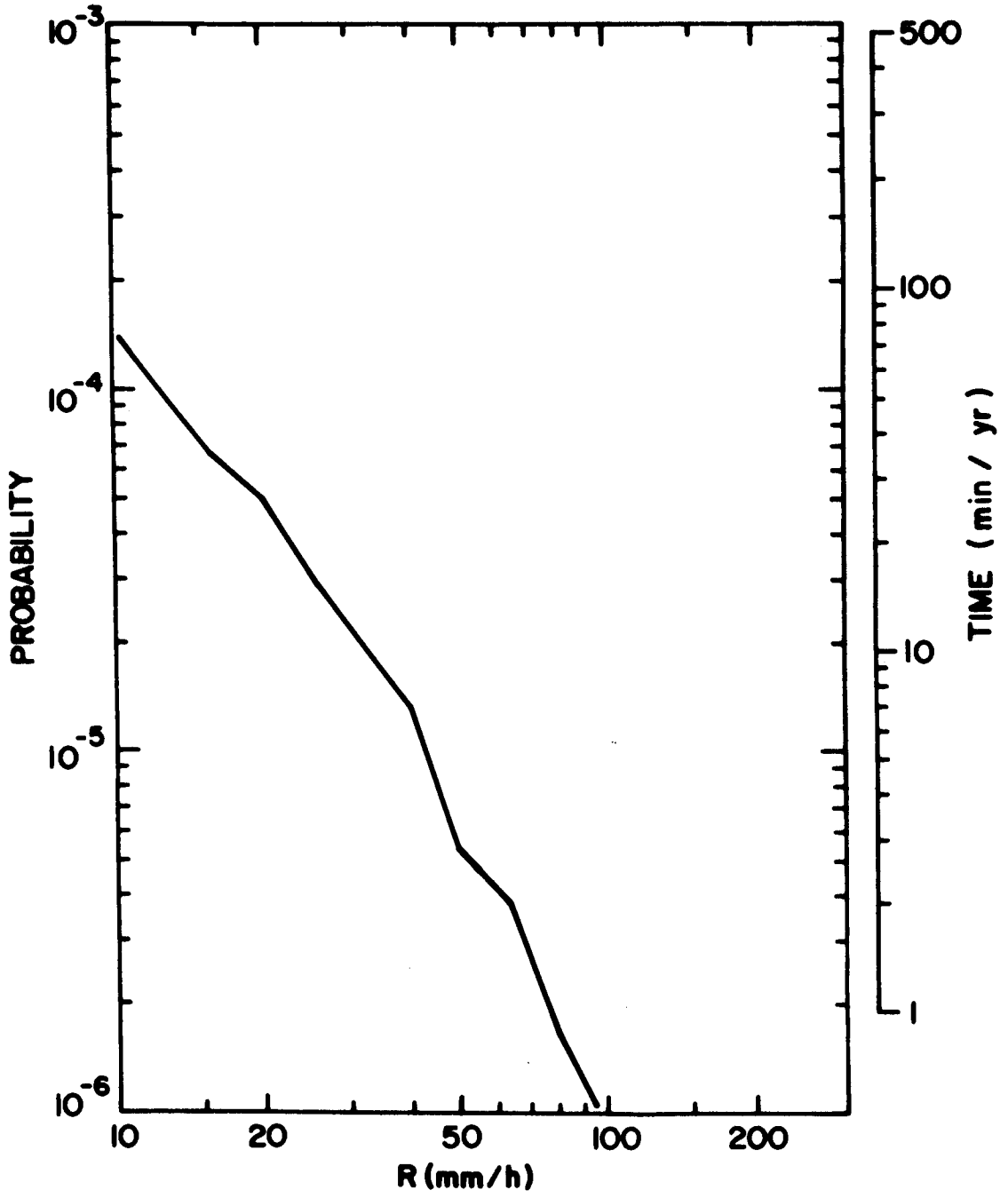

Figure 86. Long term average probability of exceeding a given rainfall rate at Watino, Alta.

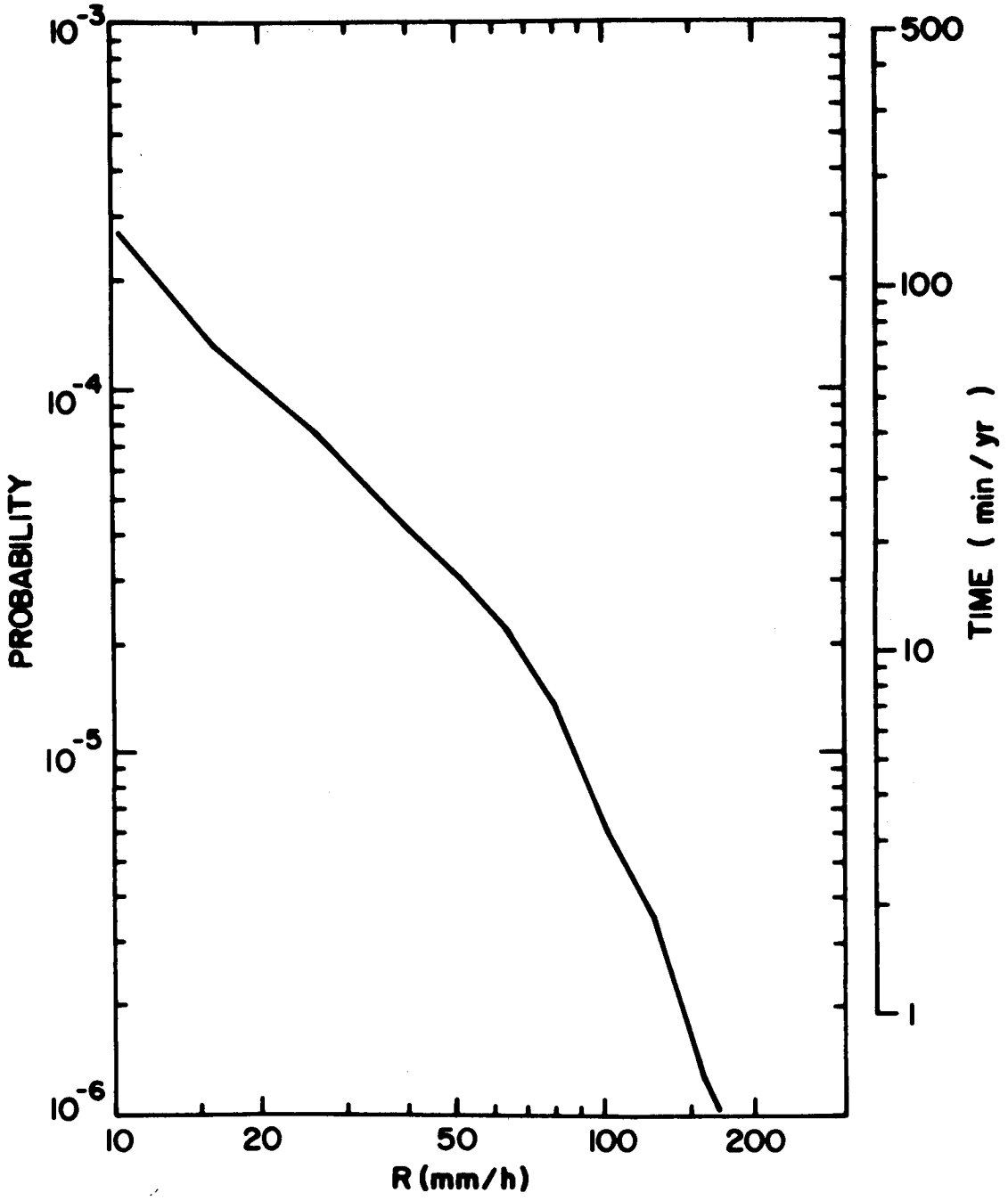

Figure 87. Long term average probability of exceeding a given rainfall rate at Weyburn, Sask.

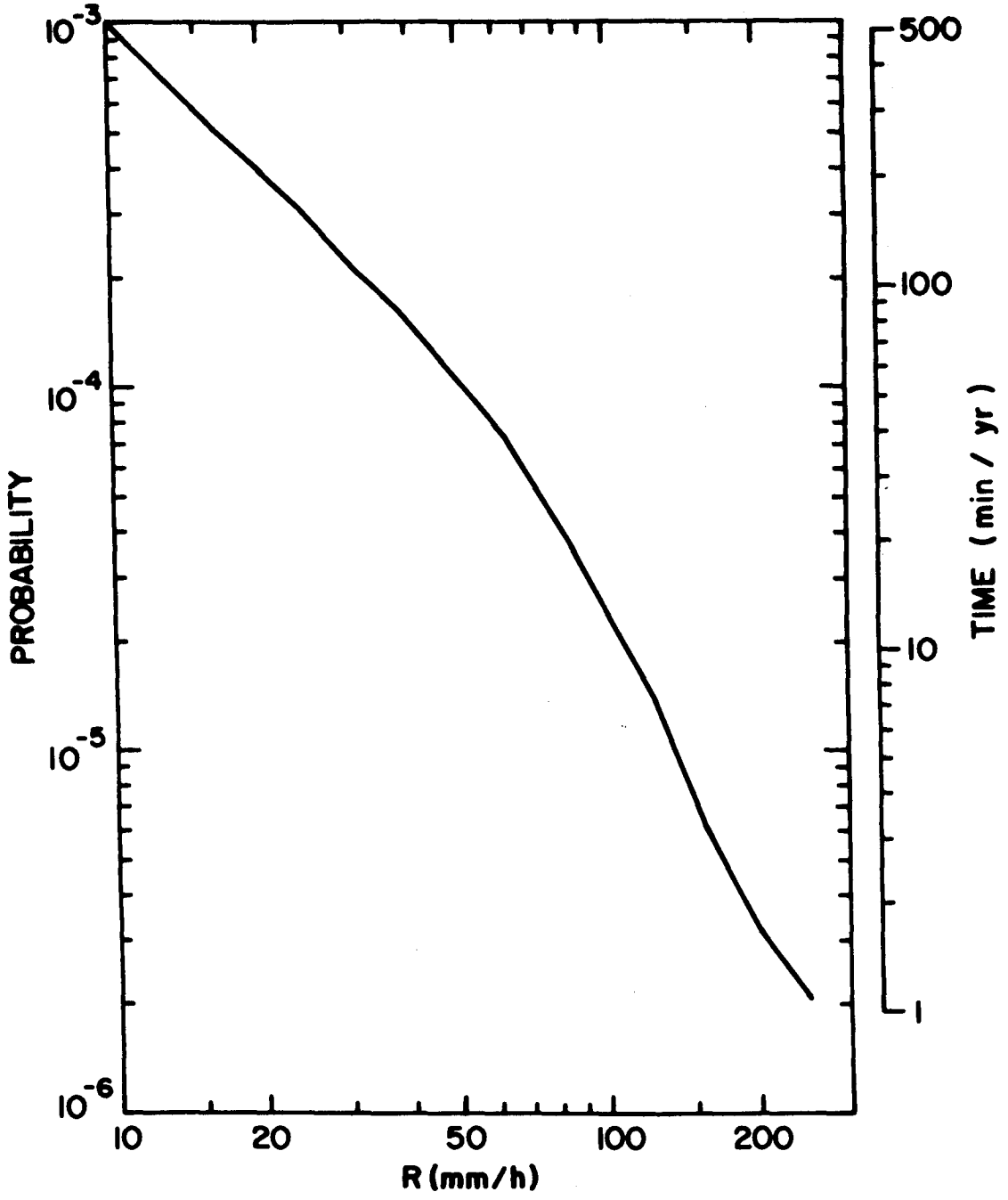

Figure 88. Long term average probability of exceeding a given rainfall rate at Windsor, Ont.

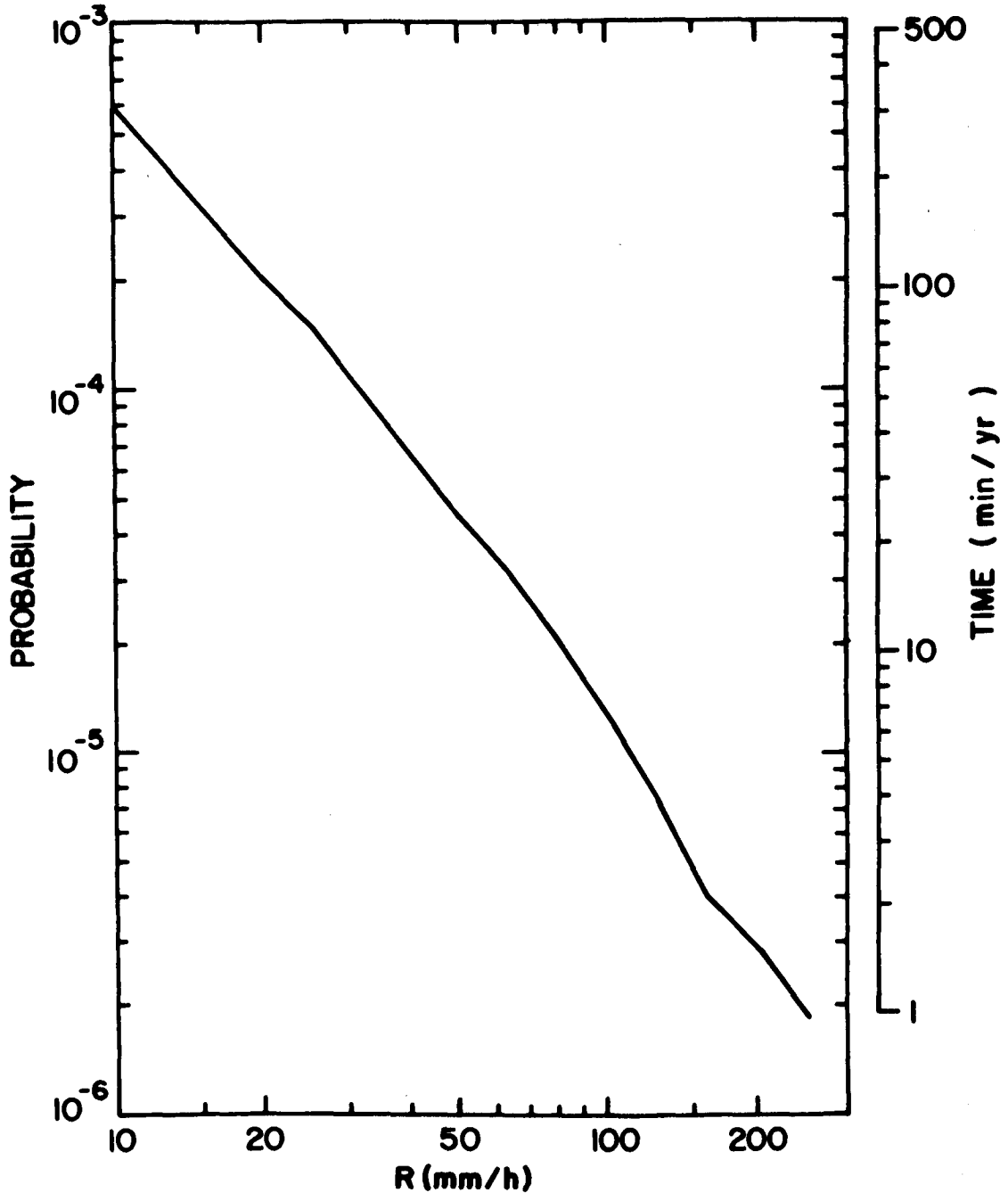

Figure 89. Long term average probability of exceeding a given rainfall rate at Winnipeg, Man.

CRC DOCUMENT CONTROL DATA

1. **ORIGINATOR:** Department of Communications/Communications Research Centre

2. **DOCUMENT NO:** CRC Report No. 1329-E

3. **DOCUMENT DATE:** November 1979

4. **DOCUMENT TITLE:** High-Intensity Rainfall Statistics for Canada

5. **AUTHOR(s):** B. Segal

6. **KEYWORDS:**
(1) Atmospheric Precipitation
(2) Microwave Attenuation
(3) Climatology

7. **SUBJECT CATEGORY (FIELD & GROUP: COSATI)**

04 Atmospheric Sciences

04 01 Atmospheric Physics

8. **ABSTRACT:** Not applicable to this report.

9. **CITATION:**

Government of Canada
Gouvernement du Canada